MIMICAD TECHNICAL REPORT NO. 7

Electromagnetic Modeling of Microstrip Circuit Discontinuities and Antennas of Arbitrary Shape

by

Jian-Xiong Zheng

Department of Electrical and Computer Engineering
University of Colorado
Boulder, Colorado 80309-0425

Work described in this report has been supported by the MIMICAD Center and the National Science Foundation.

January 1991

Zheng, Jian-Xiong (Ph.D., Electrical Engineering)

Electromagnetic Modeling of Microstrip Circuit Discontinuities and Antennas of Arbitrary Shape

Thesis directed by Professor D. C. Chang

In this thesis, a spatial-domain mixed-potential integral equation algorithm is developed for the analysis of microstrip discontinuities and antennas of arbitrary shape. The algorithm is based upon roof-top basis functions on a rectangular and triangular mixed-grid, polynomial curve-fitting of the Green's functions and analytical evaluation of the resulting quadruple moment integrals.

A microstrip structure of arbitrary shape is first broken up into a group of small rectangular cells and triangular cells with the rectangular cells in the regular region and triangular cells to fit the non-regular boundary. The current density distribution is expressed linearly in terms of the normal current components across cell boundaries, which are constrained to be continuous across and constant along each cell boundary.

An mixed-potential integral equation is formulated and then solved by the Galerkin method to yield a matrix equation. The resultant matrix elements contain quadruple moment integrals, whose integrands are known only in terms of so-called Sommerfeld integrals and are singular. The singularities in these integrals are first extracted and the remainder terms are then numerically evaluated and curve-fitted into polynomials.

The quadruple integrals are solved analytically to save computational time and improve numerical accuracy.

An accurate and efficient de-embedding technique is developed to

solve the network S-parameters and the complex wave propagation constants by detecting the standing waves in microstrip structures at three uniformly spaced points.

A general network connection algorithm is introduced to accomplish network connection among elements after the S-matrices of these elements are evaluated from the electromagnetic simulation.

The algorithm is well implemented into a general FORTRAN program. And a graphic-aided gridding program is developed to construct the geometry files of describing the microstrip structures being analyzed.

The code is used to analyze various kinds of passive microstrip circuits. Good agreement with experimental results is observed. It is found that the metallic loss, reflections from junctions and coupling between striplines are the dominant factors of affecting the performance of a microstrip circuit. The radiation loss is negligibly small for a typical MMIC microstrip circuit.

Some bandwidth broadening mechanisms for microstrip patch antennas are discovered from numerical simulation. Multi-loaded resonant frequency concept is applied to achieve significant bandwidth improvement.

ACKNOWLEGEMENTS

I would like to express my appreciation and thanks to Dr. David C. Chang. He suggested the investigations covered in this thesis and has contributed a lot, especially the " P-mesh " idea, to the methods of attack. I have also benifited very much from his guidance, technical insight, and time toward this project. Dr. Chang has also broadened the scope of my graduate education. I am very grateful to be working on Dr. Chang's direction and I sincerely appreciate his guidance.

I also wish to thank Dr. Edward F. Kuester and other members of the committee: Dr. K. C. Gupta, Dr. John Dunn, Dr. Richard Booton and Dr. William Jones, for their comments and suggestions on the writing of the dissertation.

The author would like to thank Dr. Doris Wu, Dr. Abdelaziz Benalla and other staff and students of the MIMICAD center for their discussions and assistance.

Special thanks to Dr. Martin Herman in Hughes Aircraft Company and Dr. C. Goldsmith in Texas Instrument for supplying the experimental data.

CONTENTS

TABLES

TABLE

FIGURES

FIGURE

CHAPTER 1

INTRODUCTION

1.1 Background

The rapidly advancing technology in microwave/millimeter-wave integrated circuits (MMICs) has made it possible to fabricate complicated components, such as amplifiers, transceivers and radiators with both active devices and passive elements, into a single chip. such circuits generally have very complicated geometry (see Fig. 1.1). But their basic elements are planar structures such as microstrip patches and lines, configured in such a way as to act as resonators, couplers, and transmission lines interconnecting active devices and passive elements.

Basically, there are three commonly-used planar transmission-line structures: (1) microstrip lines; (2) co-planar waveguides; (3) slotted-lines [45]. Compared to traditional microwave circuits with waveguide structures of hollow metallic waveguides and coaxial-lines, the MMIC monolithic circuits have the advantage of smaller size, higher functionality, better performance and reliability, and last but not least, more manufacturability. However, unlike conventional waveguide systems, MMICs lack tuning capability once a circuit is fabricated. Accurate EM modeling is therefore necessary in order to minimize the number of design iterations or even achieve a first pass design.

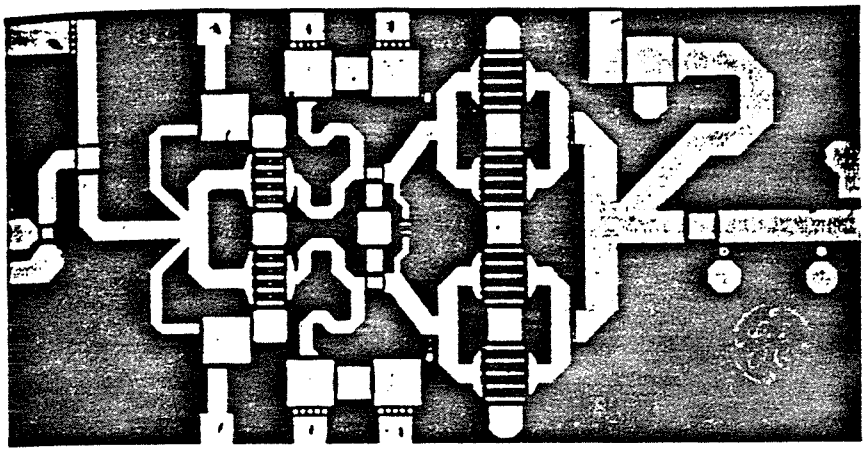

Figure 1.1: A C-band 3-watt, 2-stage amplifier [1].

The dominant mode of wave propagation for many of these guided-wave structures is quasi-TEM at low frequencies. At higher frequencies, it consists of both transverse and longitudinal field components and has no cut-off frequency. Unlike in conventional waveguide structures, analytical determination of the characteristics of the quasi-TEM mode and higher order modes is not available. Furthermore, because they are also open wave-guiding structures, radiation as well as reflection of incident waves occurs at circuit junctions and bends, in a manner not predictable by conventional transmission-line theory. In addition, parasitic couplings among the closely packed circuit elements have pronounced effects on circuit performance at high frequency range.

In this thesis, a versatile, accurate and efficient electromagnetic simulation algorithm is developed for the analysis of this kind of circuit. Emphasis is on microstrip circuits.

Before we proceed to the detailed theoretical derivation in the following chapters, we shall provide first a review on the analysis methods for MMICs in Sections 1.2 and 1.3. The configuration of the chapters, the assumptions and some frequently used notations in this thesis will be discussed in Sections 1.4 and 1.5, respectively.

1.2 Microstrip Circuit Analysis Methods

The simplest and most efficient method for analyzing microstrip circuits is the quasi-static analysis. There are basically two types of quasi-static analyses: (1)two-dimensional analysis for the transmission-line parameters [2]; and (2)three-dimensional analysis for the discontinuity parameters [3]-[6]. In quasi-static analyses, it is assumed that the dominant effect associated with a circuit discontinuity can be obtained from the solution of the Laplace equation.

This technique ignores the longitudinal field components and is valid usually for low frequency microstrip circuits [7]-[9]. The dispersive effects obviously can not be modeled in the quasi-static analyses.

Another commonly-used approximate method in analyzing microstrip circuits at low frequencies is the so-called 2-D planar circuit analysis in which microstrip circuits are replaced by parallel-plate waveguides with magnetic walls (see Fig. 1.2) so that the dynamic nature of a microstrip discontinuity can be analyzed by a combination of mode and point-matching techniques [10]-[14]. By using the known properties for closed waveguides of specific geometries such as rectangular, triangular and circular sections, complex geometries can be handled using the segmentation techniques [15]-[17]. Some empirical or analytical formulas are utilized to calculate the equivalent width of a microstrip and the effective dielectric constant of the structure. The radiative coupling among discontinuities is then taken into account in the multi-port model [17] by adding some equivalent magnetic currents on magnetic walls. Although dispersive and coupling effects can be taken into consideration in this manner, it will be demonstrated in Chapter 6 that such a method is still frequency limited.

Full-wave methods in principle numerically solve the exact Maxwell's equations without the use of approximations in the mathematical model. They can generally be catagorized into two basic groups: (1) Finite difference and finite element methods in either time or frequency domain [19]-[22]; (2) Integral equation methods [29] - [39].

In time-domain finite difference approaches, the partial derivatives

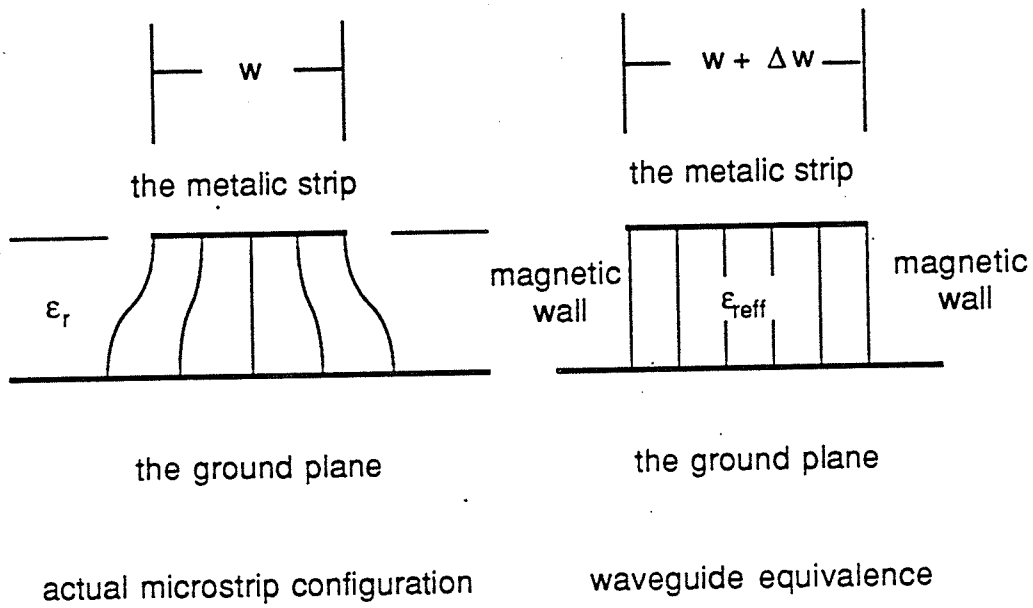

Figure 1.2: The waveguide equavalence of the waveguide methods.

both in time and spatial directions in the Maxwell's equations are approximated by the finite differences and the resulting equation is solved to find the field distribution as a function of space and time [19]. The advantage of finite difference approaches is that the algorithm is very straight-forward to implement and there is no need to invert large matrices. However, because they solve electric and magnetic fields in a three-dimensional space, the number of unknowns is substantially larger than that in integral equation methods, in which two-dimensional current density distribution on a microstrip structure is evaluated. They also encounter difficulty in modeling structures other than that can be divided into a group of rectangular shapes. Generally, very fine gridding has to be used when some non-rectangular structures are analyzed [22] (see Fig. 1.3). In addition, absorbing boundary conditions are typically used to reduce an open-system problem to a finite-region problem. These however are only approximate conditions and often may lead to unstable solutions [22]. Furthermore, a considerable time history has to be established before one can extract the solution at a given frequency with a reasonable degree of resolution. Henceforth, it may be computationally more intensive than a frequency-domain solution if only a small number of frequency points is desired.

Finite element frequency-domain method is similar to the finite difference in that they both deal directly with the differential-form of the Maxwell equation for vector electric and magnetic fields in space [23,24]. The difference is that finite element method uses a tetrahedral division instead of a cubic division so that it can more easily be used to analyze arbitrary structures. Spurious solutions occassionally can occur as a result of over-specifying the

continuity condition of the field components at the interface of any two different materials. Besides, large even though sparse matrices are encountered in finite element method.

Similar solution of electric and magnetic fields in space is also found in the method of lines algorithm [26,25]. It has the same disadvantage as the finite element method.

1.3 Frequency-Domain Integral Equation Methods

The algorithm developed in this thesis is based upon an integral equation formulation, and we seek the solution of the electric or magnetic current density distribution on a guiding structure instead of electric and magnetic field components in a volume outside of the structure. In microstrip circuits, a guiding structure is generally a thin metallic strip and, therefore, the solution process is concerned only with the current density distribution over a two-dimensional region and as a result involves much smaller number of unknowns than finite difference and finite element methods. An electric field integral equation (EFIE) is typically in the form:

$$\int_S \bar{\bar{G}}(x,y;x',y') \cdot \bar{J}(x',y')\, dx'\, dy' \;=\; -\bar{E}_i(x,y) \tag{1.1}$$

where $\bar{\bar{G}}(x,y;x',y')$ is the dyadic Green's function; $\bar{E}_i(x,y)$ is the incident field; $\bar{J}(x',y')$ is the unknown surface current density distribution on S as shown in Fig. 1.4. In a microstrip structure, S is the metallic strip.

To solve the electric field integral equation, it is typical to expand the two dimensional current density distribution into some complete set of basis functions (see (1.2)).

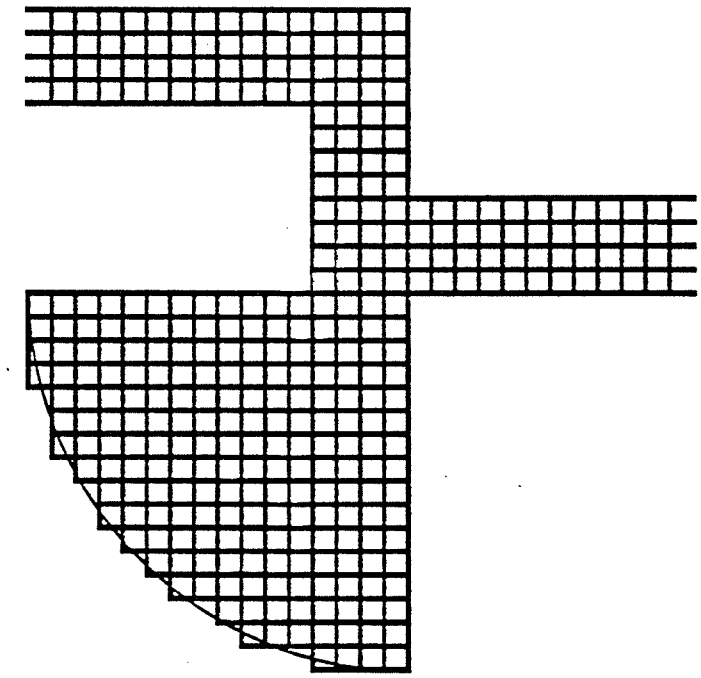

Figure 1.3: A rectangular grid for a microstrip structure.

$$\bar{J}(x,y) = \sum_{n=1}^{\infty} I_n \, \bar{B}_n(x,y) \tag{1.2}$$

where $\bar{B}_n(x,y)$, $n = 1,2,3,...,$ and I_n are the basis functions and the corresponding coefficients.

Substitution of (1.2) into (1.1) yields the following equation

$$\sum_{n=1}^{\infty} I_n \int_s \bar{\bar{G}}(x,y;x',y') \cdot \bar{B}_n(x',y') \, dx' \, dy' \; = \; -\bar{E}_i(x,y) \tag{1.3}$$

A matrix equation is subsequently obtained if we multiply both sides of (1.3) by a set of test functions $\bar{T}_m(x,y)$, $m = 1,2,3,...,$ integrate them over the surface of the structure and then truncate the infinite number of basis functions and test functions into finite number of them.

$$\sum_{n=1}^{M} Z_{m,n} \, I_n \; = \; V_m \; ; \; m = 1,2,...,M \tag{1.4}$$

where M is the number of basis functions or test functions after truncated,

$$Z_{m,n} = \int_s dx \, dy \int_s dx' \, dy' \, \bar{T}_m(x,y) \cdot \bar{\bar{G}}(x,y;x',y') \cdot \bar{B}_n(x',y') \tag{1.5}$$

$$V_m = -\int_s dx \, dy \, \bar{E}_i(x,y) \cdot \bar{T}_m(x,y) \tag{1.6}$$

The method is commonly referred to as the Galerkin method when $\bar{T}_m(x,y) = \bar{B}_m(x,y)$. Clearly, the efficiency of the above described procedure depends upon the choice of basis functions and evaluation of the moment integrals involved. A set of basis functions in which (1.2) converges rapidly can reduce the size of the matrix and, therefore, the number of integrals.

Basis functions can be full-domain basis functions or sub-domain basis functions. Full-domain basis functions are generally very efficient, but can only

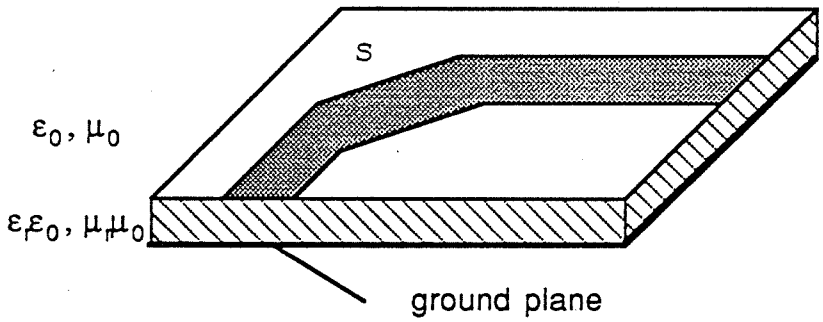

Figure 1.4: A microstrip structure.

be found in regular regions, such as a rectangle or a circle. Therefore, they can only be used for structures of regular shape. Sub-domain basis functions are more versatile. They can be used to fit complicated geometries. But, generally, we have to use a large number of them even for simple structures.

Integral equation methods can also be sub-divided into two groups: spectral-domain methods and spatial-domain methods. They differ in the way they evaluate the moment integrals in (1.5). In spectral domain methods [34]-[40], the Green's function in (1.5) is expressed in terms of a double Fourier transform with respect to x and y. The two surface integrals are evaluated analytically in the transform domain resulting in only the inverse transform of known, but complex integrands, to be performed numerically. Spectral-domain methods are efficient when few basis functions, in the form of full domain functions, can yield convergent results.

When a complicated microstrip structure, such as a patch with a slot or a corner cut, is considered, sub-domain basis functions on cells appear to be the only logical choices. The microstrip structure in this case is divided into rectangular and/or triangular cells. Generally, simple sub-domain basis functions, such as pulse functions and roof-top functions, are employed in order to simplify the evaluation of the moment integrals. Even so, many basis functions result from the process and spectral-doman methods can no longer be used efficiently.

1.4 Configuration of the Chapters

The algorithm developed in this thesis is a spatial-domain mixed potential integral equation (MPIE) method [29]-[32], [41]-[44]. It is based upon the roof-top basis functions over a rectangular and triangular mixed-grid and

analytical evaluation of the resulting quadruple moment integrals with static singular integrands.

In Chapter 2, we will derive the mixed-potential equation for microstrip structures from the fields of a horizontally-placed current density distribution over a grounded dielectric slab. The roof-top basis functions over a rectangular and triangular mixed-grid are introduced in Chapter 3. The pseudo-mesh (or P-mesh) concept will also be discussed in Chapter 3. Application of the roof-top basis functions and test functions to the mixed-potential equation results with a large number of quadruple moment integrals. An analytical integration technique will be illustrated in Chapter 4 to evaluate these integrals. A comparison between the analytical and numerical integration schemes will also be provided in Chapter 4.

For microstrip structures, especially circuit problems, we are ultimately more interested in network parameters than in current distributions. Several de-embedding techniques have been developed and they will be discussed in Chapter 5.

Since the P-mesh algorithm makes use of rectangular cells for the regular region and triangular cells for irregular region of a microstrip structure of general shape, planar structures of general shape can be analyzed efficiently using the P-mesh code. The applications of P-mesh in analyzing microstrip circuits of different structures will be discussed in Chapter 6. Chapter 7 discusses the use of the P-mesh code in analyzing microstrip antennas.

1.5 Assumptions and Notations

The Physical world is a very complicated system. Mathematics is developed to model the physical world and the modeling can never be exact. In

the P-mesh algorithm, some approximations have to be made in order to simplify the analysis of encountered problems. The first approximation we make is that the dielectric slab and the ground plane of a microstrip structure are infinitely extended. This assumption is commonly accepted since the radiation as well as the reactive fields decays rapidly away from the strips and since the surface-wave field is usually very weak when the substrate thickness is much smaller than the wavelength in the substrate material. The second approximation we have made is that we assume that the microstrip can be modeled by a perfectly conducting and infinitely-thin conductor. As we will demonstrate in Section 2.4, such an assumption can be remedied by introducing an equivalent surface impedance on the microstrip surface.

Time convention $e^{j\omega t}$ and metric system are adopted in this thesis. Some commonly used notations will be defined in the following. They will be used consistently in the thesis except in Chapter 4. In Chapter 4, a very complicated analytical integration techniques will be discussed and a lot of notations will be used in the intermediate procedures. The following defined notations will not be valid and some of them will be used for other purposes in Chapter 4.

ε — permittivity;

ε_0 — permittivity in air;

ε_r — substrate relative permittivity;

μ — permeability;

μ_0 — permeability in air;

μ_r — substrate relative permeability;

h — substrate thickness;

σ — conductivity of a microstrip;

λ_g — waveguide wavelength;

$\gamma = \alpha + j\,\beta$ — complex propagation constant;

ω — angular frequency;

k_n — wave propagation constant in substrates;

k_0 — wave propagation constant in free space or air.

The References for Chapter 1

[1] W. H. Perkins, N. Jansen, T. A. Midford, W. C. Niehaus, D. H. Reep and J. Tenedorio " MIMIC technology transportability," **IEEE MTT Intern. Microwave Symposium Digest**, pp. 109-112, Dallas, May 1990.

[2] H. A. Wheeler, " Transmission-line properties of parallel strips separated by a dielectric sheet, " **IEEE Trans. on Microwave Theory Tech.**, Vol. MTT-13, pp. 172-185, Feb. 1965.

[3] A. Farrar and A. T. Adams, " Matrix methods for microstrip three-dimensional problems," **IEEE Trans. on Microwave Theory Tech.**, Vol. MTT-20, pp. 497-504, 1972.

[4] A. Farrar and A. T. Adams, " Computation of lumped microstrip capacitances by matrix methods — rectangular sections and end effects", **IEEE Trans. on Microwave Theory Tech.**, Vol. MTT-19, pp. 495-496, Aug. 1971.

[5] P. Benedek and P. Silvester, " Equivalent capacitances for microstrip gaps and steps," **IEEE Trans. on Microwave Theory Tech.**, Vol. MTT-20, pp. 729-733, 1972.

[6] A. F. Thomson and A. Gopinath, " Calculation of microstrip discontinuity inductances," **IEEE Trans. on Microwave Theory Tech.**, Vol. MTT-23, pp. 648-654, 1975.

[7] D. C. Chang and E. F. Kuester, " An analytic theory for narrow open microstrips," **Arch. Elek. Ubertragung.**, Vol. 33, pp. 199-206, Feb. 1979.

[8] E. J. Denlinger, " A frequency dependent solution for microstrip transmission lines," **IEEE Trans. on Microwave Theory Tech.**, Vol. MTT-19, pp.30-39, Jan. 1971.

[9] E. F. Kuester and D. C. Chang, " Theory of dispersion in microstrip arbitrary width," **IEEE Trans. on Microwave Theory Tech.** , Vol. MTT-28, pp. 259-265, March 1980.

[10] I Wolff, G. Kompa, and R. Mehran, " Calculation method for microstrip discontinuities and T-junctions, " **Electron. Lett.**, Vol. 8, pp. 177-179, 1972.

[11] G. Kompa, " *S*-matrix computation of microstrip discontinuities with a planar waveguide model, " **Arch. Elec. Ubertragung.** , Vol. 30, pp. 58-64, 1975.

[12] R. P. Owens, " Predicted frequency dependence of microstrip characteristic impedance using the planar-waveguide model, " **Electron. Lett.**, Vol. 12, pp. 260-270, 1976.

[13] W. Menzel and I Wolff, " A method calculating the frequency-dependent properties of microstrip discontinuities, " **IEEE Trans. on Microwave Theory Tech.** , Vol. MTT-25, pp. 107-112, Feb. 1977.

[14] T. S. Chu, T. Itoh, " Comparative study of mode matching formulations of microstrip discontinuity problems," **IEEE Trans. on Microwave Theory Tech.**, Vol. MTT-33, pp. 1018-1023, Oct. 1985.

[15] T. Okoshi, Y. Uehara and T. Takeuchi, " The segmentation method: an approach to the analysis of microwave planar lines," **IEEE Trans. on Microwave Theory Tech.** , Vol. MTT-24, pp. 662-668, Oct. 1976.

[16] R. Chadha and K. C. Gupta, " Segmentation method using impedance matrices for analysis of planar microwave circuits, " **IEEE Trans. on Microwave Theory Tech.**, Vol. MTT-29, pp. 71-74, Jan. 1981.

[17] A. Sabban and K. C. Gupta, " A planar-lumped model for coupled microstrip line discontinuities," **IEEE Trans. on Microwave Theory Tech. Special Issue**, MTT-38, Dec. 1990, to be published.

[18] R. F. Harrington, **Field Computations by Moment Methods.** New York: Macmillan, 1968.

[19] X. Zhang and K. K. Mei, "Time-domain finite difference approach to the calculation of the frequency-dependent characteristics of microstrip discontinuities," **IEEE Trans. on Microwave Theory Tech.**, vol. MTT-36, pp. 1775-1787, Dec. 1988.

[20] X. Zhang, J. Fang, K. K. Mei and Y. Liu, " Calculations of the dispersive characteristics of microstrips by the time-domain finite difference method, " **IEEE Trans. on Microwave Theory Tech.** , Vol. MTT-36, pp. 263-267, Feb. 1988.

[21] C. J. Railton and J. P. McGeehau, " Analysis of microstrip discontinuities using the finite difference time-domain technique, " **IEEE MTT-S Digest**, pp. 1009-1012, June 1989.

[22] M. Rittwegar and I. Wolff, "Analysis of complex passive (M)MIC-components using the finite difference time-domain approach," **IEEE MTT Intern. Microwave Symposium Digest**, pp. 1147-1150, May 1990.

[23] B. M. A. Rahman and J. B. Davies, " Finite-element analysis of optical and microwave waveguide problems," **IEEE Trans. on Microwave Theory Tech.**, Vol. MTT-32, pp. 20-28, Jan. 1984.

[24] M. Koshiba, K. Hayata and M. Suzuki, " Improved finite-element formulation in terms of the magnetic-field vector for dielectric waveguides," **IEEE Trans. on Microwave Theory Tech.**, Vol. MTT-33, pp. 227-233, March 1985.

[25] Z. Q. Chen and B. Gao, " Deterministic approach to full-wave analysis of discontinuities in MIC's using the method of lines," **IEEE Trans. on Microwave Theory Tech.**, Vol. MTT-37, pp. 606-611, March 1989.

[26] S. B. Worm and R. Pregla, " Hybrid-mode analysis of arbitrarily shaped planar microwave structures," **IEEE Trans. on Microwave Theory Tech.** , Vol. MTT-32, pp. 191-196, 1984.

[27] A. W. Glisson and D. R. Wilton, " Simple and efficient numerical methods for problems of electromagnetic radiation and scattering from surfaces, " **IEEE Trans. on Antennas Propag.**, Vol. AP-28, pp. 593-603, Sep. 1980.

[28] S. M. Rao, D. R. Wilton and A. W. Glisson, " Electromagnetic scattering by surfaces of arbitrary shape, " **IEEE Trans. on Antennas Propag.** , Vol. AP-30, pp. 409-418, 1982.

[29] D. I. Wu, D. C. Chang and B. I. Brim, "Accurate numerical modeling of microstrip junctions and discontinuities," **Intern. Journal of Microwave Millimeter-wave Computer Aided Engineering**, to be published.

[30] J. R. Mosig, "Arbitrarily shaped microstrip structures and their analysis with a mixed potential integral equation," **IEEE Trans. on Microwave Theory Tech.**, MTT-36, pp. 314-323, February 1988.

[31] W. Wertgen and R. H. Jansen, " Efficient direct and iterative electrodynamic analysis of geometrically complex MIC and MMIC structures," **Intern. Journal of Numerical Modeling: Electronic Networks, Devices and Fields**, Vol.2, 153-186, 1989.

[32] R. W. Jackson, " Full-wave, finite element analysis of irregular microstrip discontinuities," **IEEE Trans. on Microwave Theory Tech.**, MTT-37, pp. 81-89, January 1989.

[33] J. C. Rautio and R. F. Harrington, " Preliminary results of a time-harmonic electromagnetic analysis of shielded microstrip circuits, " **27th Automatic RF Techniques Group Conference Digest**, Baltimore, pp. 121-134, June 1986.

[34] R. Mittra and T. Itoh, " A new technique for the analysis of the dispersion characteristics of microstrip lines," **IEEE Trans. on Microwave Theory Tech.** , Vol. MTT-19, pp. 47-56, Jan. 1971.

[35] T. Itoh and R. Mittra, " Spectral-domain approach for calculating the dispersion characteristics of microstrip lines," **IEEE Trans. on Microwave Theory Tech.** , Vol. MTT-21, pp. 496-499, July 1973.

[36] R. H. Jansen, " High-speed computation of single and coupled microstrip parameters including dispersion, high-order modes loss and finite strip thickness, " **IEEE Trans. on Microwave Theory Tech.** , Vol. MTT-26, pp. 75-82, Jan. 1978.

[37] E. F. Kuester and D. C. Chang, " An appraisal of methods for compuation of the dispersion characteristics of open microstrip, " **IEEE Trans. on Microwave Theory Tech.** , Vol. MTT-27, pp. 691-694, July, 1979.

[38] P. B. Katehi and N. G. Alexopoulos, " Frequency-dependent characteristics of microstrip discontinuities in millimeter-wave integrated circuits," **IEEE Trans. on Microwave Theory Tech.**, Vol. MTT-33, pp. 1029-1035, Oct. 1985.

[39] R. W. Jackson and D. M. Pozar, " Full-wave analysis of microstrip open-end and gap discontinuities," **IEEE Trans. on Microwave Theory Tech.**, Vol. MTT-33, pp. 1036-1042, Oct. 1985.

[40] Shih-chang Wu, Hung-Yu Yang and N. G. Alexopoulos, " A rigorous dispersive characteristics of microstrip cross and tee-junctions," **IEEE MTT Intern. Microwave Symposium Digest,** pp. 1151-1154, May 1990.

[41] D. C. Chang and J. X. Zheng, " Numerical modeling of planar circuits with pseudo meshes," **National Science Meeting Digest**, pp. 265, Boulder, CO, Jan. 1990.

[42] J. X. Zheng and D. C. Chang, " Convergence of the numerical solution for a microstrip junction based upon a triangular cell expansion," **National Science Meeting Digest**, pp.212, Boulder, CO, Jan. 1990.

[43] J. X. Zheng and D. C. Chang, " Numerical modeling of chamfered bends and other microstrip junctions of general shape in MMICs," **IEEE MTT Intern. Microwave Symposium Digest**, pp. 709-712, Dallas , May 1990.

[44] D. C. Chang and J. X. Zheng, " Electromagnetic modeling of passive circuit elements in MMIC," **IEEE Trans. Microwave Theory Tech.**, to be published.

[45] D. I. Wu and D. C. Chang, " A review on the electromagnetic properties of the guiding structures in MMIC, " to be published.

[46] R. R. Romanofsky, " Analytical and experimental procedures for determining propagation characteristics of millimeter-wave gallium arsenide microstrip lines," **NASA Technical Paper 2899**, 1989.

CHAPTER 2

MIXED-POTENTIAL INTEGRAL EQUATION FORMULATION OF MICROSTRIP STRUCTURES

2.1 Introduction

The formulation of mixed-potential integral equation (MPIE) can be traced back to the well-known work of Harrington [1]. It has been widely used in solving scattering problems [2,3]. Basically, it transforms the expression for the induced electric field given in (1.3) in terms of the dot product of a dyadic Green's function $\bar{\bar{G}}$ with the unknown current $\bar{J}$, to one involving two scalar Green's functions, one associated with the current and the other with the charge distribution on the structure. The detailed derivation of such an equation as applied to microstrip structure will be given in the following sections.

For planar structures, the MPIE formulation has at least two distinctive advantages when compared with a typical electric field integral equation(EFIE): one is that the Green's functions involved in the kernel of a MPIE are scalar functions of electric and magnetic types and they usually can be represented by one-dimensional Sommerfeld integrals. The other is that the singularity in the Green's functions of both types is of the order of $1/R$, where $R = |\bar{r} - \bar{r}'|$ is the distance between the source and observation points; We will show in Chapeter 4 that the moment integrals associated with this singular term are in fact known analytically in a closed-form for both rectangles and

triangles.

To find the Green's functions of electromagnetic boundary problems, one usually starts by seeking solutions that satisfy all the necessary boundary conditions in the spectral or the Fourier transform domain, which are often referred to as the Sommerfeld integrals. For an $\hat{x}$-directed dipole over a ground plane as shown in Fig. 2.1, the electric vector potential $\bar{\Pi} = \Pi_x \hat{x}$ of free space case was first expanded into a spectral-integral of cylindrical waves in Sommerfeld's derivation [4]. Then, the plane wave reflection concept is used to include the half-space dielectric medium by enforcing the field continuity conditions on the boundary between air and the dielectric medium. The electric field and magnetic field are finally expressed in terms of two components Π_x and Π_z of the eletric vector potential. Alternatively, one can also use a pair of scalar functions, or the Whittaker potentials U and V to represent the fields [7].

In Section 2.2, we will find the Green's functions, or the Whittaker potentials U and V for a horizontal electric current source over a grounded dielectric slab. Then, in Section 2.3, we will discuss how a representation can be casted into the form of a scalar magnetic potential and a scalar electric potential for the mixed-potential integral equation. Finally, we will develop the formulation of the mixed-potential integral equation for an arbitrary metallic strip on the dielectric slab in Section 2.4.

2.2 The Green's Functions of a Horizontally-Placed Current Density Distribution over a Grounded Dielectric Slab

For a horizontal current density distribution $\bar{J}(x', y')$ of arbitrary shape located at $z = z'$ as shown in Fig. 2.2, the horizontal field components at (x, y, z) can be written as [7]

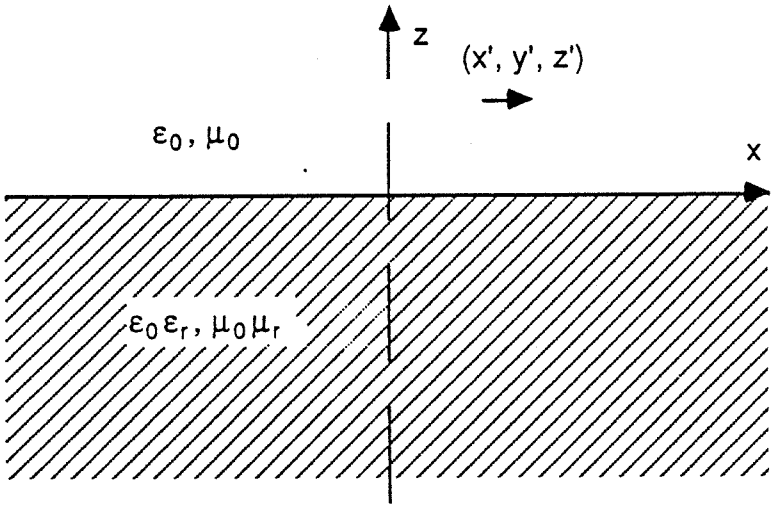

Figure 2.1: A horizontal dipole over a half-space dielectric medium.

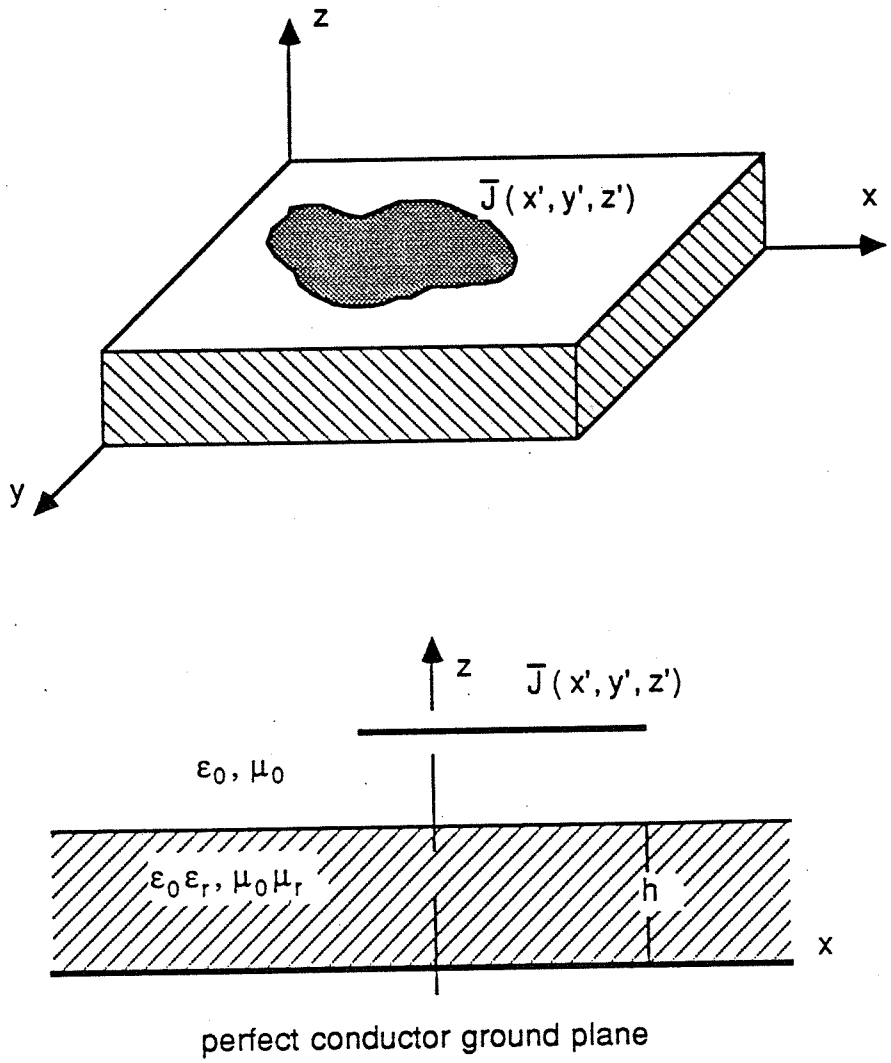

Figure 2.2. A horizontally-placed current density distribution over a grounded dielectric slab.

$$\bar{E}_t = \nabla_t \frac{\partial V}{\partial z} - j\omega\mu \ \nabla_t \times (\hat{z}U) \tag{2.1}$$

$$\bar{H}_t = \nabla_t \frac{\partial U}{\partial z} + j\omega\varepsilon \ \nabla_t \times (\hat{z}V) \tag{2.2}$$

where $\bar{E}_t$ and $\bar{H}_t$ are the horizontal electric and magnetic fields, respectively;

$$\varepsilon = \begin{cases} \varepsilon_0 & \text{in the air region;} \\ \varepsilon_0\varepsilon_r & \text{in the dielectric slab region.} \end{cases} \tag{2.3}$$

$$\mu = \begin{cases} \mu_0 & \text{in the air region;} \\ \mu_0\mu_r & \text{in the dielectric slab region.} \end{cases} \tag{2.4}$$

$$\nabla_t = \hat{x}\frac{\partial}{\partial x} + \hat{y}\frac{\partial}{\partial y} \tag{2.5}$$

The Whittaker potentials satisfy the wave equation in the two regions, or

$$(\nabla^2 + k^2) \begin{Bmatrix} U \\ V \end{Bmatrix} = 0 \, ; \, z \neq z' \tag{2.6}$$

where k is the wavenumber in both media

$$k = \begin{cases} k_0 \, ; & z > h \\ k_n \, ; & z < h \end{cases} \tag{2.7}$$

$$k_0^2 = \omega^2 \mu_0 \varepsilon_0 \tag{2.8}$$

$$k_n^2 = k_0^2 \mu_r \varepsilon_r \tag{2.9}$$

h is the substrate thickness (see Fig. 2.2);

$$\nabla = \nabla_t + \hat{z}\frac{\partial}{\partial z} \tag{2.10}$$

To solve the boundary problem, we have to express the field quantities U, V, $\bar{E}_t$ and $\bar{H}_t$ in terms of their double Fourier transforms with respect to x and y. We use uppercase calligraphic letters $\mathcal{U}$, $\mathcal{V}$, $\bar{\mathcal{E}}_t$ and $\bar{\mathcal{H}}_t$ to denote the corresponding Fourier transforms of the fields. The double Fourier transform and the inverse transform are defined as

$$\left\{ \begin{array}{c} \mathcal{U}(\alpha,\beta,z) \\ \mathcal{V}(\alpha,\beta,z) \end{array} \right\} = \left(\frac{1}{2\pi}\right)^2 \int_{-\infty}^{\infty} dx \int_{-\infty}^{\infty} dy \left\{ \begin{array}{c} U(x,y,z) \\ V(x,y,z) \end{array} \right\} \mathrm{e}^{j(\alpha x+\beta y)} \tag{2.11}$$

$$\left\{ \begin{array}{c} U(x,y,z) \\ V(x,y,z) \end{array} \right\} = \int_{-\infty}^{\infty} d\alpha \int_{-\infty}^{\infty} d\beta \left\{ \begin{array}{c} \mathcal{U}(\alpha,\beta,z) \\ \mathcal{V}(\alpha,\beta,z) \end{array} \right\} \mathrm{e}^{-j(\alpha x+\beta y)} \tag{2.12}$$

Then, we have

$$\bar{\mathcal{E}}_t = \tilde{\nabla}_t \frac{\partial \mathcal{V}}{\partial z} - j\omega\mu(\tilde{\nabla}_t \times \hat{z})\mathcal{U} \tag{2.13}$$

$$\bar{\mathcal{H}}_t = \tilde{\nabla}_t \frac{\partial \mathcal{U}}{\partial z} + j\omega\varepsilon(\tilde{\nabla}_t \times \hat{z})\mathcal{V} \tag{2.14}$$

where $\tilde{\nabla}_t$ is the corresponding operator of ∇_t in the Fourier transform domain, and it is

$$\tilde{\nabla}_t = -j(\alpha\hat{x} + \beta\hat{y}) \tag{2.15}$$

The continuity conditions on $z = z'$ plane are

$$\hat{z} \times \bar{E}_t|_{z=z'^-}^{z=z'^+} = 0 \tag{2.16}$$

$$\hat{z} \times \bar{H}_t|_{z=z'^-}^{z=z'^+} = \bar{J}(x', y') \tag{2.17}$$

In the Fourier transform domain, we have

$$\hat{z} \times \bar{\mathcal{E}}_t|_{z=z'^-}^{z=z'^+} = 0 \tag{2.18}$$

$$\hat{z} \times \bar{\mathcal{H}}_t|_{z=z'^-}^{z=z'^+} = \bar{\mathcal{J}}(\alpha, \beta) \tag{2.19}$$

or,

$$\bar{\mathcal{E}}_t|_{z=z'^-}^{z=z'^+} = 0 \tag{2.20}$$

$$\bar{\mathcal{H}}_t|_{z=z'^-}^{z=z'^+} = \bar{\mathcal{J}}(\alpha, \beta) \times \hat{z} \tag{2.21}$$

where $\bar{\mathcal{J}}(\alpha, \beta) = \hat{x}\mathcal{J}_x + \hat{y}\mathcal{J}_y$ is the Fourier transform of the current density distribution $\bar{J}(x, y) = \hat{x}J_x + \hat{y}J_y$.

Considering the continuity condition of the tangential electric field on $z = z'$, and the wave nature of the fields, we can intuitively assume

$$\mathcal{U} = \begin{cases} A_u(\alpha, \beta)\, \mathrm{e}^{-u_0|z-z'|} + B_u(\alpha, \beta)\, \mathrm{e}^{-u_0(z+z'-2h)} & ;\ z > h \\ C_u(\alpha, \beta)\, \sinh(u_n z)\, \mathrm{e}^{-u_0(z'-h)} & ;\ z < h \end{cases} \tag{2.22}$$

$$\mathcal{V} = \begin{cases} Sgn(z-z')\, A_v(\alpha, \beta)\, \mathrm{e}^{-u_0|z-z'|} + B_v(\alpha, \beta)\, \mathrm{e}^{-u_0(z+z'-2h)} & ;\ z > h \\ C_v(\alpha, \beta)\, \cosh(u_n z)\, \mathrm{e}^{-u_0(z'-h)} & ;\ z < h \end{cases} \tag{2.23}$$

where $A_{u,v}$, $B_{u,v}$ and $C_{u,v}$ are the coefficients to be solved;

$$Sgn(z-z') = \begin{cases} +1 & ; z > z' \\ -1 & ; z < z' \end{cases} \tag{2.24}$$

$$u_0 = \sqrt{\alpha^2 + \beta^2 - k_0^2}\ ,\ \mathrm{Re}(u_0) > 0 \tag{2.25}$$

$$u_n = \sqrt{\alpha^2 + \beta^2 - k_n^2} \tag{2.26}$$

The tangential electric and magnetic fields must be continuous across the dielectric surface $z = h$. Then, we obtain from (2.13) and (2.14),

$$\tilde{\nabla}_t \frac{\partial \mathcal{V}}{\partial z} - j\omega\mu_0(\tilde{\nabla}_t \times \hat{z})\mathcal{U}\,|_{z=z'-}^{z=z'+} = 0 \tag{2.27}$$

$$\tilde{\nabla}_t \frac{\partial \mathcal{U}}{\partial z} + j\omega\varepsilon_0(\tilde{\nabla}_t \times \hat{z})\mathcal{V}\,|_{z=z'-}^{z=z'+} = \bar{\mathcal{J}}(\alpha,\beta) \times \hat{z} \tag{2.28}$$

Condition (2.27) is automatically satisfied from the assumption of the $\mathcal{U}$ and $\mathcal{V}$ in (2.22) and (2.23). From (2.22), (2.23) and (2.28), we write

$$-2u_0\tilde{\nabla}_t A_u(\alpha,\beta) + j2\omega\varepsilon_0(\tilde{\nabla}_t \times \hat{z})A_v(\alpha,\beta) = \bar{\mathcal{J}}(\alpha,\beta) \times \hat{z} \tag{2.29}$$

Taking dot product of $\tilde{\nabla}_t$ with (2.29) yields

$$A_u(\alpha,\beta) = \frac{\tilde{\nabla}_t \cdot (\bar{\mathcal{J}}(\alpha,\beta) \times \hat{z})}{-2u_0\,\tilde{\nabla}_t \cdot \tilde{\nabla}_t} \tag{2.30}$$

Taking dot product of $(\tilde{\nabla}_t \times \hat{z})$ with (2.29) yields

$$A_v(\alpha,\beta) = \frac{(\tilde{\nabla}_t \times \hat{z}) \cdot \left[\bar{\mathcal{J}}(\alpha,\beta) \times \hat{z}\right]}{j2\omega\varepsilon_0(\tilde{\nabla}_t \times \hat{z}) \cdot (\tilde{\nabla}_t \times \hat{z})} \tag{2.31}$$

The following two vector formulas are utilized to simplify (2.31).

$$\bar{a} \times (\bar{b} \times \bar{c}) = (\bar{a} \cdot \bar{c})\bar{b} - (\bar{a} \cdot \bar{b})\bar{c} \tag{2.32}$$

$$\bar{a} \cdot (\bar{b} \times \bar{c}) = (\bar{a} \times \bar{b}) \cdot \bar{c} \tag{2.33}$$

Finally, we obtain

$$A_v(\alpha, \beta) = \frac{\tilde{\nabla}_t \cdot \bar{\mathcal{J}}(\alpha, \beta)}{j2\omega\varepsilon_0 \tilde{\nabla}_t \cdot \tilde{\nabla}_t} \tag{2.34}$$

The B_u, C_u, B_v and C_v in (2.22) and (2.23) have to be found by invoking the tangential electric and magnetic field continuity conditions across the dielectric surface $z = h$. From (2.13) and (2.14), the continuity conditions for $\hat{\mathcal{E}}_t$ and $\hat{\mathcal{H}}_t$ result in that $\mu\mathcal{U}$, $\varepsilon\mathcal{V}$, $\mathcal{U}'_z$ and $\mathcal{V}'_z$ are also continuous at $z = h$. We obtain

$$A_u + B_u = \mu_r C_u \sinh(u_n h) \tag{2.35}$$

$$-A_v + B_v = \varepsilon_r C_v \cosh(u_n h) \tag{2.36}$$

$$u_0(A_u - B_u) = u_n C_u \cosh(u_n h) \tag{2.37}$$

$$u_0(-A_v - B_v) = u_n C_v \sinh(u_n h) \tag{2.38}$$

B_u, C_u, B_v and C_v are easily solved from (2.35) - (2.38).

$$B_u = \Gamma_u A_u \tag{2.39}$$

$$C_u = \frac{1+\Gamma_u}{\mu_r \sinh(u_n h)} A_u \tag{2.40}$$

$$B_v = \Gamma_v A_v \tag{2.41}$$

$$C_v = \frac{-1+\Gamma_v}{\varepsilon_r \cosh(u_n h)} A_v \tag{2.42}$$

where

$$\Gamma_u = \frac{\mu_r u_0 \sinh(u_n h) - u_n \cosh(u_n h)}{\mu_r u_0 \sinh(u_n h) + u_n \cosh(u_n h)} \tag{2.43}$$

$$\Gamma_v = \frac{u_n \sinh(u_n h) - \varepsilon_r u_0 \cosh(u_n h)}{u_n \sinh(u_n h) + \varepsilon_r u_0 \cosh(u_n h)} \tag{2.44}$$

We will establish the integral equation by enforcing the boundary condition on the tangential electric field in the source region. Only the horizontal electric field in the air region will be involved and it will be discussed next.

From (2.22), (2.23), (2.39) and (2.41), we write

$$\mathcal{U} = A_u F_u(\alpha, \beta, z) \tag{2.45}$$

$$\mathcal{V} = A_v \left[Sgn(z - z') \, \mathrm{e}^{-u_0 |z-z'|} + \Gamma_v \, \mathrm{e}^{-u_0 (z+z'-2h)} \right] \tag{2.46}$$

and

$$\frac{\partial \mathcal{V}}{\partial z} = -u_0 A_v F_v(\alpha, \beta, z) \tag{2.47}$$

where

$$F_{u,v}(\alpha,\beta,z) = \mathbf{e}^{-u_0|z-z'|} + \Gamma_{u,v}\,\mathbf{e}^{-u_0(z+z'-2h)} \tag{2.48}$$

Substituting (2.45) and (2.47) into (2.13) gives the horizontal electric field in the air region.

$$\bar{\mathcal{E}}_t = \tilde{\nabla}_t\,[-u_0\,A_v\,F_v(\alpha,\beta,z)] - j\omega\mu_0(\tilde{\nabla}_t \times \hat{z})\;[A_u\,F_u(\alpha,\beta,z)] \tag{2.49}$$

where the A_u and A_v are given in (2.30) and (2.31), respectively.

The spatial-domain horizontal electric field can be obtained from the double inverse Fourier transform of $\bar{\mathcal{E}}_t$.

2.3 The Scalar Magnetic and Electric Potentials for the Microstrip Structure

We have solved the horizontal electric field of a horizontally-placed electric current distribution (see (2.49)) in Section 2.2. We can re-organize (2.49) into a mixed-potential form. It is noticed that the vector operation in the second term of the right-hand side of (2.49) can be simplified as follow:

$$\begin{aligned}&(\tilde{\nabla}_t \times \hat{z})\left[\bar{\mathcal{J}}(\alpha,\beta)\cdot(\tilde{\nabla}_t \times \hat{z})\right]\\ &= (\tilde{\nabla}_t \times \hat{z}) \times [(\tilde{\nabla}_t \times \hat{z}) \times \bar{\mathcal{J}}(\alpha,\beta)] + [(\tilde{\nabla}_t \times \hat{z})\cdot(\tilde{\nabla}_t \times \hat{z})]\bar{\mathcal{J}}(\alpha,\beta)\end{aligned} \tag{2.50}$$

The first term on the left-hand side of (2.50) is

$$(\tilde{\nabla}_t \times \hat{z}) \times [(\tilde{\nabla}_t \times \hat{z}) \times \bar{\mathcal{J}}] \;=\; (\tilde{\nabla}_t \times \hat{z}) \times [(\tilde{\nabla}_t \cdot \bar{\mathcal{J}})\hat{z} - (\hat{z}\cdot\bar{\mathcal{J}})\tilde{\nabla}_t]$$

$$
\begin{aligned}
&= (\tilde{\nabla}_t \cdot \bar{\mathcal{J}})(\tilde{\nabla}_t \times \hat{z}) \times \hat{z} \\
&= -(\tilde{\nabla}_t \cdot \bar{\mathcal{J}})\, \tilde{\nabla}_t
\end{aligned}
\tag{2.51}
$$

The second term on the left-hand side of (2.50) is

$$
[(\tilde{\nabla}_t \times \hat{z}) \cdot (\tilde{\nabla}_t \times \hat{z})]\bar{\mathcal{J}} = (\tilde{\nabla}_t \cdot \tilde{\nabla}_t)\bar{\mathcal{J}} \tag{2.52}
$$

Substituting (2.51) into (2.50) and, then, (2.30), (2.34), (2.50) and (2.52) into (2.49) yield

$$
\bar{\mathcal{E}}_t = -j\omega \frac{\mu_0 F_u}{2u_0} \bar{\mathcal{J}}(\alpha,\beta) - \tilde{\nabla}_t [\frac{u_0^2 F_v + k_0^2 F_u}{j2\omega\varepsilon_0 u_0 \tilde{\nabla}_t \cdot \tilde{\nabla}_t}\ \tilde{\nabla}_t \cdot \bar{\mathcal{J}}(\alpha,\beta)] \tag{2.53}
$$

Therefore, the horizontal electric field from a current density distribution on a horizontal patch s at $z = z'$ is obtained by taking the inverse Fourier transform of (2.53).

$$
\bar{E}_t = -j\,\omega\,\bar{A}_t\ -\ \nabla_t \phi \tag{2.54}
$$

where

$$
\phi = \frac{1}{4\pi\varepsilon_0} \int_s ds' [-\frac{1}{j\omega}\ \nabla'_t \cdot \bar{J}(x',y')]\, G_e(\rho; z, z') \tag{2.55}
$$

$$
\nabla'_t = \hat{x}\frac{\partial}{\partial x'} + \hat{y}\frac{\partial}{\partial y'} \tag{2.56}
$$

and $G_{m,e}$ are the magnetic and electric potentials, respectively; $ds' = dx'\,dy'$.

$$
G_m(\rho; z, z') = \frac{1}{2\pi} \int_{-\infty}^{\infty} d\alpha \int_{-\infty}^{\infty} d\beta\, \frac{F_u}{u_0}\, \mathrm{e}^{-j[\alpha(x-x')+\beta(y-y')]} \tag{2.57}
$$

$$G_e(\rho; z, z') = \frac{1}{2\pi} \int_{-\infty}^{\infty} d\alpha \int_{-\infty}^{\infty} d\beta \, \frac{u_0^2 F_v + k_0^2 F_u}{u_0 (\alpha^2 + \beta^2)} \, \mathrm{e}^{-j[\alpha(x-x')+\beta(y-y')]} \tag{2.58}$$

$$\rho = \sqrt{(x-x')^2 + (y-y')^2} \tag{2.59}$$

The horizontal part of the dyadic Green's function corresponding to that in (1.1) is easily obtained as

$$\bar{\bar{G}}_t = G_m(\hat{x}\hat{x} + \hat{y}\hat{y}) + \nabla_t \nabla_t \cdot [G_e(\hat{x}\hat{x} + \hat{y}\hat{y})] \tag{2.60}$$

The double Fourier transforms in (2.57) and (2.58) can be further reduced to single Fourier-Bessel type integrals with the following change of variables:

$$\lambda = \sqrt{\alpha^2 + \beta^2} \tag{2.61}$$

$$\theta_\lambda = \arctan(\frac{\beta}{\alpha}) \tag{2.62}$$

The integration with respect to θ_λ can be expressed in terms of the zero-th order Bessel function $J_0(\lambda\rho)$. We finally have

$$G_m(\rho; z, z') = \int_0^{\infty} d\lambda \, J_0(\lambda\rho) \, \frac{\lambda F_u}{u_0} \tag{2.63}$$

$$G_e(\rho; z, z') = \int_0^{\infty} d\lambda \, J_0(\lambda\rho) \, \frac{u_0^2 F_v + k_0^2 F_u}{u_0 \lambda} \tag{2.64}$$

where,

$$u_0 = \sqrt{\lambda^2 - k_0^2}\,;\; Re(u_0) \leq 0\,;\; Im(u_0) \leq 0\,. \tag{2.65}$$

$$u_n = \sqrt{\lambda^2 - k_n^2}\,;\; Re(u_n) \leq 0\,;\; Im(u_n) \leq 0\,. \tag{2.66}$$

For the case $\varepsilon_r = 1$ and $\mu_r = 1$, or there is no dielectric slab, the $G_{m,e}(\rho; z, z')$ can be solved analytically in a closed form

$$G_{m,e}(\rho; z, z') = \frac{\mathrm{e}^{-jk_0 R}}{R} - \frac{\mathrm{e}^{-jk_0 R'}}{R'} \tag{2.67}$$

where

$$R = \sqrt{\rho^2 + (z - z')^2} \tag{2.68}$$

$$R' = \sqrt{\rho^2 + (z + z')^2} \tag{2.69}$$

For most of the microstrip structures, thin metallic strips are etched on the dielectric slab. The integral equation is established based upon the tangential field on the strips. Therefore, we can just consider the case with $z = z' = h$. The $G_{m,e}(\rho; z, z')$ are functions of ρ only, or

$$G_m(\rho) = \int_0^\infty d\lambda\, J_0(\lambda\rho)\, \frac{2\mu_r\, \lambda}{D_{tm}} \tag{2.70}$$

$$G_e(\rho) = \int_0^\infty d\lambda\, J_0(\lambda\rho)\, \frac{2\lambda[u_0 + \mu_r u_n \tanh(u_n h)]}{D_{te}\, D_{tm}} \tag{2.71}$$

where

$$D_{tm} = \mu_r\, u_0 + u_n\, \coth(u_n\, h) \tag{2.72}$$

$$D_{te} = \varepsilon_r \, u_0 + u_n \, \tanh(u_n \, h) \tag{2.73}$$

2.4 Mixed-Potential Integral Equation

When we assume that the metallic strip in a microstrip structure s (see Fig. 1.4) is a perfect conductor, we can establish the integral equation straight-forwardly. An impressed electric field $\bar{E}^i$ induces a scattered current density distribution $\bar{J}(x,y)$ on the metallic strip, and the $\bar{J}(x,y)$ creates scattered field $\bar{E}$. The integral equation is established by enforcing the boundary condition that the total tangential electric field vanishes on the microstrip, or

$$\bar{E}_t(x,y) + \bar{E}_t^i(x,y) = 0 \, ; \, (x,y) \in s \tag{2.74}$$

where $\bar{E}_t(x,y)$ is expressed in (2.54) and $\bar{E}_t^i(x,y)$ is the tangential impressed electric field [1].

In fact, metallic strips can no longer be approximated as perfect conductors at high frequency range of microwave or at millimeter-wave range. As we will demonstrate in Chapter 6, metallic loss is significant beyond 10GHz for MMIC circuits. From the plane wave incident analysis, we can take the conductor loss into consideration by imposing an equivalent surface impedance on the metallic strips. This surface impedance has a non-trivial dependence on the conductivity, the shape of the cross section and the edge of a metallic strip, as well as the operation frequency for a finite dimensional microstrip line [10]-[12].

When the approximate impedance boundary condition is introduced, (2.74) becomes

$$\bar{E}_t(x,y) + \bar{E}_t^i(x,y) = Z_s(x,y)\,\bar{J}(x,y)\,;\,(x,y) \in s \tag{2.75}$$

Z_s is the surface impedance of the metallic strip. It is a function of position and frequency, etc. A simplified formula is obtained in [13] by neglecting the shape dependence of the Z_s and assuming negligible skin depth compared to strip thickness.

$$Z_s = \sqrt{\frac{\mu_0}{\epsilon_0 - j\sigma/\omega}} \tag{2.76}$$

where σ is the conductivity.

Strictly speaking, (2.75) should be applied to the whole surface, including the top and bottom and the edge surface of the microstrip structure under investigation [14]. But, it will increase the computational effort substantially without increasing accuracy much. The formula is applied to microstrip problems in [15] by just taking the s as either the top surface or the bottom surface.

A more general and accurate formula is derived for position not very close to the edge of a strip [16].

$$Z_s = \sqrt{\frac{\mu_0}{\epsilon_0 - j\sigma/\omega}}\,\frac{1 + e^{-jk_s t}}{2} \tag{2.77}$$

where k_s is the wave number of the strip material; t is the strip thickness. Obviously, (2.77) can be reduced to (2.76) only when $k_s t << 1$, or the strip thickness is much less than the skin depth.

A more rigorous formula is being derived for implementation in MPIE formulation [17]. The detail is beyond the topic of this thesis.

In fact, the imperfection in the ground plane can also be modeled using the impedance boundary condition in (2.76).

The References for Chapter 2

[1] R. F. Harrington, **Field Computations by Moment Methods**. New York: Macmillan, 1968.

[2] A. W. Glisson and D. R. Wilton, " Simple and efficient numerical methods for problems of electromagnetic radiation and scattering from surfaces, " **IEEE Trans. on Antennas Propag.**, Vol. AP-28, pp. 593-603, Sep. 1980.

[3] S. M. Rao, D. R. Wilton and A. W. Glisson, " Electromagnetic scattering by surfaces of arbitrary shape, " **IEEE Trans. on Antennas Propag.** , Vol. AP-30, pp. 409-418, 1982.

[4] A. J. W. Sommerfeld, **Lectures on Theoretical Physics**. New York, Academic Press, Vol. 6 **Partial differential equations in physics**, 1956.

[5] J. R. Wait, **Electromagnetic Waves in Stratified Media**. Oxford, New York, Pergemon Press, 1970.

[6] V. A. Strattron, **Electromagnetic Theory**. New York, McGraw - Hill Book Co., 1941.

[7] E. F. Kuester and D. C. Chang, **Electromagnetic Boundary Problems**. Course Notes for ECEN 5144, Chapter 1, University of Colorado at Boulder, 1988.

[8] J. A. Kong, **Theory of Electromagnetic Waves**. New York: Wiley, 1975.

[9] B. L. Brim and D. C. Chang, " Accelerated numerical computation of the spatial domain dyadic Green's functions of a grounded dielectric slab," **National Science Meeting Digest**, pp. 164, Boulder,CO, Jan. 1987.

[10] L. Lewin, " A method of avoiding the edge current divergence in perturbation loss calculation, " **IEEE Trans. on Microwave Theory and Tech.**, Vol. MTT-32, pp. 717-719, 1984.

[11] L. A. Vainshtein and S. M. Zhurav, " Strong skin effect at the edges of metal plates," [Russian], **Pis'ma Zh. Tekh. Fiz.** , Vol. 12, pp.723-729,

1986. [Engl. transl. in **Sov. Tech. Phys. Lett.**, Vol. 12, pp. 298-299, 1986]

[12] E. L. Barsotti, **Effect of strip edge shape on microstrip conductor loss.** Master Degree Thesis, Unversity of Colorado at Boulder, 1990.

[13] T. B. A. Senior, " Impedance boundary conditions for imperfectly conducting surfaces, " **Applied Scientific Research,** Section B, Vol. 17, pp. 418-436, 1960.

[14] S. T. Peng, C-K. C. Tzuang and C. D. Chen, " Full-wave analysis of lossy transmission line incorporating the metal modes," **IEEE Intern. Microwave Symposium Digest,** Vol. 1, pp. 171-174, Dallas, TX, May 1990.

[15] J. R. Mosig, "Arbitrarily shaped microstrip structures and their analysis with a mixed potential integral equation," **IEEE Trans. on Microwave Theory Tech.**, MTT-36, pp. 314-323, February 1988.

[16] D. C. Chang, private communication.

[17] E. F. Kuester, private communication.

CHAPTER 3

ROOF-TOP FUNCTIONS ON A RECTANGULAR AND TRIANGULAR MIXED GRID

3.1 Introduction

In Chapter 2, we have established the mixed-potential integral equation in (2.75). As mentioned in Section 1.3, a set of complete basis functions is used to expand the current density distribution.

$$\bar{J}(x,y) = \sum_{m=1}^{\infty} I_m \bar{B}_m(x,y) \tag{3.1}$$

where I_m are the unknown coefficients.

To solve the unknown coefficients I_m from (2.75), we have to take the inner product of a set of complete test functions $\bar{T}_m(x,y), m = 1,2,...$ with (2.75). The procedure creates an infinite-dimensional problem and can not be solved exactly. Finite truncation of the basis functions and test functions yields a matrix equation

$$\sum_{m'=1}^{M} Z_{m,m'} I_{m'} = V_m \; ; \; m = 1,2,...,M \tag{3.2}$$

where $Z_{m,m'}$ is obtained from (2.54), (2.75) and (3.1).

$$Z_{m,m'} = \int_s ds \, \bar{T}_m(x,y) \cdot [j\omega \bar{A}_{t,m'} + \nabla_t \phi_{m'} + Z_s \bar{B}_{m'}(x,y)] \tag{3.3}$$

$$V_m = \int_s ds\, \bar{T}_m(x,y) \cdot \bar{E}_t^i(x,y) \tag{3.4}$$

$$ds = dx\, dy \tag{3.5}$$

$$\bar{A}_{t,m'} = \frac{\mu_0}{4\pi} \int_s ds'\, \bar{B}_{m'}(x',y')\, G_m(\rho; z, z') \tag{3.6}$$

$$\phi_{m'} = \frac{1}{4\pi\varepsilon_0} \int_s ds' \left[-\frac{1}{j\omega}\ \nabla_t' \cdot \bar{B}_{m'}(x',y')\right] G_e(\rho; z, z') \tag{3.7}$$

The first term in (3.3) is

$$\frac{j\omega\mu_0}{4\pi} \int_s ds \int_s ds'\, \bar{T}_m(x,y) \cdot \bar{B}_{m'}(x',y')\, G_m(\rho) \tag{3.8}$$

The second term is expanded as

$$\begin{aligned}
&\int_s ds\, \bar{T}_m(x,y) \cdot \nabla_t \phi_{m'} \\
&= \int_s ds \left\{ \nabla_t \cdot [\bar{T}_m(x,y)\, \phi_{m'}] - \nabla_t \cdot \bar{T}_m(x,y)\, \phi_{m'} \right\} \\
&= \oint_c dl\, \hat{n} \cdot \bar{T}_m(x,y)\, \phi_{m'} - \int_s ds\ \nabla_t \cdot \bar{T}_m(x,y)\, \phi_{m'} \\
&= \frac{1}{j4\pi\omega\varepsilon_0} \int_s ds \int_s ds'\ \nabla_t \cdot \bar{T}_m(x,y)\ \nabla_t' \cdot \bar{B}_{m'}(x',y')\, G_e(\rho)
\end{aligned} \tag{3.9}$$

where c is the edge of the microstrip structure s and $\hat{n}$ is the outer-going normal component of the edge on the plane of the strip. The condition that the normal component of the test functions or $\bar{T}_m(x,y)$ is continuous across cell boundaries and vanishes on the boundary of the structure has been used in deriving the last step of (3.9).

The matrix elements in (3.3) can be simplified as

$$Z_{m,m'} = \frac{j\omega\mu_0}{4\pi}\int_s ds \int_s ds' \,[\bar{T}_m(x,y)\cdot\bar{B}_{m'}(x',y')\,G_m(\rho) - \frac{1}{k_0^2}\,\nabla_t\cdot\bar{T}_m(x,y)\;\nabla_t'\cdot\bar{B}_{m'}(x,y)\,G_e(\rho)] + Z_s\int_s ds\,\bar{T}_m(x,y)\cdot\bar{B}_{m'}(x,y) \tag{3.10}$$

Now, the matrix equation is established. The remaining problem is to choose the basis functions $\bar{B}_m(x,y)$ and test functions $\bar{T}_m(x,y)$, and to evaluate the quadruple moment integrals in (3.10).

For a microstrip structure of arbitrary shape, full-domain functions obviously are difficult to apply. Consequently, the issue reduces to what type of sub-domain basis functions are most effective in representing the current density distribution on a microstrip structure.

A wire-mesh model was developed in [1] for solving scattering problems, in which the solid conducting surface is physically replaced by mesh of thin wires conforming to the contour of the original surface. Such a model however is not suitable for antenna and circuit problems, in which accurate current distributions and therefore input impedances are desired [2].

Rectangular cells used in conjunction with the MPIE formulation have been adopted previously to model current density distribution on microstrip patch antennas and microstrip circuit discontinuities [3] - [6]. For instance, in [3], the microstrip structure is divided into two sets of rectangular cells and pulse basis-functions are used to approximate the charge and current distribution separately. A special form of linear " roof-top" basis functions is used to approximate the current distribution in [4]-[7], again for a set of rectangular cells. These basis functions obviously are most appropriate when the structure under investigation can be in fact naturally divided into rectangular cells, but would not be efficient when cells of reasonable size can not be fitted into the

boundaries of a structure.

An implicit requirement in choosing basis and test functions is that the normal current density component is continuous on cell boundaries to avoid a possible δ-function in the integrand of (3.10) from $\nabla_t \cdot \bar{T}_m(x,y)$ or $\nabla'_t \cdot \bar{B}_n(x',y')$. An interesting exception to this is the so-called constant current/ constant charge method in which the $\bar{T}_m$ and $\nabla_t \cdot \bar{T}_m$ are treated as independent quantities first. They are then related back to each other by shifting the x-component and y-component current cells by half with respect to the charge cells in the x-direction and the y-directions, respectively [3].

In addition to rectangular cells, triangular cells with roof-top basis function expansion has been tried in [11]. The current distribution in this case is expressed in terms of the nodal currents at its vertices. Boundary conditions at the edges of a microstrip structure are difficult to enforce in this case, particularly when non-rectangular corners are encountered. Furthermore, it has been demonstrated in [11] that for a given structure, the rate of convergence for such a scheme may depend upon the particular orientation of the cells selected.

As stated in [13], what distinguishes the new algorithm we developed here from other similar use of roof-top basis functions to approximate the current density distribution on a microstrip structure is that we are able to use a combination of rectangular and triangular cells in a self-consistent manner in order to take into account the regularity in shape over major portion of a microstrip structure, while still preserving the flexibility to model junctions of arbitrary shape locally (see Fig 3.1). This self-consistency is derived from the observation that in order to avoid the unphysical occurance of a δ-function charge density in the numerical process, only the normal component of the

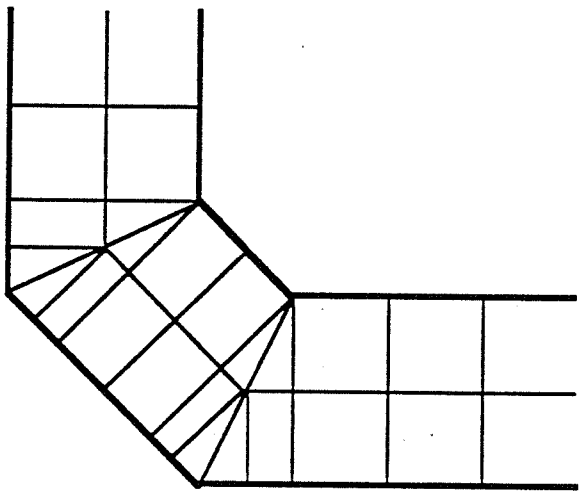

Figure 3.1: A rectangular and triangular mixed-grid.

current density, but **not** the entire current density, is required to be continuous across a cell boundary. Thus, instead of expressing the current density distribution in terms of **vector** nodal currents at the three vertices of a triangular cell [11], we can implement a modified version in which the current density distribution is expressed in terms of the normal components on the three sides. In order to solve for the current uniquely, we further impose an additional requirement that these normal components have to remain constant across their respective boundaries. In the case of a rectangular cell, two of the four additional conditions can be shown to be redundant and thus the number of equations is again reduced to six for the six unknown coefficients.

The roof-top functions on rectangular cells and triangular cells will be introduced in Sections 3.2 and 3.3, respectively. Section 3.4 will discuss the **Pseudo-mesh** concept. The expansion of the vector current on a microstrip structure in terms of the pseudo-mesh currents will be provided in Section 3.5. The matrix equation will be re-stated in Section 3.6 with matrix elements expressed in terms of the roof-top functions.

3.2 Roof-Top Functions on Rectangular Cells

Denote the side formed by nodes i and j by side (i,j) (see Fig. 3.2). We can express the current density distribution $\bar{J}_\alpha(x,y)$ in rectangle α in terms of the normal components $I_\alpha^{i,j}$ on the sides, where the subscript α and the superscripts i,j mean the side (i,j) of cell α.

$$\bar{J}_\alpha(x,y) = \sum_{i=1}^{4} I_\alpha^{i,i+1} \bar{D}_\alpha^{i,i+1}(x,y) \; ; \; (x,y) \in \text{rectangle } \alpha \qquad (3.11)$$

where $\bar{D}_{\alpha}^{i,i+1}$ is the expression for the corresponding roof-top function to the side $(i, i+1)$ of cell α (see Fig. 3.2). The direction of $\bar{D}_{\alpha}^{i,i+1}$ is always defined to be incoming. Since a rectangular cell has four vertices or nodes, we can consider i as a cyclic number so that $i = i - 4$ or $i > 4$ and $i = i + 4$ for $i < 1$.

$\bar{D}_{\alpha}^{i,i+1}$ should be parallel to side $(i+1, i+2)$ and side $(i-1, i)$ as shown in Fig. 3.2. Therefore, we can write

$$\bar{D}_{\alpha}^{i,i+1}(x,y) = \frac{(x_{i-1} - x_i)\hat{x} + (y_{i-1} - y_i)\hat{y}}{d_{i-1,i}} (a + b\,x + c\,y) \tag{3.12}$$

where the a, b and c are yet unknown constants and the $d_{i-1,i}$ is the distance between nodes $(i-1)$ and i, or

$$d_{i-1,i} = \sqrt{(x_{i-1} - x_i)^2 + (y_{i-1} - y_i)^2} \tag{3.13}$$

Expression for a, b and c are determined by the requirement that the $\bar{D}_{\alpha}^{i,i+1}$ has a magnitude of 1 on side $(i, i+1)$ and vanishes on the opposite side, i.e. side $(i+2, i+3)$:

$$\begin{cases} a + b\,x_{i-1} + c\,y_{i-1} = 0 \\ a + b\,x_i + c\,y_i = 1 \\ a + b\,x_{i+1} + c\,y_{i+1} = 1 \end{cases} \tag{3.14}$$

Equation (3.14) can easily be solved using Cramer's rule.

$$\begin{bmatrix} a \\ b \\ c \end{bmatrix} = \frac{1}{\triangle_{i-1,i,i+1}} \begin{bmatrix} (x_{i+1} - x_i)y_{i-1} - (y_{i+1} - y_i)x_{i-1} \\ y_{i+1} - y_i \\ x_i - x_{i+1} \end{bmatrix} \tag{3.15}$$

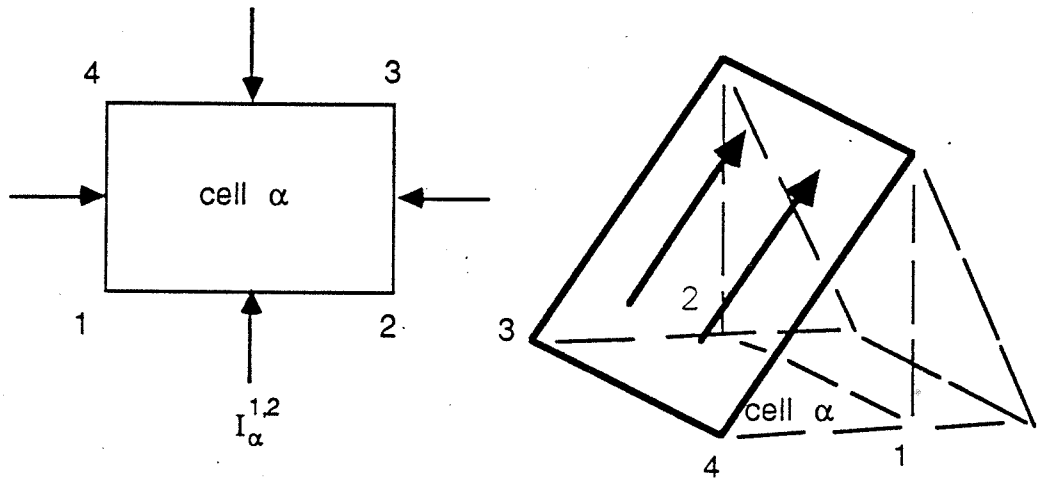

Figure 3.2: The roof-top function on a rectangular cell.

where

$$\triangle_{i-1,i,i+1} = \begin{vmatrix} 1 & x_{i-1} & y_{i-1} \\ 1 & x_i & y_i \\ 1 & x_{i+1} & y_{i+1} \end{vmatrix} \tag{3.16}$$

Substituting (3.15) into (3.12) yields

$$\bar{D}_\alpha^{i,i+1}(x,y) = \frac{[(y_{i+1}-y_i)(x-x_{i-1}) - (x_{i+1}-x_i)(y-y_{i-1})]}{\triangle_{i-1,i,i+1}} \cdot \frac{(x_{i-1}-x_i)\hat{x} + (y_{i-1}-y_i)\hat{y}}{d_{i-1,i}} \; ; \; (x,y) \in \text{rectangle } \alpha \tag{3.17}$$

The divergence of the cell current density distribution can be written as

$$\bigtriangledown \cdot \bar{J}_\alpha(x,y) = \sum_{i=1}^{4} I_\alpha^{i,i+1} Q_\alpha^i \; ; \; (x,y) \in \text{rectangle } \alpha \tag{3.18}$$

where

$$Q_\alpha^i = -\frac{1}{d_{i-1,i}} \tag{3.19}$$

3.3 Roof-Top Functions on Triangular Cells

As in the case of a rectangular cell, the current density and its divergence on a triangular cell α can also be expressed as

$$\bar{J}_\alpha(x,y) = \sum_{i=1}^{3} I_\alpha^{i,i+1} \bar{D}_\alpha^{i,i+1}(x,y) \; ; \; (x,y) \in \text{triangle } \alpha \tag{3.20}$$

$$\bigtriangledown \cdot \bar{J}_\alpha(x,y) = \sum_{i=1}^{3} I_\alpha^{i,i+1} Q_\alpha^i \; ; \; (x,y) \in \text{triangle } \alpha \tag{3.21}$$

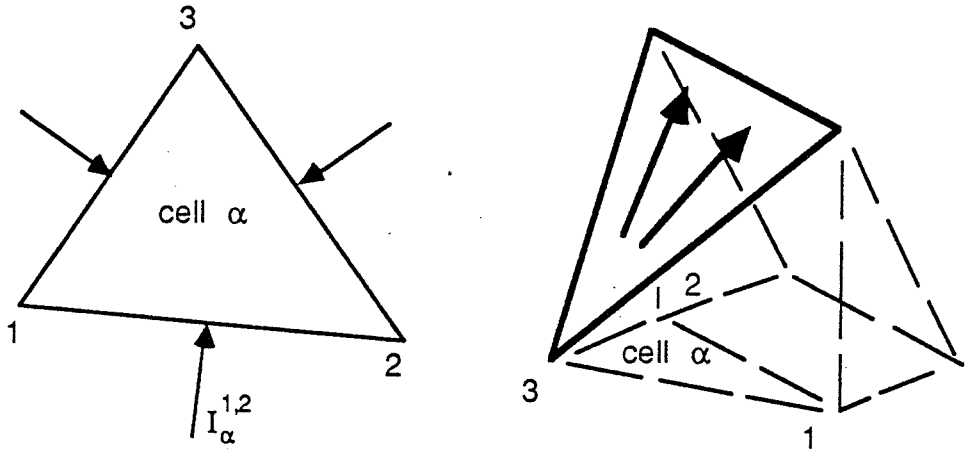

Figure 3.3: The roof-top function on a triangular cell.

and, similarly, $i = i - 3$ for $i > 3$, or $i = i + 3$ for $i < 1$.

The difference is that the $\bar{D}_{\alpha}^{i,i+1}$ for a triangle changes direction at different location of the cell. For the triangle α shown in Fig. 3.3, the roof-top function for side $(i, i+1)$ is a vector parallel to side $(i-1, i)$ at node i, parallel to side $(i-1, i+1)$ at node $(i+1)$ and vanished at node $(i-1)$. The incoming normal component is defined as 1 on side $(i, i+1)$. Obviously, the total current density over the normal current density at node i is $d_{i-1,i}/h_{i,i+1}$, where $h_{i,i+1}$ is the height of the triangle on side $(i, i+1)$ (see Fig. 3.3). The $d_{i-1,i}$ is the distance between nodes $(i-1)$ and i. Then, we can write

$$\begin{aligned} \bar{D}_{\alpha}^{i,i+1}(x_i, y_i) &= \frac{d_{i-1,i}}{h_{i,i+1}} \frac{(x_{i-1} - x_i)\hat{x} + (y_{i-1} - y_i)\hat{y}}{d_{i-1,i}} \\ &= \frac{(x_{i-1} - x_i)\hat{x} + (y_{i-1} - y_i)\hat{y}}{h_{i,i+1}} \end{aligned} \tag{3.22}$$

Similarly,

$$\bar{D}_{\alpha}^{i,i+1}(x_{i+1}, y_{i+1}) = \frac{(x_{i-1} - x_{i+1})\hat{x} + (y_{i-1} - y_{i+1})\hat{y}}{h_{i,i+1}} \tag{3.23}$$

From (3.22), we can assume

$$\begin{aligned} \bar{D}_{\alpha}^{i,i+1}(x, y) = \tfrac{1}{h_{i,i+1}} \quad & \{[(x_{i-1} - x_i) + s\,(x - x_i) + t\,(y - y_i)]\hat{x} + \\ & [(y_{i-1} - y_i) + u\,(x - x_i) + v\,(y - y_i)]\hat{y}\} \end{aligned} \tag{3.24}$$

where s, t, u and v are some constants to be determined.

Setting $(x, y) = (x_{i-1}, y_{i-1})$ and (x_{i+1}, y_{i+1}) in (3.24) and equating its values at the two points to zero and (3.23) respectively, we obtain

$$\begin{cases} s = -1 \\ t = 0 \\ u = 0 \\ v = -1 \end{cases} \tag{3.25}$$

and therefore,

$$\bar{D}_{\alpha}^{i,i+1}(x,y) = -\frac{d_{i,i+1}}{|\triangle_{i-1,i,i+1}|}[(x - x_{i-1})\hat{x} + (y - y_{i-1})\hat{y}] \tag{3.26}$$

$$Q_{\alpha}^{i} = -\frac{2d_{i,i+1}}{|\triangle_{i-1,i,i+1}|} \tag{3.27}$$

where $h_{i,i+1} = d_{i,i+1}/|\triangle_{i-1,i,i+1}|$ is made use of in deriving (3.26).

3.4 Pseudo-Mesh Current Distribution Representation

Since, for both rectangular and triangular cells, we can express the current density in a cell by the normal current density across its boundary and since each of these normal current densities is assumed to be constant along the boundary, we can now characterize the current in the cell by the **total current flow** into and out of each of the sides of the cell. Topologically, this is the same as replacing the microstrip structure by equivalent meshes, and the current distribution on the surface area of a cell by the current flow along corresponding meshes as shown in Fig. 3.4.

Unlike a real mesh structure, however, the net amount total current flows into and out of a "junction" does not follow the conventional Kirchhoff's law. In fact, the difference between the incoming current and the outgoing current contributes to the charge distribution on the cell. The requirement

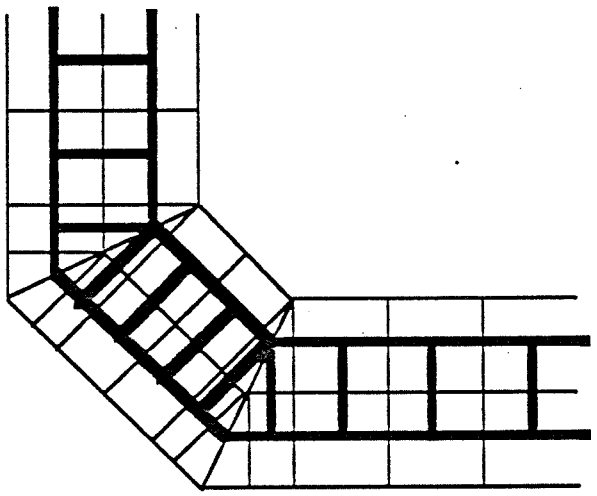

Figure 3.4: Current flow in a wire mesh.

that the normal component of current must vanish at the edges of a microstrip circuit can be easily implemented by "opening" the corresponding meshes connected to the edges. We should note that the use of triangular " meshes " captures fully the physical phenomenum of a current flow round the corner of a bend. Thus, one of the advantages for the P-mesh representation is that it can be constructed according to the physical intuition a designer has, and such intuition usually results in fast convergence of the computational process.

3.5 The Global Expression for Current Distribution

In Sections 3.2 and 3.3, we have discussed the roof-top basis functions on individual cells. To complete the P-mesh development, we still need to integrate the individual current unknowns, i.e. $I_\alpha^{i,i+1}$ for the cell α into a global set of "mesh" currents I_m, $m = 1, 2, ..., M$ where M is the total number of interconnecting "meshes". As we mentioned earlier, "meshes" at the boundary of a microstrip structure are "disconnected" since the normal current at the edge of a boundary cell is zero. For adjacent cells α and α', at the common boundary describable either by $(\alpha; i, i+1)$ or $(\alpha'; i', i'+1)$ (see Fig. 3.5), the unknown current across this boundary is now expressed in terms of the mesh current I_m so that

$$I_m = I_\alpha^{i,i+1} = -I_{\alpha'}^{i',i'+1} \tag{3.28}$$

The roof-top basis function corresponding to this unknown current is

$$\bar{H}_m = \bar{D}_\alpha^{i,i+1} - \bar{D}_{\alpha'}^{i',i'+1} \tag{3.29}$$

The divergence of the roof-top basis function is

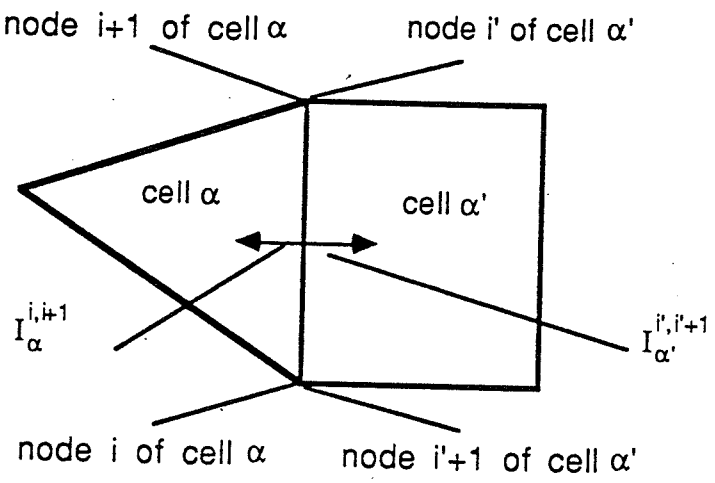

Figure 3.5: The side current for two adjacent cells.

$$P_m = Q^i_\alpha - Q^{i'}_{\alpha'} \tag{3.30}$$

Therefore, the P-mesh current distribution on a structure can finally be expressed as

$$\bar{J}(x,y) = \sum_{m=1}^{M} I_m \bar{H}_m(x,y) \tag{3.31}$$

The $\bar{H}_m$, $m = 1,2,...$ are the corresponding $\bar{B}_m$ and $\bar{T}_m$, $m = 1,2,...$ discussed in Section 3.1.

3.6 Matrix Solution to the MPIE

The $\bar{H}_m$ in (3.29) are used as both the basis functions $\bar{B}_m$ and the test functions $\bar{T}_m$ of a microstrip structure. We have established the matrix equation in (3.2) and we write down it again here.

$$\sum_{m'=1}^{M} Z_{m,m'} I_{m'} = V_m \; ; \; m = 1,2,...,M \tag{3.32}$$

Substituting (3.31) into (3.10) yields

$$Z_{m,m'} = \frac{j\omega\mu_0}{4\pi} \int_{s_m} ds \int_{s_{m'}} ds' \, K_{m,m'}(x,y;x',y') + Z_s \int_{s_m} ds \, \bar{H}_m(x,y) \cdot \bar{H}_{m'}(x,y) \tag{3.33}$$

$$K_{m,m'}(x,y;x',y') = G_m(\rho)\bar{H}_m(x,y) \cdot \bar{H}_{m'}(x',y') - \frac{1}{k_0^2} G_e(\rho) \, P_m \, P_{m'} \tag{3.34}$$

$$V_m = \int_{s_m} ds \, \bar{H}_m(x,y) \cdot \bar{E}_i(x,y) \tag{3.35}$$

$$\rho = \sqrt{(x-x')^2 + (y-y')^2} \tag{3.36}$$

The surface integration on s_m has to be carried out over the two adjacent cells, s_α and $s_{\alpha'}$ which share a common boundary or "mesh" m, i.e. $m = (\alpha; i, i+1) = (\alpha'; i', i'+1)$. It is noticed that the matrix element $Z_{m,m'}$ consists of quadruple integrals of the form

$$\int_{\text{cell }\alpha} ds \int_{\text{cell }\alpha'} ds' G_{m,e}(\rho)\, x^\mu y^\nu x'^{\mu'} y'^{\nu'} \; ; \; \mu, \nu, \mu', \nu' \geq 0 \;\&\; 0 \leq \mu+\nu, \mu'+\nu' \leq 1 \tag{3.37}$$

For planar structures, the $G_{m,e}$ in (3.37) are Sommerfeld integrals as we derived in Chapter 2. They can not be evaluated analytically. Some semi-analytical expressions of $G_{m,e}$ have to be found for efficient evaluation of the quadruple integrals.

The References for Chapter 3

[1] J. H. Richmond, " A wire-grid model for scattering by conducting bodies," **IEEE Trans. on Antennas Propag.** , Vol. AP-14, pp. 782-786, Nov. 1966.

[2] A. W. Glisson and D. R. Wilton, " Simple and efficient numerical methods for problems of electromagnetic radiation and scattering from surfaces, " **IEEE Trans. on Antennas Propag.**, Vol. AP-28, pp. 593-603, Sep. 1980.

[3] D. I. Wu, D. C. Chang and B. I. Brim, "Accurate numerical modeling of microstrip junctions and discontinuities," **Intern. Journal of Microwave Millimeter-wave Computer Aided Engineering**, to be published.

[4] J. R. Mosig, "Arbitrarily shaped microstrip structures and their analysis with a mixed potential integral equation," **IEEE Trans. on Microwave Theory Tech.**, MTT-36, pp. 314-323, February 1988.

[5] W. Wertgen and R. H. Jansen, " Efficient direct and iterative electrodynamic analysis of geometrically complex MIC and MMIC structures," **International Journal of Numerical Modeling: Electronic Networks, Devices and Fields**, Vol.2, 153-186, 1989.

[6] R. W. Jackson, " Full-wave, finite element analysis of irregular microstrip discontinuities," **IEEE Trans. on Microwave Theory Tech.**, MTT-37, pp. 81-89, January 1989.

[7] J. C. Rautio and R. F. Harrington, " Preliminary results of a time-harmonic electromagnetic analysis of shielded microstrip circuits, " **27th Automatic RF Techniques Group Conference Digest**, Baltimore, pp. 121-134, June 1986.

[8] P. B. Katehi and N. G. Alexopoulos, " Frequency-dependent characteristics of microstrip discontinuities in millimeter-wave integrated circuits," **IEEE Trans. on Microwave Theory Tech.**, MTT-33, pp. 1029-1035, Oct. 1985.

[9] R. W. Jackson and D. M. Pozar, " Full-wave analysis of microstrip open-end and gap discontinuities," **IEEE Trans. on Microwave Theory Tech.**, MTT-33, pp. 1036-1042, Oct. 1985.

[10] D. C. Chang and J. X. Zheng, " Numerical modeling of planar circuits with pseudo meshes," **National Science Meeting Digest**, pp. 265, Boulder, CO, Jan. 1990.

[11] J. X. Zheng and D. C. Chang, " Convergence of the numerical solution for a microstrip junction based upon a triangular cell expansion," **National Science Meeting Digest**, pp.212, Boulder, CO, Jan. 1990.

[12] J. X. Zheng and D. C. Chang, " Numerical modeling of chamfered bends and other microstrip junctions of general shape in MMICs," **IEEE MTT Intern. Microwave Symposium Digest**, pp. 709-712, Dallas, TX , May 1990.

[13] D. C. Chang and J. X. Zheng, " Electromagnetic modeling of passive circuit elements in MMIC," **IEEE Trans. on Microwave Theory Tech.**, to be published.

[14] B. L. Brim and D. C. Chang, " Accelerated numerical computation of the spatial domain dyadic Green's functions of a grounded dielectric slab," **National Science Meeting Digest**, pp. 164, Boulder,CO, Jan. 1987.

[15] B. L. Brim and D. C. Chang, " The use of subsectional uniform distributions in the Galerkin-moment method solution of electromagnetics problems, " **National Science Meeting Digest**, pp. 8, Boulder, CO, Jan. 1988.

CHAPTER 4

ANALYTICAL EVALUATION OF THE QUADRUPLE MOMENT INTEGRALS IN MATRIX ELEMENTS

4.1 Introduction

The matrix elements have been expressed in terms of some quadruple integrals with integrands involving the Green's functions and linear basis and test functions (see (3.37)). As mentioned in Chapter 3, the Green's functions are Sommerfeld integrals and can not be evaluated analytically. When the source point and the field point are both on the dielectric slab, the Green's functions are of the form

$$G_m(\rho) = \int_0^\infty d\lambda\, J_0(\lambda\rho)\, \frac{2\mu_r\, \lambda}{D_{tm}} \tag{4.1}$$

$$G_e(\rho) = \int_0^\infty d\lambda\, J_0(\lambda\rho)\, \frac{2\lambda[u_0 + \mu_r u_n \tanh(u_n h)]}{D_{te}\, D_{tm}} \tag{4.2}$$

All the parameters have been defined in Chapter 2 and will not be repeated here. Let's first see the large argument behaviour of the integrands. When $\lambda \to \infty$,

$$u_0 \text{ or } u_n \sim \lambda \tag{4.3}$$

$$\tanh(u_n h) \sim 1 \tag{4.4}$$

and,

$$D_{tm} \sim (\mu_r + 1)\lambda \tag{4.5}$$

$$D_{te} \sim (\varepsilon_r + 1)\lambda \tag{4.6}$$

Therefore, the asymptotic behaviour of the integrands in (4.1) and (4.2) is of the order of $J_0(\lambda\rho)$, integration of the term results in $1/\rho$ [1], or

$$\int_0^\infty d\lambda\, J_0(\lambda\rho) = \frac{1}{\rho} \tag{4.7}$$

Equation (4.7) corresponds to the direct (not including the image) field of a static source and has a singularity at $\rho = 0$. In order to avoid difficulty in numerical computation of these integrals, we first extract the term from the integrands of (4.1) and (4.2) to obtain [5]

$$G_{m,e} = G^{sg}_{m,e} + G^{sm}_{m,e} \tag{4.8}$$

where

$$G^{sg}_m = \frac{2\mu_r}{\mu_r + 1}\frac{1}{\rho} \tag{4.9}$$

$$G^{sm}_m = \int_0^\infty 2J_0(\lambda\rho)[\frac{\mu_r\lambda}{D_{tm}} - \frac{\mu_r}{\mu_r + 1}]d\lambda \tag{4.10}$$

$$G^{sg}_e = \frac{2}{\varepsilon_r + 1}\frac{1}{\rho} \tag{4.11}$$

$$G^{sm}_e = \int_0^\infty 2J_0(\lambda\rho)\{\frac{\lambda[u_0 + \mu_r u_n \tanh(u_n h)]}{D_{tm}\, D_{te}} - \frac{1}{\varepsilon_r + 1}\}d\lambda \tag{4.12}$$

For $\rho = 0$, the integrals in (4.10) and (4.12) are evaluated along the real axis of the complex λ plane with a deformation to avoid the singularities between $\lambda = k_0$ and $\lambda = k_n$. For $\rho > 0$, however, we found it more convenient to first transform the integration from 0 to ∞ to that from $-\infty$ to ∞ with the $J_0(\lambda\rho)$ replaced with $\frac{1}{2}H_0^2(\lambda\rho)$ [4]. And then, the integration contour is deformed onto both sides of a branch cut defined by $Re(u_0) = 0$, in the lower half plane [5] (see Fig. 4.1). Since $G_{m,e}^{sm}$ are smooth functions of ρ [5], we can first compute a number of them with different ρ, and then curve-fit them piecewise into some range-dependent polynomial of finite order.

$$G_{m,e}(\rho) = \sum_{p=-1}^{M_p} C_p^{m,e}(\alpha, \alpha')\rho^p. \tag{4.13}$$

where $C_p^{m,e}$ are the coefficients from the curve-fitting; M_p is the order of the polynomials; the α and α' are the indices of two cells, within the range of which the polynomial is valid.

The process is easily done since $G_{m,e}$ are functions of ρ only. In practical programing, we assume $\mu_r = 1$ and there is no dielectric loss. It must be noted that the assumptions are not an inherent limitation of the algorithm.

Based upon the expression in (4.13), we can re-express the quadruple integrals in the matrix elements (see (3.32) - (3.37) of Chapter 3) by individual integrals of the following form:

$$Q(\alpha, \alpha', \mu, \nu, \mu', \nu', p) = \int_{\text{cell }\alpha} ds \int_{\text{cell }\alpha'} ds' \rho^p x^\mu y^\nu x'^{\mu'} y'^{\nu'} \; ; p = -1, 0, ..., N_p. \tag{4.14}$$

where

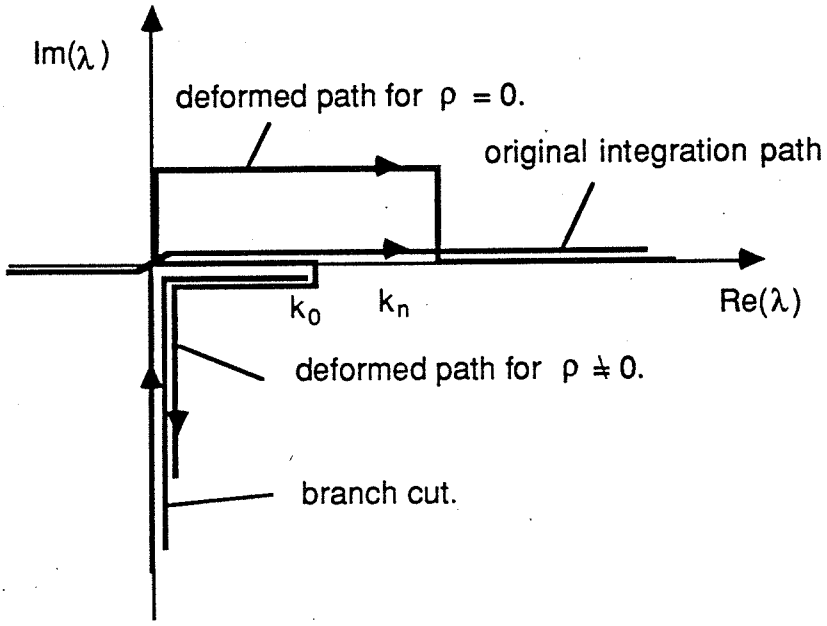

Figure 4.1: The deformed integration contours.

$$\rho = \sqrt{(x - x')^2 + (y - y')^2} \tag{4.15}$$

When the two cells are rectangular cells and $\mu = \nu = \mu' = \nu' = 0$, the integral has been evaluated in [6]. In this chapter, we will show that the integrals for all the cases can be solved analytically [9]. Unfortunately, since no explicit recurrence relations among different combinations of μ, ν, μ', ν' and p are found, we have to solve each case individually. Only the cases with $p \leq 4$ will be included, even though in principle, other cases can be derived as well.

The quadruple integration in (4.14) involves two triangular or rectangular cells, and the integration process is closely related to the evaluation of the area of an arbitrary polygon. The process evaluating the area of or an integral over an arbitrary polygon will be demonstrated first in Section 4.2.

For the cases with even p in (4.14), the terms related to ρ can be broken up into some terms with separable x, y, x' and y', and the quadruple integrals can be reduced to the summation and product of some double integrals with integrands of power functions of x and y or x' and y'. The integrals with even p in (4.14) will be solved in Section 4.3.

For odd p cases, the integrals can be evaluated in a similar way, but the two-double integrals have to be solved simutaneously. The final process involves change of integration variables and is very complicated. We will discuss such process in Sections 4.4-4.5. In the final section, we will include a comparison between the analytical technique and a numerical technique.

4.2 The Evaluation of Double Integrals over an Arbitrary Polygon

Let's first consider evaluating the area of an arbitrarily oriented triangle α or $\triangle ABC$ as shown in Fig. 4.2. The area is defined as

$$S_{\triangle ABC} = \int_{\triangle ABC} dx\, dy \tag{4.16}$$

We can break the triangle into two smaller triangles $\triangle ABD$ and $\triangle BCD$, where point D has the same x-coordinate as point B. The integration with respect to y is evaluated first.

$$S_{\triangle ABD} = \int_{x_{\alpha,1}}^{x_{\alpha,2}} dx\, y \,|_{y=y_{\alpha,3}+(x-x_{\alpha,3})(y_{\alpha,1}-y_{\alpha,3})/(x_{\alpha,1}-x_{\alpha,3})}^{y=y_{\alpha,1}+(x-x_{\alpha,1})(y_{\alpha,2}-y_{\alpha,1})/(x_{\alpha,2}-x_{\alpha,1})} \tag{4.17}$$

$$S_{\triangle BCD} = \int_{x_{\alpha,2}}^{x_{\alpha,3}} dx\, y \,|_{y=y_{\alpha,3}+(x-x_{\alpha,3})(y_{\alpha,1}-y_{\alpha,3})/(x_{\alpha,1}-x_{\alpha,3})}^{y=y_{\alpha,2}+(x-x_{\alpha,2})(y_{\alpha,3}-y_{\alpha,2})/(x_{\alpha,3}-x_{\alpha,2})} \tag{4.18}$$

The sum of $S_{\triangle ABD}$ and $S_{\triangle BCD}$ is the area of triangle $\triangle ABC$ or $S_{\triangle ABC}$.

$$S_{\triangle ABC} = \sum_{i=1}^{3} \int_{x_{\alpha,i}}^{x_{\alpha,i+1}} dx\, y(x,i) \tag{4.19}$$

where

$$y(x,i) = y_{\alpha,i} + \frac{y_{\alpha,i+1} - y_{\alpha,i}}{x_{\alpha,i+1} - x_{\alpha,i}}(x - x_{\alpha,i}) \tag{4.20}$$

and $x_{\alpha,4} = x_{\alpha,1}$ and $y_{\alpha,4} = y_{\alpha,1}$.

The final integral in (4.19) can easily be done. It is noticed that the nodal index goes clockwise in Fig. 4.2. When the nodal index goes counter-clockwise, we have a sign difference between the area and the summation in (4.19). Therefore, we have to define that the nodal index is in a clockwise order whenever the above integration scheme is used. A special case with $x_{\alpha,i} = x_{\alpha,i+1}$

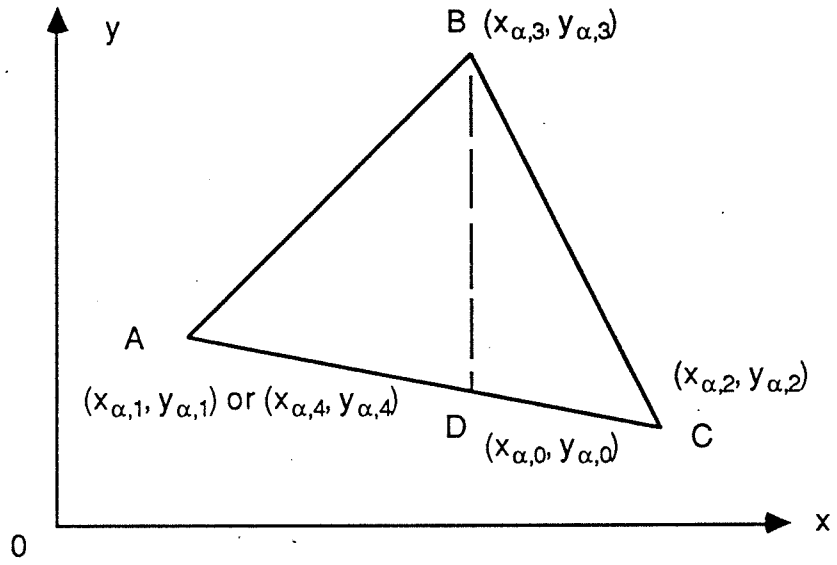

$$x_{\alpha,0} = x_{\alpha,3}$$

$$y_{\alpha,0} = y_{\alpha,1} + \frac{y_{\alpha,2} - y_{\alpha,1}}{x_{\alpha,2} - x_{\alpha,1}} (x_{\alpha,3} - x_{\alpha,1})$$

Figure 4.2: An arbitrary triangle.

in (4.19) may be encoutered. In this case, either $\triangle ABD$ or $\triangle BCD$ vanishes and the corresponding term can be dropped.

Obviously, we can extend the technique to the integration of an integrand over an arbitrary polygon.

$$D[f(x,y)] = \int_{\text{polygon }\alpha} f(x,y)dxdy \tag{4.21}$$

After the integration with respect to y, we obtain

$$D[f(x,y)] = \sum_{k=1}^{M_\alpha} \int_{x_{\alpha,k}}^{x_{\alpha,k+1}} f_y(x)dx \tag{4.22}$$

where M_α is the number of sides in the polygon;

$$f_y(x) = \int f(x,y)dy. \tag{4.23}$$

The only requirement for the procedure is that the integral in (4.22) and (4.23) can be solved analytically in a closed-form.

4.3 The Evaluation of $\mathbf{Q(\alpha, \alpha', i, j, i', j', p), p = 0, 2, 4}$

We have learned from Section 4.1 that the quadruple integrals of even p cases over two arbitrarily oriented cells α and α' shown in Fig. 4.3 can be reduced to the summation and product of some double integrals of the form

$$S(\alpha, i, j) = \int_{\text{cell }\alpha} ds\, x^i y^j \tag{4.24}$$

Following the procedure discussed in Section 4.2, we obtain

$$S(\alpha, i, j) = \frac{1}{j+1} \sum_{k=1}^{M_\alpha} C(x_{\alpha,k}, y_{\alpha,k}, x_{\alpha,k+1}, y_{\alpha,k+1}, 0, i, j+1) \tag{4.25}$$

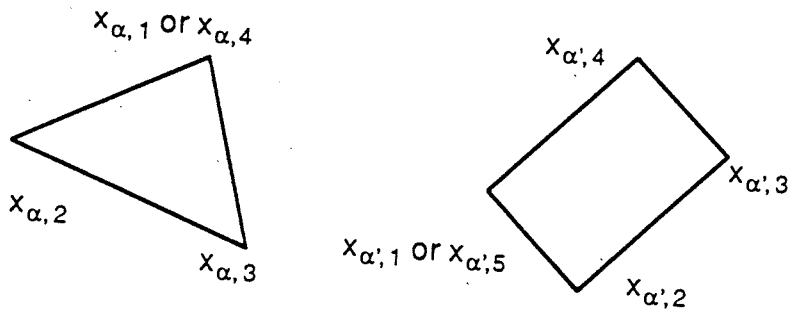

Figure 4.3: Two arbitrarily oriented cells.

where

$$C(x_{\alpha,1}, y_{\alpha,1}, x_{\alpha,2}, y_{\alpha,2}, p, i, j) = \int_{x_{\alpha,1}}^{x_{\alpha,2}} dx\, \rho^p x^i y^j|_{y=y_{\alpha,1}+(y_{\alpha,2}-y_{\alpha,1})(x-x_{\alpha,1})/(x_{\alpha,2}-x_{\alpha,1})} \tag{4.26}$$

The $C(x_{\alpha,1}, y_{\alpha,1}, x_{\alpha,2}, y_{\alpha,2}, p, i, j)$, $p \geq -1$, $i, j \geq 0$ can be solved analytically and are listed in Appendix B.

By expanding the integrands of $Q(\alpha, \alpha', i, j, i', j', p)$ with $p = 0, 2, 4$ into power series of x, y, x' and y', and making use of (4.24), we can obtain

$$Q(\alpha, \alpha', i, j, i', j', 0) = S_p(\alpha, \alpha', i, j, i', j') \tag{4.27}$$

$$Q(\alpha, \alpha', i, j, i', j', 2) = \sum_{r=0}^{2} (-1)^r \frac{2!}{r!\,(2-r)!} S_s(\alpha, \alpha', i, j, i', j', 2, r) \tag{4.28}$$

$$Q(\alpha, \alpha', i, j, i', j', 4) = Q_1(\alpha, \alpha', i, j, i', j') + Q_2(\alpha, \alpha', i, j, i', j') \tag{4.29}$$

where

$$S_p(\alpha, \alpha', i, j, i', j') = S(\alpha, i, j)\, S(\alpha', i', j') \tag{4.30}$$

$$S_s(\alpha, \alpha', i, j, i', j', r, t) = S_p(\alpha, \alpha', i+r-t, j, i'+t, j') + S_p(\alpha, \alpha', i, j+r-t, i', j'+t) \tag{4.31}$$

$$Q_1(\alpha, \alpha', i, j, i', j') = \sum_{r=0}^{4} (-1)^r \frac{4!}{r!\,(4-r)!} S_s(\alpha, \alpha', i, j, i', j', 4, r) \tag{4.32}$$

$$Q_2(\alpha,\alpha',i,j,i',j') = 2\sum_{r=0}^{2}(-1)^r \frac{2!}{r!(2-r)!} S_p(\alpha,\alpha',i+2-r,j+2-t,i'+r,j'+t) \tag{4.33}$$

4.4 The Evaluation of the Integrations with Respect to y and y′ in $Q(\alpha,\alpha',i,j,i',j',p), p = -1,1,3$

As discussed in Section 4.1, the analytical evaluation of the quadruple integrals for odd p cases is very complicated. The difficulty arises from the fact that the integrands are not separable into two independent double integrals. The two double integrals have to be solved simutaneously. But, the same technique in Section 4.2 can be applied to solve the integrations with respect to y and y' first. The process yields

$$Q(\alpha,\alpha',i,j,i',j',p) = \sum_{k=1}^{M_\alpha}\sum_{k'=1}^{M_{\alpha'}} \int_{x_{\alpha,k}}^{x_{\alpha,k+1}} dx \int_{x_{\alpha',k'}}^{x_{\alpha',k'+1}} dx' F(i,j,i',j',p)|_{y(k),y'(k')}. \tag{4.34}$$

where

$$y(k) = y_{\alpha,k} + (y_{\alpha,k+1} - y_{\alpha,k})(x - x_{\alpha,k})/(x_{\alpha,k+1} - x_{\alpha,k}) \tag{4.35}$$

$$y'(k') = y_{\alpha',k'} + (y_{\alpha',k'+1} - y_{\alpha',k'})(x' - x_{\alpha',k'})/(x_{\alpha',k'+1} - x_{\alpha',k'}) \tag{4.36}$$

$$F(i,j,i',j',p) = \int dy \int dy' \rho^p x^i y^j x'^{i'} y'^{j'}. \tag{4.37}$$

$F(i,j,i',j',p)$ are functions of x, y, x' and y'. For conciseness, the variables are not included in $F(i,j,i',j',p)$. The process to obtain the $F(i,j,i',j')$

is similar to what described in Section 4.2. We will use the $F(0,0,0,0,-1)$ as an example of illustration.

$$\begin{aligned} F(0,0,0,0,-1) &= \int dy \int dy' \frac{1}{\rho} \\ &= \int dy \, \ln(\rho + y' - y) \\ &= (y - y') \ln(\rho + y' - y) + \rho \end{aligned} \tag{4.38}$$

In fact, there should be some additional analytic functions of x and x', or constants with respect to y and y', in $F(0,0,0,0,-1)$ as well as all the other $F(j,k,m,n,p)$. But, the remaining double integrations of these additional functions in (4.34) vanish and will not affect our final solutions. Therefore, the additional functions are neglected. The final expressions of $F(i,j,i',j',p)$, $p = -1, 1, 3$ are listed in the following:

$$F(0,0,0,0,-1) = (y - y') \ln(\rho + y' - y) + \rho \tag{4.39}$$

$$F(0,0,1,0,-1) = x' \, F(0,0,0,0,-1) \tag{4.40}$$

$$F(1,0,0,0,-1) = x \, F(0,0,0,0,-1) \tag{4.41}$$

$$F(0,0,0,1,-1) = y' \, F(0,0,0,0,-1) + FA(0,1,-1) \tag{4.42}$$

where

$$FA(0,1,-1) = \frac{1}{4}[3(y - y')\rho + 2(y - y')^2 \ln(\rho + y' - y) +$$

$$(x-x')^2\ln(\rho+y-y')] \tag{4.43}$$

$$F(0,1,0,0,-1) = y'\,F(0,0,0,0,-1) + FA(1,0,-1) \tag{4.44}$$

where

$$\begin{aligned} FA(1,0,-1) &= \frac{1}{4}[(y-y')\rho + 2(y-y')^2\ln(\rho+y'-y) - \\ &\quad (x-x')^2\ln(\rho+y-y')] \end{aligned} \tag{4.45}$$

$$F(1,0,1,0,-1) = x\,x'\,F(0,0,0,0,-1) \tag{4.46}$$

$$F(0,1,1,0,-1) = x'\,F(0,1,0,0,-1) \tag{4.47}$$

$$F(1,0,0,1,-1) = x\,F(0,0,0,1,-1) \tag{4.48}$$

$$\begin{aligned} F(0,1,0,1,-1) &= y'^2\,F(0,0,0,0,-1) + y'\,[FA(0,1,-1) + \\ &\quad FA(1,0,-1)] + FA(1,1,-1) \end{aligned} \tag{4.49}$$

where

$$\begin{aligned} FA(1,1,-1) &= \frac{1}{9}[4(y-y')^2\rho + (x-x')^2\rho + \\ &\quad 3(y-y')^2\ln(\rho+y'-y)] \end{aligned} \tag{4.50}$$

$$F(0,0,0,0,1) = \frac{1}{6}\{3(x-x')^2[(y-y')\ln(\rho+y'-y)+\rho]-\rho^3\} \tag{4.51}$$

$$F(0,0,1,0,1) = x'\,F(0,0,0,0,1) \tag{4.52}$$

$$F(1,0,0,0,1) = x\,F(0,0,0,0,1) \tag{4.53}$$

$$F(0,0,0,1,1) = y'\,F(0,0,0,0,1) + FA(0,1,1) \tag{4.54}$$

where

$$\begin{aligned} FA(0,1,1) \;=\; & \frac{1}{48}\,[13(x-x')^2(y-y')\rho - \\ & 2(y-y')^3\rho + 3(x-x')^4\,\ln(\rho+y-y') + \\ & 12(y-y')^2(x-x')^2\,\ln(\rho+y'-y)] \end{aligned} \tag{4.55}$$

$$F(0,1,0,0,1) = y'\,F(0,0,0,0,1) + FA(1,0,1) \tag{4.56}$$

$$\begin{aligned} FA(1,0,1) \;=\; & \frac{1}{16}\,[(x-x')^2(y-y')\rho - 2(y-y')^3\rho + \\ & 4(y-y')^2(x-x')^2\,\ln(\rho+y'+y) - \\ & (x-x')^4\,\ln(\rho+y-y')] \end{aligned} \tag{4.57}$$

$$F(1,0,1,0,1) = xx'\,F(0,0,0,0,1) \tag{4.58}$$

$$F(0,1,1,0,1) = x'\,F(0,1,0,0,1) \tag{4.59}$$

$$F(1,0,0,1,1) = x\,F(0,0,0,1,1) \tag{4.60}$$

$$F(0,1,0,1,1) = y'^2\,F(0,0,0,0,1) + y'[FA(0,1,1) + FA(1,0,1)] + FA(1,1,1) \tag{4.61}$$

where

$$\begin{aligned} FA(1,1,1) \;=\; & \frac{1}{90}[-3(y-y')^4\,\rho + 14(y-y')^2(x-x')^2\rho + \\ & 2(y-y')^4\rho + 15(y-y')^3(x-x')^2\,\ln(\rho+y'-y)] \end{aligned} \tag{4.62}$$

$$\begin{aligned} F(0,0,0,0,3) \;=\; & \frac{1}{40}[-2(y-y')^4\,\rho - 9(x-x')^2(y-y')^2\rho + \\ & 8(x-x')^4\rho + 15(x-x')^4(y-y')\,\ln(\rho+y'-y)] \end{aligned} \tag{4.63}$$

$$F(0,0,1,0,3) = x'\,F(0,0,0,0,3) \tag{4.64}$$

$$F(1,0,0,0,3) = x\,F(0,0,0,0,3) \tag{4.65}$$

$$F(0,0,0,1,3) = y'\,F(0,0,0,0,3) \;+\; FA(0,1,3) \tag{4.66}$$

where

$$FA(0,1,3) = \frac{1}{480}[-4(y-y')^5\rho - 28(y-y')^3(x-x')^2\rho + 81(y-y')(x-x')^4\rho + 90(y-y')^2(x-x')^4 \ln(\rho+y'-y) + 15(x-x')^6 \ln(\rho+y-y')] \quad (4.67)$$

$$F(0,1,0,0,3) = y' F(0,0,0,0,3) + FA(1,0,3) \quad (4.68)$$

where

$$FA(1,0,3) = \frac{1}{96}[-4(y-y')^5\rho - 16(x-x')^2(y-y')^3\rho + 3(x-x')^4(y-y')\rho + 18(x-x')^4(y-y')^2 \ln(\rho+y'-y) - 3(x-x')^6 \ln(\rho+y-y')] \quad (4.69)$$

$$F(1,0,1,0,3) = xx' F(0,0,0,0,3) \quad (4.70)$$

$$F(0,1,1,0,3) = x' F(0,1,0,0,3) \quad (4.71)$$

$$F(1,0,0,1,3) = x F(0,0,0,1,3) \quad (4.72)$$

$$F(0,1,0,1,3) = y'^2 F(0,0,0,0,3) + y'[FA(0,1,3) + FA(1,0,3)] + FA(1,1,3) \quad (4.73)$$

where

$$FA(1,1,3) = \frac{1}{840}[-6(y-y')^6\rho - 249(y-y')^4(x-x')^2\rho + 10(y-y')^2(x-x')^4\rho + 148(x-x')^6\rho + 105(y-y')^3(x-x')^4 \ln(\rho+y'-y)] \quad (4.74)$$

It is clear from (4.34) the basic elements in the remaining double integrals are over the x-x' plane as shown in Fig. 4.4 and are of the form

$$I(i,j,i',j',p) = \int_{x_{\alpha,k}}^{x_{\alpha,k+1}} dx \int_{x_{\alpha',k'}}^{x_{\alpha',k'+1}} dx' F(i,j,i',j',p)|_{y(k),y'(k')} \quad (4.75)$$

where $y(k)$ and $y'(k')$ are defined in (4.35) and (4.36), respectively.

The evaluation of the integrations with respect to x and x' will be discussed in the next section.

4.5 The Evaluation of the Integrations with Respect to x and x' in $Q(\alpha,\alpha',i,j,i',j',p), p = -1,1,3$

We have solved the integrations with respect to y and y' in last section. The basic elements in the remaining double integrations with respect to x and x' are listed in (4.75). The integrand in (4.75) contains functions of ρ,

$$\rho = \sqrt{s^2+t^2} \quad (4.76)$$

where

$$s = x - x' \quad (4.77)$$

$$t = y - y' \quad (4.78)$$

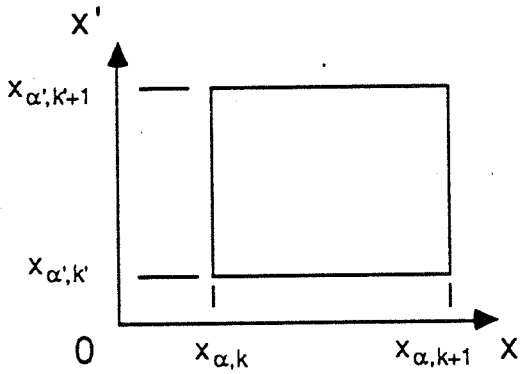

Figure 4.4: The integration domain in the x-x' plane.

It is pretty difficult to solve the double integrals in (4.75) without any integration domain transform since the ρ has a very complicated function dependence on the integration variables x and x'.

We first define some intermediate variables,

$$y(k) = a + b\,x \tag{4.79}$$

$$y'(k') = c + d\,x' \tag{4.80}$$

or

$$a = y_{\alpha,k} - x_{\alpha,k}\,b \tag{4.81}$$

$$b = \frac{y_{\alpha,k+1} - y_{\alpha,k}}{x_{\alpha,k+1} - x_{\alpha,k}} \tag{4.82}$$

$$c = y_{\alpha',k'} - x_{\alpha',k'}\,d \tag{4.83}$$

$$d = \frac{y_{\alpha',k'+1} - y_{\alpha',k'}}{x_{\alpha',k'+1} - x_{\alpha',k'}} \tag{4.84}$$

The a, b, c and d are obtained directly from (4.35) and (4.36).

There are two cases we have to consider: (a) $b = d$, or the two lines $(x_{\alpha,k}, y_{\alpha,k})$-$(x_{\alpha,k+1}, y_{\alpha,k+1})$ and $(x_{\alpha',k'}, y_{\alpha',k'})$-$(x_{\alpha',k'+1}, y_{\alpha',k'+1})$ are parallel, or s and t in (4.77) and (4.78) are linearly dependent; (b) $b \neq d$, or the two lines are not parallel, or s and t are linearly independent. We will discuss the two cases in the following two sub-sections, respectively.

4.5.1 The evaluation of the double integrals I(i,j,i',j',p), p = −1, 1, 3 with linarly dependent (x − x') and (y − y') As mentioned earlier, we have to transform the integration domain in the x-x' plane to another domain with simpler function dependence of the integrands on the integration variables. It is noticed that $s = x - x'$ and $t = y - y'$ can be used to simplify the expressions of $F(i,j,i',j',p)$ (see Section 4.4). We can use s as one of the integration variable in the transformed integration domain. But t can not be used as the other integration variable since it is linearly dependent on s in this case. Therefore, we define the transform as

$$\begin{cases} s = x - x' \\ v = x + x' \end{cases} \tag{4.85}$$

We can obtain from $b = d$ and (4.79)-(4.84)

$$\begin{cases} x &= \frac{1}{2}(v+s) \\ x' &= \frac{1}{2}(v-s) \\ y &= a + \frac{1}{2}bs + \frac{1}{2}bv \\ y' &= c - \frac{1}{2}bs + \frac{1}{2}bv \end{cases} \tag{4.86}$$

The integration domain of a rectangle (see Fig. 4.4) in the x-x' plane is transformed to a rotated rectangle in the s-v domain as shown in Fig. 4.5. The absolute value of the Wronskian is

$$\left| \frac{\partial x}{\partial s}\frac{\partial x'}{\partial v} - \frac{\partial x}{\partial v}\frac{\partial x'}{\partial s} \right| = \frac{1}{2} \tag{4.87}$$

From (4.39)-(4.74), we can see the integrands have very simple function relations, such as x, x', y, y', $x\,x'$, y'^2, $x'\,y'$ and $x\,y'$, to v. When $v = \lambda\, s + \xi$,

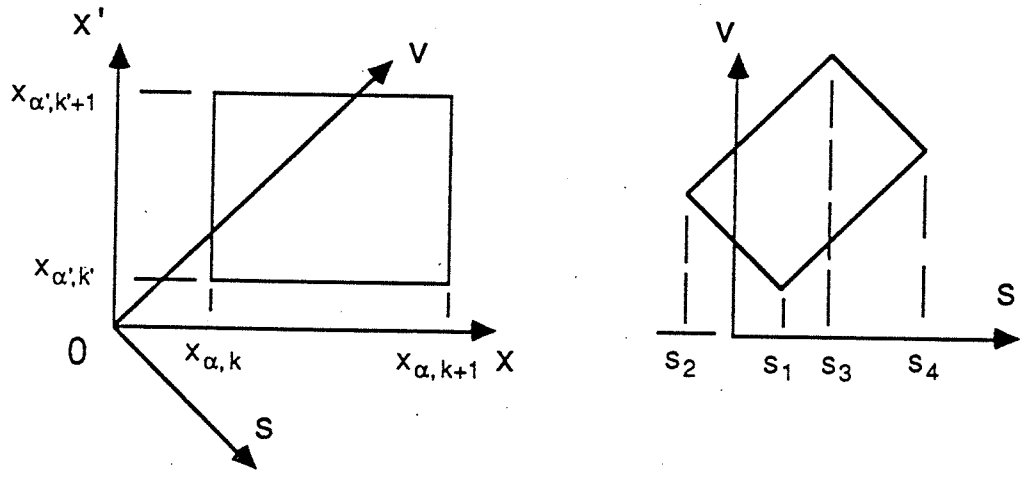

Figure 4.5: The integration domain in the s-v plane.

where λ and ξ are constants, the integrations with respect to v of such functions yield

$$\int x'\,dv = \frac{1}{4}\left[(1-2\lambda)\,s^2 + 2\,\xi\,(\lambda-1)\,s + \xi^2\right] \tag{4.88}$$

$$\int x\,dv = \frac{1}{4}\left[(1+2\lambda)\,s^2 + 2\,\xi\,(\lambda+1)\,s + \xi^2\right] \tag{4.89}$$

$$\int y'\,dv = \frac{1}{4}[(4c+b\xi)\xi + 2(2\lambda\,c - b\,\xi + \lambda\,b\,\xi)\,s + b(1-2\lambda)\,s^2] \tag{4.90}$$

$$\int x\,x'\,dv = \frac{1}{12}\left[-2\lambda\,s^3 + 3\lambda\,\xi^2\,s + \xi^3\right] \tag{4.91}$$

$$\begin{aligned}\int y'^2\,dv \;=\; & \frac{1}{12}\Big\{\xi(12\,c^2 + 6\,c\,b\,\xi + b^2\,\xi^2) + 3[b\,\xi(\lambda-1)(b\,\xi+4c) + 4\,c^2\,\lambda]\,s + \\ & 6\,b[c(1-2\lambda) + b\,\xi(1-\lambda)]\,s^2 + b^2\,(4\lambda-3)\,s^3\Big\}\end{aligned} \tag{4.92}$$

$$\begin{aligned}\int x'\,y'\,dv \;=\; & \frac{1}{12}\Big\{b\,(4\lambda-3)\,s^3 + 3[2\,b\,\xi\,(1-\lambda) + c\,(1-2\lambda)]\,s^2 + \\ & 3\,\xi\,(\lambda-1)(b\,\xi+2c)\,s + \xi^2\,(b\,\xi+3\,c)\Big\}\end{aligned} \tag{4.93}$$

$$\begin{aligned}\int x\,y'\,dv \;=\; & \frac{1}{12}\Big\{-2\,b\,\lambda\,s^3 + 3\,c\,(2\lambda+1)\,s^2 + \\ & 3\,\xi\,[2\,c\,(\lambda+1) + b\,\lambda\,\xi] + \xi^2\,(3\,c + b\,\xi)\Big\}\end{aligned} \tag{4.94}$$

(4.86) has been used in deriving (4.88) and (4.94) and the a, b and c are defined in (4.81)-(4.83).

The double integration technique discussed in Section 4.2 is, again, used to yield after the integration with respect to v

$$I(0,0,0,0,-1) = \frac{1}{2}\sum_{m=1}^{4}\int_{s_m}^{s_{m+1}} ds\,[t\,\ln(\rho - t) + \rho]v(m) \tag{4.95}$$

where the $\frac{1}{2}$ is from the Wronskian [3] and,

$$v(m) = \lambda_m\, s + \xi_m \tag{4.96}$$

$$\lambda_m = \frac{v_{m+1} - v_m}{s_{m+1} - s_m} \tag{4.97}$$

$$\xi_m = v_{m+1} - \lambda_m\, s_{m+1} \tag{4.98}$$

The s_m, t_m and v_m are defined as

$$\begin{cases} s_{1 \text{ or } 5} = x_{\alpha,k} - x_{\alpha',k'}\ , & t_{1 \text{ or } 5} = y_{\alpha,k} - y_{\alpha',k'}\ , & v_{1 \text{ or } 5} = x_{\alpha,k} + x_{\alpha',k'} \\ s_2 = x_{\alpha,k} - x_{\alpha',k'+1}\ , & t_2 = y_{\alpha,k} - y_{\alpha',k'+1}\ , & v_2 = x_{\alpha,k} + x_{\alpha',k'+1} \\ s_3 = x_{\alpha,k+1} - x_{\alpha',k'+1}\ , & t_3 = y_{\alpha,k+1} - y_{\alpha',k'+1}\ , & v_3 = x_{\alpha,k+1} + x_{\alpha',k'+1} \\ s_4 = x_{\alpha,k+1} - x_{\alpha',k'}\ , & t_4 = y_{\alpha,k+1} - y_{\alpha',k'}\ , & v_4 = x_{\alpha,k+1} + x_{\alpha',k'} \end{cases} \tag{4.99}$$

They are the physical coordinates of the parallelogram's vertices in the s-v plane as shown in Fig. 4.5.

We can write from (4.95)

$$\begin{aligned} I(0,0,0,0,-1) \;=\; & \frac{1}{2}\sum_{m=1}^{4}[\lambda_m\, G(s_m, t_m, s_{m+1}, t_{m+1}, 1) + \\ & \xi_m\, G(s_m, t_m, s_{m+1}, t_{m+1}, 0)] \end{aligned} \tag{4.100}$$

where

$$G(s_m, t_m, s_{m+1}, t_{m+1}, n) = CL(s_m, t_m, s_{m+1}, t_{m+1}, -1, n, 1) + C(s_m, t_m, s_{m+1}, t_{m+1}, 1, n, 0) \quad (4.101)$$

$$CL(s_m, t_m, s_{m+1}, t_{m+1}, \gamma, \mu, \nu) = \int_{s_m}^{s_{m+1}} ds\, s^\mu t^\nu \ln(\rho + \gamma t)|_{t=t_m+(s-s_m)\frac{t_{m+1}-t_m}{s_{m+1}-s_m}} \quad \gamma = -1 \text{ or } 1 \quad (4.102)$$

$C(s_m, t_m, s_{m+1}, t_{m+1}, \gamma, \mu, \nu)$ is defined in (4.26). Both integrals in (4.26) and (4.102) are solved analytically in Appendix B.

Similarly, the integrals $I(i, j, i', j', p)$ of other combinations are solved in the same way by making use of the integrals in (4.88)-(4.94). The final results are listed in Appendix F.

4.5.2 The evaluation of the double integrals I(i,j,i',j',p), p = −1, 1, 3 with linear independent (x − x') and (y − y') When $b \neq d$ in (4.82) and (4.84), the $(x - x')$ and $(y - y')$ are linear independent. We can transform the integration domain in the x-x' plane, which is a rectangle(see Fig. 4.4), into a parallelogram in the s-t plane as shown in Fig. 4.6. s and t are defined as

$$\begin{cases} s = x - x' \\ t = y - y' \end{cases} \quad (4.103)$$

We can obtain

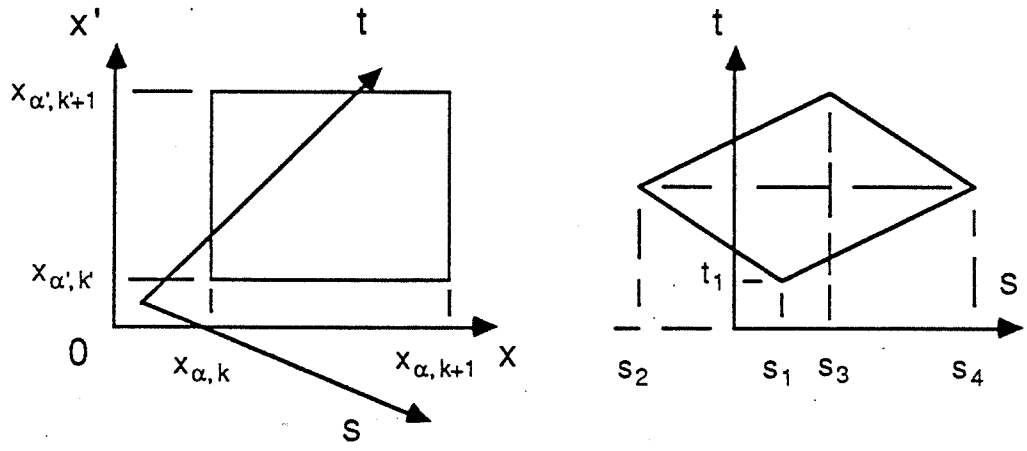

Figure 4.6: The integration domain in the s-t plane.

$$\begin{cases} x &= [t - d\,s - (a-c)]/(b-d) = \alpha_1 + \beta_1\, s + \gamma_1\, t \\ x' &= [t - b\,s - (a-c)]/(b-d) = \alpha_2 + \beta_2\, s + \gamma_2\, t \\ y &= a + b\,x = \alpha_3 + \beta_3\, s + \gamma_3\, t \\ y' &= c + d\,x' = \alpha_4 + \beta_4\, s + \gamma_4\, t \end{cases} \tag{4.104}$$

α_i, β_i and γ_i are explicitly given in (4.104).

To eliminate the sign confusion in the integration process (see Section 4.2), we have to define the vertex indices in the following way.

$$\begin{cases} s_{k,k'} = x_{\alpha,k} - x_{\alpha',k'}, & t_{k,k'} = y_{\alpha,k} - y_{\alpha',k'} \\ s_{k,k'+1} = x_{\alpha,k} - x_{\alpha',k'+1}, & t_{k,k'+1} = y_{\alpha,k} - y_{\alpha',k'+1} \\ s_{k+1,k'+1} = x_{\alpha,k+1} - x_{\alpha',k'+1}, & t_{k+1,k'+1} = y_{\alpha,k+1} - y_{\alpha',k'+1} \\ s_{k+1,k'} = x_{\alpha,k+1} - x_{\alpha',k'}, & t_{k+1,k'} = y_{\alpha,k+1} - y_{\alpha',k'} \end{cases} \tag{4.105}$$

$$\begin{cases} s_2 = min(s_{k,k'}, s_{k,k'+1}, s_{k+1,k'+1}, s_{k+1,k'}) \\ s_4 = max(s_{k,k'}, s_{k,k'+1}, s_{k+1,k'+1}, s_{k+1,k'}) \end{cases} \tag{4.106}$$

t_2 and t_4 are the corresponding t coordinates. Upon the definition of (s_2, t_2) and (s_4, t_4), (s_1, t_1) and (s_3, t_3) are defined such that

$$\begin{cases} t_1 < t_2 + \frac{t_4 - t_2}{s_4 - s_2}(s_1 - s_2) \\ t_3 > t_2 + \frac{t_4 - t_2}{s_4 - s_2}(s_3 - s_2) \end{cases} \tag{4.107}$$

The physical meaning of the definition is clearly shown in Fig. 4.6. The Wronskian for the transformation is defined as

$$\begin{aligned} \triangle &= Sign[(x_{\alpha,k+1} - x_{\alpha,k})(x_{\alpha',k'+1} - x_{\alpha',k'})] \left| \frac{\partial x}{\partial s}\frac{\partial x'}{\partial t} - \frac{\partial x}{\partial t}\frac{\partial x'}{\partial s} \right| \\ &= \frac{Sign[(x_{\alpha,k+1} - x_{\alpha,k})(x_{\alpha',k'+1} - x_{\alpha',k'})]}{|b-d|} \end{aligned} \tag{4.108}$$

We have from (4.39)

$$F(0,0,0,0,-1) = t\,\ln(\rho - t) + \rho \tag{4.109}$$

Integration of the term over the domain in the s-t plane yields

$$\begin{aligned} I(0,0,0,0,-1) &= \triangle \sum_{m=1}^{4} \int_{s_m}^{s_{m+1}} ds\,[D(s,t,1,0) + DL(s,t,-1,1)]|_{t(s,m)} \\ &= \triangle \sum_{m=1}^{4} GD(s_m,t_m,s_{m+1},t_{m+1},0,0) \end{aligned} \tag{4.110}$$

where

$$t(s,m) = t_m + \frac{t_{m+1} - t_m}{s_{m+1} - s_m}(s - s_m) \tag{4.111}$$

$$D(s,t,\mu,\nu) = \int dt\, t^{\nu}\, \rho^{\mu}\, dt \tag{4.112}$$

$$\begin{aligned} DL(s,t,\mu,\nu) &= \int dt\, t^{\nu}\, \ln(\rho + \mu\, t) \\ & \qquad \mu = -1 \text{ or } 1 \end{aligned} \tag{4.113}$$

$$\begin{aligned} GD(s_m,t_m,s_{m+1},t_{m+1},\nu,\gamma) &= E(s_m,t_m,s_{m+1},t_{m+1},1,\nu,\gamma) + \\ & \qquad EL(s_m,t_m,s_{m+1},t_{m+1},-1,\nu+1,\gamma) \end{aligned} \tag{4.114}$$

$$E(s_m,t_m,s_{m+1},t_{m+1},\mu,\nu,\gamma) = \int_{s_m}^{s_{m+1}} ds\, s^{\gamma}\, D(s,t,\mu,\nu) \tag{4.115}$$

$$EL(s_m, t_m, s_{m+1}, t_{m+1}, \mu, \nu, \gamma) = \int_{s_m}^{s_{m+1}} ds\, s^\gamma\, DL(s, t, \mu, \nu) \qquad (4.116)$$

$D(s, t, \mu, \nu)$ and $DL(s, t, \mu, \nu)$ can be solved analytically and are listed in Appendix A. $E(s_m, t_m, s_{m+1}, t_{m+1}, \mu, \nu, \gamma)$ and $EL(s_m, t_m, s_{m+1}, t_{m+1}, \mu, \nu, \gamma)$ can also be solved. They are expressed in terms of $C(s_m, t_m, s_{m+1}, t_{m+1}, \mu, \nu, \gamma)$ and $CL(s_m, t_m, s_{m+1}, t_{m+1}, \mu, \nu, \gamma)$, which are defined in (4.26) and (4.102), in Appendix C.

Similarly, the integrals $I(i, j, i', j', p)$ of other combinations are evaluated in the same way. The final results are listed in Appendix F.

4.6 Comparison between the Analytical Integration Scheme and a Numerical Integration Scheme

The complexity in the analytical integration of the quadruple integrals raises a question whether numerical integration schemes will do a better job for the smooth terms in the Green's functions.

No matter what scheme we use, the current algorithm should be used in a not very low frequency. The reason for this is that the size of cells in the de-embedding regions (see the next chapter) is chosen to be proportional to the waveguide wavelength λ_g in order to reduce the number of cells in the de-embedding arms, which are about $0.5\lambda_g$ long, at low frequency. The ratio of cell size over substrate thickness might be very large at low frequency and the image term of the Green's functions on longer varies slowly over the same cell. Hence, the smooth term requires more higher-order terms in the polynomials, which further compounds the complexity in deriving an analytical expression. The other choice is to extract the static parts of the image terms and solve

the whole or part of the corresponding quadruple integrals analytically. Again, this will increase computational time.

In practical programming, a 6-term (the highest order of the polynomials is 4) analytical scheme is used to yield stable results as long as $h/\lambda_g > 0.001$, where h and λ_g are the substrate thickness and the waveguide wavelength, respectively.

Since the effect of a junction discontinuity decrease as the operating frequency also decreases, the constraint that $h/\lambda_g > 0.001$ does not appear to to a serious one.

A four-point numerical scheme was successfully used in [8] when the two cells are rectangular cells and the basis functions are pulse functions. Similar formulation is not found for arbitrary triangular cells. A numerical integration scheme is developed based upon the idea of dividing a cell into some smaller cells with sampling points at the center of the smaller cells as shown in Fig. 4.7. Comparison shows that the 6-term analytical scheme is computationally equivalent to the 9-point numerical scheme. The 9-point scheme generally can provide network s- parameters of reasonable accuracy when the substrate thickness is not very small ($> 1/100\lambda_g$). But, accurate determination of current distribution, especially the phase, on a structure needs a scheme of at least 25 sampling points, which is about $(25/9)^2 - 1 \approx 6.7$ times slower than the analytical scheme.

The analytical scheme is a better choice in considering stability, accuracy and efficiency.

In practical programing, 6-term curve-fitting is only used for cells that are close to each other. When the two cells are far away, fewer terms

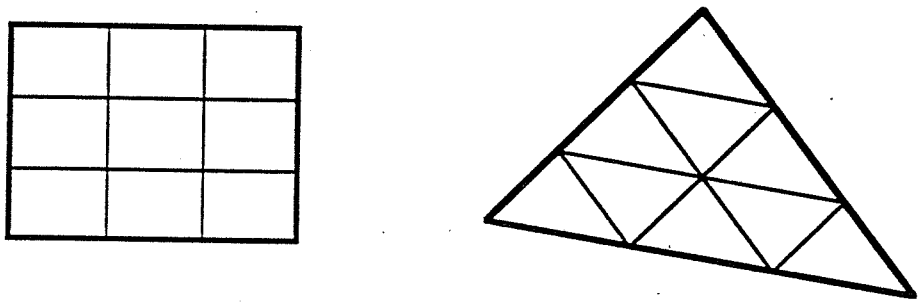

Figure 4.7: 9- point numerical integration scheme.

are used to save computational time. Also, the quadruple integrals of different combinations are evaluated simutaneously, instead one by one, to make use of the fact that they have many common terms.

The References for Chapter 4

[1] Y. L. Luke, **Integrals of Bessel functions.** McGrqw Hill Book Company, Inc., 1962

[2] A. Milton and A. S. Iren, **Handbook of mathematical functions: with formulas, graphs and mathematical tables.** New York Dover Publications , 1965.

[3] D. L. Kuipers and D. R. Timman, **Handbook of Mathematics.** Pergaman Press Ltd., pp.179-182, 1969.

[4] A. J. W. Sommerfeld, **Lectures on Theoretical Physics.** New York, Academic Press, Vol. 6 **Partial differential equations in physics,** 1956.

[5] B. L. Brim and D. C. Chang, " Accelerated numerical computation of the spatial domain dyadic Green's functions of a grounded dielectric slab," **National Science Meeting Digest,** pp. 164, Boulder,CO, Jan. 1987.

[6] B. L. Brim and D. C. Chang, " Closed-form expressions for static coupling between two coplanar polygon, " **National Science Meeting Digest,** pp. 60, Boulder, CO, Jan. 1987.

[7] S. Vijayakumar and D. E. Cormack, " An invariant imbedding method for singular integral evaluation on finite domains, " **SIAM J. Appl. Math.,** Vol. 48, No. 6, pp, 1335-1349, Dec. 1988.

[8] D. I. Wu, D. C. Chang and B. I. Brim, "Accurate numerical modeling of microstrip junctions and discontinuities," **Intern. Journal of Microwave Millimeter-wave Computer Aided Engineering,** to be published.

[9] D. C. Chang and J. X. Zheng, " Electromagnetic modeling of passive circuit elements in MMIC," **IEEE Trans. on Microwave Theory Tech.,** to be published.

CHAPTER 5

DE-EMBEDDING OF NETWORK PARAMETERS

5.1 Introduction

The bulk of the P-mesh algorithm has been discussed in Chapters 2, 3 and 4. Using the formulas, we can solve the current distribution induced on a microstrip structure by an excitation. But, the current distribution is not the final result we need. What we need are the network parameters, such as the impedance or admittance or scattering matrices. When any one set of these parameters are known, the performance of a network is defined.

In microstrip antenna problems, a current dipole is usually used to approximate the actual probe feed or edge feed [1]. Input impedance or admittance can be found once the voltage across the source dipole is computed from the solved current distribution on the patch. De-embedding in such a problem is relatively straight-forward. However, the accuracy associated with the use of a source dipole with an assumed current distribution can not be easily assessed. Alternatively, we can assume a constant electric field across a break in a microstrip structure as a "voltage source" to induce the current. Input admittance of the structure can then be obtained from the current of the gap [2,10]. Unfortunately, the admittance obtained in this manner contains a capacitance of unknown nature, due to the physical nature of a gap. This leads to the conclusion that characterizing a microstrip structure by input impedance in the case of a known current source or by input admittance in the

case of a known voltage source is not very satisfactory in any event.

One way to avoid this problem is to characterize a microstrip discontinuity by the reflection and transmission waves, or the scattering parameters on the microstrip. There are two fundamental methods of measuring S-parameters in experimental environments [3]. One is to detect the standing-wave distribution along the transmission line of a port as shown in Fig. 5.1 (slotted line technique); the other is to calculate both magnitude and phase of the incident and reflected waves by measuring power at some different positions (reflectometer).

In a CAD program, it is not straight-forward to calculate the power of the incident wave and reflected wave at a point along a strip-line since it involves evaluation of the field around the strip-line from the solved current distribution. The " slotted-line technique " is rather simple for CAD purposes since the standing-wave feature is possesed by the current distribution.

Numerical results reveal that the solved current distribution along the feed-line of a typical microstrip circuit or antenna is very close to a sinusoidal function just 0.1-0.2 waveguide wavelength away from junctions and other discontinuities [4] (see Fig. 5.2). Therefore, we can assume the current distribution as

$$I(z) = a\, e^{-\gamma z} - b\, e^{\gamma z} \tag{5.1}$$

where a and b are the incoming wave and outgoing wave in a port; $\gamma = \alpha + j\beta$ is the complex propagation constant; z is the port linear coordinate.

The process solving the a, b and γ, in turn, the S-parameters of a network is called de-embedding. Some techniques have been introduced to

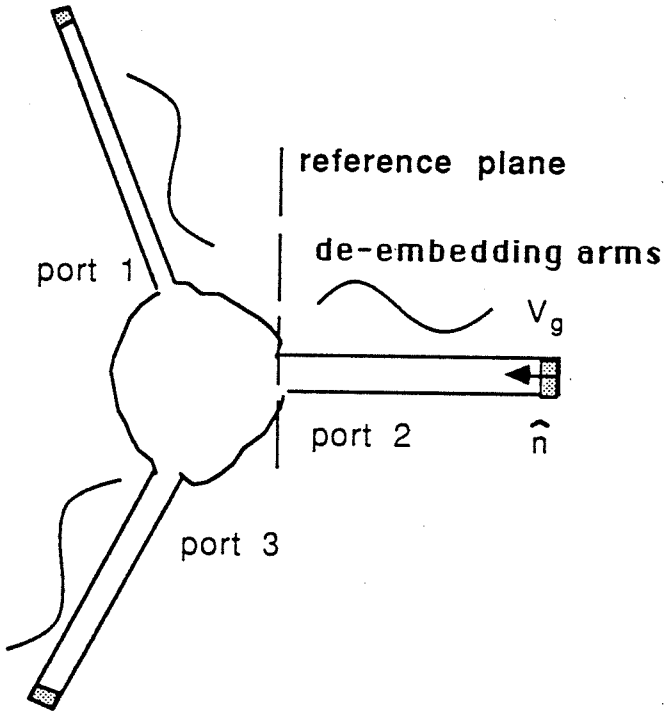

Figure 5.1: A network and its de-embedding arms.

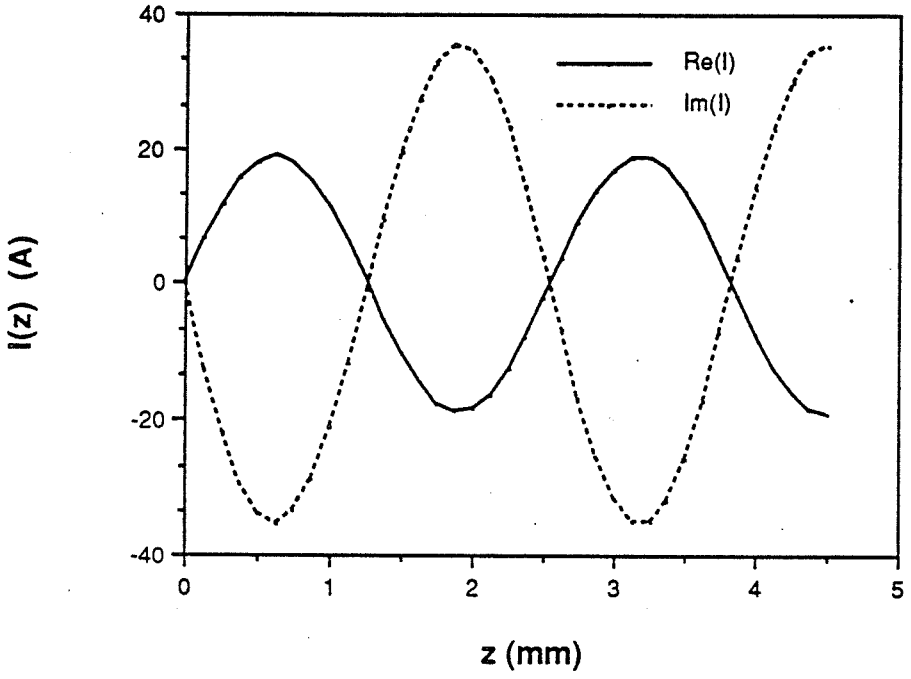

Figure 5.2: The current distribution along an open-end structure.

cast the current distribution on a de-embedding arm into the sinusoidal form of (5.1) before solving the matrix equations [5,6]. These methods require accurate determination of the wave propagation constant before the matrix solution. Three de-embedding techniques have been developed for the P-mesh algorithm. They will be discussed in Section 5.2.

For an N-port network, we need to detect the incoming wave and outgoing wave on each port in N-different excitation states. Section 5.3 will demonstrate the solution process for the S-matrix from the solved incoming waves and outgoing waves.

When a large circuit is considered, we have to break it into small pieces for efficient analysis. The solved S-parameters of each piece are then used to construct the S-matrix of the whole circuit. A general network connection algorithm will be discussed in Section 5.4.

Accuracy is the other important consideration than efficiency and versatility in developing an algorithm. The convergence characteristics of a de-embedding technique affects the accuracy of an algorithm very much. Some convergence study has been done for the P-mesh algorithm and the de-embedding techniques. An example will be provided in Section 5.5.

In the processes, we alway use a voltage gap source at the far end of the de-embedding arm of a port as shown in Fig. 5.1. In fact, the de-embedding techniques developed here only require an excitation no matter what kind of excitation it is as long as the excitation is far from de-embedding regions.

5.2 De-embedding of Incoming and Outgoing Waves and Propagation Constants of a Network

It has been mentioned that three de-embedding techniques have been developed for extraction of the incoming wave a, outgoing wave b and propagation constant γ along a microstrip. To identify them, we will call them: (1) zero-crossing method; (2) additional strip method; (3) curve-fitting method. They will be illustrated in the following subsections.

The common feature of the three de-embedding techniques is that all of them extract the standing waves and waveguide wavelength along the de-embedding arm of a port. It is also possible to solve the input impedance at a source by first defining an equivalent characteristic impedance, and then transform it back to S-parameters [10]. This technique will not be included here.

5.2.1 Zero-crossing de-embedding technique The technique can only handle lossless cases (or $\gamma = j\beta$).

In (5.1), we express the current distribution in a wave form. When we expand the exponential terms, we obtain

$$I_r(z) = A \sin[\beta(z - z_r)] \tag{5.2}$$

$$I_i(z) = B \sin[\beta(z - z_i)] \tag{5.3}$$

where A and B are the maximum values of the real part $I_r(z)$ and imaginary part $I_i(z)$ of $I(z)$.

Comparing (5.1) with (5.2) and (5.3), we obtain

$$A \sin[\beta(z - z_r)] = |a| \cos(\beta z - \theta_a) - |b| \cos(\beta z + \theta_b) \tag{5.4}$$

$$B \sin[\beta(z - z_i)] = -|a| \sin(\beta z - \theta_a) - |b| \sin(\beta z + \theta_b) \tag{5.5}$$

where

$$a = |a| e^{j\theta_a} \tag{5.6}$$

$$b = |b| e^{j\theta_b} \tag{5.7}$$

It is not difficult to find

$$|a| = \frac{1}{2}\sqrt{A^2 + B^2 + 2AB \sin[\beta(z_r - z_i)]} \tag{5.8}$$

$$\tan\theta_a = \frac{A \cos(\beta z_r) - B \sin(\beta z_i)}{-A \sin(\beta z_r) - B \cos(\beta z_i)} \tag{5.9}$$

$$|b| = \frac{1}{2}\sqrt{A^2 + B^2 - 2AB \sin[\beta(z_r - z_i)]} \tag{5.10}$$

$$\tan\theta_b = \frac{A \cos(\beta z_r) + B \sin(\beta z_i)}{A \sin(\beta z_r) - B \cos(\beta z_i)} \tag{5.11}$$

Obviously, a and b can be evaluated if the magnitude A and zero-crossing z_r of the real part, the magnitude B and zero-crossing z_i of the imaginary part of the current distribution and the wave propagation constant β are solved.

To evaluate the β, we can detect two consecutive zero-crossings of the real part and/or the imaginary part of the current. Their distance is $\lambda_g/2$. Then,

$$\beta = 2\pi/\lambda_g \tag{5.12}$$

A, B, z_r and z_i are easily obtained by matching both the real and the imaginary parts of the computed current distribution along the center of a microstrip de-embedding arm. The method was previously studied in [8] and was found to be relatively sensitive to the higher order modes from junctions and excitation regions. Typically, we need some isolation sections and the de-embedding arms require at least $1.5\,\lambda_g$ long.

The method is found to be more accurate when both I_r and I_i should be comparable.

5.2.2 Additional strip method Generally speaking, the computational effort for modeling a microstrip structure comes from two major parts. The first is the time it takes to compute the matrix elements and the so-called filling time is proportional to N_c^2, where N_c is the number of cells. The second part is from the inversion of the matrix equation and it is proportional to N_c^3. When the number of cells is less than about 1000, the filling time typically dominate the inversion time. The second portion becomes the most important part after the number of cells exceeds about 1000. For a simple junction, bend or resonator problem, the number of cells is generally much less than 100.

No matter which portion is the dominant part, computational time increases much faster than N_c. For a given problem, reducing the number of

cells, or even breaking a large size problem into several small size problems means saving in computational resource.

Our experience with the de-embedding technique discussed earlier is that only 10-20% of the cells are actually required in the junction region with the rest in the de-embedding arms. Generally, since we can not reduce the number of cells in a junction region without sacrifiing accuracy, the question becomes whether we can shorten the length of a de-embedding arm.

We know from (5.1) that we can solve a and b by detecting the current distribution at two or more different points from the least square curve-fitting algorithm when the γ is known. An alternative to the first method is then to introduce an additional strip of sufficient length and use it to determine the waveguide wavelength λ_g using the zero-crossing method. The real part of γ is obtained by comparing the a and b solved at two different positions. In this way, only a de-embedding arm of about $0.5\lambda_g$ is needed to attach to each port of a network.

5.2.3 Curve-fitting technique A curve-fitting technique has been developed in [8], in which the current distribution on a long section of a de-embedding arm is curve-fitted using a least-square algorithm. But, it is noticed that there are only three complex unknowns in (5.1) — a, b and γ. These unknowns in principle can be determined analytically if we sample the current values at three equally spaced points. Assuming the separation of two consecutive points of the three is z_0, we obtain

$$z = -z_0 \; : \; I_1 = a\, e^{\gamma z_0} - b\, e^{-\gamma z_0} \tag{5.13}$$

$$z = 0 : I_2 = a - b \tag{5.14}$$

$$z = z_0 : I_3 = a\,e^{-\gamma z_0} - b\,e^{\gamma z_0} \tag{5.15}$$

Summation of (5.13) and (5.15) yields

$$2\,(a - b)\cosh(\gamma z_0) = (I_1 + I_3) \tag{5.16}$$

Substituting (5.14) into (5.16) gives

$$\cosh(\gamma z_0) = \frac{I_1 + I_3}{2\,I_2} \tag{5.17}$$

A unique γ can be solved from (5.17) as long as $\beta z_0 < \frac{\pi}{2}$. Then, the incident and reflected wave can be obtained from either two of (5.13), (5.14) and (5.15) provided we avoid the situation where $|I_2| << |I_1|$ and $|I_3|$. This technique is in general more efficient than the first two methods.

5.3 Multi-Port Network De-embedding

Obviously, the process discussed in Section 5.2 can be directly used to give the reflection coefficient of a one-port network. For an N-port network problem, however, we have to provide N different excitation states for the network and detect the a, b and γ for each port in each state in order to extract the S-matrix.

Using a_i^j and b_i^j to denote the incoming wave and outgoing wave at port i in the j-th state. We have

$$b_i^j = \sum_{k=1}^{N} S_{i,k}\,a_k^j \;;\; i,j = 1,2,...,N. \tag{5.18}$$

We have N^2 equations and N^2 unknowns — $S_{i,k}, i, k = 1, 2, ..., N$. It is a linear equation and alway has unique solution as long as the N-number of states are linear independent. In fact, (5.18) can be reduced to N-number of $N \times N$-matrix equations different only in the right-hand sides.

It should be noted that (5.18) works only when the N-ports have the same transverse geometry. When the ports don't have the same transverse geometry, we have to do the following process

$$S'_{i,j} = \sqrt{S_{i,j}\, S_{j,i}} \tag{5.19}$$

The reason is that the solution of (5.18) is the pre-normalized S-matrix. Generally, normalization involves the characteristic impedances of the ports. The need to define a characteristic impedance, however, can be avoided by invoking the condition $S'_{i,j} = S'_{j,i}$ for passive and isotropic networks.

5.4 A General Network Connection Algorithm

Network connection formulas can be found in many books [9]. Here, a general network connection formulation will be introduced. The most important features for this algorithm are its simpleness and its application in network synthesis.

To simplify our discussion, we will consider an N-port network $[S]$ with its i-th port and j-th port connected to a 2-port network $[S^c]$ (see Fig. 5.3). More complicated connections can be done in the same way.

The S-matrices of the N-port network and the two-port connection network are given by

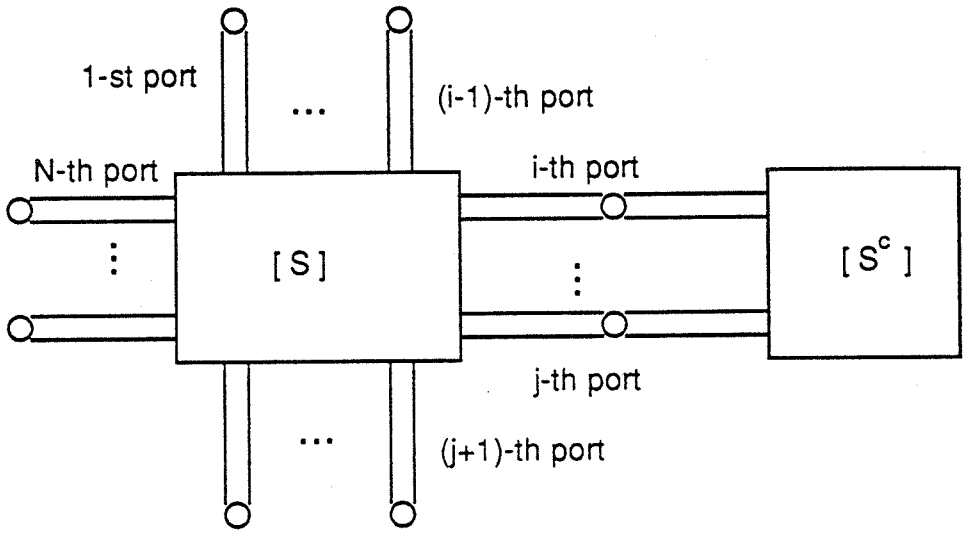

Figure 5.3: A network connection.

$$[S] = \begin{bmatrix} S_{1,1} & S_{1,2} & \cdots & S_{1,i} & \cdots & S_{1,j} & \cdots & S_{1,N} \\ S_{2,1} & S_{2,2} & \cdots & S_{2,i} & \cdots & S_{2,j} & \cdots & S_{2,N} \\ \vdots & \vdots & \ddots & \vdots & \ddots & \vdots & \ddots & \vdots \\ S_{i,1} & S_{i,2} & \cdots & S_{i,i} & \cdots & S_{i,j} & \cdots & S_{i,N} \\ \vdots & \vdots & \ddots & \vdots & \ddots & \vdots & \ddots & \vdots \\ S_{j,1} & S_{j,2} & \cdots & S_{j,i} & \cdots & S_{j,j} & \cdots & S_{j,N} \\ \vdots & \vdots & \ddots & \vdots & \ddots & \vdots & \ddots & \vdots \\ S_{N,1} & S_{N,2} & \cdots & S_{N,i} & \cdots & S_{N,j} & \cdots & S_{N,N} \end{bmatrix} \tag{5.20}$$

$$[S^c] = \begin{bmatrix} S^c_{i,i} & S^c_{i,j} \\ S^c_{j,i} & S^c_{j,j} \end{bmatrix} \tag{5.21}$$

We can write

$$[b] = [S][a] \tag{5.22}$$

where $[a]$ and $[b]$ are the incoming wave and outgoing wave vectors.

We still know

$$\begin{bmatrix} a_i \\ a_j \end{bmatrix} = [S^c] \begin{bmatrix} b_i \\ b_j \end{bmatrix} \tag{5.23}$$

We can put (5.23) into (5.20) to get the new S-matrix. For such a simple connection, the above process is easily done. But, it is very sophisticated for complicated connections such as $[S^c]$ is a multi-port network and the connection is among several big networks. It is very important to find an easy way to simplify the process.

Let's re-write (5.23) in a global form.

$$\begin{bmatrix} 0 & 0 & \dots & a_i & \dots & a_j & \dots & 0 \end{bmatrix}^t = [S^c]_g\,[b] \tag{5.24}$$

where the superscript t means transpose; $[S^c]_g$ is the global form of the connection matrix,

$$[S^c]_g = \begin{bmatrix} 0 & 0 & \dots & 0 & \dots & 0 & \dots & 0 \\ 0 & 0 & \dots & 0 & \dots & 0 & \dots & 0 \\ \vdots & \vdots & \ddots & \vdots & \ddots & \vdots & \ddots & \vdots \\ 0 & 0 & \dots & S^c_{i,i} & \dots & S^c_{i,j} & \dots & 0 \\ \vdots & \vdots & \ddots & \vdots & \ddots & \vdots & \ddots & \vdots \\ 0 & 0 & \dots & S^c_{j,i} & \dots & S^c_{j,j} & \dots & 0 \\ \vdots & \vdots & \ddots & \vdots & \ddots & \vdots & \ddots & \vdots \\ 0 & 0 & \dots & 0 & \dots & 0 & \dots & 0 \end{bmatrix} \tag{5.25}$$

If we fill the zeros on the left-hand side of (5.24), we have to add the corresponding elements in the right-hand side. The process yields

$$[a] = [S^c]_g\,[b] + [T]\,[a] \tag{5.26}$$

where the $[T]$ matrix is the unit matrix $[I]$ with the 1's in (i,i)-th and (j,j)-th elements replaced with 0's, or

$$[T] = \begin{bmatrix} 1 & 0 & \dots & 0 & \dots & 0 & \dots & 0 \\ 0 & 1 & \dots & 0 & \dots & 0 & \dots & 0 \\ \vdots & \vdots & \ddots & \vdots & \ddots & \vdots & \ddots & \vdots \\ 0 & 0 & \dots & 0 & \dots & 0 & \dots & 0 \\ \vdots & \vdots & \ddots & \vdots & \ddots & \vdots & \ddots & \vdots \\ 0 & 0 & \dots & 0 & \dots & 0 & \dots & 0 \\ \vdots & \vdots & \ddots & \vdots & \ddots & \vdots & \ddots & \vdots \\ 0 & 0 & \dots & 0 & \dots & 0 & \dots & 1 \end{bmatrix} \tag{5.27}$$

Substituting (5.26) into (5.22) and re-organizing the equation yield

$$[b] = [S'][a] \tag{5.28}$$

where $[S']$ is the new S-matrix,

$$[S'] = ([I] - [S][S^c]_g)^{-1}[S][T] \tag{5.29}$$

The i-th column and j-th column of $[S']$ vanish. The outgoing waves at i-th port and j-th port are, in fact, explicitly expressed in terms of the i-th row and j-th row of $[S']$ and the incoming waves at ports other than i-th port and j-th port.

Obviously, for other connections, we can just change the corresponding $[S^c]_g$ matrix in (5.25) and the $[T]$ matrix in (5.27). And the modification is alway simple no matter how complicated the connection is.

Another important feature is that the formulation can be used in network synthesis. When an $[S]$ is known, what kind of $[S^c]_g$ should we use to achieve the desired $[S']$? The problem can be solved under some conditions.

The discussion will not be included since it is beyond the subject of this thesis.

5.5 Accuracy in the P-mesh Computation

In this section, a microstrip of finite length is used to study the convergence of the P-mesh algorithm.

We have three parameters to adjust: (1) N_t — number of cells in the transverse direction; (2) N_w — number of cells per waveguide wavelength; (3) L — length of the de-embedding arms.

The longer a de-embedding arm is, the less effect the higher-order modes would have on the network parameter solution. But, a longer de-embedding arm will not necessarily yield a better result. This is because we always solve the incoming wave a and outgoing wave b in the de-embedding region and transfer them back to the network reference plane (see Fig. 5.1). When we have a longer de-embedding arm, the a and b in the de-embedding region should be more accurate, but the a and b at the reference plane will be affected more by the error in γ.

An actual grid with $N_t = 3$ is shown in Fig. 5.4. Narrower cells are used on the edge to simulate the edge condition. The magnitude and phase of the reflection coefficient Γ are shown in Fig. 5.5 as a function of frequency using different values of N_t, N_w and L, while the guided wavelength and attenuation constant are shown in Fig. 5.6. Because of the memory limitation in a workstation, the maximum number of cells used in this study is about 300. Generally speaking, a 4-digit accuracy in the complex value of Γ and γ can be achieved even for $N_t = 1$, $N_w = 20$ and $L = 0.5\lambda_g$. While we have not yet performed a more exhaustive convergence study, it is sufficent to state that the various limitations we place on the numerical integration of the Green's

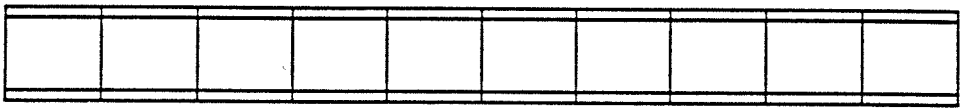

Nt = 3
Nw=20
w = 0.074 mm
h = 0.100 mm
ε_r = 12.9
σ = 4.55E7 s/m

Figure 5.4: An actual grid of an open-end structure.

functions G_e and G_m, the nature of curve-fitting them by polynomials of finite order, the size placement and aspect ratio of the cells, truncation error as well contribute to the ultimate accuracy of the P-mesh algorithm.

As mentioned in Section 4.6, the length of a de-embedding arm is adjusted to be proportional to the waveguide wavelength in order to obtain consistent accuracy. The question is whether we should keep the aspect ratio of the cell size over the substrate thickness unchanged or we should keep the number of cells in the de-embedding arm unchanged. If we keep the aspect ratio unchanged, we can reduce the error at low frequency resulting from large aspect ratio. But, we need large number of cells in a de-embedding arm, which is proportional to waveguide wavelength, at low frequency. If we keep the number of cells unchanged and change the size of the cells in a de-embedding arm in a whole frequency range, we will not have the memory problem. But, the low frequency solution will be affected by the numerical error resulting from large aspect ratio.

Furthermore, the present model relies upon the use of the equivalent surface impedance to account for the finite conductivity and finite cross-section of the metallic strips, which itself is only an approximation of the actual physical model. This leads us to conclude that the attempt to establish an error bound using a direct comparision with the measured results is indeed desired.

Radiation has been suspected to be one of the causes why transmission line theory and other equivalent methods don't work well for the analysis of typical MMIC circuits at high frequency ranges. It is found that the radiation loss is so small that we can hardly detect it. As we will demonstrate later, the metallic loss and the dynamic reactances associated with junctions and

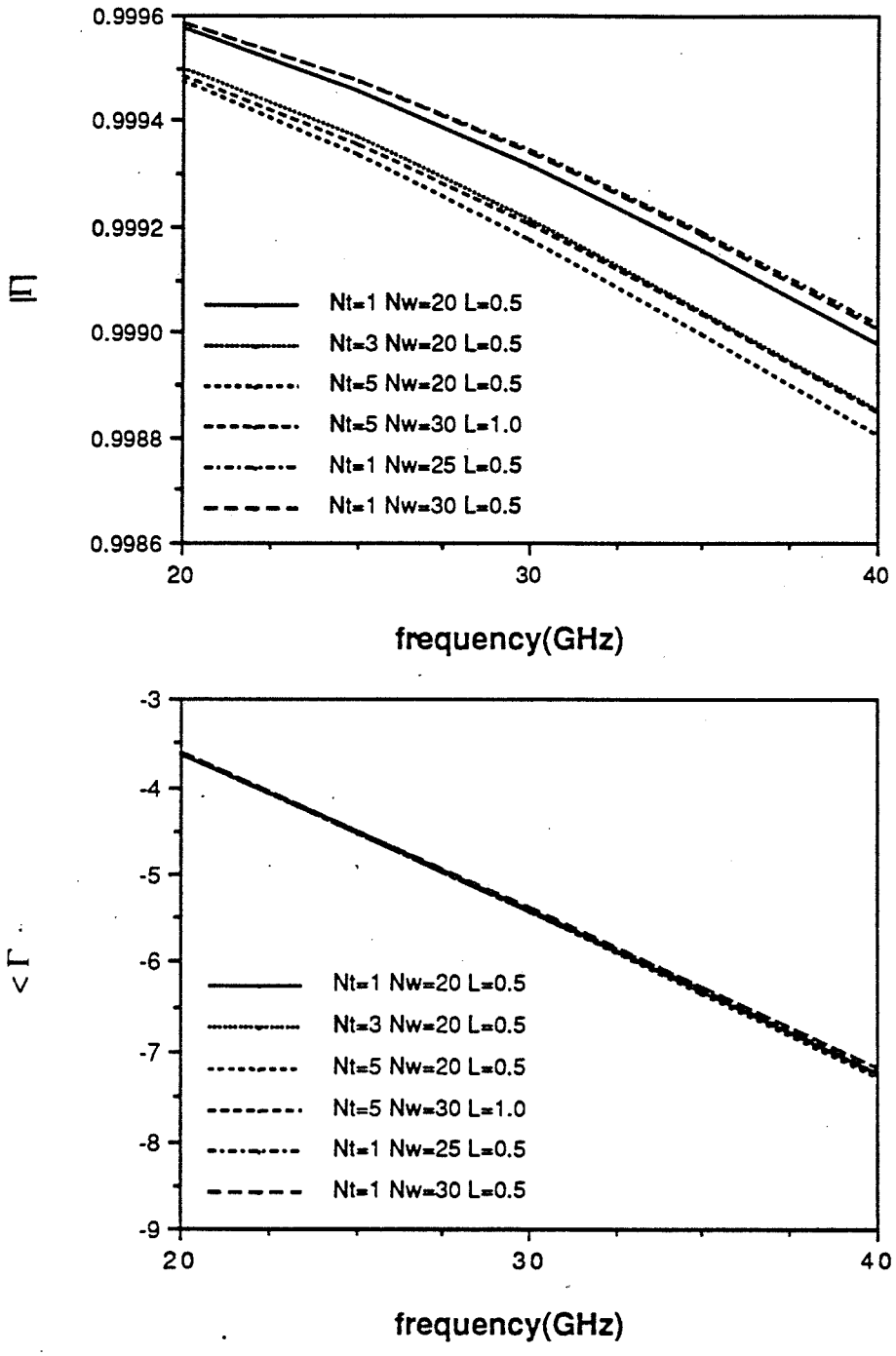

Figure 5.5. The magnitude and phase frequency response of reflection coefficient.

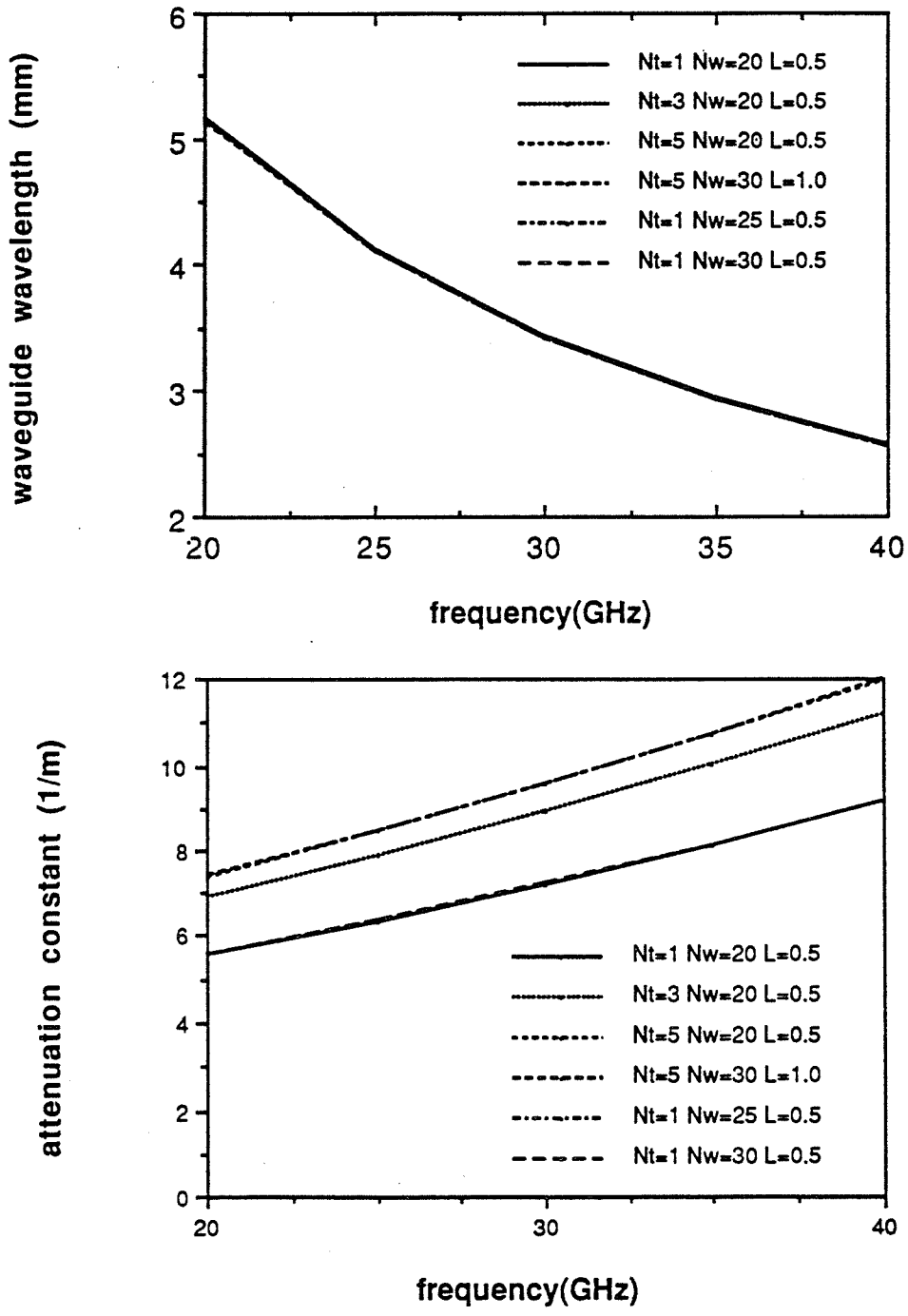

Figure 5.6. The waveguide wavelength and attenuation constant of the structure.

Table 5.1: The error-bounds of the parameters.

parameter	small value	large value
λ_g	$< 0.5\%$	$< 0.5\%$
resonant frequency	$< 0.5\%$	$< 0.5\%$
$\|S_{i,j}\|$	< 2.0 dB	$< 1.5\%$
$\angle S_{i,j}$	$< 0.2°$	$< 1.5\%$

bends play much more important roles in performance degradation at high frequencies.

For microstrip circuits of those dimensions typically used in MMICs, the effect of higher order mode is always very small just $0.1 \sim 0.2\ \lambda_g$ away from junctions. In fact, we de-embed all the parameters $0.25\lambda_g$ away from the discontinuities and very accurate results are obtaind. To give an idea of the accuracy of the P-mesh code with $N_t = 1$ and $N_w = 20$ when the strip width is less than $5\%\lambda_g$, we list the error-bounds for the main parameters in Table 5.1.

In the analysis of microstrip circuits and antennas in the following chapters, we always use $N_t = 1$ and $N_w = 20$.

The References for Chapter 5

[1] K. R. Carver and J. W. Mink, " Microstrip antenna technology, " **IEEE Trans. on Antenna Propagat.**, AP-29, pp. 2 - 24, Jan. 1981.

[2] P. B. Katehi and N. G. Alexopolous, " Frequency-dependent characteristics of microstrip discontinuities in millimeter-wave integrated circuits," **IEEE Trans. on Microwave Theory Tech.**, MTT-30, pp. 1029-1035, October 1985.

[3] G. F. Engen, **Microwave Circuit Theory and Foundation of Microwave Methology** . Priliminary draft, 1988.

[4] D. C. Chang and J. X. Zheng, " Electromagnetic modeling of passive circuit elements in MMIC," **IEEE Trans. on Microwave Theory Tech.**, to be published.

[5] W. Menzel and I. Wolff, " A method for calculating the frequency-dependent properties of microstrip discontinuities," **IEEE Trans. on Microwave Therory Tech.**, MTT-25, pp. 107-112, Feb. 1977.

[6] D. I. Wu and D. C. Chang, " Solving microstrip discontinuity problems using an embeded technique, " **Joint IEEE-AP/URSI Conference Digest**, Dallas, TX, May 1990.

[7] J. R. Mosig, "Arbitrarily shaped microstrip structures and their analysis with a mixed potential integral equation," **IEEE Trans. on Microwave Theory Tech.**, MTT-36, pp. 314-323, February 1988.

[8] D. I. Wu, D. C. Chang and B. I. Brim, "Accurate numerical modeling of microstrip junctions and discontinuities," **Intern. Journal of Microwave Millimeter-wave Computer Aided Engineering**, to be published.

[9] K. C. Gupta, **Computer-Aided Microstrip Antenna Design** . Course notes of ECEN 5004, Chapter 6, University of Colorado at Boulder, 1990.

[10] J. C. Moore, J. X. Zheng, E. F. Kuester, D. C. Chang, " De-embedding characteristic impedance and S-parameters from numerically determined

current distributions of planar junctions," to be published.

CHAPTER 6

MICROSTRIP CIRCUITS

6.1 Introduction

The most direct application of the P-mesh algorithm introduced in Chapter 2, 3 and 4 is on the analysis of microstrip circuits. Although very much has been done on modeling microstrip discontinuities [1]-[19], most work deals with simple discontinuities, such as open-end, gap, step or straight bend structures, and some with large strip width to substrate thickness ratios. In this chapter, we will be concentrated on industrial MMIC circuits and our aim is to start with relatively simple structures, and then proceed to treat the more complicated ones in order to demonstrate the importance of including not only the junction reactances but also parasitic couplings in modeling circuit behaviour in an accurate manner.

In what follows, we divide microstrip passive elements or circuits into three catagories: (1) bends and junctions in Section 6.2; (2) resonant structures in Section 6.3; (3) and composite structures in Section 6.4. The notations defined in Section 1.5 and Section 5.5 will be used.

Although the examples we use in this chapter assume no dielectric loss, it would be relatively straight-forward either by replacing the current subroutines for computing Green's functions with the one including loss, or by analytic continuation of real permittivity into a complex one where change in a physical quantity of interest, say the scattering matrix $[S]$ due to dielectric loss

can be obtained from computing its first derivative with respect to ε_r, when the structure is not close to resonances [27].

All the computations are performed in the HP/350 workstation enviroment. It takes about 10 minutes to fill the matrix and 0.5 minutes to solve the matrix for a 100 cell problem. An additional 0.7 minutes is used to evaluate the Green's functions. It has been mentioned in Chapter 5 and now is repeated here that the computational time is almost proportional to the square of cell number when we have much less than 1000 cells. When the number of cells exceeds 1000 very much, the computational time increases as N_c^3. Generally, less than 100 cells are used for most junctions, bends and other simple two-port or three-port network problems.

6.2 Microstrip Bends and Junctions

6.2.1 ϕ-bends Right-angle bends (see Fig. 6.2) have been well analyzed, but they are not often used in circuit design. A bend with an arbitrary bending angle ϕ (see Fig. 6.1), on the other hand, has not been analyzed before, even though they are much more frequently encountered. Because P-mesh can fit a structure of general shape with a combination of triangles and rectangles, computation for a ϕ-bend is, in fact, straight-forward and the results for various bending angles are shown in Fig. 6.1 for the two quantities of interest $|S_{1,1}|$ and $\angle S_{2,1}$. Because $|S_{2,1}|$ is very close to 1 and $\angle S_{1,1}$ is very close to $-90°$, they will not be shown here. Clearly, for typical MMIC dimensions, little radiation is observed for all angles and reflection from the junction is negligibly small for bending angles ϕ less than 45° even at the high end of the microwave spectrum.

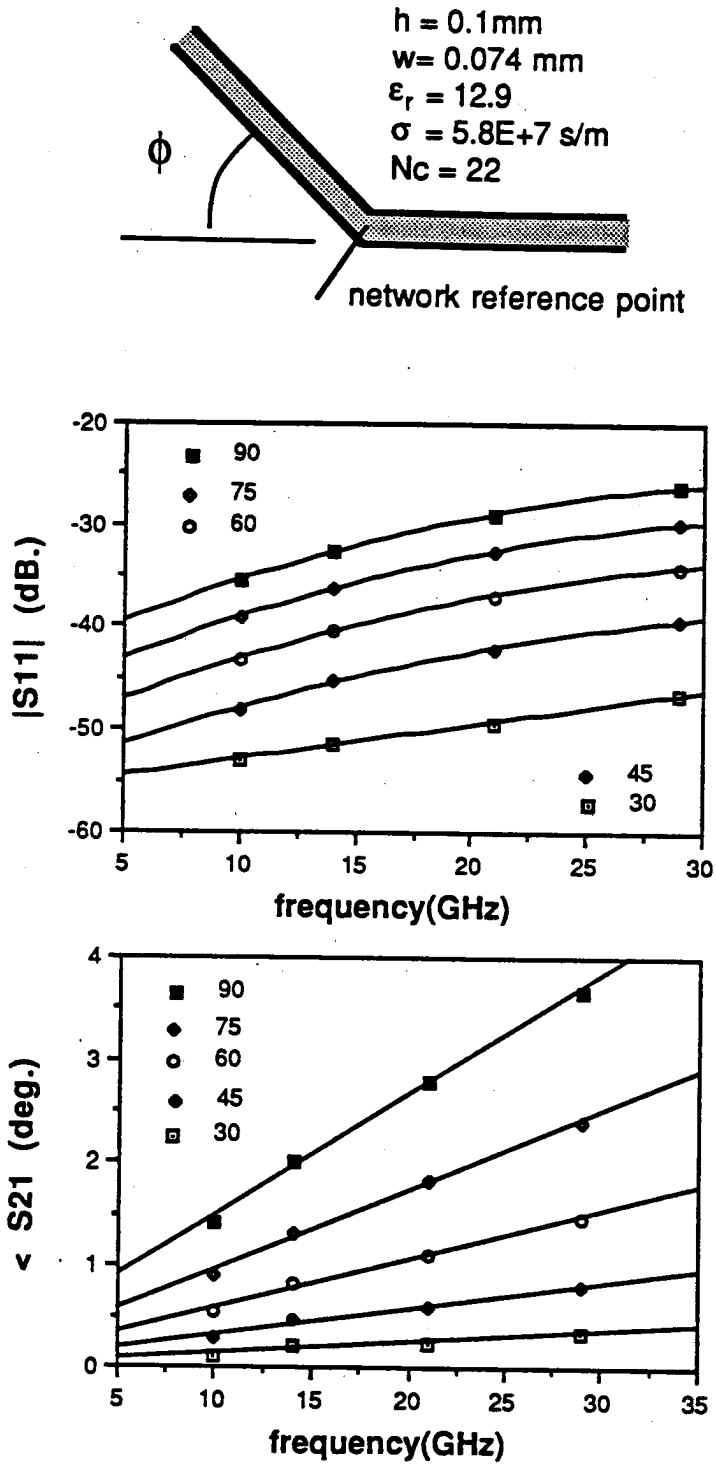

Figure 6.1: The frequency responses of a ϕ-bend.

6.2.2 Right-angle, chamfered or double-bends For many non-MMIC applications, such as those encountered in printed-circuit antenna feed networks, radiation from a right-angle bend (Fig. 6.2a) could become more significant. In such an event, a chamfered-bend (Fig. 6.2b) can significantly reduce radiation as well as reflection losses. One can further speculate that a double-bend (Fig. 6.2c) could produce even higher performance than a chamfered corner. Fig. 6.3 and 6.4 seem to confirm this and more. Reflection from a bend can be in fact optimized in a given frequency range by adjusting the length of the double-bend section. Due to the cancelation of the reflected waves from the two junctions of about $\lambda_g/4$ in separation, the total reflection $|S_{11}|$ from the junctions reaches its minimum value at 24 GHz and is below -44 dB over the entire range from 0 - 27 GHz.

6.2.3 *U*-**bends** *U*-bends are often used to achieve desirable phase shift between two ports in MMICs. Fig. 6.5 shows a typical *U*-bend structure. The comparison among our numerical result and the result obtained from the conventional transmission line theory is shown in Fig. 6.6 and 6.7. The value of $|S_{11}|$ reaches a minimum at 37 GHz due to the cancellation of reflections at the junctions, what could not be caught in the transmission line analysis.

It is noticed that accumulation of the reflection from each bend can produce noticeable resonances in the circuit (see Fig. 6.9) when three *U*-bends are cascaded together (see Fig. 6.8) to form a serpentile line structure. At resonance, the total loss, as computed from the expression $1 - |S_{1,1}|^2 - |S_{2,1}|^2$, is about 12.5% of the incident power. Part of this loss is due to finite conductivity of the strip (our calculation indicates that even at 10 GHz, the loss is still as high as 6.5%). Fig. 6.9 shows the comparison between the results of

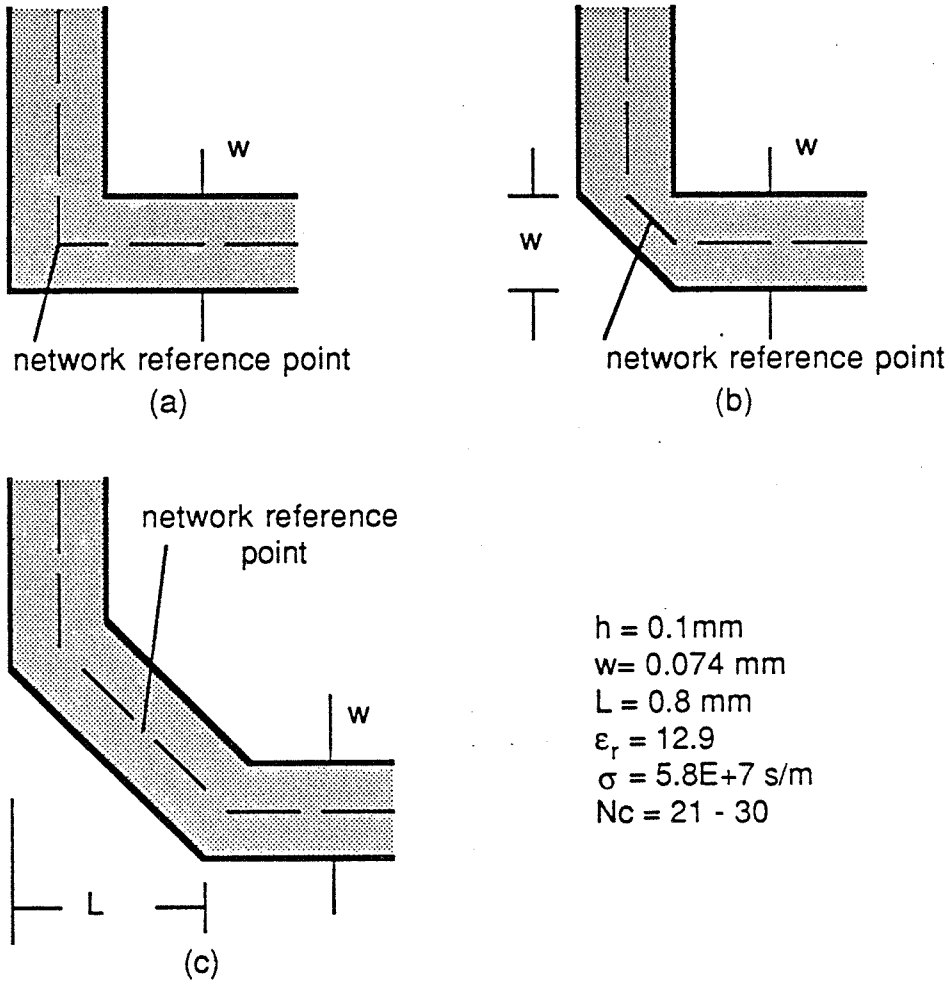

Figure 6.2. Configurations of a right-angle bend, chamfered bend and double-bend.

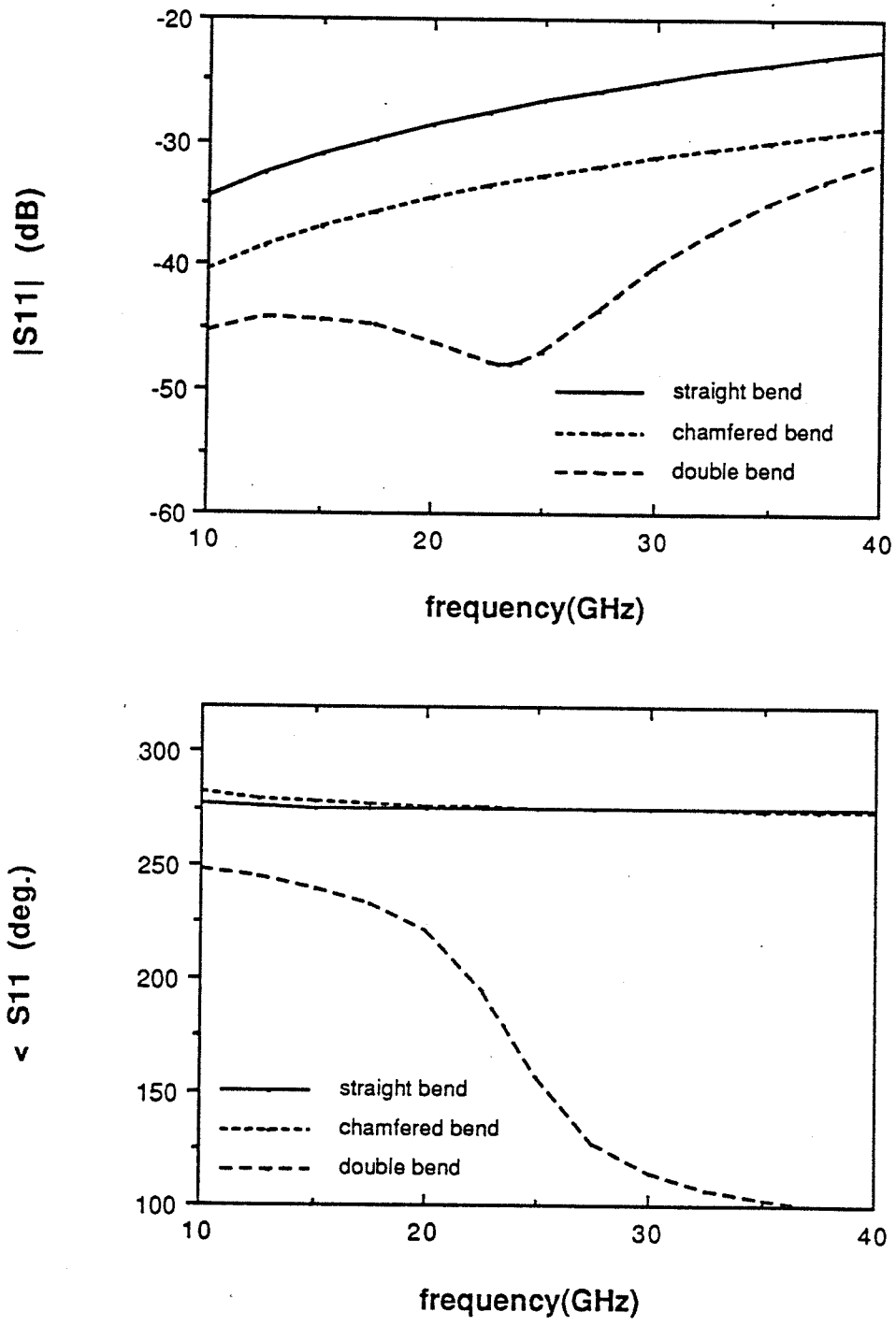

Figure 6.3. The frequency responses of S_{11} of the right-angle bend, chamfered bend and double-bend.

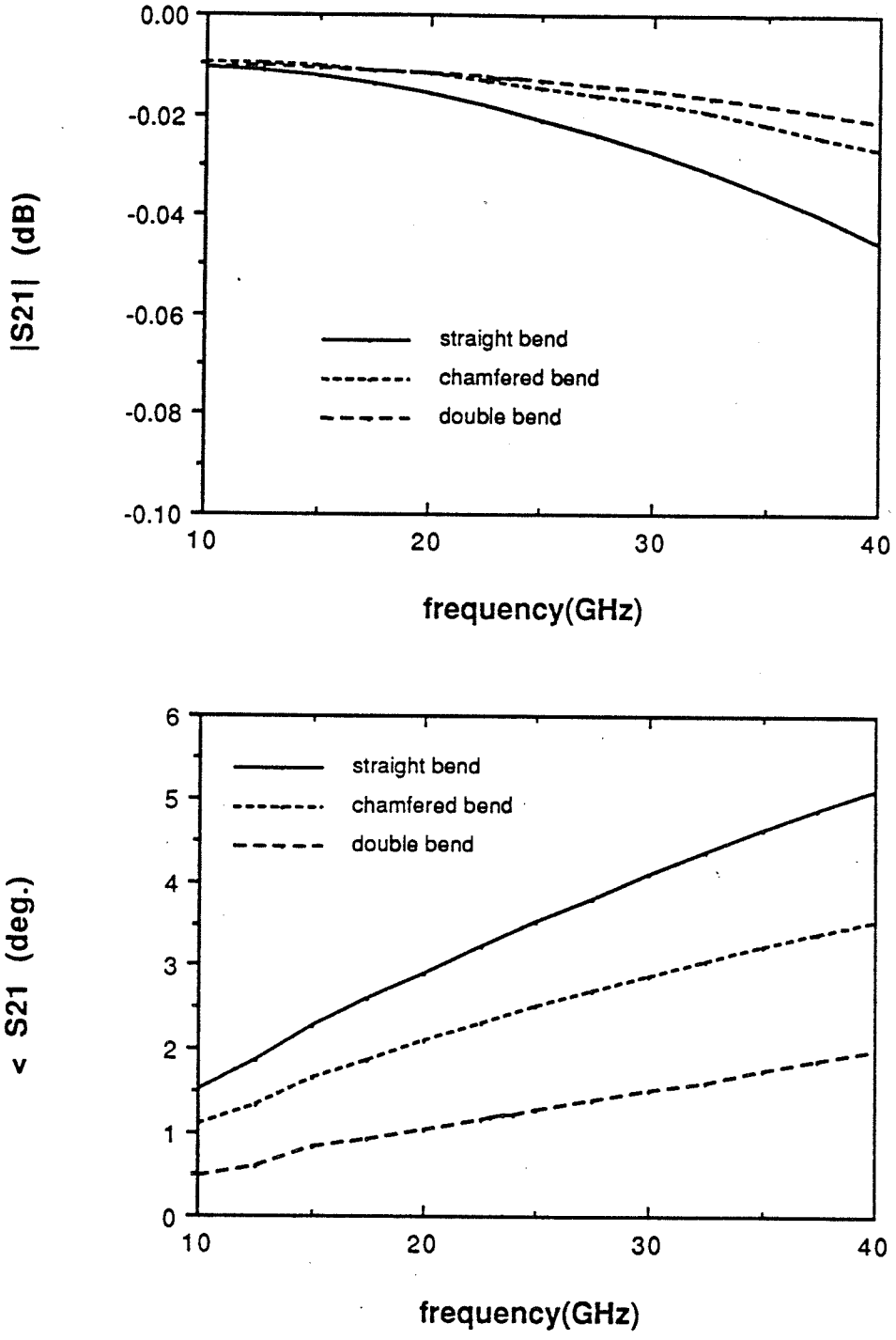

Figure 6.4. The frequency responses of S_{21} of the right-angle bend, chamfered bend and double-bend.

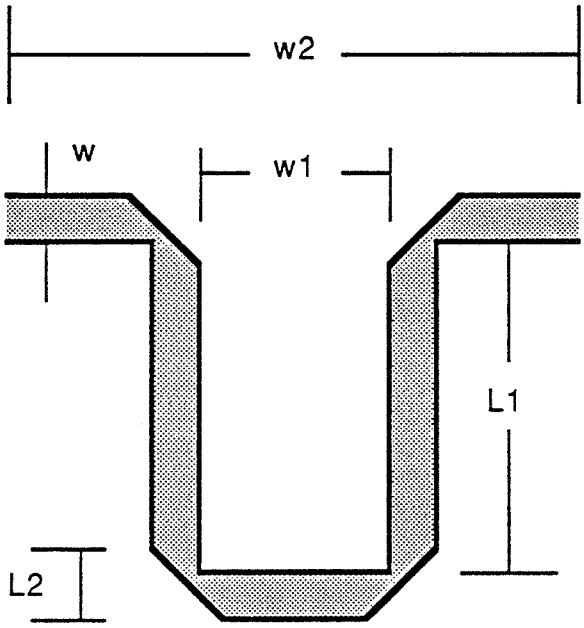

w = 0.075 mm
h = 0.1016 mm
ε_r = 12.9
σ = 4.55E7 s/m
L1 = 0.114 mm
L2 = 0.322 mm
w1 = 0.168 mm
w2 = 0.560 mm
Nc = 43

Figure 6.5: Configuration of a U - bend.

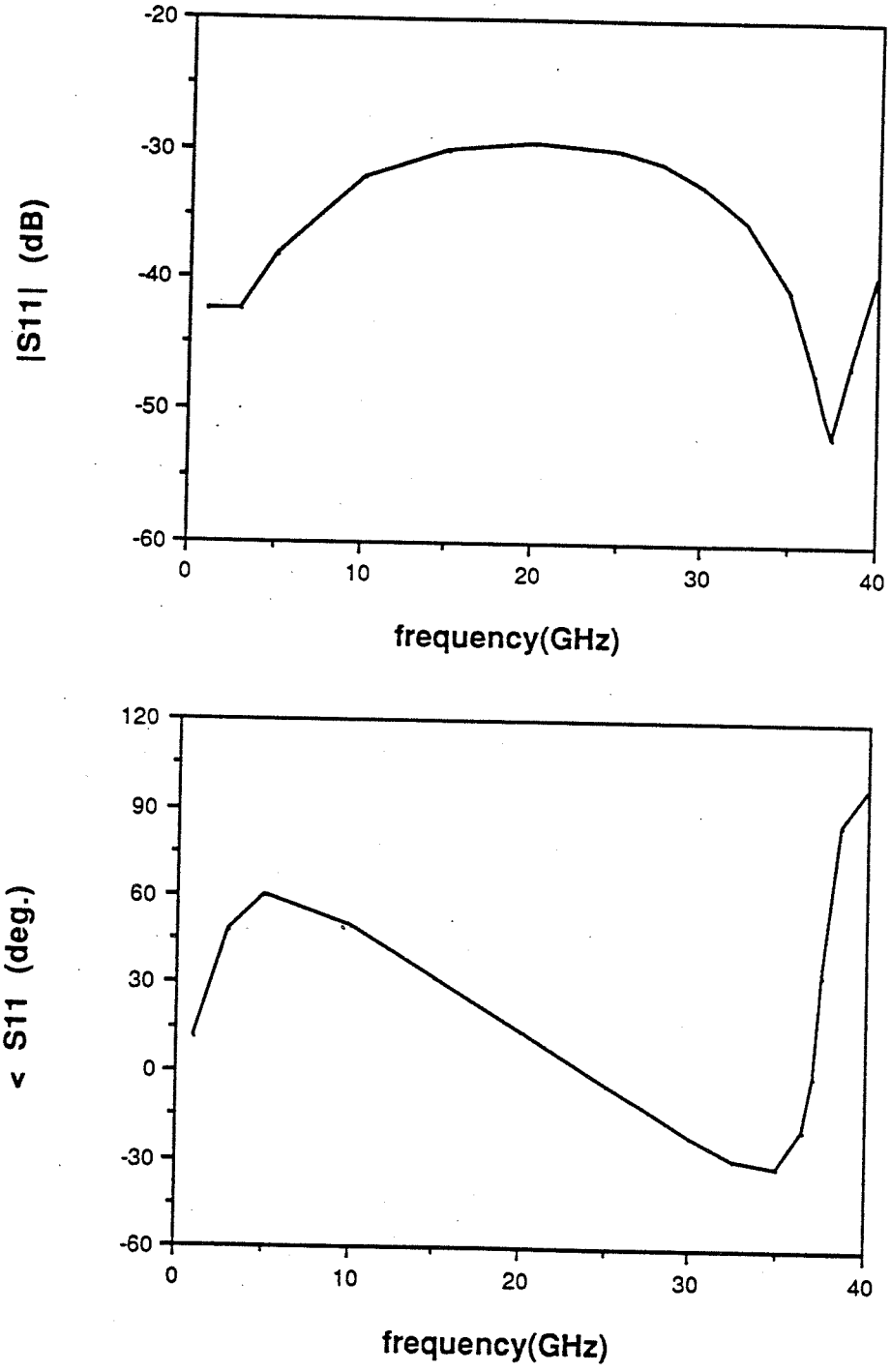

Figure 6.6: The frequency response of $S_{1,1}$ for the U - bend.

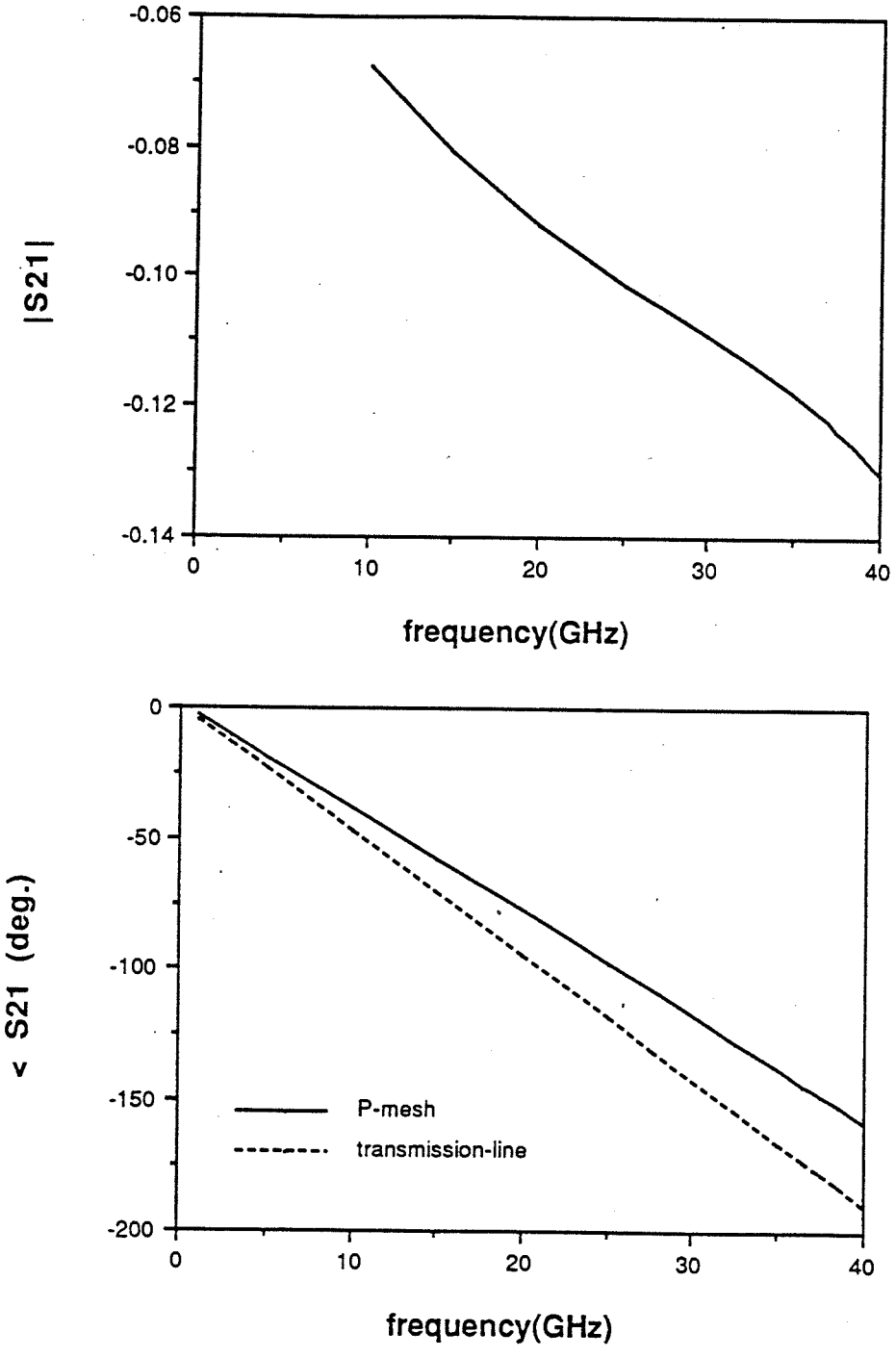

Figure 6.7: The frequency response of $S_{2,1}$ for the U - bend.

layout connection (analyzing the set of cascaded U-bends in its entirety) and network connection (analyzing one U-bend and connecting them together). The difference between them accounts for the coupling effect between the U-bends, which is very significant when the circuit is at resonance.

The above example clearly demonstrates that the reflection from bends, the metallic loss and the coupling effect among different parts of a circuit can have great impact on the performance of a MMIC circuit.

6.2.4 Y-junctions T-junctions can be handled by many theories and will not be discussed here. Fig. 6.10 shows a symmetric Y-junction. It is not surprising that we get $|S_{ii}| \approx 0.333$ and $|S_{ij}| \approx 0.667$, $i \neq j$ over the whole frequency range since very little radiation is expected. However, the reactive stored energy at the junction could in fact produce phase shift of a few degrees in $S_{1,1}$ and $S_{2,1}$, which is not expected in a typical transmission-line analysis by which $\angle S_{1,1} = 180°$ and $\angle S_{2,1} = 0°$ are predicted (Fig. 6.10). Non-symmetric Y-junctions and T-junctions can be modeled easily using the P-mesh code, as well.

6.3 Resonant Structures

6.3.1 Double-stub band-stop filter A double-stub band-stop structure shown in Fig. 6.11 was previously fabricated and measured for the purpose of determining the parasitic coupling of two parallel stubs [22]. The interesting phenomenon is that two local minima are observed in the response of $|S_{21}|$ (see Fig. 6.11). It happens even the stub separation is as large as $\lambda_g/4$. Static theory and all the commercial softwares predict only one local minimum [22]. In fact, since the two stubs are identical in length, only one minimum is expected if we break the structure into two single-stub structures

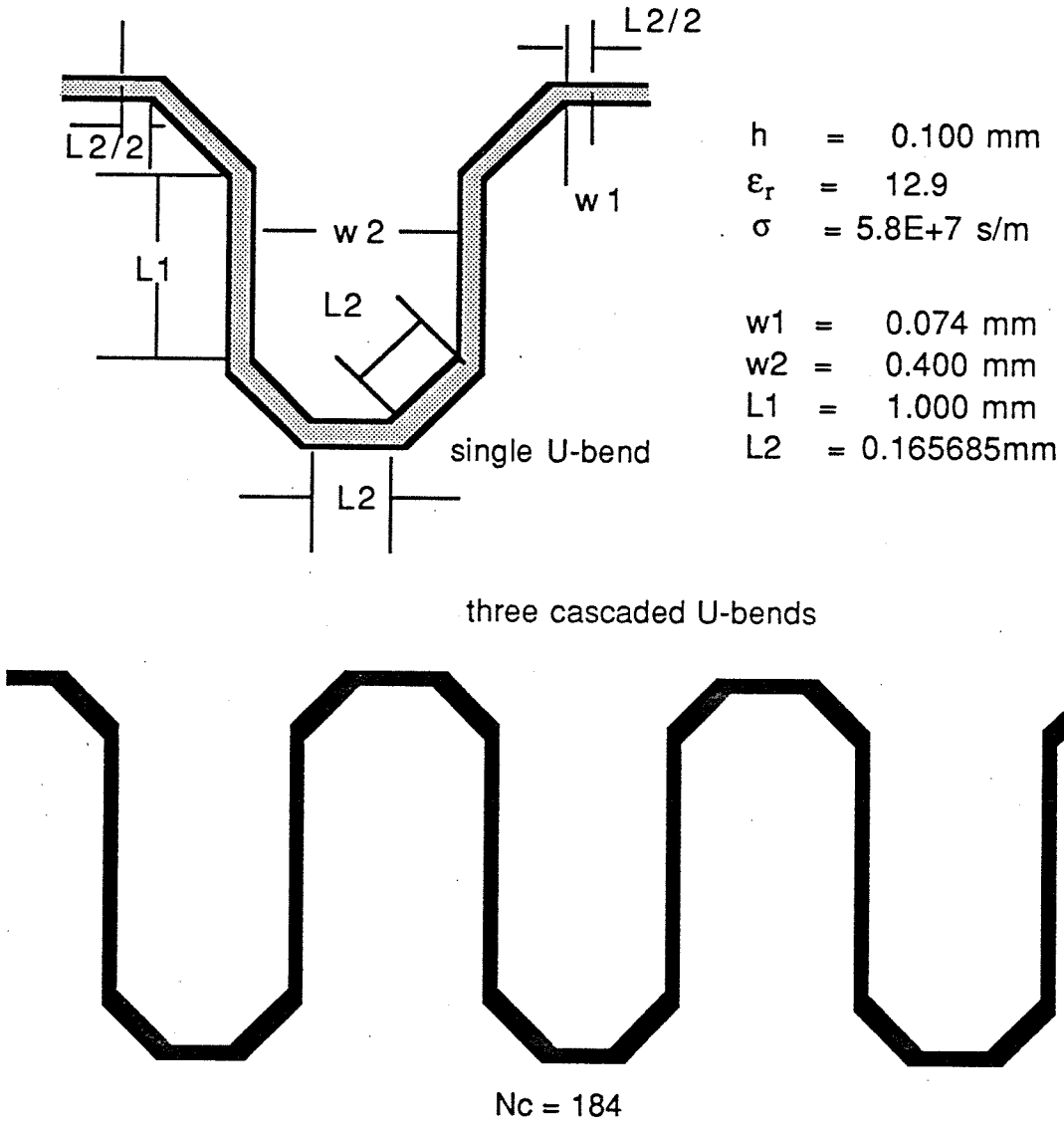

Figure 6.8: The structure of three cascaded U - bends.

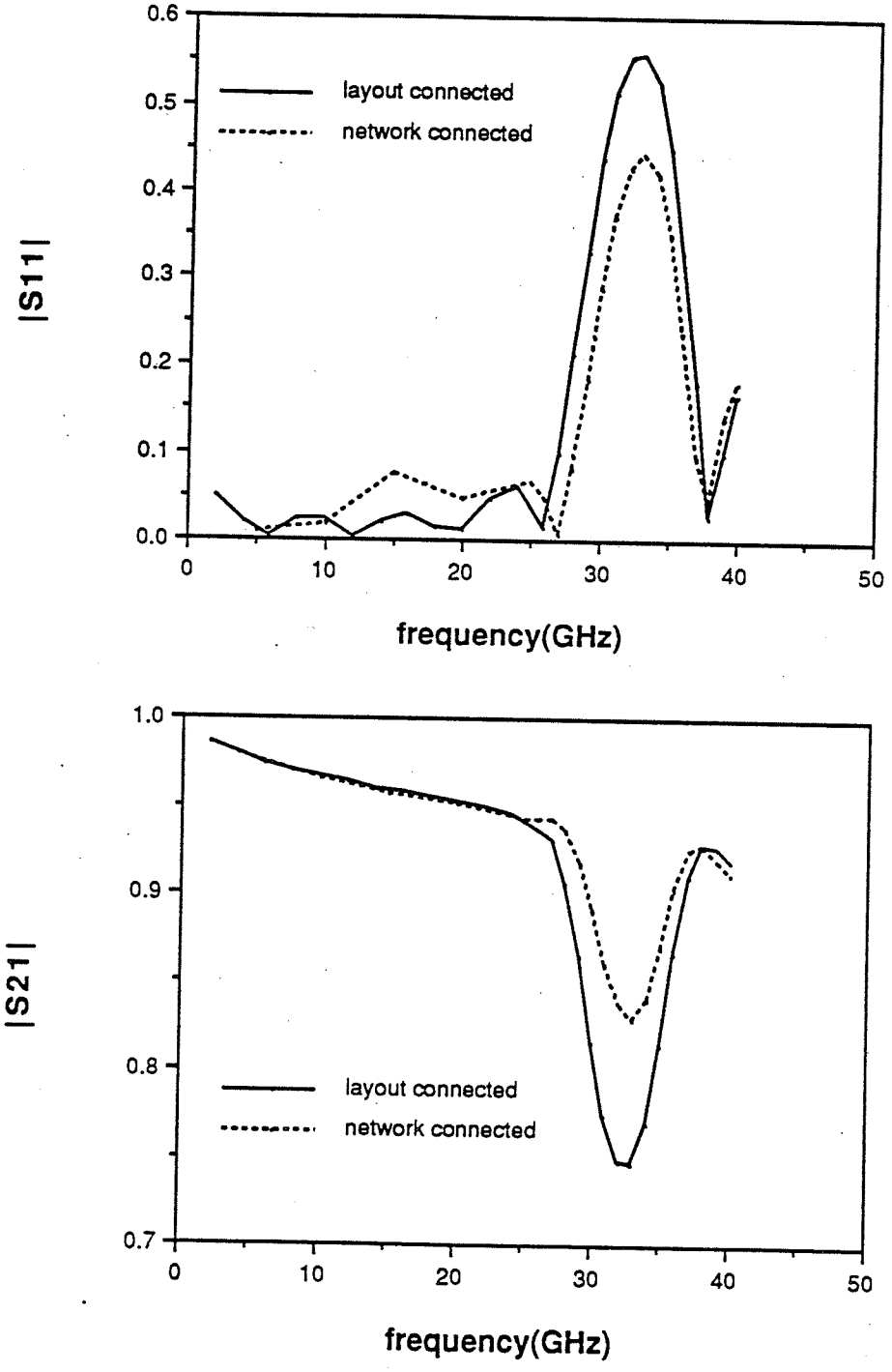

Figure 6.9: The frequency responses of the three cascaded U - bends.

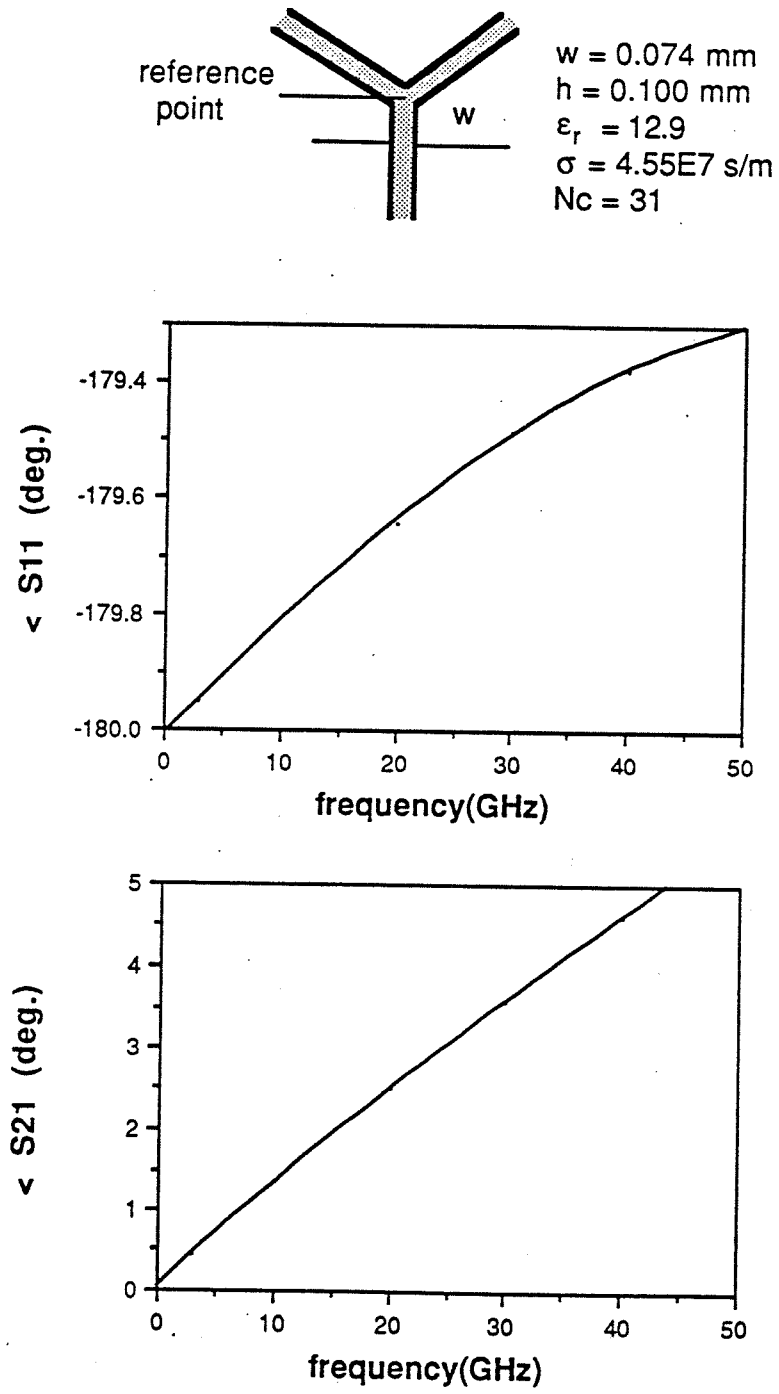

Figure 6.10: A symmetric Y-junction and its frequency responses.

and connect them without considering the coupling effect. This is indeed the situation when we use the P-mesh to simulate the two stubs individually even though radiation from the end of the stub and from the junction are included implicitly. This leads us to the conclusion that for many applications, parasitic coupling could be a major factor in limiting a designer's ability to compact the circuit layout, unless some form of circuit compensation is provided. In addition to the numerical result generated by P-mesh, also shown in Fig. 6.11 are the measured result [23] and results produced by other numerical and/or circuit analysis methods [20,24]. Although a more comprehensive test program for the validation of the P-mesh code is beyond the scope of this thesis, Fig. 6.11 nevertheless provides a good indication regarding the kind of accuracy involved.

6.3.2 A band-pass structure A band-pass structure is shown in Fig. 6.12. A high-Q resonance occurs at 24.3 GHz. Comparison between the perfect conductor case and the actual copper strip case is also available in Fig. 6.12. Surprisingly, 37% of the power is lost at the resonant frequency for the copper strip case, whereas only $1 - (|S_{11}|^2 + |S_{21}|^2) = 1\%$ is observed in the case of a perfect conductor. It means that the radiation loss for this structure is about 1%. This again confirms the notion that for circuit dimensions typically encountered in MMICs, metallic loss often dominates, and by comparision, radiation loss usually is very insignificant. It is also noticed that, even though the loss in the copper strip case is much higher than that in the perfect conductor case, the bandwidth doesn't change very much, however.

6.4 Composite Structures

Directional couplers are often used in detecting signals from one stripline to another. The structure of a directional coupler is shown in Fig. 6.13

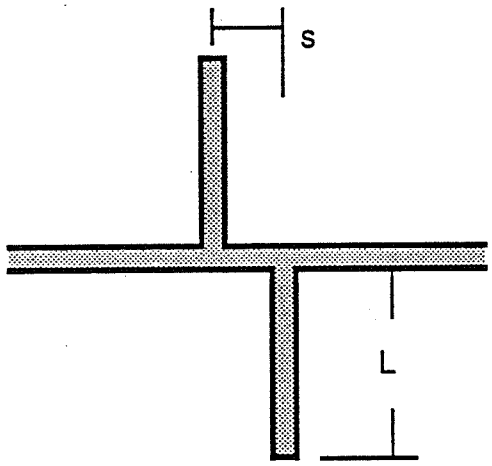

w = 0.1219 mm
h = 0.127 mm
ε_r = 9.9
σ = 4.55E7 s/m
L = 2.921 mm
s = 0.7569 mm
Nc = 35

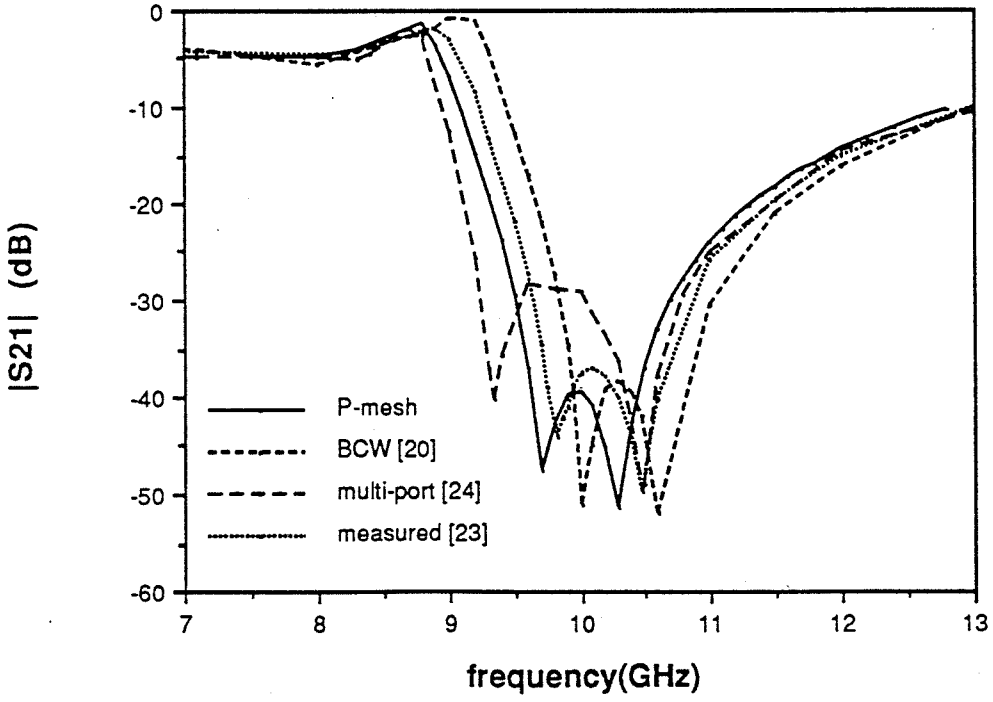

Figure 6.11: A double-stub structure and its frequency response.

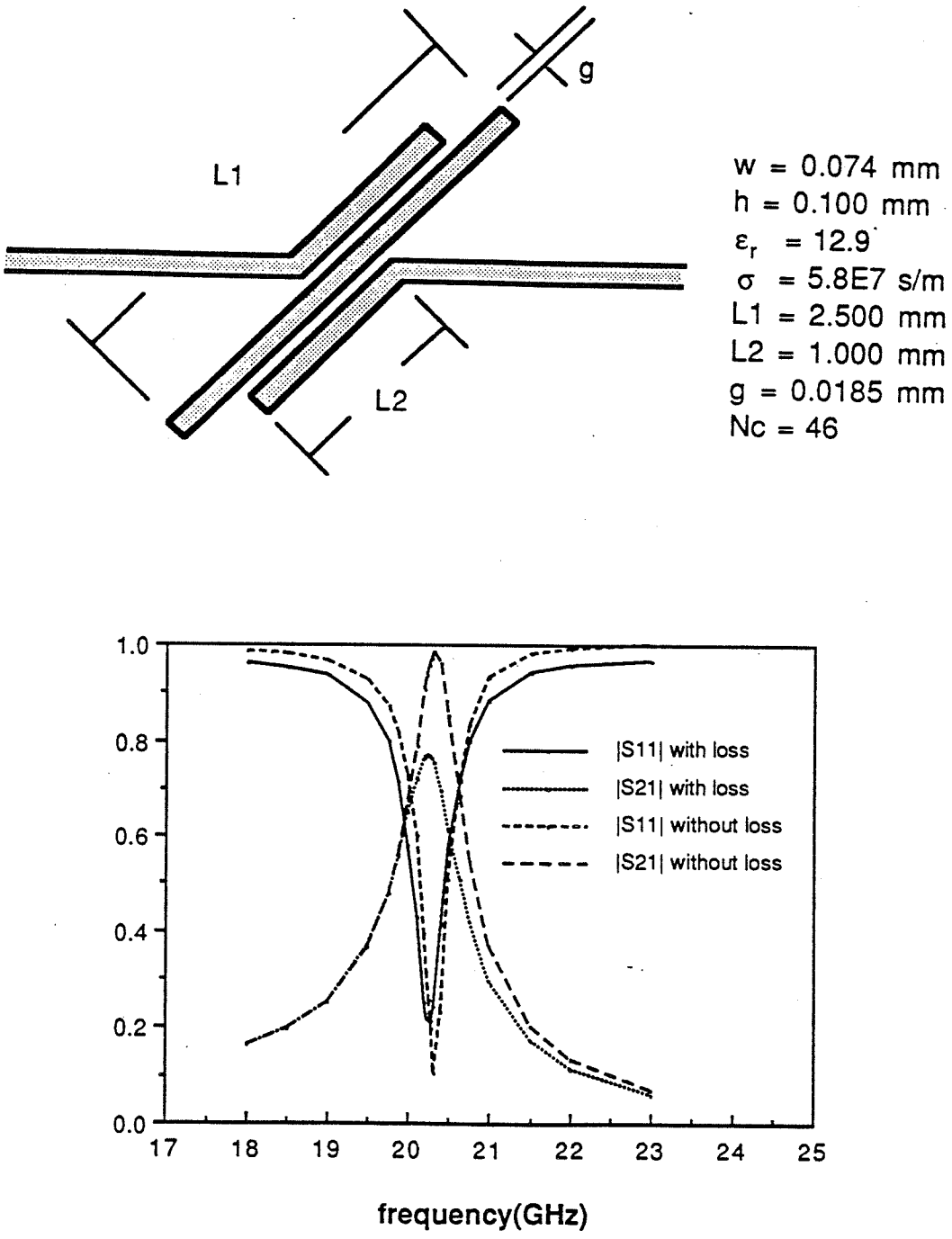

Figure 6.12: A band-pass structure and its frequency responses.

for two sets of parameters. As shown in Fig. 6.14, for the coupler with a longer length, up to -10dB of signal can be transmitted from port 1 to port 3, while the transmission to port 4 is always below -20dB. Almost the same $|S_{31}|$ is obtained when we reduce the gap width from 0.074mm to 0.020mm. Instead, the $|S_{11}|$ and $|S_{41}|$ increase a lot. One way to increase $|S_{31}|$ is to increase the strip width in the coupling sections to create a stronger resonant-type coupler. However, both the directional property and bandwidth will be reduced. Fig. 6.15, on the other hand, shows that a very short coupler can achieve significant coupling and reasonable isolation. The direction of the coupler, is no longer from 1 to 3, but from 1 to 4.

6.5 Conclusions

We have demonstrated some applications of P-mesh algorithm in analyzing microstrip circuit discontinuities. They are far from exhaustive. Two additional structures are shown: one represents an inter-digitated capacitor with 6 fingers (Fig. 6.16 and 6.17), and the other is a five-port junction (Fig. 6.18 - 6.20). These figures serve to demonstrate that provided the memory and computation time are allowed for, P-mesh can in fact simulate circuit configurations of more complex nature. In the next chapter, the use of P-mesh as a numerical test bed for new microstrip antenna structures will be discussed in some detail. Insofar as MMICs are concerned, the following conclusions appear to be in order:

(a) Radiation is negligible;

(b) Coupling between elements may significantly alter the circuit behaviour of a passive MMIC element.

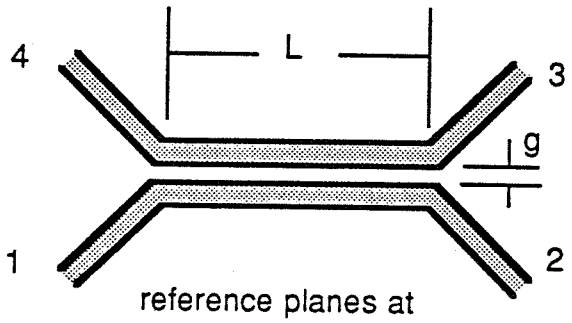

A long directional coupler:

w = 0.074 mm
h = 0.100 mm
L = 4.000 mm
g = 0.074 mm
ε_r = 12.9
σ = 5.8E7 s/m
Nc = 84

A short directional coupler:

w = 0.0254 mm
h = 0.1524 mm
L = 1.524 mm
g = 0.010922 mm
ε_r = 12.9
σ = 1.5E7 s/m
Nc = 68

Figure 6.13: Directional couplers.

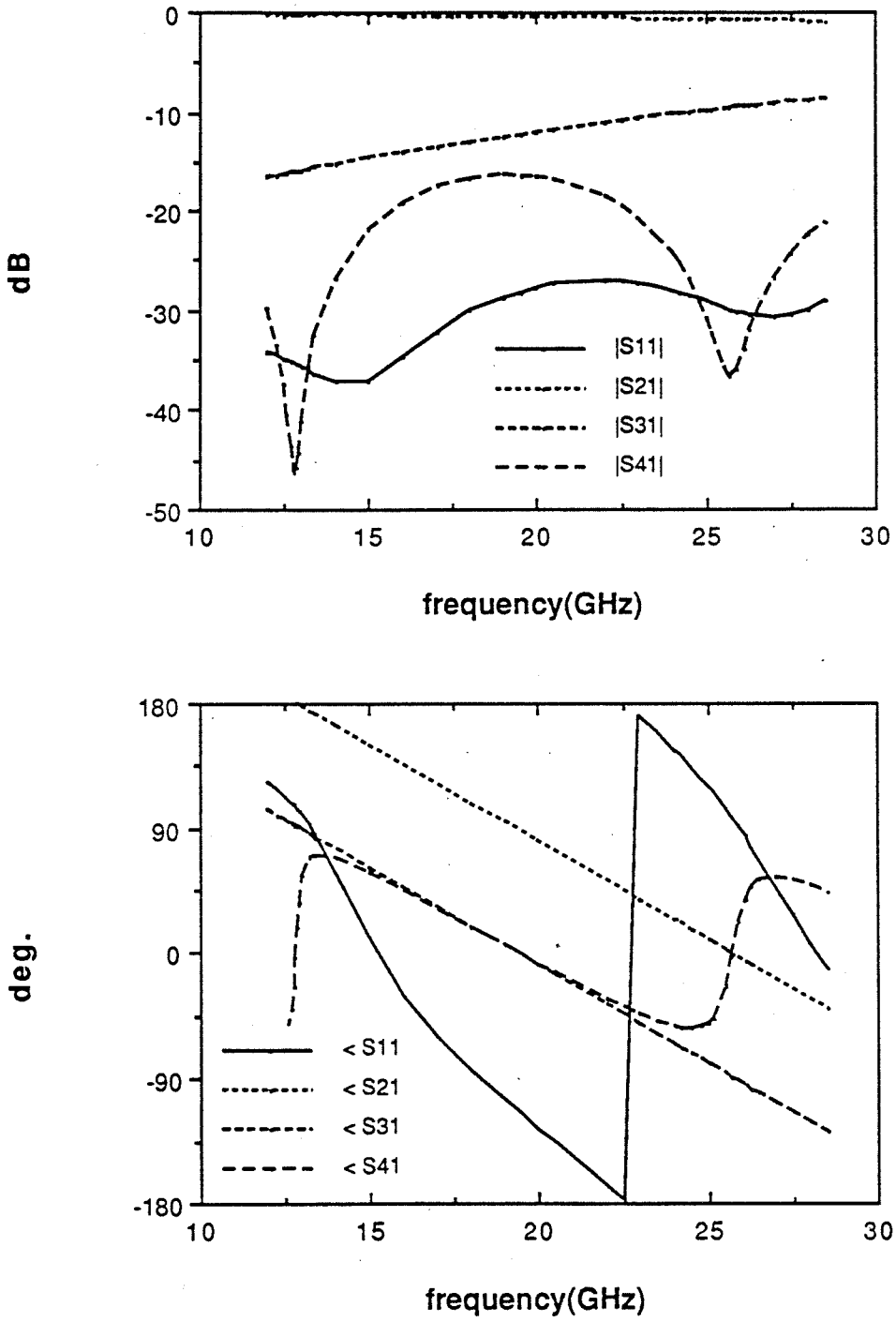

Figure 6.14: The frequency responses of the long coupler.

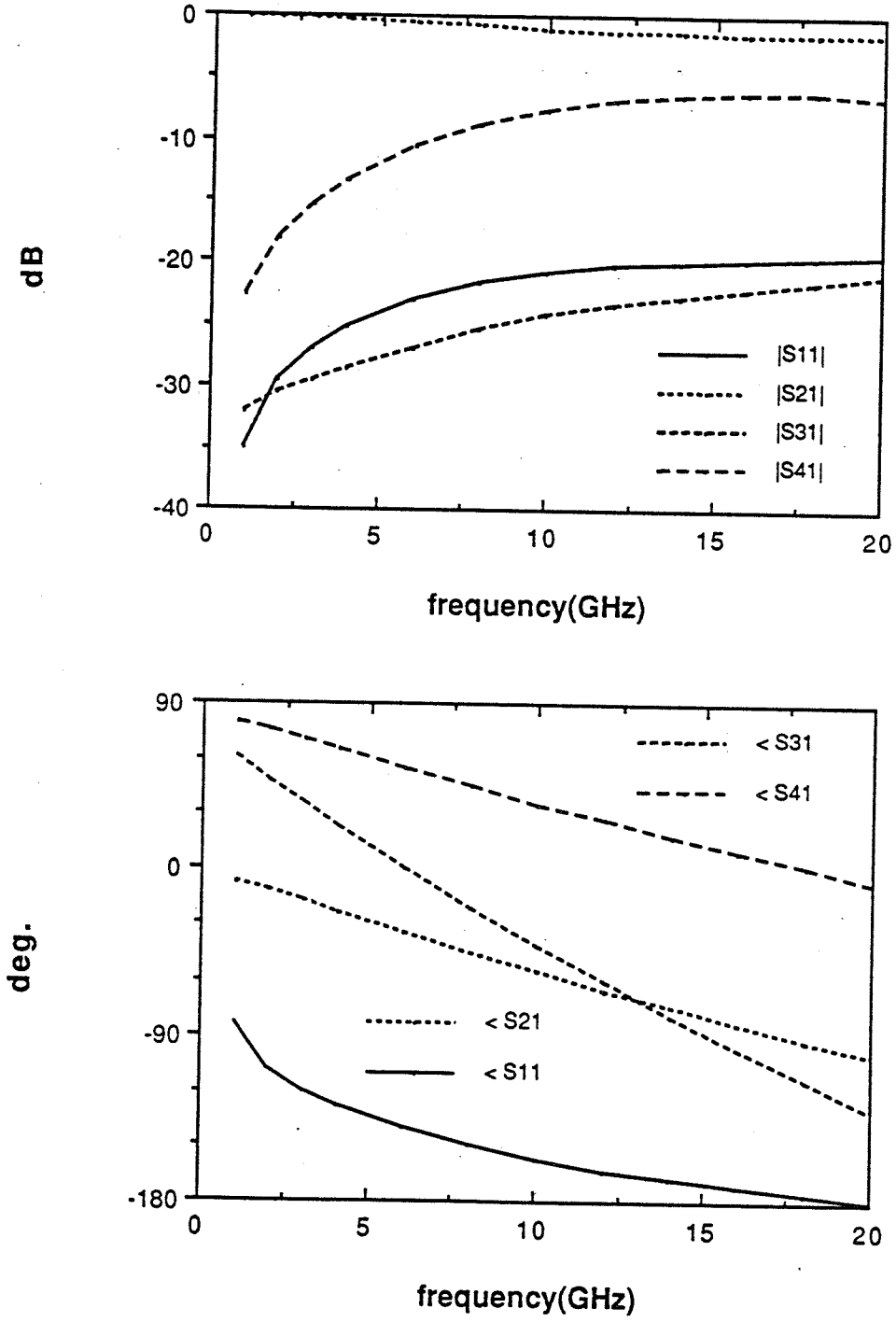

Figure 6.15: The frequency responses of the short coupler.

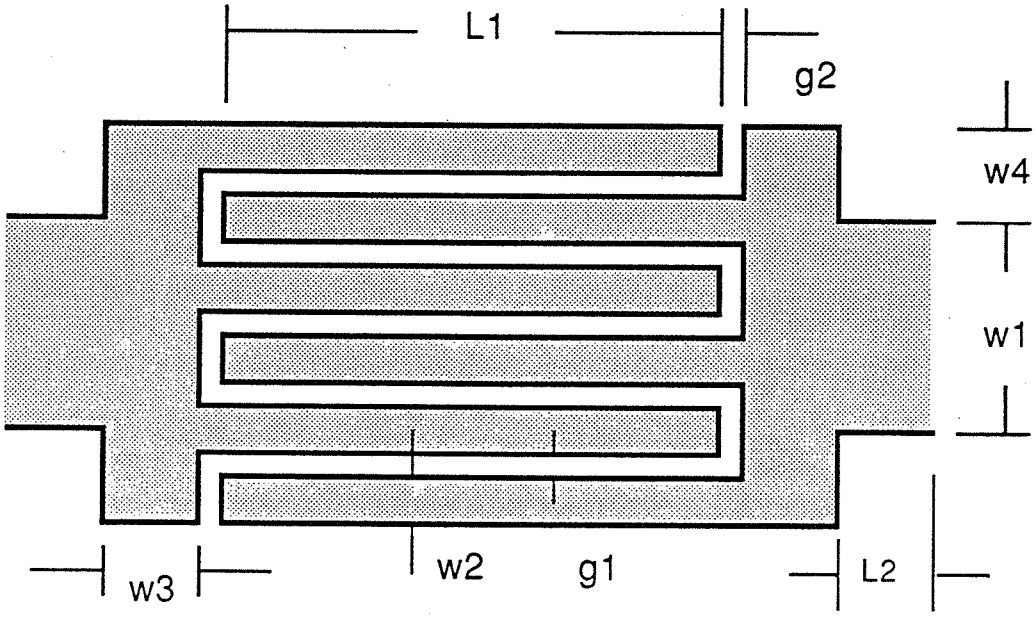

h = 0.100 mm
ε_r = 12.9
σ = 4.55E7 (s/m)
L1 = 0.260 mm
L2 = 0.037 mm
w1= 0.050 mm
w2= 0.015 mm
w3= 0.050 mm
w4= 0.0325mm
g1 = 0.005 mm
g2 = 0.017 mm
Nc = 176

Figure 6.16: The configuration of an inter-digitated capacitor.

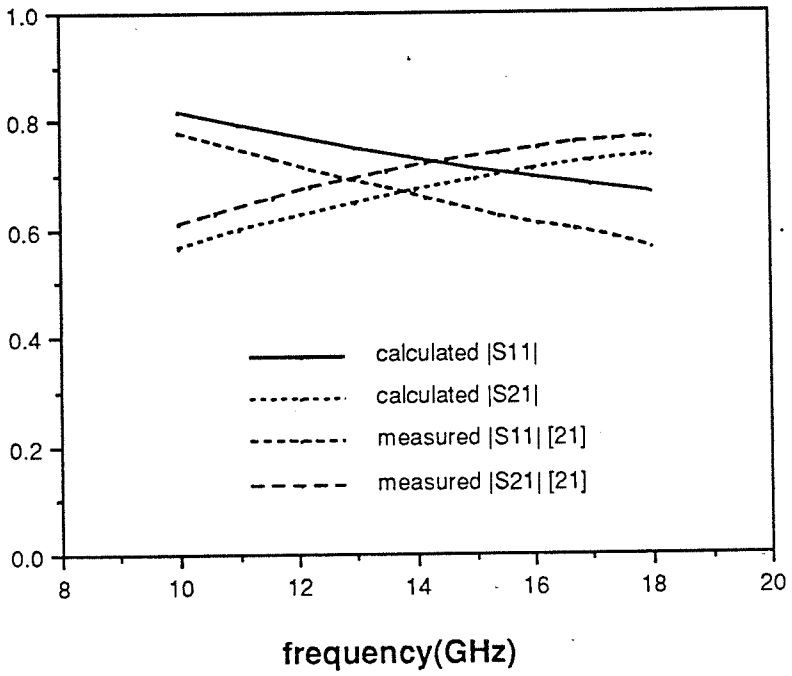

Figure 6.17. The magnitude frequency responses of the inter-digitated capacitor.

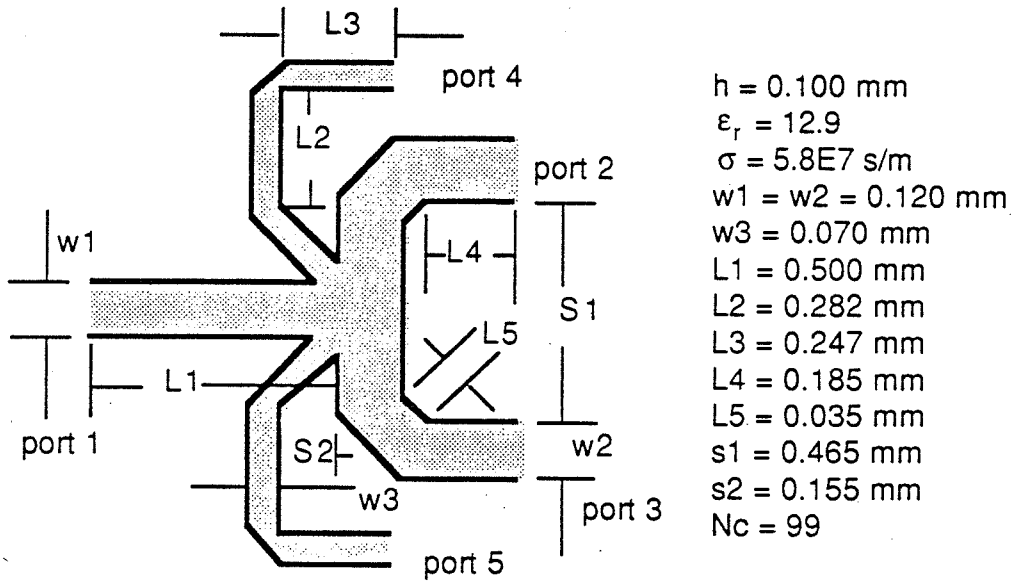

Figure 6.18: A complex matching network.

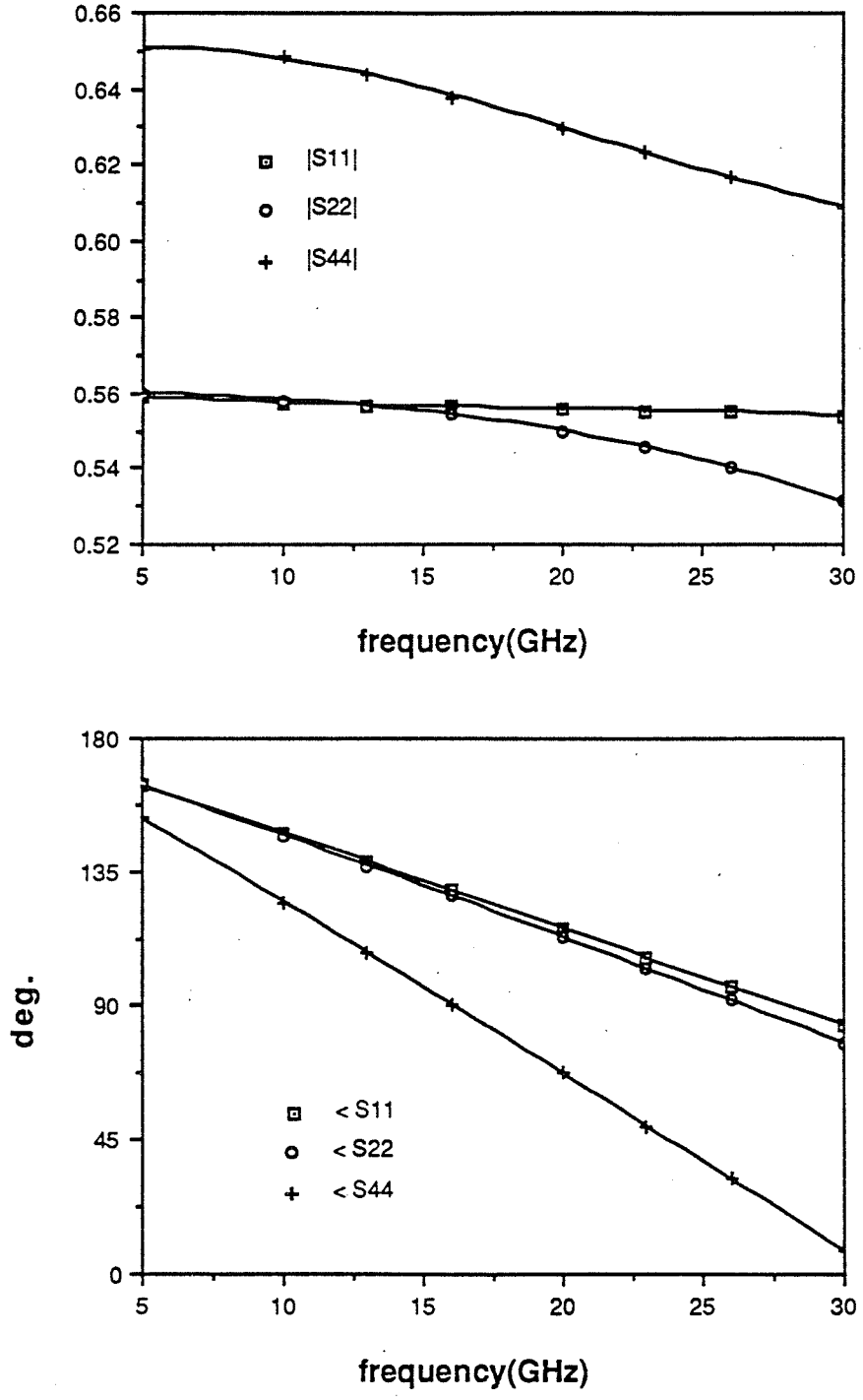

Figure 6.19: The frequency responses $S_{i,i}$ of the complex matching network.

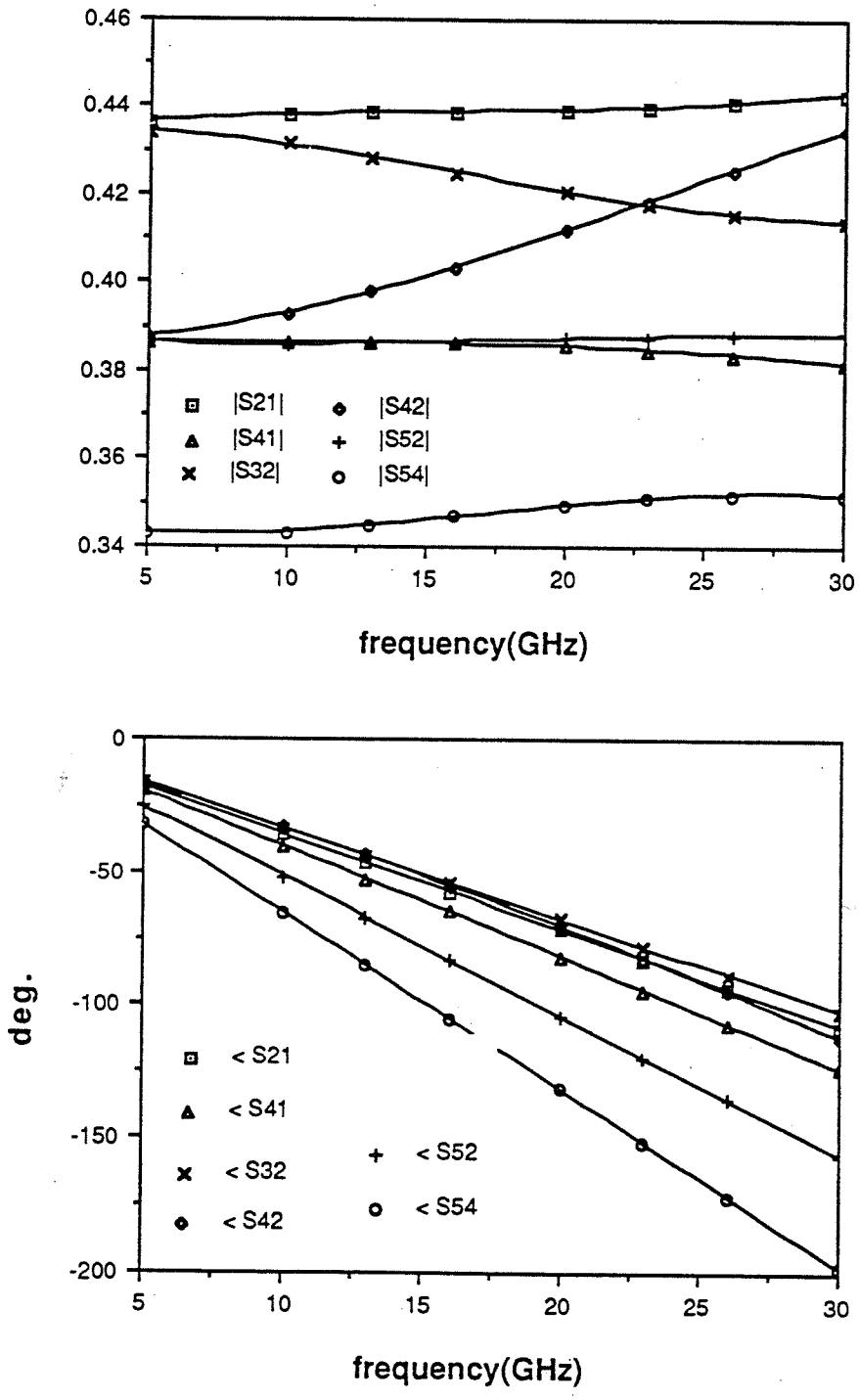

Figure 6.20: The frequency responses $S_{i,j}$ of the complex matching network.

(c) Metallic loss is an important loss factor whenever resonance is encountered.

(d) Accumulation of small reflections from junctions and bends may result in resonances and the resonances may cause a significant insertion loss in circuits.

The References for Chapter 6

[1] A. Farra and A. T. Adams, " Matrix methods for microstrip three-dimensional problems," **IEEE Trans. on Microwave Theory Tech.**, Vol. MTT-20, pp.497-504, 1972.

[2] I. Wolff, G. Kompa and R. Mehran, " Calculation method for microstrip discontinuities and T-junctions", **Electronics Lett.**, Vol. 11, pp. 177-179, 1972.

[3] P. Silvester and P. Benedek, " Microstrip discontinuity capacitance for right-angle bends, T-junctions and crossings," **IEEE Trans. on Microwave Theory Tech.**, Vol. MTT-21, pp. 341-346, 1973.

[4] A. F. Thompson and A. Gopinath, " Calculation of microstrip discontinuity inductances," **IEEE Trans. on Microwave Theory Tech.**, Vol. MTT-23,1975.

[5] P. Anders and F. Arndt, " Microstrip discontinuities capacitances and inductances for double steps, mitered bends with arbitrary angle and asymmetric right-angle bends," **IEEE Trans. on Microwave Theory Tech.**, Vol. MTT-28, pp. 1213-1217, Nov. 1980.,

[6] R. Chadha and K. C. Gupta, " Segmentation method using impedance matrices for analysis of planar microwave circuits, " **IEEE Trans. on Microwave Theory Tech.**, Vol. MTT-29, pp. 71-74, Jan. 1981.

[7] N. H. L. Koster and R. H. Jansen, " The equivalent circuit of the asymmetrical series gap in microstrip and suspended-substrate lines," **IEEE Trans. on Microwave Theory Tech.**, Vol. MTT-30, pp. 1273-1279, 1982.

[8] T. S. Chu, T. Itoh, " Comparative study of mode matching formulations fo microstrip discontinuity problems," **IEEE Trans. on Microwave Theory Tech.**, Vol. MTT-33, pp. 1018-1023, Oct. 1985.

[9] N. H. L. Koster and R. H. Jansen, " The microstrip step discontinuity: A revised description, " **IEEE Trans. on Microwave Theory Tech.**, Vol. MTT-34, pp. 213-223, Feb. 1986.

[10] J. R. Mosig, "Arbitrarily shaped microstrip structures and their analysis with a mixed potential integral equation," **IEEE Trans. on Microwave Theory Tech.**, MTT-36, pp. 314-323, February 1988.

[11] W. Wertgen and R. H. Jansen, " Efficient direct and iterative electrodynamic analysis of geometrically complex MIC and MMIC structures," **Intern. Journal of Numerical Modeling: Electronic Networks, Devices and Fields**, Vol.2, 153-186, 1989.

[12] R. W. Jackson, " Full-wave, finite element analysis of irregular microstrip discontinuities," **IEEE Trans. on Microwave Theory Tech.**, MTT-37, pp. 81-89, January 1989.

[13] P. B. Katehi and N. G. Alexopoulos, " Frequency-dependent characteristics of microstrip discontinuities in millimeter-wave integrated circuits," **IEEE Trans. on Microwave Theory Tech.**, MTT-33, pp. 1029-1035, Oct. 1985.

[14] R. W. Jackson and D. M. Pozar, " Full-wave analysis of microstrip open-end and gap discontinuities," **IEEE Trans. on Microwave Theory Tech.**, MTT-33, pp. 1036-1042, Oct. 1985.

[15] J. C. Rautio and R. F. Harrington, " An electromagnetic time-harmonic analysis of shielded microstrip circuits," **IEEE Trans. on Microwave Theory Tech.**, Vol. MTT-35, pp. 726-730, Aug. 1987.

[16] J. C. Rautio and R. F. Harrington, " An efficient electromagnetic analysis of arbitrary microstrip circuits," **IEEE MTT Intern. Microwave Symposium Digest**, pp. 295-298, 1987.

[17] Z. Q. Chen and B. Gao, " Deterministic approach to full-wave analysis of discontinuities in MIC's using the method of lines," **IEEE Trans. on Microwave Theory Tech.**, Vol. MTT-37, pp. 606-611, March 1989.

[18] H. Y. Yang, N. G. Alexopoulos and D. R. Jackson, " Microstrip open-end and gap discontinuities in a substrate-superstrate structure," **IEEE Trans. on Microwave Theory Tech.**, Vol. MTT-37, pp. 1542-1546, Oct. 1989.

[19] S. Nam, H. Ling and T. Itoh, " Characterization of uniform microstrip line and its discontinuities using time-domain method of lines," **IEEE Trans. on Microwave Theory Tech.**, Vol. MTT-37, pp. 2051-2057, Dec. 1989.

[20] D. I. Wu, D. C. Chang and B. I. Brim, "Accurate numerical modeling

of microstrip junctions and discontinuities," **Intern. Journal of Microwave Millimeter-wave Computer Aided Design**, to be published.

[21] M. Herman, Hughes Aircraft Company, private communication.

[22] M. Goldfarb and P. A. Platzker, " The effect of electromagnetic coupling on MMIC design," **Intern. Journal of Microwave Millimeter-wave Computer Aided Design**, to be published.

[23] C. Goldsmith, Texas Instrument, private communication.

[24] A. Sabban and K. C. Gupta, " A planar-lumped model for coupled microstrip line discontinuities," **IEEE Trans. on Microwave Theory Tech. Special Issue**, MTT-38, Dec. 1990, to be published.

[25] K. Larson and J. Dunn, University of Colorado at Boulder, private communication.

[26] J. X. Zheng and D. C. Chang, " Computer-aided design of electromagnetically-coupled and tuned, wide band microstrip patch antennas," **IEEE AP-Symposium Digest** , pp.1120-1123, Dallas, TX, May 1990.

[27] E. F. Kuester and D. C. Chang, **Theory of Waveguides and Transmission Lines** . Course notes of ECEN 5114, Chapter 3, University of Colorado at Boulder, 1989.

CHAPTER 7

MICROSTRIP PATCH ANTENNAS

7.1 Introduction

Microstrip patch antennas have received extensive attention because of their advantages of light weight, low profile, small size, ease of fabrication and comformality, etc. [1]. Many algorithms and theories have been developed for the analysis of microstrip patch antennas and dipoles. Among them are the transmission-line theory [3], cavity model [4]-[6], Weiner-Hopf method [9], multi-port network method [10,11], moment methods [12] - [18] and finite-element method [19]. Except in [4], most of them are designed for structures of regular shape, such as rectangular patches, circular patches and elliptical patches. As a result, they have difficulty in analyzing irregularities such as a rectangular patch with a corner cut or a slot (see Fig. 7.1). Obviously, the P-mesh algorithm has no problem in analyzing this kind of structure. In fact, the P-mesh algorithm can, at the expense of more computational time, provide much more accurate results than the ordinary spectral-domain moment methods [14,15] since the small cells can accomodate more rapid variation of current distribution on the antenna structure.

The major disadvantage of microstrip antennas is narrow bandwidth

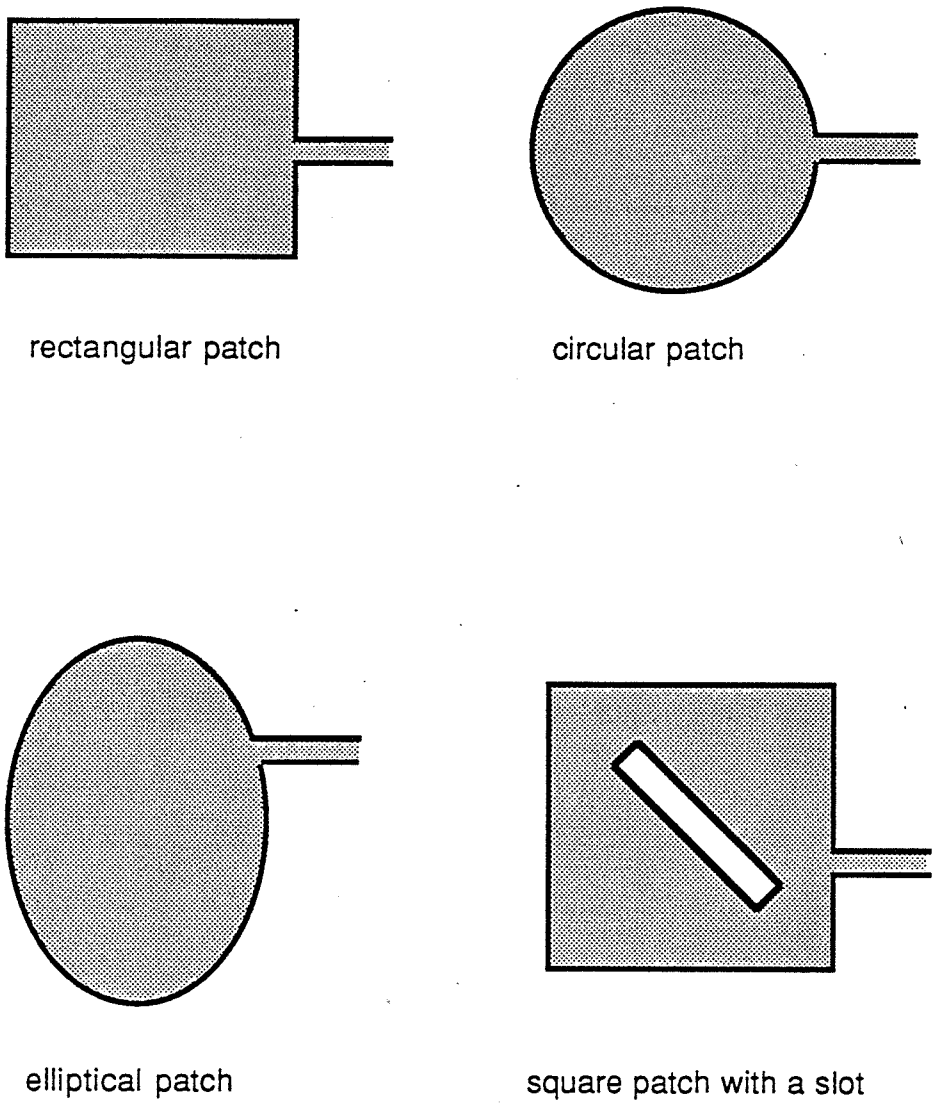

Figure 7.1: Microstrip antennas.

[1]. The reason for narrow bandwidth can be explained either from the viewpoint of small radiating aperture around the antenna perimeter, or the viewpoint that any radiation from the current on the patch is offset by the corresponding image current on the ground plane. Attempts to broaden the bandwidth by increasing the substrate thickness [15,18,20,21] have been partially successful, primarily because it is accomplished at the expense of a stronger surface-wave excitation.

An alternative to a thicker substrate is to introduce additional parasitic elements [22] - [28] by either placing them on the same planar surface or stacking them on different layers (see Fig. 7.2). In both cases, a wider bandwidth is achieved when individual resonances are coupled strongly together. Unfortunately, the horizontal parasitic element arrangement is often difficult to realize because of the space constraint in an array configuration. The vertical arrangement, on the other hand, is difficult to fabricate and has an impedance matching problem [29]. It is noticed that a broad-band gap coupled microstrip antenna made of strongly coupled narrow strips was reported to realize an 8 times bandwidth broadening compared to the solid patch of same size [30].

Electromagnetically-coupled microstrip antennas (see Fig. 7.3) have been shown to possess a wider bandwidth [29]. The patch antenna is typically placed on a superstrate which is, generally, made of honeycomb or other low dielectric constant materials to reduce the surface waves. A tuning stub is typically added to match the input impedance of the antenna to that of the feed-line [21]. Electromagnetic modeling of such a structure with a closely-spaced stub is given in Section 7.3. We will demonstrate in the same section how the inductive coupling between the tuning stub and the patch antenna

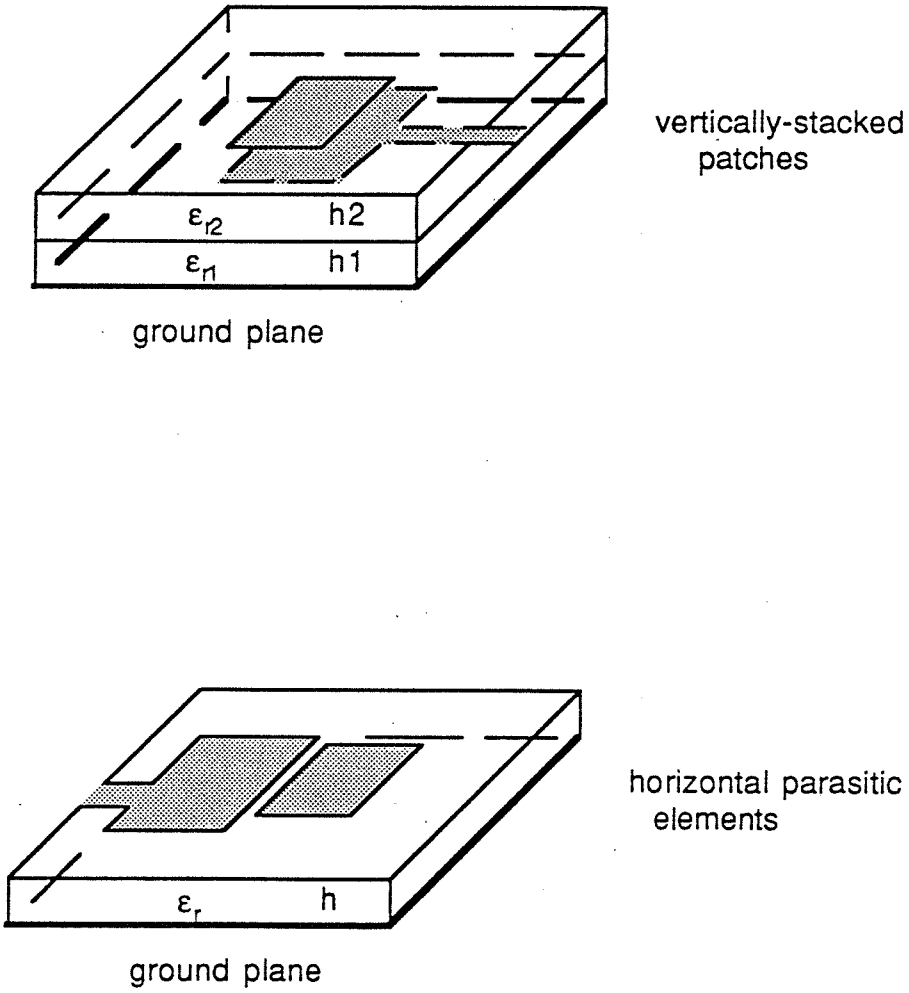

Figure 7.2: Microstrip antennas using parasitic elements.

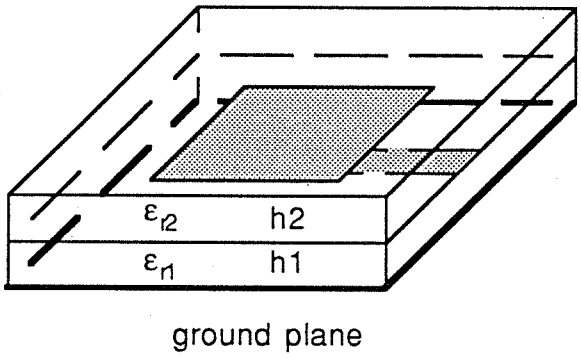

Figure 7.3: Electromagnetically-coupled microstrip antennas.

can be utilized to broden the antenna bandwidth. Another wide-band scheme with two closely-coupled 45° - 45° - 90° triangles on the same substrate will be discussed in Section 7.4.

Corporate feed networks are commonly used in the design of microstrip arrays [31] (see Fig. 7.4). Metallic loss caused by the feed network is often a prohibiting factor at high frequency. A series-fed microstrip antenna array, as shown in Fig. 7.5, has the advantage of smaller conduction loss. However, because the width may vary from element to element, the beam-pointing direction of such an array is often very sensitive to the change in the operating frequency. In Section 7.5, we will discuss how one can avoid such difficulty by using identical patches in a coupled series-fed configuration.

7.2 Numerical Consideration

In Section 5.5, we demonstrated that accurate results can be obtained using about 20 cells per waveguide wavelength in the longitudinal direction ($N_w = 20$) and 1 cell in the transverse direction ($N_t = 1$) along a typical MMIC microstrip line.

To determine whether the same criterion is suitable in analyzing microstrip patch antennas in which much lower dielectric constant substrates are used, we have included a comparative study of several commonly used methods for microstrip patch antennas. The dimensions of the microstrip patch antenna fed at the radiating edge by a narrow microstrip is shown in Fig. 7.6. Good agreement is obtained when the criterion of $N_w = 20$ and $N_t = 1$ is used (see Fig. 7.7, frequency beginning at 1.197GHz with step of 0.01GHz). We found a higher degree of accuracy can be achieved when we use some narrow cells on the edges of both the patch and the feed-line to simulate the edge effect. This

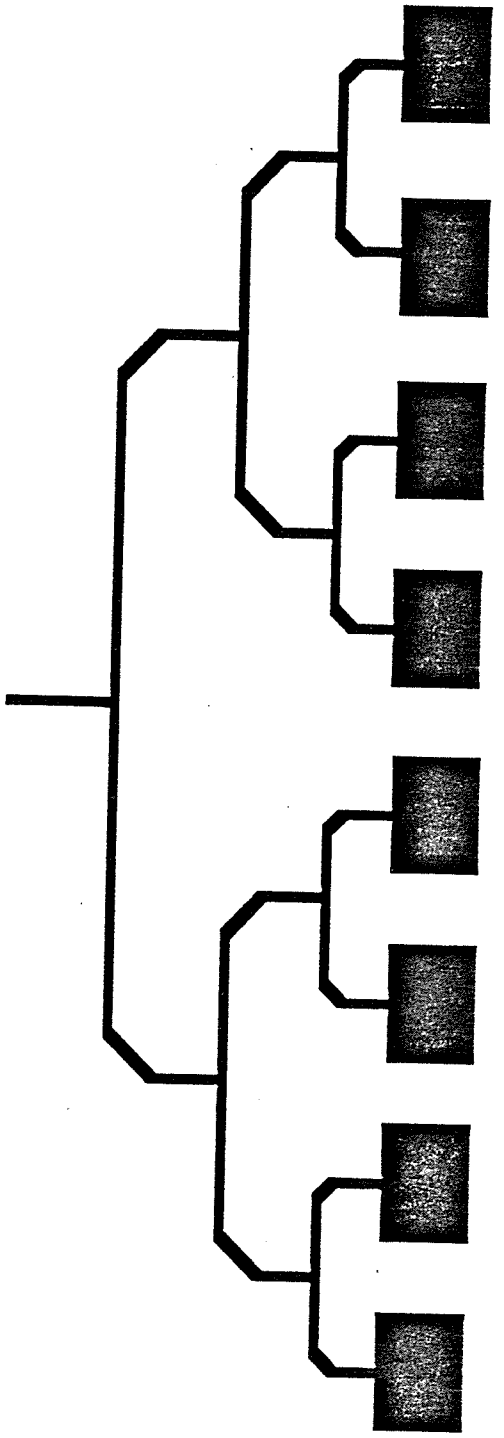

Figure 7.4: A power division network in microstrip arrays.

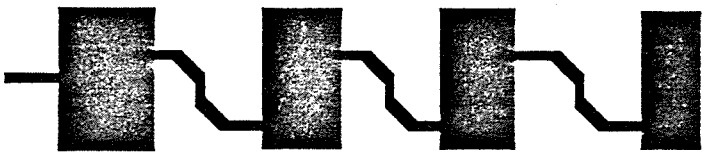

Figure 7.5: A series-fed microstrip antenna array.

becomes important particularly when the patch is edge-coupled to a feed-line (Section 7.5) and/or to a tuning element (Section 7.3).

7.3 Wide-Band Microstrip Patch Antennas

The current P-mesh code can directly be applied to planar microstrip antennas with a single layer, or to vertically-stacked antennas with an air-substrate (extension to a multiple-layer dielectric substrate will not be included in this thesis because of the lack of a suitable Green's function program). The objective of this section is to demonstrate how wide-band patch antennas can be derived using strongly coupled resonances.

Fig. 7.9 shows the typical frequency response of a microstrip patch with dimensions as shown in Fig. 7.8. The bandwidth, defined as $VSWR \leq 2$, of such a structure is about 1%, due to the fact that the substrate thickness is usually small in this case.

To increase the bandwidth, a superstrate is added, the antenna is now placed on the superstrate and electromagnetically, or more precisely capacitively coupled to the feed-line which remains on the substrate surface (Fig. 7.10). Fig. 7.11 shows a substantial amount of power is reflected back even at resonace since the antenna is no longer impedance-matched to the feed-line.

To provide a better impedance match, a tuning stub is added to the feed-line of the antenna (see Fig. 7.12). The tuned frequency responses with optimal stub locations (distance from the end of the patch) based upon the transmission-line theory are shown in Fig. 7.13. It is noticed that the farther the stub is from the patch, the narrower the bandwidth is. The question is whether the transmission-line theory works for closely placed stubs.

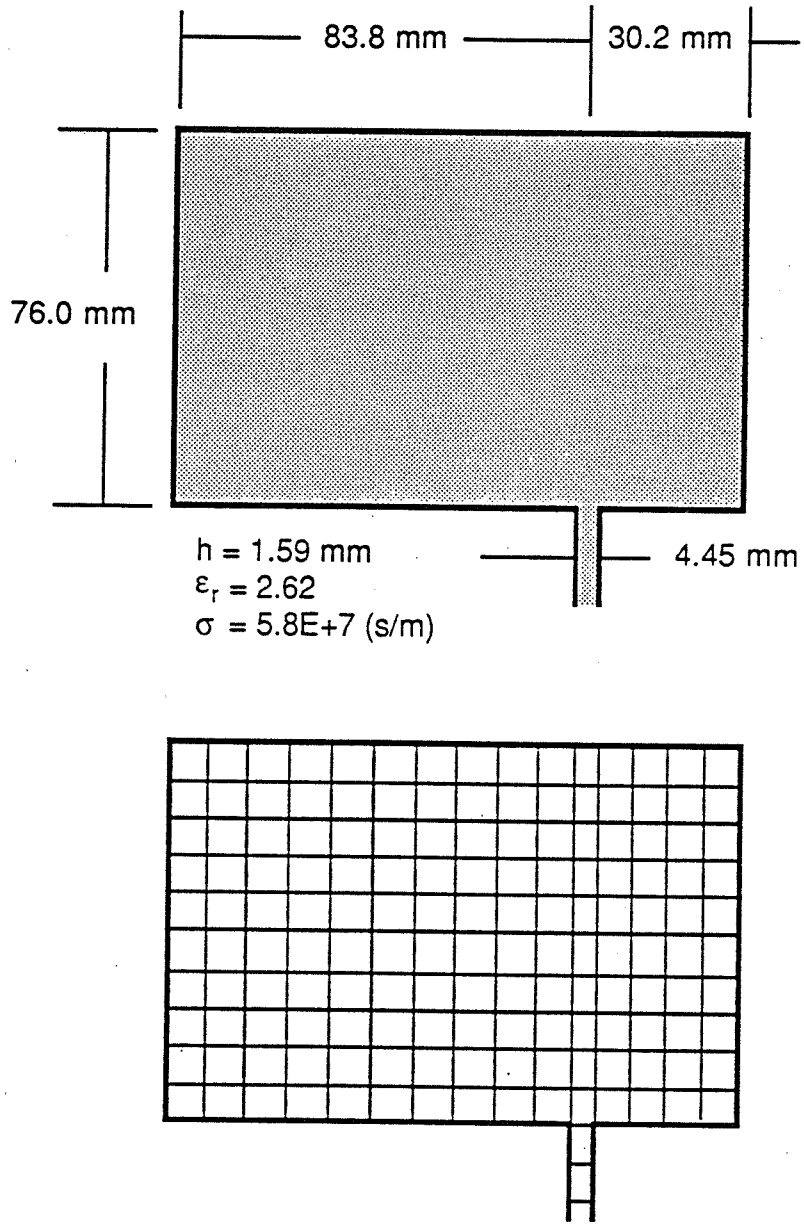

Figure 7.6. A direct line-fed microstrip patch antenna and its grided structure

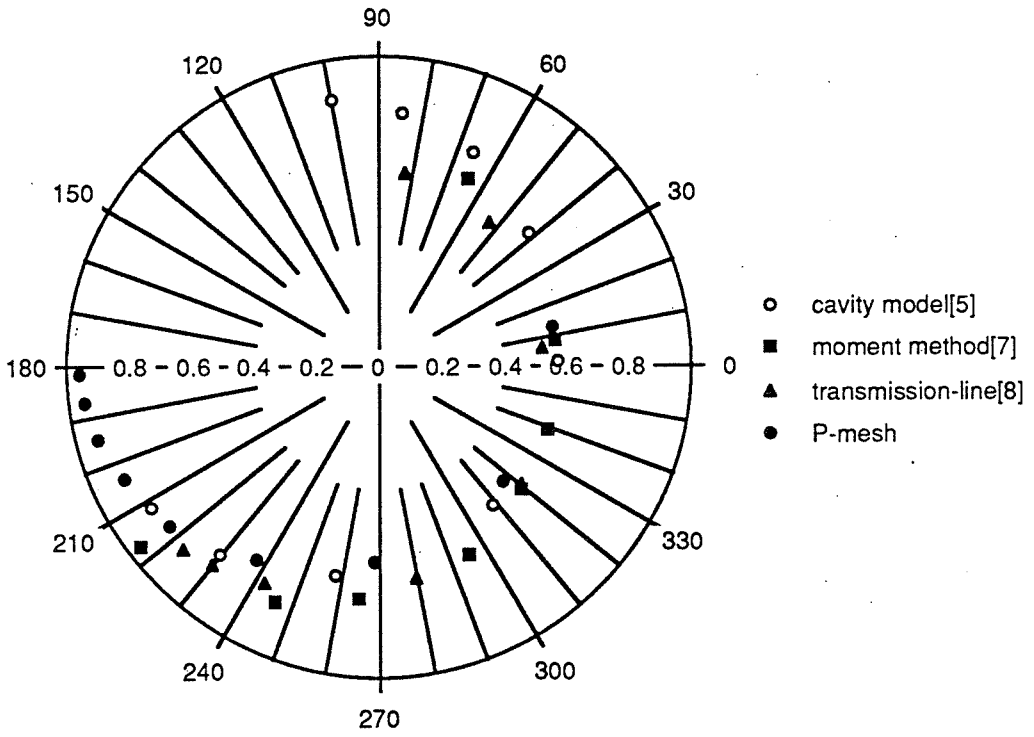

Figure 7.7. The frequency response of the direct line-fed microstrip patch antenna.

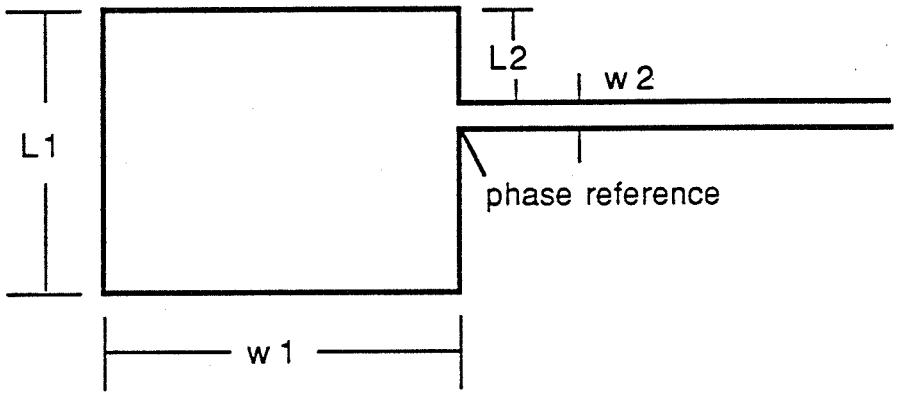

h = 1.0mm
ε_r = 1.0
L1=50mm
L2=13.75mm
w1=60mm
w2=5mm

Figure 7.8: A one-layer microstrip patch antenna.

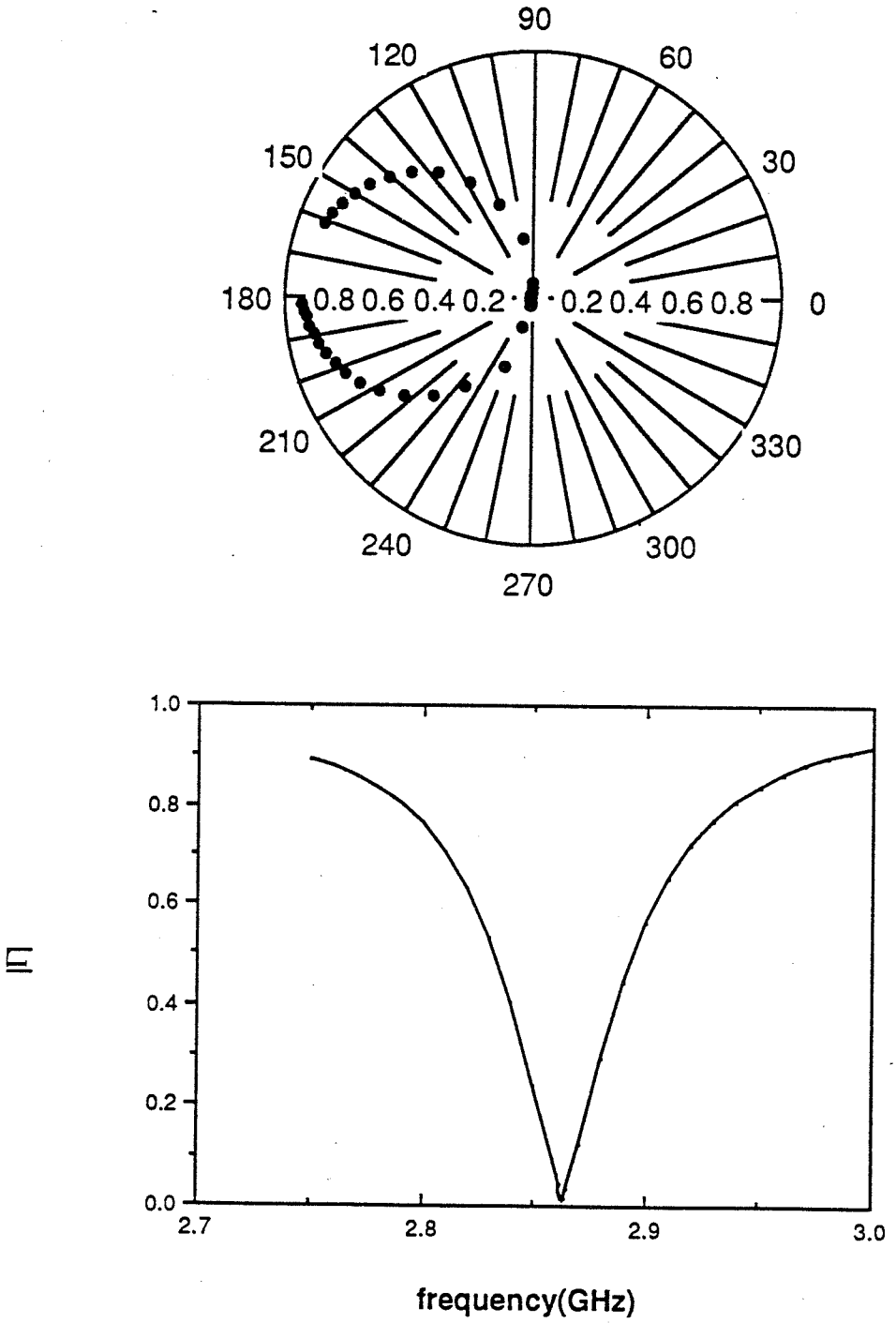

Figure 7.9. The frequency response of the one-layer microstrip patch antenna.

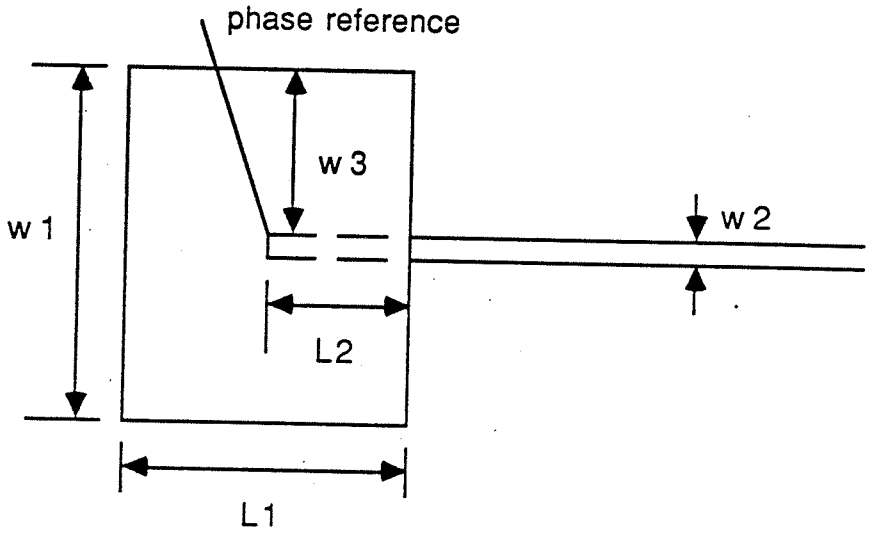

The patch is on the second substrate.
The feeding network is on the first substrate.

h1= 1.0mm
h2= 4.0mm
ε_{r1}= 1.0
ε_{r2} = 1.0
L1=50.0mm
L2=25.0mm
w1=60.0mm
w2=5.0mm
w3=27.5mm

Figure 7.10. The configuration of a double-layer electromagnetically-coupled fed microstrip antenna.

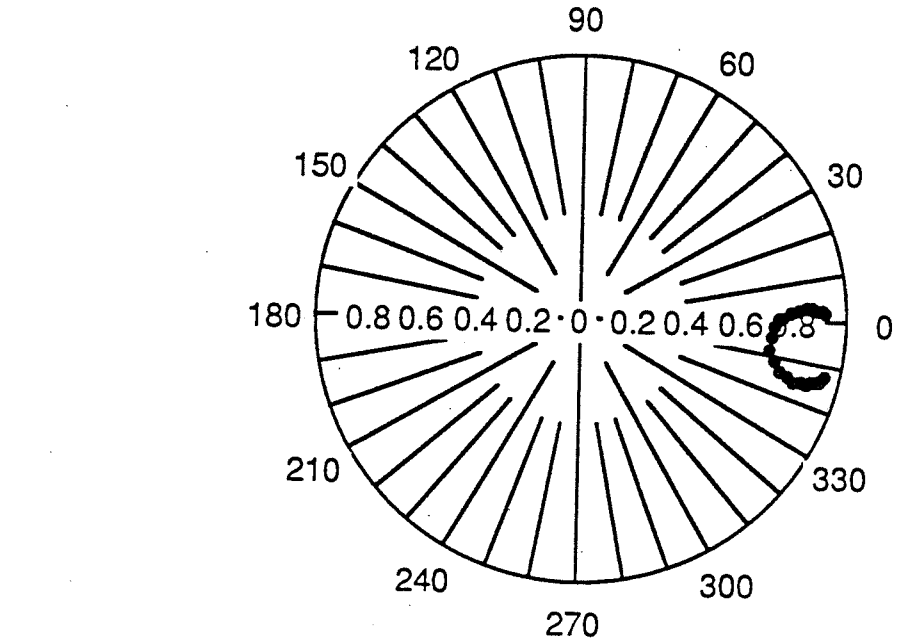

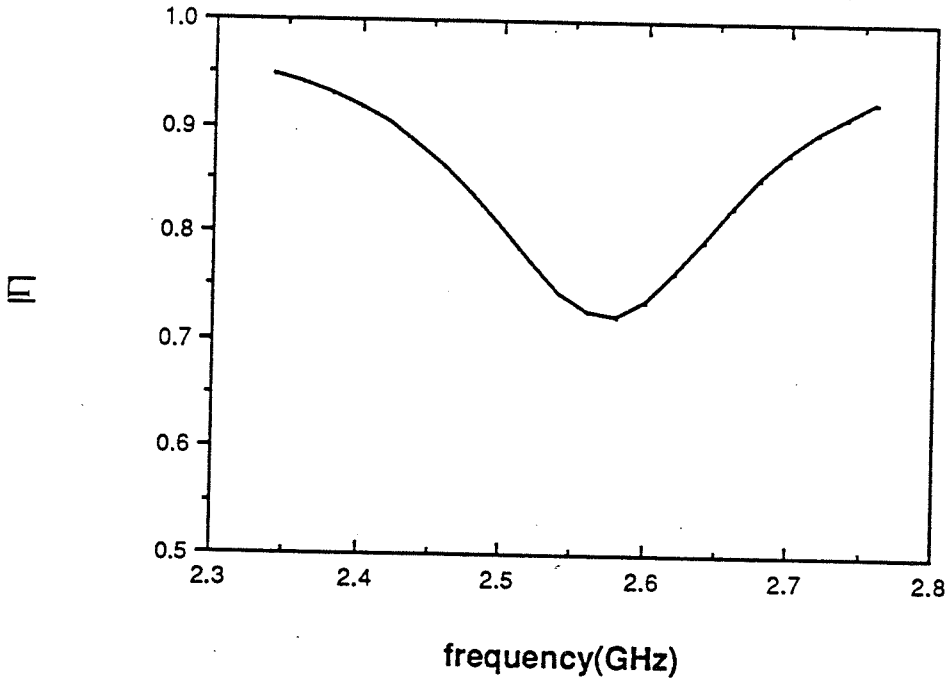

Figure 7.11. The frequency response of the double-layer electomagnetically-coupled fed antenna.

The stub is also optimized using the P-mesh code and the optimized dimensions of the configuration is shown in Fig. 7.12. The P-mesh code predicts that the location of the stub is 33.8mm away from the end (see Fig. 7.12) of the feed-line compared to 35.2mm based upon transmission-line theory. The frequency response based upon the P-mesh code compared with the corresponding one based upon the transmission-line theory is shown in Fig. 7.13. It is noticed that the EM modeling predicts a narrower bandwidth (5%) than the transmission-line theory (8%). The strong coupling between the patch and the stub is clearly seen from the non-symmetric $\hat{y}$-directed current density distribution in the $\hat{x}$-direction as shown in Fig. 7.14.

In fact, 5% bandwidth is not the best we can do for such a double-layer antenna. A slotted patch antenna and its frequency response are shown in Fig. 7.15 and 7.16. Surprisingly, the impedance bandwidth is doubled to about 10%. It is explained that the two stubs, including the one under the patch, serve as two different feeds. The stub under the patch is more a capacitive feed from the end. The stub parallel to the edge of the patch is more an inductive feed along the stub. The two feeds form two different loaded resonances and each of the stubs serves as the matching network of the other. It was suspected that the two minima could be from two different resonances in the two directions. But, the current distributions tell that both $\hat{x}$ and $\hat{y}$-directed current have almost the same amplitude in the whole frequency range, and there is no indication of two resonant frequencies in two different directions. Fig. 7.17 shows a typical x and y-directed current distribution. It is very clear the current is forced to orient itself in the slot direction.

A typical E-plane (defined as parallel to the slot) radiation pattern

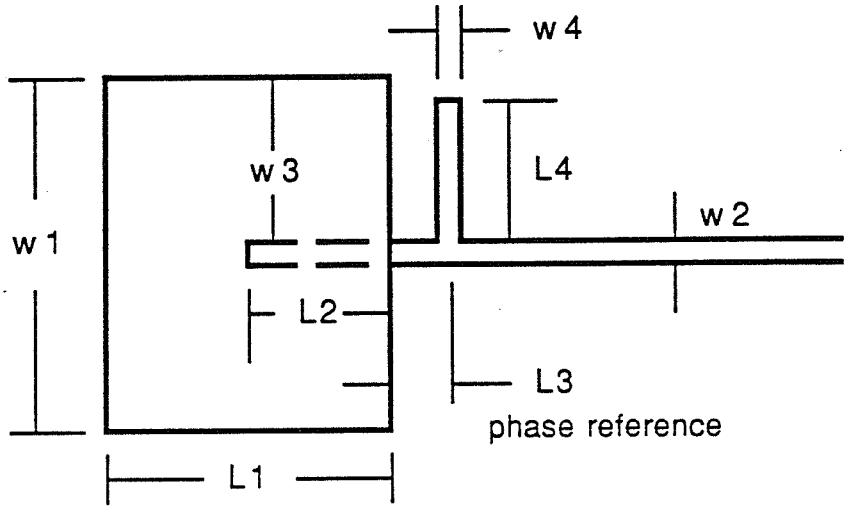

The patch is on the second substrate.
The feeding network is on the first substrate.

h1 = 1.0 mm
h2 = 4.0 mm
ε_{r1} = 1.0
ε_{r2} = 1.0
L1=50.0mm
L2=25.0mm
L3=8.8mm
L4=24.0mm
w1=60.0mm
w2=5.0mm
w3=27.5mm
w4=2.0mm

Figure 7.12. The configuration of a double-layer electromagnetically-coupled fed microstrip antenna with a tuning-stub.

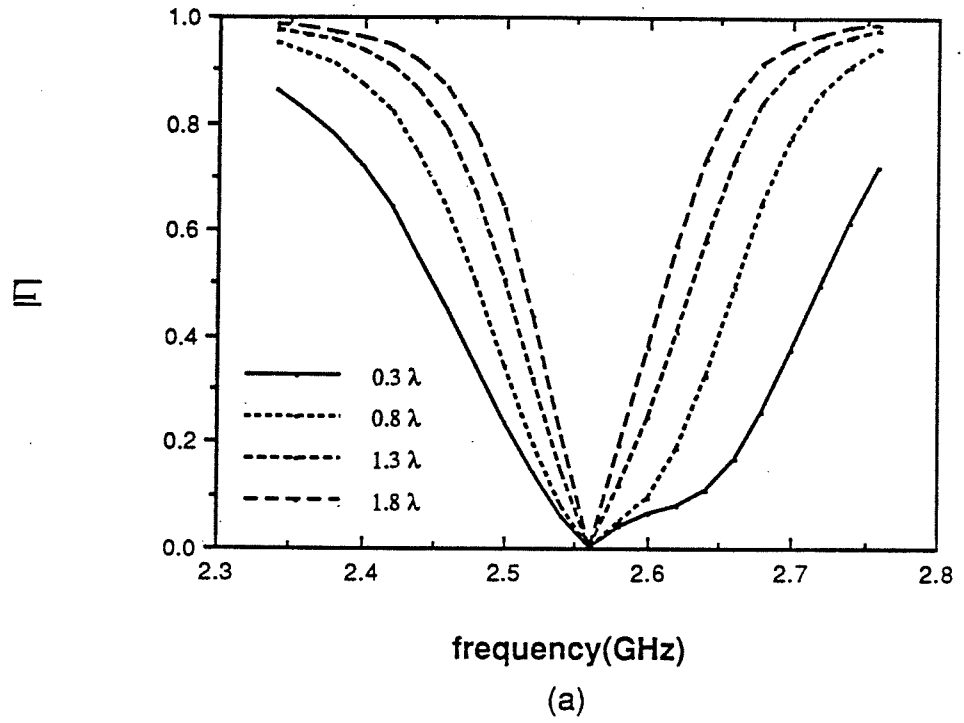

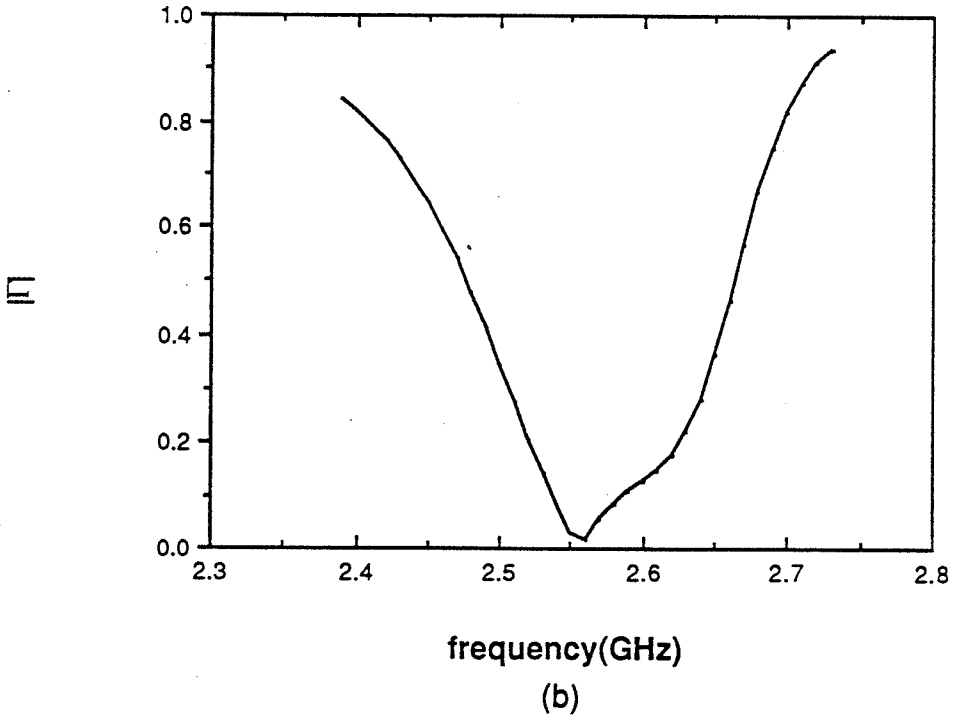

Figure 7.13. The frequency response of the double-layer electromagnetically-coupled fed microstrip antenna with a tuning-stub.

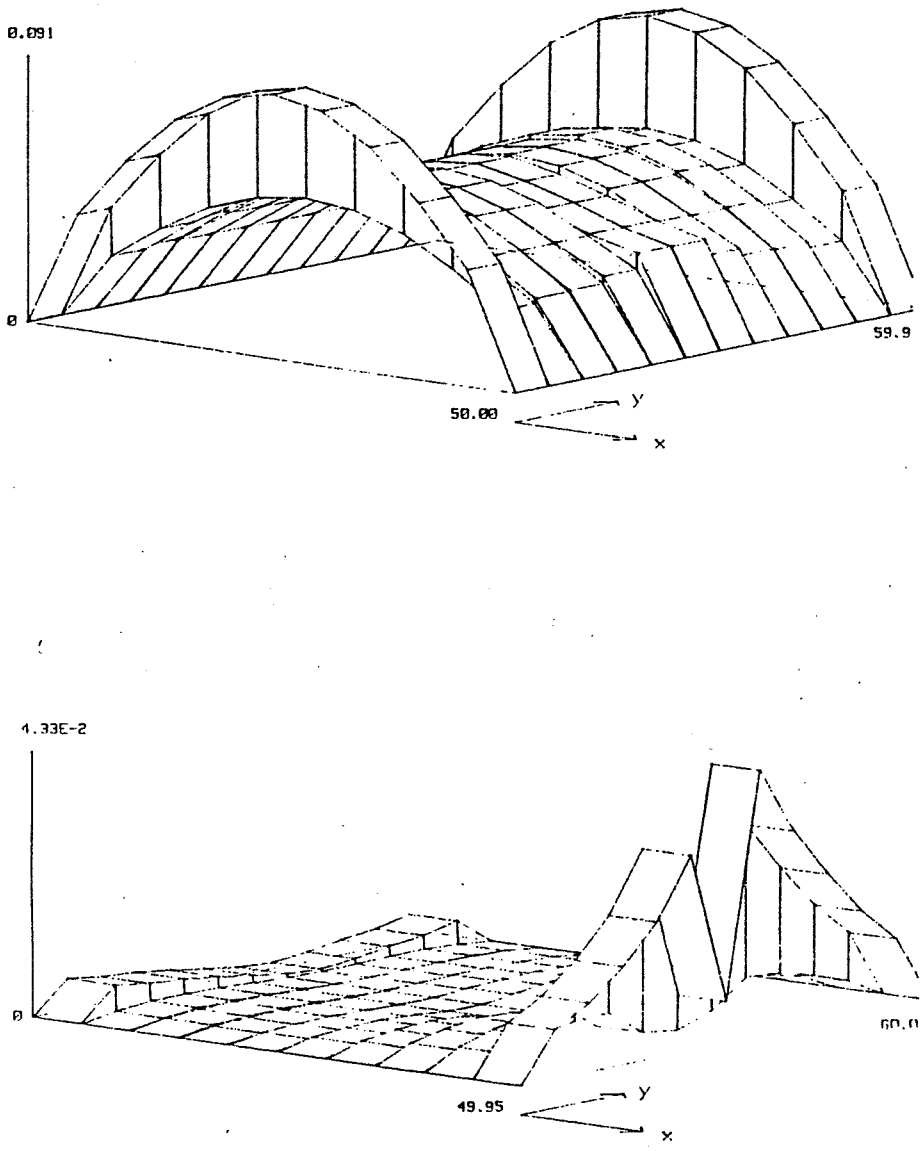

Figure 7.14. The current distribution of the double-layer electromagnetically-coupled fed microstrip antenna with a tuning-stub.

at three different frequencies is dipicted in Fig. 7.18. The cross-polarization is lower than -19dB for both E-plane and H-plane patterns in the whole frequency range. The advantage of such a configuration is that the slotted patch doubles the bandwidth apparently without sacrificing anything.

Since the antenna and the tuning stubs are placed in different layers, a question naturally arises as to whether the antenna performance is sensitive to alignment error. A sensitivity analysis was consequently performed and the result is dipicted in Fig. 7.19. The dx and dy in the figure are the offsets of the feeding network with respect to the location of the patch in Fig. 7.15. Obviously, the location error between the patch and the feeding network has little effect on the frequency response. But the error in the feeding network, such as the length and the location of the stubs do have substantial effect on the frequency response.

7.4 A Microstrip Antenna with two Triangular Patches

Another example of wide-band microstrip antennas is a composite structure consisted of two 45° - 45° - 90° triangular patches on the same substrate (see Fig. 7.20). We know such a triangular patch has approximately the same Q-factor as the corresponding square patch [32], and therefore it should have the same bandwidth as a square patch. A coupled resonance phenomenon occurs when two triangular patches of slightly different dimensions are facing each other. For comparision, a rectangular patch of somewhat larger size is also shown in Fig. 7.20. Their frequency responses are compared in Fig. 7.21. It is of interest to note that the impedance bandwidth of the double-patch structure is increased substantially (to about 2.5%) compared to the rectangular patch

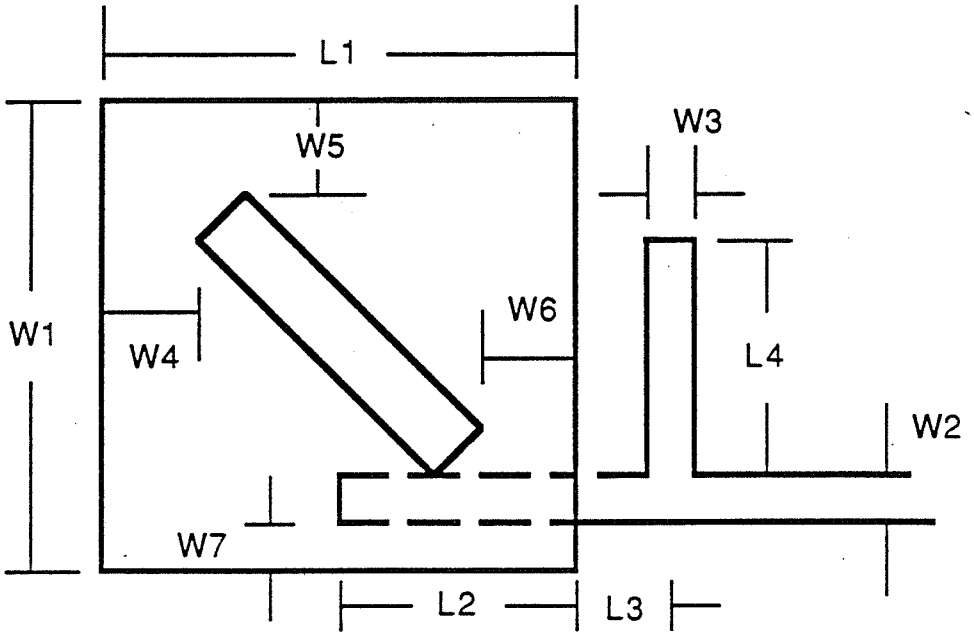

The patch is on the second substrate.
The feeding network is on the first substrate.

h1= 1.0
h2= 4.0
ε_{r1} = 1.0
ε_{r2} = 1.0
L1 = w1 = 50.0 mm
L2 =25.0 mm
L3 =10.0 mm
L4 =22.5 mm
w2=w7=5.0mm
w3=2.0mm
w4=w5=w6=mm

Figure 7.15: The configuration of a slotted patch.

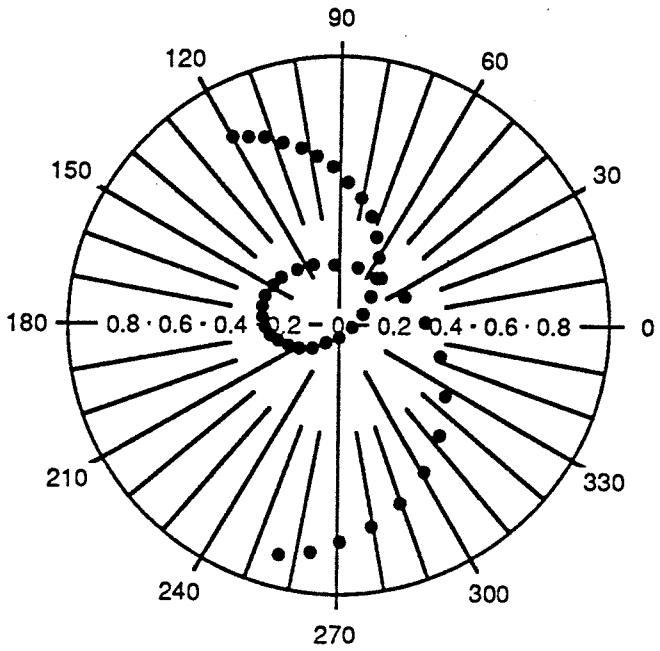

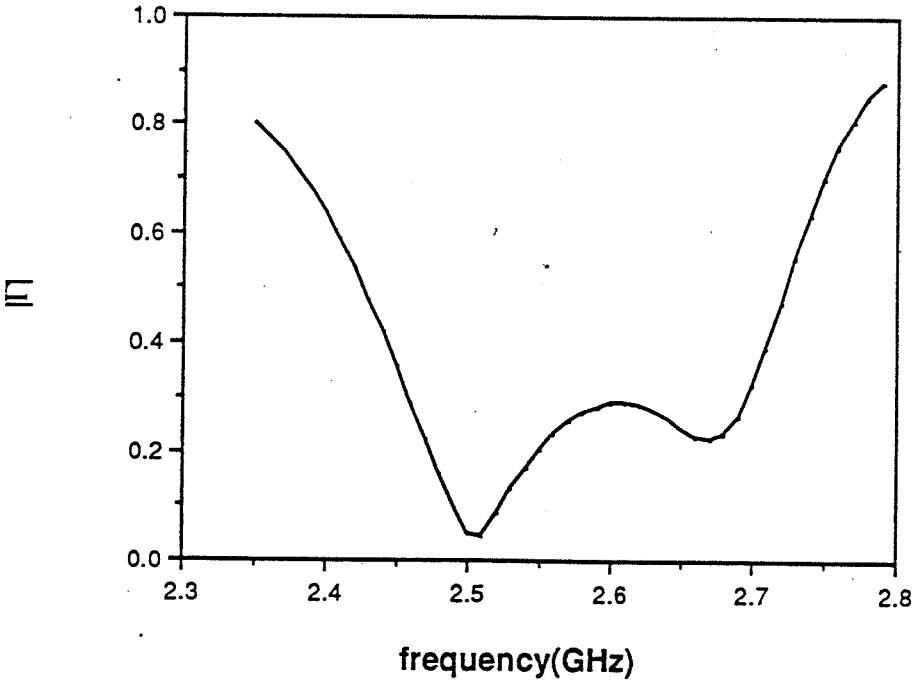

Figure 7.16: The frequency response of the slotted patch.

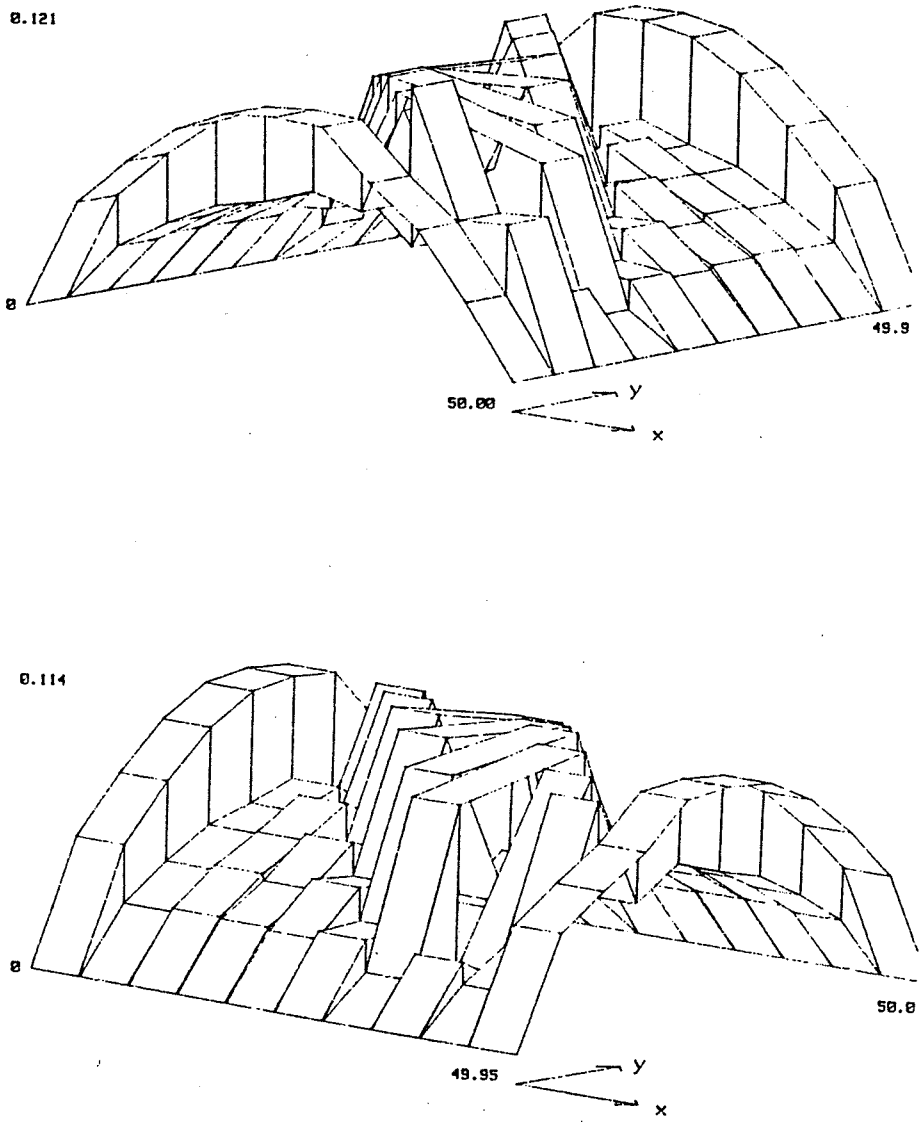

Figure 7.17: The current distributions of the slotted patch.

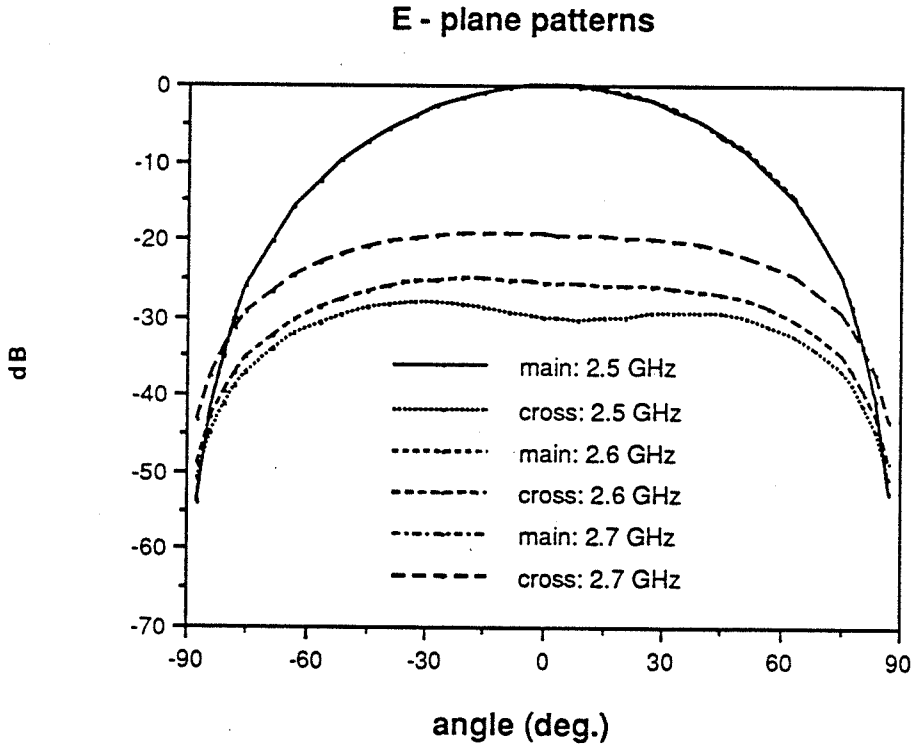

Figure 7.18: The radiation patterns of the slotted patch.

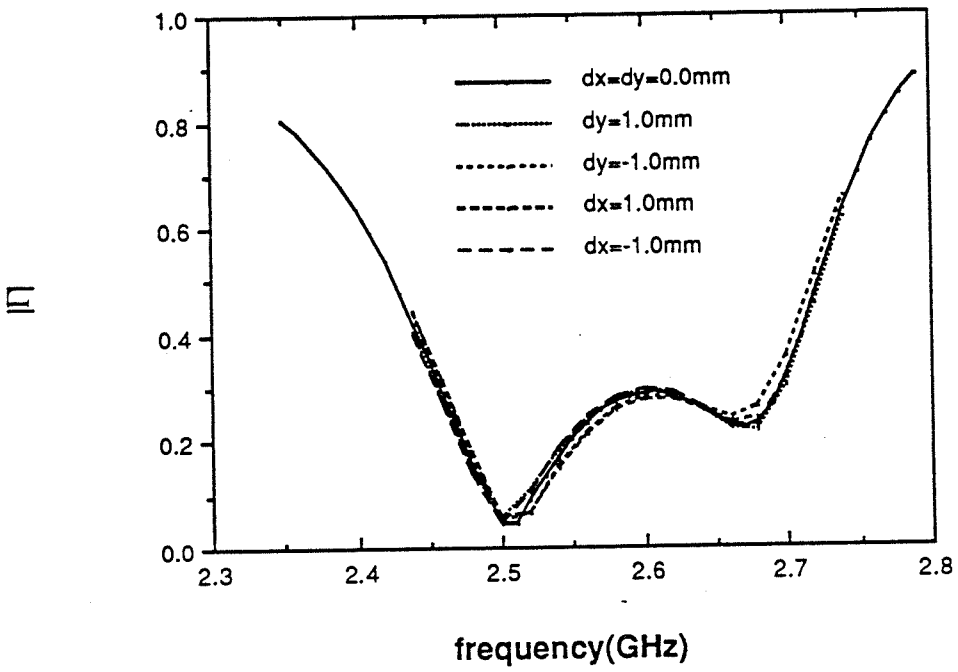

Figure 7.19: The sensitivity study of the slotted patch.

(about 1.5%) even the rectangular patch has a larger size. The E-plane patterns are shown in Fig. 7.22. Good radiation patterns are also obtained over the whole frequency range, but the cross-polarization appears to be somewhat higher than the slotted patch discussed earlier. However, we should note that the impedance bandwidth is quite sensitive to the gap width in this case.

7.5 An Edge-Coupled Microstrip Antenna Element

As mentioned in Section 7.1, metallic loss associated with a corporate feed network sometimes can be a limiting factor in array applications. On the other hand, a series-fed antenna array consisted of elements of different sizes can have a very limited beam-pointing bandwidth. In this section, an edge-coupled configuration using identical elements will be analyzed (see Fig. 7.23). The question we need to address is whether a significant amount of power can be coupled to a radiating antenna in this fashion.

As we pointed out in Section 7.2, more cells near the edge of the feed-line and the edge of the patch are needed in order to model more accurately the effect of coupling between the strip-line and the patch. A comparison is provided in Fig. 7.24 for different N_t values (number of cells on the transverse direction of the feed-line) and the Multi-port model [11]. The difference between the result using $N_t = 1$ and other values of N_t can indeed be quite significant because the edge condition is very important in this case. In the analysis follows, we consistently use $N_t = 3$.

Typical frequency responses of such a radiating edge coupled-fed antenna for different values of feed-line to patch gap width are shown in Fig. 7.25 and 7.26. The transmitted, reflected, and radiated power as a function of gap width are shown in Fig. 7.27. It is of interest to note that as much as 45% of

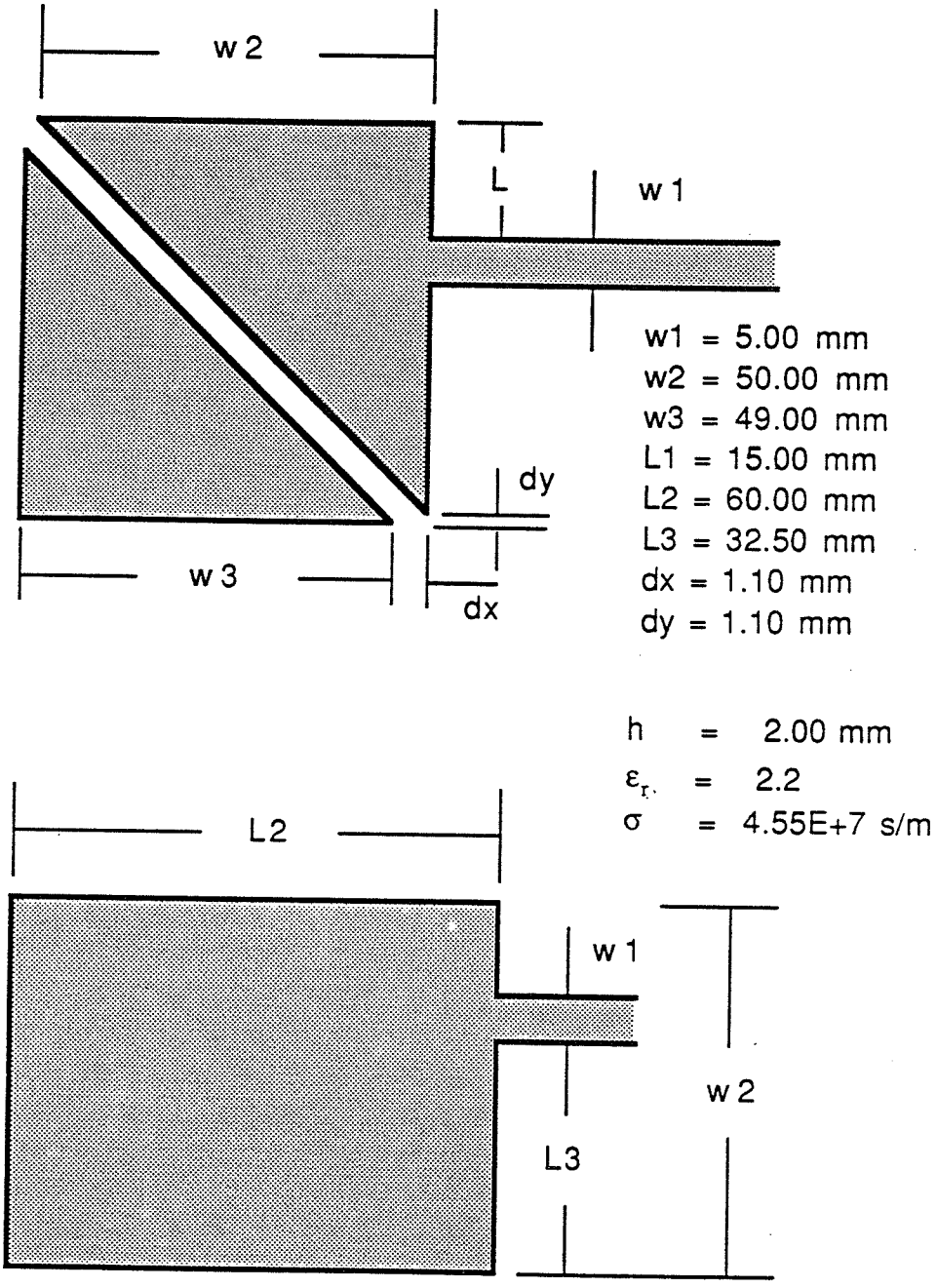

Figure 7.20. Patches of different shapes on one-layer substrate microstrip antenna.

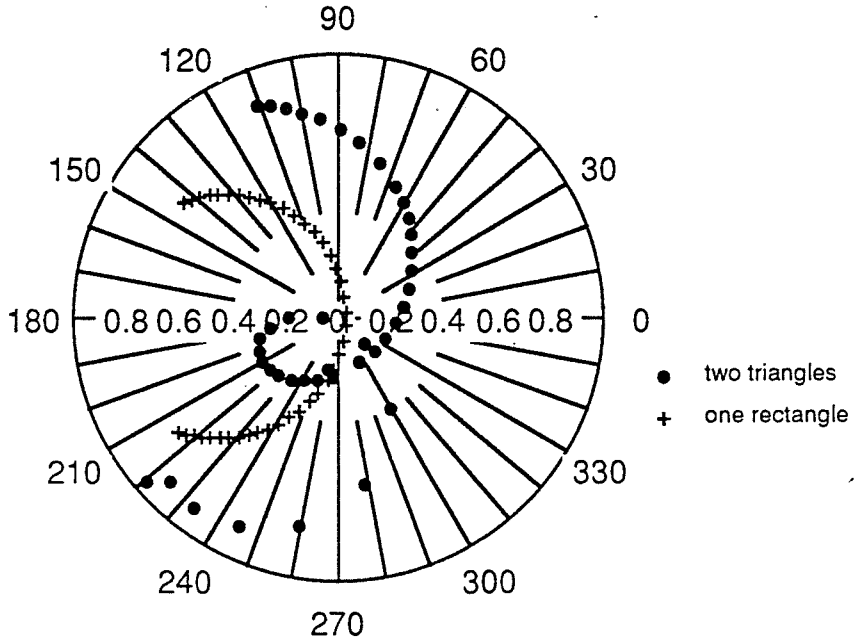

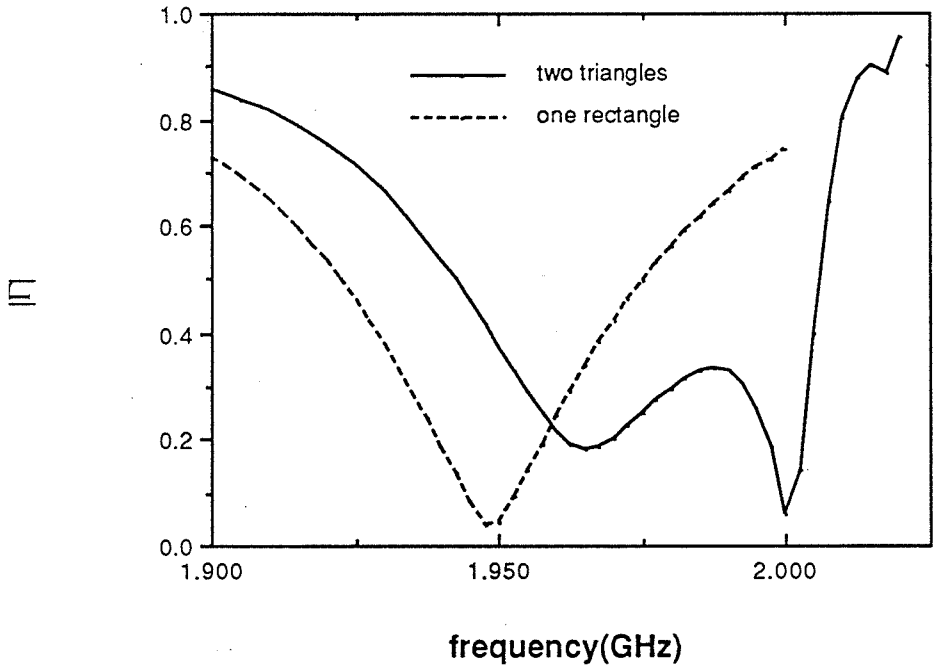

Figure 7.21: Frequency responses of the different patches.

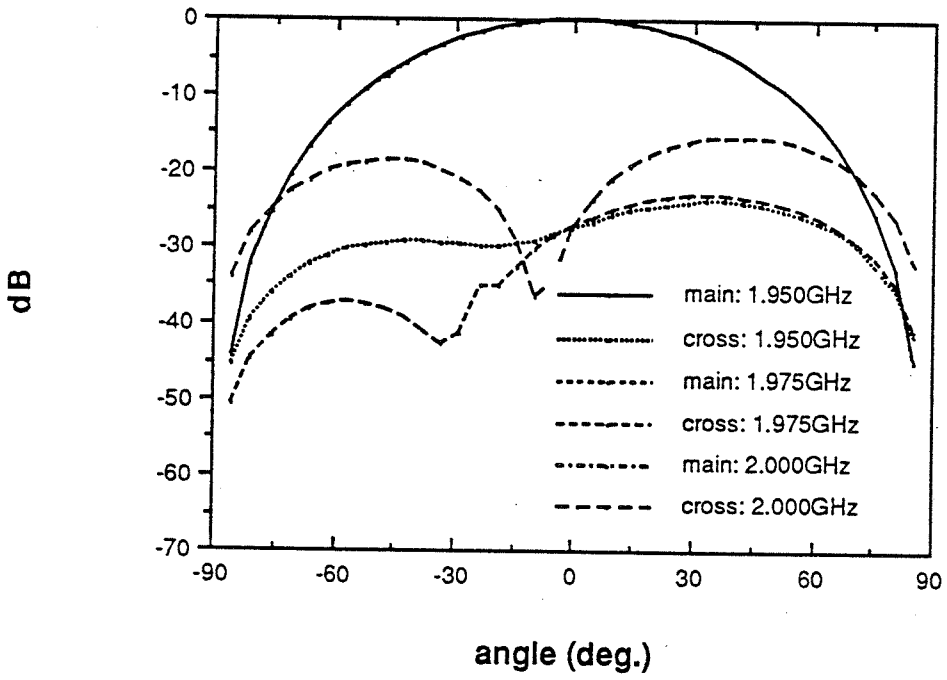

Figure 7.22: The E-plane radiation patterns of the double-patches.

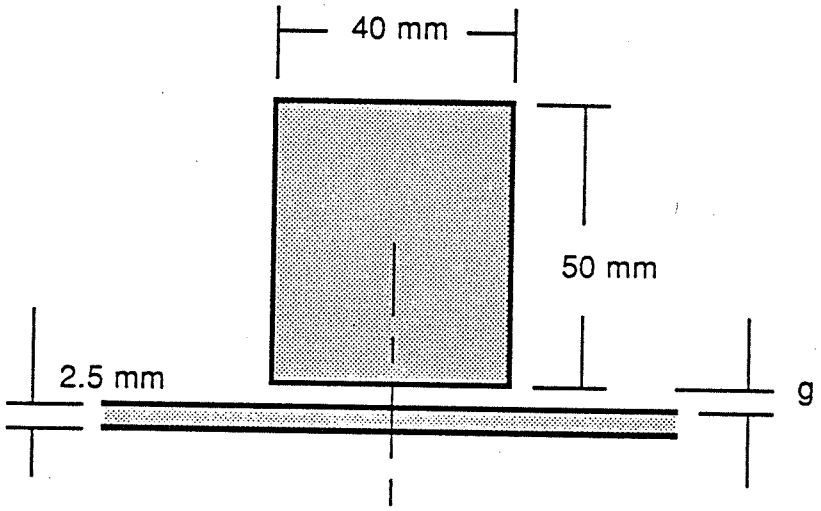

Figure 7.23: A coupled-fed microstrip patch antenna.

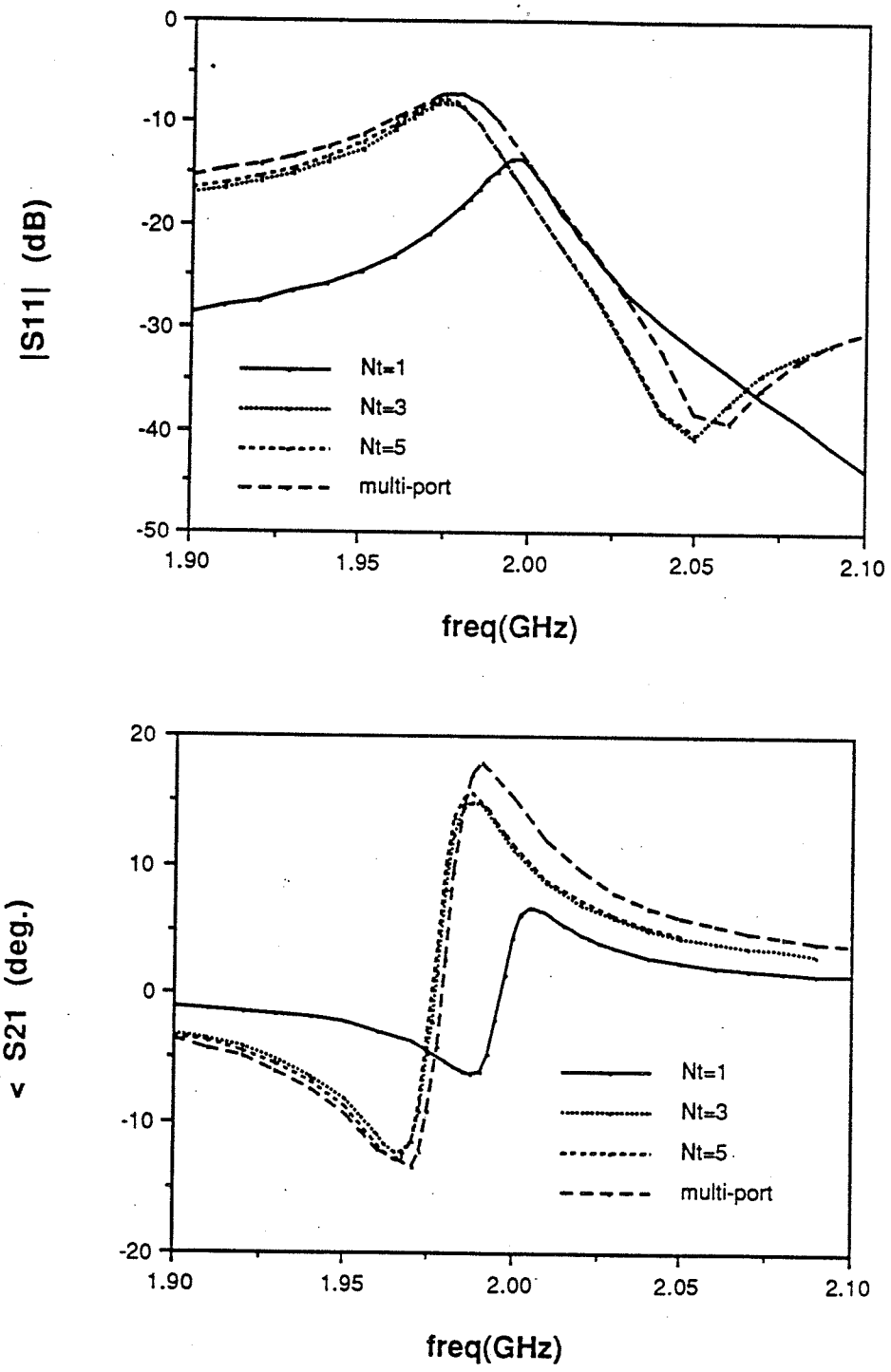

Figure 7.24: The convergence study for strip-line coupled-fed patch antenna.

the incident power can be lost. In this case, the dissipated power is very small and, therefore, we can consider the lost power is the radiated power. Except for the last one or two elements, the edge-coupled antenna can indeed be used effectively to design a series-fed array. It is also of interest to note that the phases of $S_{1,1}$ and $S_{2,1}$, measured at the symmetry plane of the antenna, are always about 180° and 0° at resonances. This feature might be helpful in array consideration.

It should be mentioned that the gap width can control the amount of power coupled to the patch only when it is a radiating-edge coupled-feed, which is capacitive, and it doesn't work well when it is a non-radiating edge coupled-feed.

7.6 Conclusions

We have demonstrated the application of the P-mesh code in the analysis and design of microstrip patch antennas. We can conclude:

(a) The edge condition of the current density distribution may be very important to the numerical accuracy of microstrip patch antennas with strong edge coupling.

(b) Multi-loaded resonances of a microstrip structure can be used to increase the bandwidth of the antenna.

(c) A configuration of two 45° - 45° - 90° triangular patches facing each other on the same substrate can increase the bandwidth substantially without occupying more space.

(d) Radiating-edge coupled antennas can be used effectively to design a series-fed array.

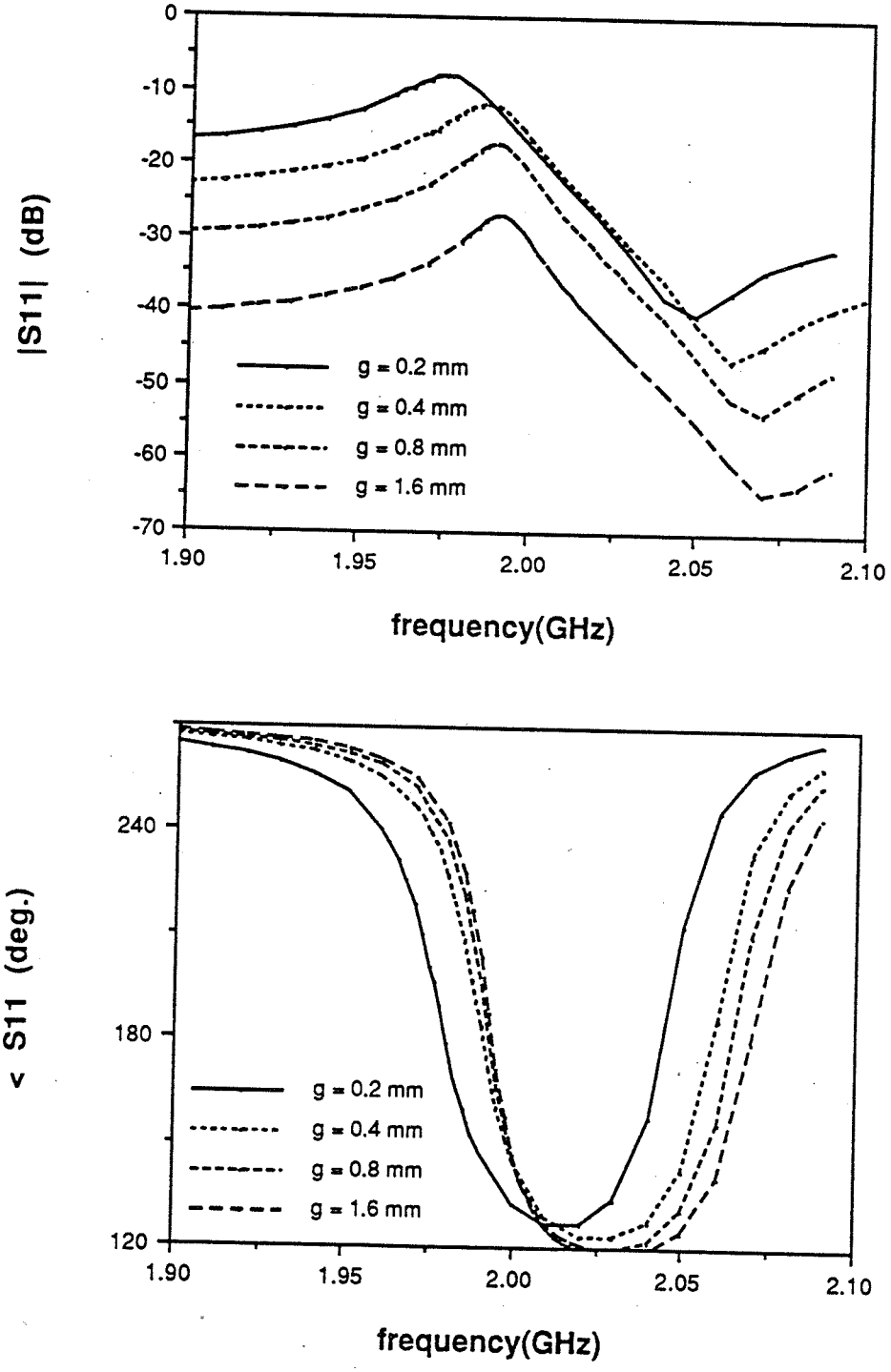

Figure 7.25. The frequency responses of $S_{1,1}$ for the coupled-fed microstrip antenna.

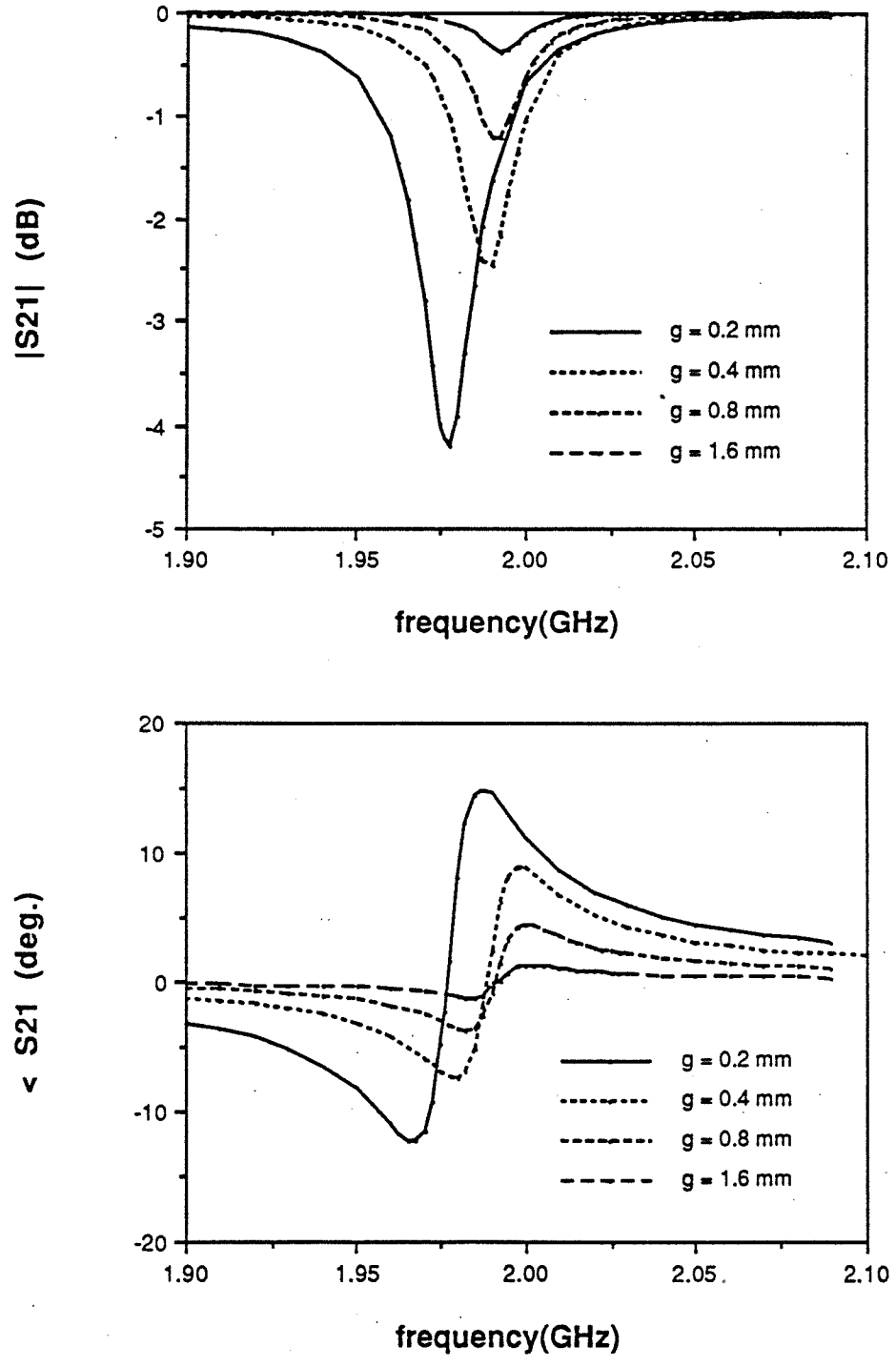

Figure 7.26. The frequency responses of $S_{2,1}$ for the coupled-fed microstrip antenna.

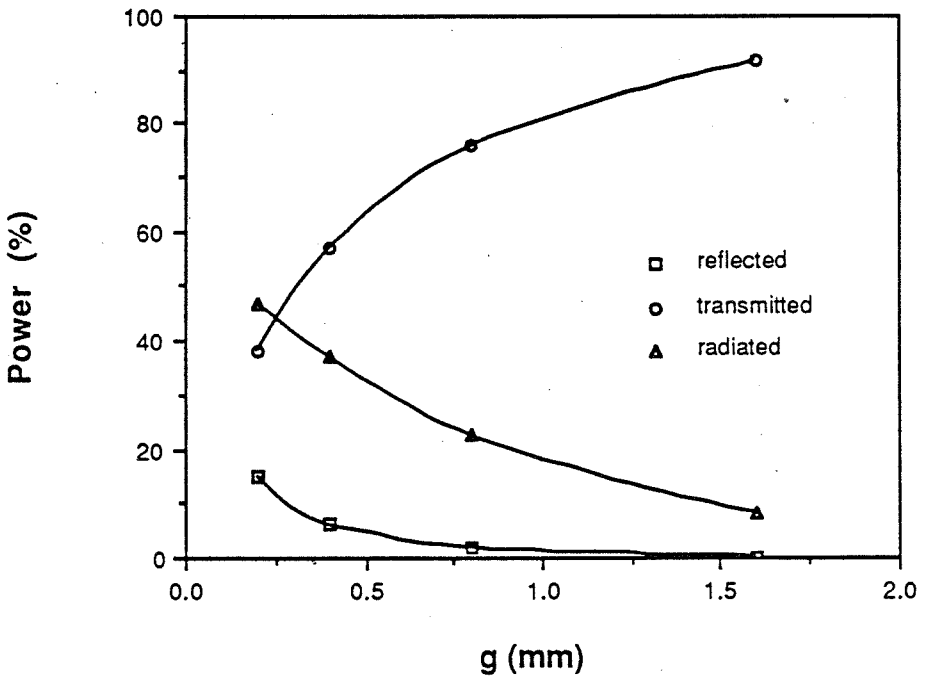

Figure 7.27. The transmitted, reflected and radiated powers as the function of gap width between the patch and the feed-line.

The References for Chapter 7

[1] J. R. James, P. S. Hall and C. Wood, **Microstrip Antenna: Theory and Design** . Peter Peregrinus LTD. , 1981.

[2] I. J. Bahl and P. Bhartia, **Microstrip Antennas**. Dedham, MA: Artech House, 1980.

[3] R. E. Munson, " Comformal microstrip antennas and microstrip phased arrays, " **IEEE Trans. on Antennas and Propagat.**, Vol, Ap-22, pp. 74-77, Jan. 1974.

[4] Y. T. Lo, D. D. Harrison, D. Solomon, G. A. Deschamps and F. R. Ore, " Study of microstrip antennas, microstrip phased arrays and microstrip feed networks, " **Rome Air Development Center Tech. Rep.** TR-77-406, Oct. 21, 1977.

[5] Y. T. Lo, D. Solomon and W. F. Richards, " Theory and experiment on microstrip antennas, " **IEEE Trans. on Antennas and Propagat.**, Vol. AP-27, pp. 137-145, 1979.

[6] W. F. Richards, Y. T. Lo and D. D. Harrison, " An improved theory for microstrip antennas and applications," **IEEE Trans. on Antennas and Propagat.**, Vol. AP-29, pp. 38-46, Jan. 1981.

[7] M. D. Deshpande and M. C. Bailey, " Input impedance of microstrip antennas, " **IEEE Trans. on Antennas and Propagat.** , Vol. AP-30, pp. 645-650, 1982.

[8] H. Pues and A. Van de Capelle, " Accurate transmission-line model for the rectangular microstrip antenna, " **IEE Proc.**, Vol. 131, Pt. H., pp. 334-340, 1984.

[9] D. C. Chang, " Analytical theory of an unloaded rectangular microstrip patch, " **IEEE Trans. on Antennas and Propagat.**, Vol. AP-29, pp. 54-62, Jan. 1981.

[10] R. Chadha and K. C. Gupta, " Segmentation method using impedance matrices for analysis of planar microwave circuits, " **IEEE Trans. on**

Microwave Theory Tech., Vol. MTT-29, pp. 71-74, Jan. 1981.

[11] A. Benella, **Multi-Port Network Model for Radiating Microstrip Patches and Applications to CAD of Microstrip Arrays.** Ph.D thesis, Dept. of ECE, University of Colorado at Boulder, May 1989.

[12] E. L. Newman, " Strip antennas in a dielectric slab, " **IEEE Trans. on Antennas and Propagat.**, Vol. AP-26, pp. 647-653, Sept. 1978.

[13] E. H. Newman and D. H. Pozar, " Electromagnetic modeling of composite wire and surface geometries," **IEEE Trans. on Antennas and Propagat.**, Vol. AP-26, pp. 784-789, Nov. 1978.

[14] T. Itoh and W. Menzel, " A full-wave analysis method for open microstrip structures," **IEEE Trans. on Antennas and Propagat.**, Vol. AP-29, pp. 63-68, Jan. 1981.

[15] W. C. Chew and J. A. Kong, " Analysis of circular microstrip disk antenna with a thick dielectric substrate, " **IEEE Trans. on Antennas and Propagat.**, Vol. AP-29, pp. 68-76, Jan. 1981.

[16] N. G. Alexopoulos, " Mutual impedance computation between printed dipoles, " **IEEE Trans. on Antennas and Propagat.**, Vol. AP-29, pp. 106-111, Jan. 1981.

[17] J. R. Mosig and F. E. Gardiol, " General integral equation formulation for microstrip antennas and scatterers, " **IEE Proc.**, Vol. 132, pp. 424-432, Dec. 1985.

[18] J. X. Zheng, **Microstrip Antennas with Thick Substrates** . Master Degree thesis, Tsinghua Univ., Beijing, China, 1986.

[19] K. R. Carver and E. L. Coffey, " Theoretical investigation of the microstrip antenna, " Physics and Sci. Lab., New Mexico State Univ. Las Cruces, Tech. Rep., PT-00929, Jan. 23, 1979.

[20] E. Chang, S. A. Zong and W. F. Richards, " An experimental investigation of electrically thick rectangular microstrip antennas, " **IEEE Trans. on Antennas Propagat.** , Vol. AP-34, pp. 767-772, Nov. 1986.

[21] D. M. Pozar and B. Kaufman, " Increasing the bandwidth of a microstrip antenna by proximity coupling, " **Electronics Lett.**, Vol. 23, pp-368-369, April 1987.

[22] C. Wood, " Improved bandwidth of microstrip antennas using parasitic elements," **IEE Proc.**, Vol. 127, pp. 231-234, Aug. 1984.

[23] S. A. Long and M. D. Walton, " A dual-frequency stacked circular-disc antenna, " **IEEE Trans. on Antennas Propagat.**, Vol. 27, pp. 270-273, March 1979.

[24] A. Sabban, " A new broad-band stacked two layer microstrip antenna," **IEEE AP-S Intern. Symposium Digest**, pp. 63-66, 1983.

[25] G. Kumar and K. C. Gupta, " Broad-band microstrip antennas using additional resonators gap coupled to radiating edges, " **IEEE Trans. on Antennas Propagat.**, Vol. 32, pp. 1375-1379, Dec. 1984.

[26] G. Kumar and K. C. Gupta, " Non-radiating edges and four edges gap-coupled multiple resonator broad band microstrip antennas," **IEEE Trans. on Antennas Propagat.**, Vol. 33, pp. 173-178, 1985.

[27] G. Dubost, G. Beauquet, J. Rocquencount and G. Bonnet, " Patch antenna bandwidth increase by means of a director, " **Electronics Lett.**, Vol. 22, pp. 1345-1347, Dec. 1986.

[28] P. S. Bhatnagar, J. P. Daniel, K. Mahdjoubl and C. Terret, " Experimental study of stacked triangular microstrip antennas, " **Electronics Lett.**, Vol. 22, pp. 864-865, 1986.

[29] J. X. Zheng and D. C. Chang, " Computer-aided design of electromagnetically-coupled and tuned, wide band microstrip patch antennas," **IEEE AP-S Intern. Symposium Digest** , pp. 1120-1123, Dallas, TX, May 1990.

[30] C. K. Aanandan, P. Mohanan and K. G. Nair, " Broad-band gap coupled microstrip antenna," **IEEE Trans. on Antennas Propagat.**, Vol. AP-38, pp. 1581-1586, Oct. 1990.

[31] R. J. Mailloux, J. F. McIlvenna and N. P. Rernweis, " Microstrip array technology, " **IEEE Trans. on Antennas Propagat.**, Vol. AP-29, pp. 25-37, Jan. 1981.

[32] E. F. Kuester and D. C. Chang, " A geometrical theory for the resonant frequencies and Q factors of some triangular microstrip patch antennas," **IEEE Trans. on Antennas and Propagat.**, Vol. AP-31, pp. 27-34, 1983.

[33] T. M. Martinson, **Edge Field Analysis of Arbitrarily Shaped Microstrip Patch Antennas.** Ph.D thesis, Dept. of ECE, University of Colorado at Boulder, 1988.

CHAPTER 8

CONCLUSIONS

The thesis has introduced a mixed-potential integral equation algorithm for the analysis of microstrip passive circuits and antennas. The primary goal is to develop an accurate and efficient CAD tool that can handle arbitrarily shaped microstrip circuits and antennas in a wide frequency range.

The algorithm began with the establishment of the mixed-potential integral equation by enforcing the boundary condition of the tangential electric field, which was expressed in terms of the current density distribution and its divergence, on the surface of a microstrip structure.

The distinguishing feature of the algorithm was the introduction of the roof-top basis functions on a combination of rectangular cells and triangular cells as the basis functions of current density distribution and the test functions for the tangential electric field. This feature makes it very efficient to use rectangular cells in the regular region and triangular cells to fit the irregular boundary of a microstrip structure.

Semi-analytical expressions for the Green's functions were obtained from extraction of the static singular parts and overlapped polynomial curve-fittings of the smooth parts of the Green's functions. The data-base for the polynomials was set up for repeated use in the evaluation of the double surface integrals or the quadruple integrals. An analytical technique was developed to

solve the quadruple integrals accurately and efficiently based upon the semi-analytical expressions of the Green's functions and the piece-wise linear current density distribution.

Other major accomplishments were the three-point curve-fitting S-parameter de-embedding scheme and efficient S-parameter de-embedding of multi-port networks. In the three-point de-embedding scheme, the current distribution along a microstrip line was detected at three uniformly spaced points for accurate determination of the complex wave propagation constant, the incoming wave and the outgoing wave. The symmetry characteristics of a passive microstrip circuit were employed to determine the S-matrix of a multi-port network of different port parameters without solving the somewhat ambiguous characteristic impedances of the ports.

A general network connection program was formulated to accomplish network inter-connections. The most important feature is its simplicity for any complicated network connection.

The algorithm was well adapted to a FORTRAN program. The program can accept cells of different sizes and orientations, and realizes true arbitrariness.

To demonstrate the versatility of the P-mesh algorithm and the P-mesh code, several structures, simple or complex, were provided for the analysis of microstrip circuit discontinuities. Good agreement between our calculated results and experimental results and results from other methods was observed. It was found that the metallic loss, mutual couplings among circuit elements and reflections from junctions are the important factors in microstrip circuit designs. On the other hand, radiation from discontinuities in a typical MMIC

circuit is generally negligibly small.

Application of the algorithm in microstrip antenna analysis was also demonstrated in the thesis. Some wide-band mechanisms were discovered from the electromagnetic simulation. It was shown that multi-loaded resonances could be used to improve the bandwidth of an antenna significantly.

Some assumptions were adopted in the algorithm developed in this thesis. It was assumed that the ground plane and substrate of a microstrip structure were infinitely extended. But, this can never be true. There is no easy way to take into consideration the finite ground plane and substrate of a microstrip structure. Fortunately, the edges of the ground planes and subtractes are generally far enough from the strips to have little effect on the field distribution. The finite thickness of the metallic strip can be approximated using the equivalent impedance boundary condition. More accurate consideration involves vertical current and is much more difficult.

The roughness or the imperfection of the ground plane can be modelled as an equivalent impedance boundary. Incorporation of an impedance boundary condition of the ground plane is non-trivial. Implementation of the P-mesh algorithm for analysis of other planar structures such as co-planar waveguides and sloted-lines can also be achieved by simply replacing the Green's functions.

A microstrip circuit generally contains not only planar structures. Some three-dimensional structures such as air-bridges and via-holes and some active elements such as transistors have to be used for circuit arrangement. Incorporation of three-dimensional elements and active elements into the P-mesh code is necessary for a layout simulation.

In this kind of integral equation methods using sub-domain basis functions, large number of basis functions are needed. Many quadruple integrals and large matrix are encounterd. Improvement has to be made to speed up the calculation. A perturbation method can be used to reduce the solution of a large structure into the solution of several small structures. An iteration method can be used to solve large matrices. It is noticed that the quadruple integrals solved in Chapter 4 are independent of frequency, substrate thickness and dielectric constant, etc. Only the coefficients in the polynomials are functions of those parameters. This characteristics can be used to significantly reduce the computational effort.

BIBLIOGRAPHY

C. K. Aanandan, P. Mohanan and K. G. Nair, " Broad-band gap coupled microstrip antenna," **IEEE Trans. on Antennas Propagat.**, Vol. AP-38, pp. 1581-1586, Oct. 1990.

N. G. Alexopoulos, " Mutual impedance computation between printed dipoles, " **IEEE Trans. on Antennas and Propagat.**, Vol. AP-29, pp. 106-111, Jan. 1981.

P. Anders and F. Arndt, " Microstrip discontinuities capacitances and inductances for double steps, mitered bends with arbitrary angle and asymmetric right-angle bends," **IEEE Trans. on Microwave Theory Tech.**, Vol. MTT-28, pp. 1213-1217, Nov. 1980.

E. L. Barsotti, **Effect of strip edge shape on microstrip conductor loss.** Master Degree Thesis, Unversity of Colorado at Boulder, 1990.

A. Benella, **Multi-Port Network Model for Radiating Microstrip Patches and Applications to CAD of Microstrip Arrays.** Ph.D thesis, Dept. of ECE, University of Colorado at Boulder, May 1989.

I. J. Bahl and P. Bhartia, **Microstrip Antennas.** Dedham, MA: Artech House, 1980.

P. Benedek and P. Silvester, " Equivalent capacitances for microstrip gaps and steps," **IEEE Trans. on Microwave Theory Tech.**, Vol. MTT-20, pp. 729-733, 1972.

P. S. Bhatnagar, J. P. Daniel, K. Mahdjoubl and C. Terret, " Experimental study of stacked triangular microstrip antennas, " **Electronics Lett.**, Vol. 22, pp. 864-865, 1986.

B. L. Brim and D. C. Chang, " Accelerated numerical computation of the spatial domain dyadic Green's functions of a grounded dielectric slab," **National Science Meeting Digest**, pp. 164, Boulder,CO, Jan. 1987.

B. L. Brim and D. C. Chang, " Closed-form expressions for static coupling between two coplanar polygon, " **National Science Meeting Digest**, pp. 60, Boulder, CO, Jan. 1987.

B. L. Brim and D. C. Chang, " The use of subsectional uniform distributions in the Galerkin-moment method solution of electromagnetics problems, " **National Science Meeting Digest**, pp. 8, Boulder, CO, Jan. 1988.

K. R. Carver and E. L. Coffey, " Theoretical investigation of the microstrip antenna, " Physics and Sci. Lab., New Mexico State Univ. Las Cruces, Tech. Rep., PT-00929, Jan. 23, 1979.

K. R. Carver and J. W. Mink, " Microstrip antenna technology, " **IEEE Trans. on Antenna Propagat.**, AP-29, pp. 2 - 24, Jan. 1981.

R. Chadha and K. C. Gupta, " Segmentation method using impedance matrices for analysis of planar microwave circuits, " **IEEE Trans. on Microwave Theory Tech.**, Vol. MTT-29, pp. 71-74, Jan. 1981.

D. C. Chang and E. F. Kuester, " An analytic theory for narrow open microstrips," **Arch. Elek. Ubertragung.**, Vol. 33, pp. 199-206, Feb. 1979.

D. C. Chang, " Analytical theory of an unloaded rectangular microstrip patch, " **IEEE Trans. on Antennas and Propagat.**, Vol. AP-29, pp. 54-62, Jan. 1981.

D. C. Chang and J. X. Zheng, " Numerical modeling of planar circuits with pseudo meshes," **National Science Meeting Digest**, pp. 265, Boulder, CO, Jan. 1990.

D. C. Chang, private communication.

D. C. Chang and J. X. Zheng, " Electromagnetic modeling of passive circuit elements in MMIC," **IEEE Trans. on Microwave Theory Tech.**, to be published.

E. Chang, S. A. Zong and W. F. Richards, " An experimental investigation of electrically thick rectangular microstrip antennas, " **IEEE Trans. on Antennas Propagat.** , Vol. AP-34, pp. 767-772, Nov. 1986.

Z. Q. Chen and B. Gao, " Deterministic approach to full-wave analysis of discontinuities in MIC's using the method of lines," **IEEE Trans. on**

Microwave Theory Tech., Vol. MTT-37, pp. 606-611, March 1989.

W. C. Chew and J. A. Kong, " Analysis of circular microstrip disk antenna with a thick dielectric substrate, " **IEEE Trans. on Antennas and Propagat.**, Vol. AP-29, pp. 68-76, Jan. 1981.

T. S. Chu, T. Itoh, " Comparative study of mode matching formulations of microstrip discontinuity problems," **IEEE Trans. on Microwave Theory Tech.**, Vol. MTT-33, pp. 1018-1023, Oct. 1985.

E. J. Denlinger, " A frequency dependent solution for microstrip transmission lines," **IEEE Trans. on Microwave Theory Tech.**, Vol. MTT-19, pp.30-39, Jan. 1971.

M. D. Deshpande and M. C. Bailey, " Input impedance of microstrip antennas, " **IEEE Trans. on Antennas and Propagat.** , Vol. AP-30, pp. 645-650, 1982.

G. Dubost, G. Beauquet, J. Rocquencount and G. Bonnet, " Patch antenna bandwidth increase by means of a director, " **Electronics Lett.**, Vol. 22, pp. 1345-1347, Dec. 1986.

G. F. Engen, **Microwave Circuit Theory and Foundation of Microwave Methology** . Priliminary draft, 1988.

A. Farrar and A. T. Adams, " Computation of lumped microstrip capacitances by matrix methods — rectangular sections and end effects", **IEEE Trans. on Microwave Theory Tech.**, Vol. MTT-19, pp. 495-496, Aug. 1971.

A. Farrar and A. T. Adams, " Matrix methods for microstrip three-dimensional problems," **IEEE Trans. on Microwave Theory Tech.**, Vol. MTT-20, pp. 497-504, 1972.

A. W. Glisson and D. R. Wilton, " Simple and efficient numerical methods for problems of electromagnetic radiation and scattering from surfaces, " **IEEE Trans. on Antennas Propag.**, Vol. AP-28, pp. 593-603, Sep. 1980.

M. Goldfarb and P. A. Platzker, " The effect of electromagnetic coupling on MMIC design," **Intern. Journal of Microwave Millimeter-wave Computer Aided Design**, to be published.

C. Goldsmith, Texas Instrument, private communication.

K. C. Gupta, **Computer-Aided Microstrip Antenna Design** . Course notes of ECEN 5004, Chapter 6, University of Colorado at Boulder, 1990.

R. F. Harrington, **Field Computations by Moment Methods**. New York: Macmillan, 1968.

M. Herman, Hughes Aircraft Company, private communication.

T. Itoh and R. Mittra, " Spectral-domain approach for calculating the dispersion characteristics of microstrip lines," **IEEE Trans. on Microwave Theory Tech.** , Vol. MTT-21, pp. 496-499, July 1973.

T. Itoh and W. Menzel, " A full-wave analysis method for open microstrip structures," **IEEE Trans. on Antennas and Propagat.**, Vol. AP-29, pp. 63-68, Jan. 1981.

R. W. Jackson and D. M. Pozar, " Full-wave analysis of microstrip open-end and gap discontinuities," **IEEE Trans. on Microwave Theory Tech.**, MTT-33, pp. 1036-1042, Oct. 1985.

R. W. Jackson, " Full-wave, finite element analysis of irregular microstrip discontinuities," **IEEE Trans. on Microwave Theory Tech.**, MTT-37, pp. 81-89, January 1989.

J. R. James, P. S. Hall and C. Wood, **Microstrip Antenna: Theory and Design** . Peter Peregrinus LTD. , 1981.

R. H. Jansen, " High-speed computation of single and coupled microstrip parameters including dispersion, high-order modes loss and finite strip thickness, " **IEEE Trans. on Microwave Theory Tech.** , Vol. MTT-26, pp. 75-82, Jan. 1978.

P. B. Katehi and N. G. Alexopoulos, " Frequency-dependent characteristics of microstrip discontinuities in millimeter-wave integrated circuits," **IEEE Trans. on Microwave Theory Tech.**, MTT-33, pp. 1029-1035, Oct. 1985.

M. Koshiba, K. Hayata and M. Suzuki, " Improved finite-element formulation in terms of the magnetic-field vector for dielectric waveguides," **IEEE Trans. on Microwave Theory Tech.**, Vol. MTT-33, pp. 227-233, March 1985.

G. Kompa, " S-matrix computation of microstrip discontinuities with a

planar waveguide model, " **Arch. Elec. Ubertragung.** , Vol. 30, pp. 58-64, 1975.

J. A. Kong, **Theory of Electromagnetic Waves.** New York: Wiley, 1975.

N. H. L. Koster and R. H. Jansen, " The equivalent circuit of the asymmetrical series gap in microstrip and suspended-substrate lines," **IEEE Trans. on Microwave Theory Tech.**, Vol. MTT-30, pp. 1273-1279, 1982.

N. H. L. Koster and R. H. Jansen, " The microstrip step discontinuity: A revised description, " **IEEE Trans. on Microwave Theory Tech.**, Vol. MTT-34, pp. 213-223, Feb. 1986.

E. F. Kuester and D. C. Chang, " An appraisal of methods for compuation of the dispersion characteristics of open microstrip, " **IEEE Trans. on Microwave Theory Tech.** , Vol. MTT-27, pp. 691-694, July, 1979.

E. F. Kuester and D. C. Chang, " Theory of dispersion in microstrip arbitrary width," **IEEE Trans. on Microwave Theory Tech.** , Vol. MTT-28, pp. 259-265, March 1980.

E. F. Kuester and D. C. Chang, " A geometrical theory for the resonant frequencies and Q factors of some triangular microstrip patch antennas," **IEEE Trans. on Antennas and Propagat.**, Vol. AP-31, pp. 27-34, 1983.

E. F. Kuester and D. C. Chang, **Electromagnetic Boundary Problems.** Course Notes for ECEN 5144, Chapter 1, University of Colorado at Boulder, 1988.

E. F. Kuester and D. C. Chang, **Theory of Waveguides and Transmission Lines** . Course notes of ECEN 5114, Chapter 3, University of Colorado at Boulder, 1989.

E. F. Kuester, private communication.

D. L. Kuipers and D. R. Timman, **Handbook of Mathematics.** Pergaman Press Ltd., pp.179-182, 1969.

G. Kumar and K. C. Gupta, " Broad-band microstrip antennas using additional resonators gap coupled to radiating edges, " **IEEE Trans.**

on Antennas Propagat., Vol. 32, pp. 1375-1379, Dec. 1984.

G. Kumar and K. C. Gupta, " Non-radiating edges and four edges gap-coupled multiple resonator broad band microstrip antennas," **IEEE Trans. on Antennas Propagat.**, Vol. 33, pp. 173-178, 1985.

K. Larson and J. Dunn, University of Colorado at Boulder, private communication.

Y. T. Lo, D. D. Harrison, D. Solomon, G. A. Deschamps and F. R. Ore, " Study of microstrip antennas, microstrip phased arrays and microstrip feed networks, " **Rome Air Development Center Tech. Rep.** TR-77-406, Oct. 21, 1977.

Y. T. Lo, D. Solomon and W. F. Richards, " Theory and experiment on microstrip antennas, " **IEEE Trans. on Antennas and Propagat.**, Vol. AP-27, pp. 137-145, 1979.

L. Lewin, " A method of avoiding the edge current divergence in perturbation loss calculation, " **IEEE Trans. on Microwave Theory and Tech.**, Vol. MTT-32, pp. 717-719, 1984.

S. A. Long and M. D. Walton, " A dual-frequency stacked circular-disc antenna, " **IEEE Trans. on Antennas Propagat.**, Vol. 27, pp. 270-273, March 1979.

Y. L. Luke, **Integrals of Bessel functions**. McGrqw Hill Book Company, Inc., 1962

R. J. Mailloux, J. F. McIlvenna and N. P. Rernweis, " Microstrip array technology, " **IEEE Trans. on Antennas Propagat.**, Vol. AP-29, pp. 25-37, Jan. 1981.

T. M. Martinson, **Edge Field Analysis of Arbitrarily Shaped Microstrip Patch Antennas**. Ph.D thesis, Dept. of ECE, University of Colorado at Boulder, 1988.

W. Menzel and I. Wolff, " A method for calculating the frequency-dependent properties of microstrip discontinuities," **IEEE Trans. on Microwave Therory Tech.**, MTT-25, pp. 107-112, Feb. 1977.

A. Milton and A. S. Iren, **Handbook of mathematical functions: with formulas, graphs and mathematical tables**. New York Dover Publications , 1965.

R. Mittra and T. Itoh, " A new technique for the analysis of the dispersion characteristics of microstrip lines," **IEEE Trans. on Microwave Theory Tech.** , Vol. MTT-19, pp. 47-56, Jan. 1971.

J. C. Moore, J. X. Zheng, E. F. Kuester, D. C. Chang, " De-embedding characteristic impedance and S-parameters from numerically determined current distributions of planar junctions," to be published.

J. R. Mosig and F. E. Gardiol, " General integral equation formulation for microstrip antennas and scatterers, " **IEE Proc.**, Vol. 132, pp. 424-432, Dec. 1985.

J. R. Mosig, "Arbitrarily shaped microstrip structures and their analysis with a mixed potential integral equation," **IEEE Trans. on Microwave Theory Tech.**, MTT-36, pp. 314-323, February 1988.

R. E. Munson, " Comformal microstrip antennas and microstrip phased arrays, " **IEEE Trans. on Antennas and Propagat.**, Vol, Ap-22, pp. 74-77, Jan. 1974.

S. Nam, H. Ling and T. Itoh, " Characterization of uniform microstrip line and its discontinuities using time-domain method of lines," **IEEE Trans. on Microwave Theory Tech.**, Vol. MTT-37, pp. 2051-2057, Dec. 1989.

E. H. Newman and D. H. Pozar, " Electromagnetic modeling of composite wire and surface geometries," **IEEE Trans. on Antennas and Propagat.**, Vol. AP-26, pp. 784-789, Nov. 1978.

E. L. Newman, " Strip antennas in a dielectric slab, " **IEEE Trans. on Antennas and Propagat.**, Vol. AP-26, pp. 647-653, Sept. 1978.

T. Okoshi, Y. Uehara and T. Takeuchi, " The segmentation method: an approach to the analysis of microwave planar lines," **IEEE Trans. on Microwave Theory Tech.** , Vol. MTT-24, pp. 662-668, Oct. 1976.

R. P. Owens, " Predicted frequency dependence of microstrip characteristic impedance using the planar-waveguide model, " **Electron. Lett.**, Vol. 12, pp. 260-270, 1976.

S. T. Peng, C-K. C. Tzuang and C. D. Chen, " Full-wave analysis of lossy transmission line incorporating the metal modes," **IEEE Intern. Microwave Symposium Digest,** Vol. 1, pp. 171-174, Dallas, TX, May 1990.

W. H. Perkins, N. Jansen, T. A. Midford, W. C. Niehaus, D. H. Reep and J. Tenedorio " MIMIC technology transportability," **IEEE MTT Intern. Microwave Symposium Digest**, pp. 109-112, Dallas, TX, May 1990.

D. M. Pozar and B. Kaufman, " Increasing the bandwidth of a microstrip antenna by proximity coupling, " **Electronics Lett.**, Vol. 23, pp-368-369, April 1987.

H. Pues and A. Van de Capelle, " Accurate transmission-line model for the rectangular microstrip antenna, " **IEE Proc.**, Vol. 131, Pt. H., pp. 334-340, 1984.

B. M. A. Rahman and J. B. Davies, " Finite-element analysis of optical and microwave waveguide problems," **IEEE Trans. on Microwave Theory Tech.**, Vol. MTT-32, pp. 20-28, Jan. 1984.

C. J. Railton and J. P. McGeehau, " Analysis of microstrip discontinuities using the finite difference time-domain technique, " **IEEE MTT-S Digest**, pp. 1009-1012, June 1989.

S. M. Rao, D. R. Wilton and A. W. Glisson, " Electromagnetic scattering by surfaces of arbitrary shape, " **IEEE Trans. on Antennas Propag.** , Vol. AP-30, pp. 409-418, 1982.

J. C. Rautio and R. F. Harrington, " Preliminary results of a time-harmonic electromagnetic analysis of shielded microstrip circuits, " **27th Automatic RF Techniques Group Conference Digest**, Baltimore, pp. 121-134, June 1986.

J. C. Rautio and R. F. Harrington, " An electromagnetic time-harmonic analysis of shielded microstrip circuits," **IEEE Trans. on Microwave Theory Tech.**, Vol. MTT-35, pp. 726-730, Aug. 1987.

J. C. Rautio and R. F. Harrington, " An efficient electromagnetic analysis of arbitrary microstrip circuits," **IEEE MTT Intern. Microwave Symposium Digest**, pp. 295-298, 1987.

W. F. Richards, Y. T. Lo and D. D. Harrison, " An improved theory for microstrip antennas and applications," **IEEE Trans. on Antennas and Propagat.**, Vol. AP-29, pp. 38-46, Jan. 1981.

J. H. Richmond, " A wire-grid model for scattering by conducting bodies," **IEEE Trans. on Antennas Propag.** , Vol. AP-14, pp. 782-786,

Nov. 1966.

M. Rittwegar and I. Wolff, "Analysis of complex passive (M)MIC-components using the finite difference time-domain approach," **IEEE MTT Intern. Microwave Symposium Digest**, pp. 1147-1150, May 1990.

R. R. Romanofsky, " Analytical and experimental procedures for determining propagation characteristics of millimeter-wave gallium arsenide microstrip lines," NASA Technical Paper 2899, 1989.

A. Sabban, " A new broad-band stacked two layer microstrip antenna," **IEEE AP-S Intern. Symposium Digest**, pp. 63-66, 1983.

A. Sabban and K. C. Gupta, " A planar-lumped model for coupled microstrip line discontinuities," **IEEE Trans. on Microwave Theory Tech. Special Issue**, MTT-38, Dec. 1990, to be published.

T. B. A. Senior, " Impedance boundary conditions for imperfectly conducting surfaces, " **Applied Scientific Research**, Section B, Vol. 17, pp. 418-436, 1960.

Shih-chang Wu, Hung-Yu Yang and N. G. Alexopoulos, " A rigorous dispersive characteristics of microstrip cross and tee-junctions," **IEEE MTT Intern. Microwave Symposium Digest**, pp. 1151-1154, May 1990.

P. Silvester and P. Benedek, " Microstrip discontinuity capacitance for right-angle bends, T-junctions and crossings," **IEEE Trans. on Microwave Theory Tech.**, Vol. MTT-21, pp. 341-346, 1973.

A. J. W. Sommerfeld, **Lectures on Theoretical Physics**. New York, Academic Press, Vol. 6 **Partial differential equations in physics**, 1956.

V. A. Strattron, **Electromagnetic Theory**. New York, McGraw - Hill Book Co., 1941.

A. F. Thomson and A. Gopinath, " Calculation of microstrip discontinuity inductances," **IEEE Trans. on Microwave Theory Tech.**, Vol. MTT-23, pp. 648-654, 1975.

L. A. Vainshtein and S. M. Zhurav, " Strong skin effect at the edges of metal plates," [Russian], **Pis'ma Zh. Tekh. Fiz.** , Vol. 12, pp.723-729,

1986. [Engl. transl. in **Sov. Tech. Phys. Lett.**, Vol. 12, pp. 298-299, 1986]

S. Vijayakumar and D. E. Cormack, " An invariant imbedding method for singular integral evaluation on finite domains, " **SIAM J. Appl. Math.**, Vol. 48, No. 6, pp, 1335-1349, Dec. 1988.

J. R. Wait, **Electromagnetic Waves in Stratified Media**. Oxford, New York, Pergemon Press, 1970.

H. A. Wheeler, " Transmission-line properties of parallel strips separated by a dielectric sheet, " **IEEE Trans. on Microwave Theory Tech.**, Vol. MTT-13, pp. 172-185, Feb. 1965.

W. Wertgen and R. H. Jansen, " Efficient direct and iterative electrodynamic analysis of geometrically complex MIC and MMIC structures," **Intern. Journal of Numerical Modeling: Electronic Networks, Devices and Fields**, Vol.2, 153-186, 1989.

I Wolff, G. Kompa, and R. Mehran, " Calculation method for microstrip discontinuities and T-junctions, " **Electron. Lett.**, Vol. 8, pp. 177-179, 1972.

C. Wood, " Improved bandwidth of microstrip antennas using parasitic elements," **IEE Proc.**, Vol. 127, pp. 231-234, Aug. 1984.

S. B. Worm and R. Pregla, " Hybrid-mode analysis of arbitrarily shaped planar microwave structures," **IEEE Trans. on Microwave Theory Tech.** , Vol. MTT-32, pp. 191-196, 1984.

D. I. Wu and D. C. Chang, " Solving microstrip discontinuity problems using an embeded technique, " **Joint IEEE-AP/URSI Conference Digest**, Dallas, TX, TX, May 1990.

D. I. Wu, D. C. Chang and B. I. Brim, "Accurate numerical modeling of microstrip junctions and discontinuities," **Intern. Journal of Microwave Millimeter-wave Computer Aided Engineering**, to be published.

D. I. Wu and D. C. Chang, " A review on the electromagnetic properties of the guiding structures in MMIC, " to be published.

H. Y. Yang, N. G. Alexopoulos and D. R. Jackson, " Microstrip open-end and gap discontinuities in a substrate-superstrate structure," **IEEE**

Trans. on Microwave Theory Tech., Vol. MTT-37, pp. 1542-1546, Oct. 1989.

X. Zhang and K. K. Mei, "Time-domain finite difference approach to the calculation of the frequency-dependent characteristics of microstrip discontinuities," **IEEE Trans. on Microwave Theory Tech.**, vol. MTT-36, pp. 1775-1787, Dec. 1988.

X. Zhang, J. Fang, K. K. Mei and Y. Liu, " Calculations of the dispersive characteristics of microstrips by the time-domain finite difference method, " **IEEE Trans. on Microwave Theory Tech.** , Vol. MTT-36, pp. 263-267, Feb. 1988.

J. X. Zheng, **Microstrip Antennas with Thick Substrates** . Master Degree thesis, Tsinghua Univ., Beijing, China, 1986.

J. X. Zheng and D. C. Chang, " Convergence of the numerical solution for a microstrip junction based upon a triangular cell expansion," **National Science Meeting Digest**, pp.212, Boulder, CO, Jan. 1990.

J. X. Zheng and D. C. Chang, " Numerical modeling of chamfered bends and other microstrip junctions of general shape in MMICs," **IEEE MTT Intern. Microwave Symposium Digest**, pp. 709-712, Dallas, TX , May 1990.

J. X. Zheng and D. C. Chang, " Computer-aided design of electromagnetically-coupled and tuned, wide band microstrip patch antennas," **IEEE AP-Symposium Digest** , pp.1120-1123, Dallas, TX, May 1990.

APPENDIX A

THE CLOSED-FORM SOLUTION OF THE $D(S,T,M,N)$ AND $DL(S,T,M,N)$

The integrals $D(s,t,m,n)$ and $DL(s,t,m,n)$ are defined in Chapter 4 and are repeated here.

$$D(s,t,m,n) = \int dt\, t^n \rho^m \; ; m = -1, 0, ... \tag{A.1}$$

$$DL(s,t,m,n) = \int dt\, t^n \ln(\rho + m\,t) \; ; m = -1 \text{ or } 1 \tag{A.2}$$

where

$$\rho = \sqrt{s^2 + t^2} \tag{A.3}$$

The solutions of the integrals should contain some arbitrary functions of s. But, these arbitrary functions of s don't affect the solution in Chapter 4 and will not be included here.

The procedure of solving the integrals is not provided here. Only the final result will be listed.

$$D(s,t,-1,0) = \ln(\rho + t) \tag{A.4}$$

$$D(s,t,-1,1) = \rho \tag{A.5}$$

$$D(s,t,-1,n) = \frac{1}{n}\left[t^{n-1}\rho - (n-1)\,s^2\,D(s,t,-1,n-2)\right]; n \geq 2 \qquad \text{(A.6)}$$

$$D(s,t,m,n) = \frac{1}{n+2}\left[t^{n+1}\rho + s^2\,D(s,t,-1,n)\right]\ ;\ n \geq 0 \qquad \text{(A.7)}$$

$$DL(s,t,-1,n) = \frac{1}{n+1}\left[t^{n+1}\,\ln(\rho - t) + D(s,t,-1,n+1)\right]\ ;\ n \geq 0 \qquad \text{(A.8)}$$

$$DL(s,t,1,n) = \frac{1}{n+1}\left[t^{n+1}\,\ln(\rho + t) + D(s,t,-1,n+1)\right]\ ;\ n \geq 0 \qquad \text{(A.9)}$$

APPENDIX B

THE CLOSED-FORM SOLUTION OF $C(S_I, T_I, S_J, T_J, M, N, K)$ AND $CL(S_I, T_I, S_J, T_J, M, N, K)$

The integrals $C(s_i, t_i, s_j, t_j, m, n, k)$ and $CL(s_i, t_i, s_j, t_j, m, n, k)$ are defined in Chapter 4 and repeated here.

$$C(s_i, t_i, s_j, t_j, m, n, k) = \int_{s_i}^{s_j} ds\, \rho^m\, s^n\, t^k \qquad -1 \leq m \leq 1 \tag{B.1}$$

$$CL(s_i, t_i, s_j, t_j, m, n, k) = \int_{s_i}^{s_j} ds\, s^n\, t^k\, \ln(\rho + m\, t) \qquad m = -1 \text{ or } 1 \tag{B.2}$$

where

$$\rho = \sqrt{s^2 + t^2} \tag{B.3}$$

$$t = a\, s + b \tag{B.4}$$

$$a = \frac{t_j - t_i}{s_j - s_i} \tag{B.5}$$

$$b = t_i - a\, s_i \tag{B.6}$$

The solution is

$$C(s_i,t_i,s_j,t_j,-1,0,0) = \frac{1}{\sqrt{1+a^2}}\,\ln(\sqrt{1+a^2}\,\rho + s + a\,t)|_{s_i}^{s_j} \qquad \text{(B.7)}$$

$$C(s_i,t_i,s_j,t_j,-1,1,0) = \frac{1}{1+a^2}\left[\rho|_{s_i}^{s_j} - a\,b\,C(s_i,t_i,s_j,t_j,-1,0,0)\right] \qquad \text{(B.8)}$$

$$\begin{aligned} C(s_i,t_i,s_j,t_j,-1,n,0) \;=\; & \frac{1}{n(1+a^2)}\left[s^{n-1}\,\rho|_{s_i}^{s_j} - \right. \\ & (2n-1)\,a\,b\,C(s_i,t_i,s_j,t_j,-1,n-1,0) - \\ & \left.(n-1)\,b^2\,C(s_i,t_i,s_j,t_j,-1,n-2,0)\right]\;;n \geq 2 \end{aligned} \qquad \text{(B.9)}$$

$$C(s_i,t_i,s_j,t_j,0,n,0) = \frac{1}{n+1}\,s^{n+1}\,|_{s_i}^{s_j}\;;\; n \geq 0 \qquad \text{(B.10)}$$

$$\begin{aligned} C(s_i,t_i,s_j,t_j,m,n,k) \;=\; & a\,C(s_i,t_i,s_j,t_j,m,n+1,k-1) + \\ & b\,C(s_i,t_i,s_j,t_j,m,n,k-1) \\ & m \geq -1\;;\; n \geq 0\;;\; k \geq 1 \end{aligned} \qquad \text{(B.11)}$$

$$\begin{aligned} C(s_i,t_i,s_j,t_j,m,n,k) \;=\; & C(s_i,t_i,s_j,t_j,m-2,n+2,k) + \\ & C(s_i,t_i,s_j,t_j,m-2,n,k+2) \\ & m \geq 2\;;\; n \geq 0\;;\; k \geq 0 \end{aligned} \qquad \text{(B.12)}$$

$$CL(s_i,t_i,s_j,t_j,m,n,0) = \frac{s^{n+1}}{n+1}\left[\ln(\rho+m\,t)-\frac{1}{n}\right]\Big|_{s_i}^{s_j} + m\,\frac{b}{n+1}\,C(s_i,t_i,s_j,t_j,-1,n,0)$$
$$m=-1 \text{ or } 1\ ;\ n\geq 0 \qquad \text{(B.13)}$$

$$CL(s_i,t_i,s_j,t_j,m,n,k) = a\,CL(s_i,t_i,s_j,t_j,m,n+1,k-1) + CL(s_i,t_i,s_j,t_j,m,n,k-1)$$
$$m=-1 \text{ or } 1\ ;\ n\geq 0\ ;\ k\geq 1 \qquad \text{(B.14)}$$

APPENDIX C

THE CLOSED FORM SOLUTION OF $E(S_I, T_I, S_J, T_J, M, N, K)$ AND $EL(S_I, T_I, S_J, T_J, M, N, K)$

The integrals $E(s_i, t_i, s_j, t_j, m, n, k)$ and $EL(s_i, t_i, s_j, t_j, m, n, k)$ are defined in Chapter 4 and repeated here.

$$E(s_i, t_i, s_j, t_j, m, n, k) = \int_{s_i}^{s_j} ds\, s^k\, D(s, t, m, n) \tag{C.1}$$

$$EL(s_i, t_i, s_j, t_j, m, n, k) = \int_{s_i}^{s_j} ds\, s^k\, DL(s, t, m, n) \tag{C.2}$$

where t is defined in (B.4); $D(s, t, m, n)$ and $DL(s, t, m, n)$ are defined in Appendix A.

The integrals can be expressed in terms of the result of Appendix B.

$$E(s_i, t_i, s_j, t_j, -1, 0, k) = CL(s_i, t_i, s_j, t_j, 1, k, 0) \tag{C.3}$$

$$E(s_i, t_i, s_j, t_j, -1, 1, k) = C(s_i, t_i, s_j, t_j, 1, k, 0) \tag{C.4}$$

$$\begin{aligned} E(s_i, t_i, s_j, t_j, -1, n, k) \;=\; & \frac{1}{n}\,[C(s_i, t_i, s_j, t_j, 1, k, n-1) - \\ & (n-1)\, E(s_i, t_i, s_j, t_j, -1, n-2, k+2)] \\ & n \geq 2 \end{aligned} \tag{C.5}$$

$$E(s_i,t_i,s_j,t_j,m,n,k) = \frac{1}{m+n+1}[C(s_i,t_i,s_j,t_j,m,k,n+1)+ m\,E(s_i,t_i,s_j,t_j,m-2,n,k+2)]$$

$$n \geq 0 \qquad \text{(C.6)}$$

$$E(s_i,t_i,s_j,t_j,m,n,k) = \frac{1}{n+1}[CL(s_i,t_i,s_j,t_j,m,k,n+1)- m\,E(s_i,t_i,s_j,t_j,-1,n+1,k)]$$

$$m = -1 \text{ or } 1 \; ; \; n \geq 0 \qquad \text{(C.7)}$$

APPENDIX D

THE EXPRESSIONS OF THE INTEGRALS INVOLVED IN APPENDIX F

The integrals $G(s_m, t_m, s_{m+1}, t_{m+1}, n)$, $H(s_m, t_m, s_{m+1}, t_{m+1}, n)$, etc., used in Section 4.5.1 and Appendix F are solved and expressed in terms of the $C(s_m, t_m, s_{m+1}, t_{m+1}, \gamma, \mu, \nu)$ and $CL(s_m, t_m, s_{m+1}, t_{m+1}, \gamma, \mu, \nu)$ defined in Appendix B. The solutions are listed next.

$$\begin{aligned} G(s_m, t_m, s_{m+1}, t_{m+1}, n) &= CL(s_m, t_m, s_{m+1}, t_{m+1}, -1, n, 1) + \\ & \quad C(s_m, t_m, s_{m+1}, t_{m+1}, 1, n, 0) \end{aligned} \tag{D.1}$$

$$\begin{aligned} H(s_m, t_m, s_{m+1}, t_{m+1}, n) &= 3\,C(s_m, t_m, s_{m+1}, t_{m+1}, 1, n, 1) + \\ & \quad 2\,CL(s_m, t_m, s_{m+1}, t_{m+1}, -1, n, 2) + \\ & \quad CL(s_m, t_m, s_{m+1}, t_{m+1}, 1, n+2, 0) \end{aligned} \tag{D.2}$$

$$\begin{aligned} K(s_m, t_m, s_{m+1}, t_{m+1}, n) &= C(s_m, t_m, s_{m+1}, t_{m+1}, 1, n, 1) + \\ & \quad 2\,CL(s_m, t_m, s_{m+1}, t_{m+1}, -1, n, 2) - \\ & \quad CL(s_m, t_m, s_{m+1}, t_{m+1}, 1, n+2, 0) \end{aligned} \tag{D.3}$$

$$\begin{aligned} L(s_m, t_m, s_{m+1}, t_{m+1}, n) &= H(s_m, t_m, s_{m+1}, t_{m+1}, n) + \\ & \quad K(s_m, t_m, s_{m+1}, t_{m+1}, n) \end{aligned} \tag{D.4}$$

$$M(s_m,t_m,s_{m+1},t_{m+1},n) = 4\,C(s_m,t_m,s_{m+1},t_{m+1},1,n,2) + C(s_m,t_m,s_{m+1},t_{m+1},1,n+2,0) + 3\,CL(s_m,t_m,s_{m+1},t_{m+1},-1,n,2) \quad \text{(D.5)}$$

$$N(s_m,t_m,s_{m+1},t_{m+1},n) = 2\,C(s_m,t_m,s_{m+1},t_{m+1},1,n+2,0) - C(s_m,t_m,s_{m+1},t_{m+1},1,n,2) + 3\,CL(s_m,t_m,s_{m+1},t_{m+1},-1,n+2,1) \quad \text{(D.6)}$$

$$P(s_m,t_m,s_{m+1},t_{m+1},n) = \frac{1}{2}[13\,C(s_m,t_m,s_{m+1},t_{m+1},1,n+2,1) - 2\,C(s_m,t_m,s_{m+1},t_{m+1},1,n,3) + 3\,CL(s_m,t_m,s_{m+1},t_{m+1},1,n+4,0) + 12\,CL(s_m,t_m,s_{m+1},t_{m+1},-1,n+2,2)] \quad \text{(D.7)}$$

$$R(s_m,t_m,s_{m+1},t_{m+1},n) = \frac{3}{2}[C(s_m,t_m,s_{m+1},t_{m+1},1,n+2,1) - 2\,C(s_m,t_m,s_{m+1},t_{m+1},1,n,3) - CL(s_m,t_m,s_{m+1},t_{m+1},1,n+4,0) + 4\,CL(s_m,t_m,s_{m+1},t_{m+1},-1,n+2,2)] \quad \text{(D.8)}$$

$$T(s_m, t_m, s_{m+1}, t_{m+1}, n) = P(s_m, t_m, s_{m+1}, t_{m+1}, n) + R(s_m, t_m, s_{m+1}, t_{m+1}, n) \quad \text{(D.9)}$$

$$\begin{aligned} V(s_m, t_m, s_{m+1}, t_{m+1}, n) = \frac{3}{5}[&-3\,C(s_m, t_m, s_{m+1}, t_{m+1}, 1, n, 4) + \\ &14\,C(s_m, t_m, s_{m+1}, t_{m+1}, 1, n+2, 2) + \\ &C(s_m, t_m, s_{m+1}, t_{m+1}, 1, n+4, 0) + \\ &15\,CL(s_m, t_m, s_{m+1}, t_{m+1}, -1, n+2, 3)] \end{aligned} \quad \text{(D.10)}$$

$$\begin{aligned} W(s_m, t_m, s_{m+1}, t_{m+1}, n) = &-2\,CL(s_m, t_m, s_{m+1}, t_{m+1}, 1, n, 4) - \\ &9\,C(s_m, t_m, s_{m+1}, t_{m+1}, 1, n+2, 2) + \\ &8\,C(s_m, t_m, s_{m+1}, t_{m+1}, 1, n+4, 0) + \\ &15\,CL(s_m, t_m, s_{m+1}, t_{m+1}, -1, n+4, 1) \end{aligned} \quad \text{(D.11)}$$

$$\begin{aligned} X(s_m, t_m, s_{m+1}, t_{m+1}, n) = \frac{1}{3}[&-4\,C(s_m, t_m, s_{m+1}, t_{m+1}, 1, n, 5) - \\ &28\,C(s_m, t_m, s_{m+1}, t_{m+1}, 1, n+2, 3) + \\ &81\,C(s_m, t_m, s_{m+1}, t_{m+1}, 1, n+4, 1) + \\ &90\,CL(s_m, t_m, s_{m+1}, t_{m+1}, -1, n+4, 2) + \\ &15\,CL(s_m, t_m, s_{m+1}, t_{m+1}, 1, n+6, 0)] \end{aligned} \quad \text{(D.12)}$$

$$
\begin{aligned}
Y(s_m, t_m, s_{m+1}, t_{m+1}, n) \;=\; & \frac{5}{3}[-4\,C(s_m, t_m, s_{m+1}, t_{m+1}, 1, n, 5) - \\
& 16\,C(s_m, t_m, s_{m+1}, t_{m+1}, 1, n+2, 3) - \\
& 3\,C(s_m, t_m, s_{m+1}, t_{m+1}, 1, n+4, 1) + \\
& 18\,CL(s_m, t_m, s_{m+1}, t_{m+1}, -1, n+4, 2) - \\
& 3\,CL(s_m, t_m, s_{m+1}, t_{m+1}, 1, n+6, 0)]
\end{aligned}
\tag{D.13}
$$

$$
\begin{aligned}
Z(s_m, t_m, s_{m+1}, t_{m+1}, n) \;=\; & X(s_m, t_m, s_{m+1}, t_{m+1}, n) + \\
& Y(s_m, t_m, s_{m+1}, t_{m+1}, n)
\end{aligned}
\tag{D.14}
$$

$$
\begin{aligned}
A(s_m, t_m, s_{m+1}, t_{m+1}, n) \;=\; & \frac{3}{7}[-6\,C(s_m, t_m, s_{m+1}, t_{m+1}, 1, n, 6) - \\
& 249\,C(s_m, t_m, s_{m+1}, t_{m+1}, 1, n+2, 4) + \\
& 10\,C(s_m, t_m, s_{m+1}, t_{m+1}, 1, n+4, 2) + \\
& 148\,C(s_m, t_m, s_{m+1}, t_{m+1}, 1, n+6, 0) + \\
& 105\,CL(s_m, t_m, s_{m+1}, t_{m+1}, -1, n+4, 3)]
\end{aligned}
\tag{D.15}
$$

APPENDIX E

THE EXPRESSIONS OF THE INTEGRALS INVOLVED IN APPENDIX G

The integrals $GD(s_m, t_m, s_{m+1}, t_{m+1}, \nu, \gamma)$, $HD(s_m, t_m, s_{m+1}, t_{m+1}, \nu, \gamma)$, etc., in Appendix G are expressed in terms of the $E(s_m, t_m, s_{m+1}, t_{m+1}, \nu, \gamma)$ and $EL(s_m, t_m, s_{m+1}, t_{m+1}, \nu, \gamma)$ listed in Appendix C. The solutions are listed next.

$$\begin{aligned} GD(s_m, t_m, s_{m+1}, t_{m+1}, \nu, \gamma) &= E(s_m, t_m, s_{m+1}, t_{m+1}, 1, \nu, \gamma) + \\ & \quad EL(s_m, t_m, s_{m+1}, t_{m+1}, -1, \nu+1, \gamma) \end{aligned} \tag{E.1}$$

$$\begin{aligned} HD(s_m, t_m, s_{m+1}, t_{m+1}, \nu, \gamma) &= \frac{1}{4}[3\,E(s_m, t_m, s_{m+1}, t_{m+1}, 1, \nu+1, \gamma) + \\ & \quad 2\,EL(s_m, t_m, s_{m+1}, t_{m+1}, -1, \nu+2, \gamma) + \\ & \quad EL(s_m, t_m, s_{m+1}, t_{m+1}, 1, \nu, \gamma+2)] \end{aligned} \tag{E.2}$$

$$\begin{aligned} KD(s_m, t_m, s_{m+1}, t_{m+1}, \nu, \gamma) &= \frac{1}{4}[E(s_m, t_m, s_{m+1}, t_{m+1}, 1, \nu+1, \gamma) + \\ & \quad 2\,EL(s_m, t_m, s_{m+1}, t_{m+1}, -1, \nu+2, \gamma) - \\ & \quad EL(s_m, t_m, s_{m+1}, t_{m+1}, 1, \nu, \gamma+2)] \end{aligned} \tag{E.3}$$

$$LD(s_m, t_m, s_{m+1}, t_{m+1}, \nu, \gamma) = HD(s_m, t_m, s_{m+1}, t_{m+1}, \nu, \gamma) +$$

$$KD(s_m, t_m, s_{m+1}, t_{m+1}, \nu, \gamma)$$

(E.4)

$$\begin{aligned} MD(s_m, t_m, s_{m+1}, t_{m+1}, \nu, \gamma) &= \frac{1}{9}[4\,E(s_m, t_m, s_{m+1}, t_{m+1}, 1, \nu+2, \gamma) + \\ & E(s_m, t_m, s_{m+1}, t_{m+1}, 1, \nu, \gamma+2) + \\ & 3\,EL(s_m, t_m, s_{m+1}, t_{m+1}, -1, \nu+2, \gamma)] \end{aligned}$$

(E.5)

$$\begin{aligned} ND(s_m, t_m, s_{m+1}, t_{m+1}, \nu, \gamma) &= \frac{1}{6}[-E(s_m, t_m, s_{m+1}, t_{m+1}, 1, \nu+2, \gamma) + \\ & 2\,E(s_m, t_m, s_{m+1}, t_{m+1}, 1, \nu, \gamma+2) + \\ & 3\,EL(s_m, t_m, s_{m+1}, t_{m+1}, -1, \nu+1, \gamma+2)] \end{aligned}$$

(E.6)

$$\begin{aligned} PD(s_m, t_m, s_{m+1}, t_{m+1}, \nu, \gamma) &= \frac{1}{48}[13\,E(s_m, t_m, s_{m+1}, t_{m+1}, 1, \nu+1, \gamma+2) - \\ & 2\,E(s_m, t_m, s_{m+1}, t_{m+1}, 1, \nu+3, \gamma) + \\ & 3\,EL(s_m, t_m, s_{m+1}, t_{m+1}, 1, \nu, \gamma+4) + \\ & 12\,EL(s_m, t_m, s_{m+1}, t_{m+1}, -1, \nu+2, \gamma+2)] \end{aligned}$$

(E.7)

$$\begin{aligned} RD(s_m, t_m, s_{m+1}, t_{m+1}, \nu, \gamma) &= \frac{1}{16}[E(s_m, t_m, s_{m+1}, t_{m+1}, 1, \nu+1, \gamma+2) - \\ & 2\,E(s_m, t_m, s_{m+1}, t_{m+1}, 1, \nu+3, \gamma) - \end{aligned}$$

$$EL(s_m, t_m, s_{m+1}, t_{m+1}, 1, \nu, \gamma+4) +$$
$$4\,EL(s_m, t_m, s_{m+1}, t_{m+1}, -1, \nu+2, \gamma+2)] \tag{E.8}$$

$$TD(s_m, t_m, s_{m+1}, t_{m+1}, \nu, \gamma) = PD(s_m, t_m, s_{m+1}, t_{m+1}, \nu, \gamma) + RD(s_m, t_m, s_{m+1}, t_{m+1}, \nu, \gamma) \tag{E.9}$$

$$\begin{aligned} VD(s_m, t_m, s_{m+1}, t_{m+1}, \nu, \gamma) = \frac{1}{90}[&-3\,E(s_m, t_m, s_{m+1}, t_{m+1}, 1, \nu+4, \gamma) + \\ &14\,E(s_m, t_m, s_{m+1}, t_{m+1}, 1, \nu+2, \gamma+2) + \\ &2\,EL(s_m, t_m, s_{m+1}, t_{m+1}, 1, \nu, \gamma+4) + \\ &15\,EL(s_m, t_m, s_{m+1}, t_{m+1}, -1, \nu+3, \gamma+2)] \end{aligned} \tag{E.10}$$

$$\begin{aligned} WD(s_m, t_m, s_{m+1}, t_{m+1}, \nu, \gamma) = \frac{1}{40}[&-E(s_m, t_m, s_{m+1}, t_{m+1}, 1, \nu+4, \gamma) - \\ &9\,E(s_m, t_m, s_{m+1}, t_{m+1}, 1, \nu+2, \gamma+2) + \\ &8\,E(s_m, t_m, s_{m+1}, t_{m+1}, 1, \nu, \gamma+4) + \\ &15\,EL(s_m, t_m, s_{m+1}, t_{m+1}, -1, \nu+3, \gamma+2)] \end{aligned} \tag{E.11}$$

$$XD(s_m, t_m, s_{m+1}, t_{m+1}, \nu, \gamma) = \frac{1}{480}[-4\,E(s_m, t_m, s_{m+1}, t_{m+1}, 1, \nu+5, \gamma) -$$

$$
\begin{aligned}
& 28\,E(s_m,t_m,s_{m+1},t_{m+1},1,\nu+3,\gamma+2)+\\
& 81\,E(s_m,t_m,s_{m+1},t_{m+1},1,\nu+1,\gamma+4)+\\
& 90\,EL(s_m,t_m,s_{m+1},t_{m+1},-1,\nu+2,\gamma+4)]+\\
& 15\,EL(s_m,t_m,s_{m+1},t_{m+1},1,\nu,\gamma+6)]
\end{aligned}
\tag{E.12}
$$

$$
\begin{aligned}
YD(s_m,t_m,s_{m+1},t_{m+1},\nu,\gamma) \;=\; & \frac{1}{96}[-4\,E(s_m,t_m,s_{m+1},t_{m+1},1,\nu+5,\gamma)-\\
& 16\,E(s_m,t_m,s_{m+1},t_{m+1},1,\nu+3,\gamma+2)+\\
& 3\,E(s_m,t_m,s_{m+1},t_{m+1},1,\nu+1,\gamma+4)+\\
& 18\,EL(s_m,t_m,s_{m+1},t_{m+1},-1,\nu+2,\gamma+4)-\\
& 3\,EL(s_m,t_m,s_{m+1},t_{m+1},1,\nu,\gamma+6)]
\end{aligned}
\tag{E.13}
$$

$$
\begin{aligned}
ZD(s_m,t_m,s_{m+1},t_{m+1},\nu,\gamma) \;=\; & XD(s_m,t_m,s_{m+1},t_{m+1},\nu,\gamma)+\\
& YD(s_m,t_m,s_{m+1},t_{m+1},\nu,\gamma)
\end{aligned}
\tag{E.14}
$$

$$
\begin{aligned}
AD(s_m,t_m,s_{m+1},t_{m+1},\nu,\gamma) \;=\; & \frac{1}{840}[-6\,E(s_m,t_m,s_{m+1},t_{m+1},1,\nu+6,\gamma)-\\
& 249\,E(s_m,t_m,s_{m+1},t_{m+1},1,\nu+4,\gamma+2)+\\
& 10\,EL(s_m,t_m,s_{m+1},t_{m+1},1,\nu+2,\gamma+4)+\\
& 148\,EL(s_m,t_m,s_{m+1},t_{m+1},1,\nu,\gamma+6)+
\end{aligned}
$$

$$105\,EL(s_m, t_m, s_{m+1}, t_{m+1}, -1, \nu+3, \gamma+4)]$$

(E.15)

APPENDIX F

THE DOUBLE INTEGRALS $\mathbf{I(I,J,I',J',P)}$, $\mathbf{P=-1,1,3}$ WITH LINARLY DEPENDENT $(\mathbf{X-X'})$ AND $(\mathbf{Y-Y'})$

The double integrals $I(i,j,i',j',p)$ with linear dependent $(x-x')$ and $(y-y')$ are defined in Section 4.4 and the solution techniques are introduced in Section 4.5.1.

The results of the integrals with all the combinations are expressed in terms of the integrals listed in Appendix D.

$$I(0,0,0,0,-1) = \frac{1}{2}\sum_{m=1}^{4}[\lambda_m\, G(s_m,t_m,s_{m+1},t_{m+1},1) + \xi_m\, G(s_m,t_m,s_{m+1},t_{m+1},0)] \tag{F.1}$$

$$I(0,0,1,0,-1) = \frac{1}{8}\sum_{m=1}^{4}[(1-2\lambda_m)\, G(s_m,t_m,s_{m+1},t_{m+1},2) + 2\xi_m(\lambda_m-1)\, G(s_m,t_m,s_{m+1},t_{m+1},1) + \xi_m^2\, G(s_m,t_m,s_{m+1},t_{m+1},0)] \tag{F.2}$$

$$I(1,0,0,0,-1) = \frac{1}{8}\sum_{m=1}^{4}[(1+2\lambda_m)\, G(s_m,t_m,s_{m+1},t_{m+1},2) + 2\xi_m(\lambda_m+1)\, G(s_m,t_m,s_{m+1},t_{m+1},1) + \xi_m^2\, G(s_m,t_m,s_{m+1},t_{m+1},0)] \tag{F.3}$$

$$
\begin{aligned}
I(0,0,0,1,-1) \;=\; & \frac{1}{8}\sum_{m=1}^{4}[b\,(1-2\lambda_m)\,G(s_m,t_m,s_{m+1},t_{m+1},2)+ \\
& 2(2\,\lambda_m\,c-b\,\xi_m+\lambda_m\,b\,\xi_m)\,G(s_m,t_m,s_{m+1},t_{m+1},1)+ \\
& (4c+b\,\xi_m)\,\xi_m\,G(s_m,t_m,s_{m+1},t_{m+1},0)+ \\
& \lambda_m\,H(s_m,t_m,s_{m+1},t_{m+1},1)+ \\
& \xi_m\,H(s_m,t_m,s_{m+1},t_{m+1},0)] \qquad \text{(F.4)}
\end{aligned}
$$

$$
\begin{aligned}
I(0,1,0,0,-1) \;=\; & \frac{1}{8}\sum_{m=1}^{4}[b\,(1-2\lambda_m)\,G(s_m,t_m,s_{m+1},t_{m+1},2)+ \\
& 2(2\,\lambda_m\,c-b\,\xi_m+\lambda_m\,b\,\xi_m)\,G(s_m,t_m,s_{m+1},t_{m+1},1)+ \\
& (4c+b\,\xi_m)\,\xi_m\,G(s_m,t_m,s_{m+1},t_{m+1},0)+ \\
& \lambda_m\,K(s_m,t_m,s_{m+1},t_{m+1},1)+ \\
& \xi_m\,K(s_m,t_m,s_{m+1},t_{m+1},0)] \qquad \text{(F.5)}
\end{aligned}
$$

$$
\begin{aligned}
I(1,0,1,0,-1) \;=\; & \frac{1}{24}\sum_{m=1}^{4}[-2\,\lambda_m\,G(s_m,t_m,s_{m+1},t_{m+1},3)+ \\
& 3\,\lambda_m\,\xi_m^2\,G(s_m,t_m,s_{m+1},t_{m+1},1)+ \\
& \xi_m^3\,G(s_m,t_m,s_{m+1},t_{m+1},0)] \qquad \text{(F.6)}
\end{aligned}
$$

$$
\begin{aligned}
I(0,1,1,0,-1) \;=\; & \frac{1}{24}\sum_{m=1}^{4}\{b(4\lambda_m-3)\,G(s_m,t_m,s_{m+1},t_{m+1},3)+ \\
& 3\,[2b\,\xi_m\,(1-\lambda_m)+c(1-2\lambda_m)]\,G(s_m,t_m,s_{m+1},t_{m+1},2)+ \\
& 3\xi_m\,(\lambda_m-1)\,(b\,\xi_m+2c)\,G(s_m,t_m,s_{m+1},t_{m+1},1)+ \\
& \xi_m^2(3c+b\,\xi_m)\,G(s_m,t_m,s_{m+1},t_{m+1},0)+
\end{aligned}
$$

$$\frac{3}{4}[(1-2\lambda_m)\,K(s_m,t_m,s_{m+1},t_{m+1},2)+$$
$$2\xi_m(\lambda_m-1)\,K(s_m,t_m,s_{m+1},t_{m+1},1)+$$
$$\xi_m^2\,K(s_m,t_m,s_{m+1},t_{m+1},0)]\} \qquad \text{(F.7)}$$

$$\begin{aligned} I(1,0,0,1,-1) \;=\; & \frac{1}{24}\sum_{m=1}^{4}\{-2b\,\lambda_m\,G(s_m,t_m,s_{m+1},t_{m+1},3)+ \\ & 3c(2\lambda_m+1)\,G(s_m,t_m,s_{m+1},t_{m+1},2)+ \\ & 3\xi_m[2c\,(\lambda_m+1)+b\,\lambda_m\,\xi_m]\,G(s_m,t_m,s_{m+1},t_{m+1},1)+ \\ & \xi_m^2\,(3c+b\,\xi_m)\,G(s_m,t_m,s_{m+1},t_{m+1},0)+ \\ & \frac{3}{4}[(1+2\lambda_m)\,H(s_m,t_m,s_{m+1},t_{m+1},2)+ \\ & 2\xi_m\,(\lambda_m+1)\,H(s_m,t_m,s_{m+1},t_{m+1},1)+ \\ & \xi_m^2\,H(s_m,t_m,s_{m+1},t_{m+1},0)]\} \end{aligned} \qquad \text{(F.8)}$$

$$\begin{aligned} I(0,1,0,1,-1) \;=\; & \frac{1}{24}\sum_{m=1}^{4}\{b^2(4\lambda_m-3)\,G(s_m,t_m,s_{m+1},t_{m+1},3)+ \\ & 6b[c(1-2\lambda_m)+b\xi_m\,(1-\lambda_m)]\cdot \\ & G(s_m,t_m,s_{m+1},t_{m+1},2)+ \\ & 3[b\xi_m\,(\lambda_m-1)\,(b\xi_m+4c)+4c^2\lambda_m]\cdot \\ & G(s_m,t_m,s_{m+1},t_{m+1},1)+ \\ & \xi_m\,(12c^2+6cb\,\xi_m+b^2\,\xi_m^2)\,G(s_m,t_m,s_{m+1},t_{m+1},0)+ \\ & \frac{3}{4}[b(1-2\lambda_m)\,L(s_m,t_m,s_{m+1},t_{m+1},2)+ \\ & 2(2\lambda_m\,c-b\,\xi_m+\lambda_m\,b\,\xi_m)\,L(s_m,t_m,s_{m+1},t_{m+1},1)+ \\ & (4c+b\,\xi_m)\,\xi_m\,L(s_m,t_m,s_{m+1},t_{m+1},0)]+ \\ & \frac{4}{3}[\lambda_m\,M(s_m,t_m,s_{m+1},t_{m+1},1)+ \end{aligned}$$

$$\xi_m\, M(s_m, t_m, s_{m+1}, t_{m+1}, 0)]\} \tag{F.9}$$

$$\begin{aligned} I(0,0,0,0,1) \;=\; & \frac{1}{12}\sum_{m=1}^{4}[\lambda_m\, N(s_m, t_m, s_{m+1}, t_{m+1}, 1) + \\ & \xi_m\, N(s_m, t_m, s_{m+1}, t_{m+1}, 0)] \end{aligned} \tag{F.10}$$

$$\begin{aligned} I(0,0,1,0,1) \;=\; & \frac{1}{48}\sum_{m=1}^{4}[(1-2\lambda_m)\, N(s_m, t_m, s_{m+1}, t_{m+1}, 2) + \\ & 2\xi_m(\lambda_m - 1)\, N(s_m, t_m, s_{m+1}, t_{m+1}, 1) + \\ & \xi_m^2\, N(s_m, t_m, s_{m+1}, t_{m+1}, 0)] \end{aligned} \tag{F.11}$$

$$\begin{aligned} I(1,0,0,0,1) \;=\; & \frac{1}{48}\sum_{m=1}^{4}[(1+2\lambda_m)\, N(s_m, t_m, s_{m+1}, t_{m+1}, 2) + \\ & 2\xi_m(\lambda_m + 1)\, N(s_m, t_m, s_{m+1}, t_{m+1}, 1) + \\ & \xi_m^2\, N(s_m, t_m, s_{m+1}, t_{m+1}, 0)] \end{aligned} \tag{F.12}$$

$$\begin{aligned} I(0,0,0,1,1) \;=\; & \frac{1}{48}\sum_{m=1}^{4}[b\,(1-2\lambda_m)\, N(s_m, t_m, s_{m+1}, t_{m+1}, 2) + \\ & 2(2\,\lambda_m\, c - b\,\xi_m + \lambda_m\, b\,\xi_m)\, N(s_m, t_m, s_{m+1}, t_{m+1}, 1) + \\ & (4c + b\,\xi_m)\,\xi_m\, N(s_m, t_m, s_{m+1}, t_{m+1}, 0) + \\ & \lambda_m\, P(s_m, t_m, s_{m+1}, t_{m+1}, 1) + \\ & \xi_m\, P(s_m, t_m, s_{m+1}, t_{m+1}, 0)] \end{aligned} \tag{F.13}$$

$$I(0,1,0,0,1) \;=\; \frac{1}{48}\sum_{m=1}^{4}[b\,(1-2\lambda_m)\, N(s_m, t_m, s_{m+1}, t_{m+1}, 2) +$$

$$2(2\,\lambda_m\,c - b\,\xi_m + \lambda_m\,b\,\xi_m)\,N(s_m,t_m,s_{m+1},t_{m+1},1) +$$
$$(4c + b\,\xi_m)\,\xi_m\,N(s_m,t_m,s_{m+1},t_{m+1},0) +$$
$$\lambda_m\,R(s_m,t_m,s_{m+1},t_{m+1},1) +$$
$$\xi_m\,R(s_m,t_m,s_{m+1},t_{m+1},0)] \qquad \text{(F.14)}$$

$$I(1,0,1,0,1) = \frac{1}{144}\sum_{m=1}^{4}[-2\,\lambda_m\,N(s_m,t_m,s_{m+1},t_{m+1},3) +$$
$$3\,\lambda_m\,\xi_m^2\,N(s_m,t_m,s_{m+1},t_{m+1},1) +$$
$$\xi_m^3\,N(s_m,t_m,s_{m+1},t_{m+1},0)] \qquad \text{(F.15)}$$

$$I(0,1,1,0,1) = \frac{1}{144}\sum_{m=1}^{4}\{b(4\lambda_m - 3)\,N(s_m,t_m,s_{m+1},t_{m+1},3) +$$
$$3\,[2b\,\xi_m\,(1-\lambda_m) + c(1-2\lambda_m)]\,N(s_m,t_m,s_{m+1},t_{m+1},2) +$$
$$3\xi_m\,(\lambda_m - 1)\,(b\,\xi_m + 2c)\,N(s_m,t_m,s_{m+1},t_{m+1},1) +$$
$$\xi_m^2(3c + b\,\xi_m)\,N(s_m,t_m,s_{m+1},t_{m+1},0) +$$
$$\frac{3}{4}[(1-2\lambda_m)\,R(s_m,t_m,s_{m+1},t_{m+1},2) +$$
$$2\xi_m(\lambda_m - 1)\,R(s_m,t_m,s_{m+1},t_{m+1},1) +$$
$$\xi_m^2\,R(s_m,t_m,s_{m+1},t_{m+1},0)]\} \qquad \text{(F.16)}$$

$$I(1,0,0,1,1) = \frac{1}{144}\sum_{m=1}^{4}\{-2b\,\lambda_m\,N(s_m,t_m,s_{m+1},t_{m+1},3) +$$
$$3c(2\lambda_m + 1)\,N(s_m,t_m,s_{m+1},t_{m+1},2) +$$
$$3\xi_m[2c\,(\lambda_m + 1) + b\,\lambda_m\,\xi_m]\,N(s_m,t_m,s_{m+1},t_{m+1},1) +$$
$$\xi_m^2\,(3c + b\,\xi_m)\,N(s_m,t_m,s_{m+1},t_{m+1},0) +$$

$$\frac{3}{4}[(1+2\lambda_m)\,P(s_m,t_m,s_{m+1},t_{m+1},2)+$$
$$2\xi_m\,(\lambda_m+1)\,P(s_m,t_m,s_{m+1},t_{m+1},1)+$$
$$\xi_m^2\,P(s_m,t_m,s_{m+1},t_{m+1},0)]\} \qquad \text{(F.17)}$$

$$\begin{aligned} I(0,1,0,1,1) \;=\; & \frac{1}{144}\sum_{m=1}^{4}\{b^2(4\lambda_m-3)\,N(s_m,t_m,s_{m+1},t_{m+1},3)+ \\ & 6b[c(1-2\lambda_m)+b\xi_m\,(1-\lambda_m)]\,N(s_m,t_m,s_{m+1},t_{m+1},2)+ \\ & 3[b\xi_m\,(\lambda_m-1)\,(b\xi_m+4c)+4c^2\lambda_m]\cdot \\ & N(s_m,t_m,s_{m+1},t_{m+1},1)+ \\ & \xi_m\,(12c^2+6cb\,\xi_m+b^2\,\xi_m^2)\,N(s_m,t_m,s_{m+1},t_{m+1},0)+ \\ & \frac{3}{4}[b(1-2\lambda_m)\,T(s_m,t_m,s_{m+1},t_{m+1},2)+ \\ & 2(2\lambda_m\,c-b\,\xi_m+\lambda_m\,b\,\xi_m)\,T(s_m,t_m,s_{m+1},t_{m+1},1)+ \\ & (4c+b\,\xi_m)\,\xi_m\,T(s_m,t_m,s_{m+1},t_{m+1},0)]+ \\ & \frac{4}{3}[\lambda_m\,V(s_m,t_m,s_{m+1},t_{m+1},1)+ \\ & \xi_m\,V(s_m,t_m,s_{m+1},t_{m+1},0)]\} \end{aligned} \qquad \text{(F.18)}$$

$$\begin{aligned} I(0,0,0,0,3) \;=\; & \frac{1}{80}\sum_{m=1}^{4}[\lambda_m\,W(s_m,t_m,s_{m+1},t_{m+1},1)+ \\ & \xi_m\,W(s_m,t_m,s_{m+1},t_{m+1},0)] \end{aligned} \qquad \text{(F.19)}$$

$$\begin{aligned} I(0,0,1,0,3) \;=\; & \frac{1}{320}\sum_{m=1}^{4}[(1-2\lambda_m)\,W(s_m,t_m,s_{m+1},t_{m+1},2)+ \\ & 2\xi_m(\lambda_m-1)\,W(s_m,t_m,s_{m+1},t_{m+1},1)+ \\ & \xi_m^2\,W(s_m,t_m,s_{m+1},t_{m+1},0)] \end{aligned} \qquad \text{(F.20)}$$

$$
\begin{aligned}
I(1,0,0,0,3) \;=\; & \frac{1}{320}\sum_{m=1}^{4}[(1+2\lambda_m)\,W(s_m,t_m,s_{m+1},t_{m+1},2)+ \\
& 2\xi_m(\lambda_m+1)\,W(s_m,t_m,s_{m+1},t_{m+1},1)+ \\
& \xi_m^2\,W(s_m,t_m,s_{m+1},t_{m+1},0)] \qquad \text{(F.21)}
\end{aligned}
$$

$$
\begin{aligned}
I(0,0,0,1,3) \;=\; & \frac{1}{320}\sum_{m=1}^{4}[b\,(1-2\lambda_m)\,W(s_m,t_m,s_{m+1},t_{m+1},2)+ \\
& 2(2\,\lambda_m\,c-b\,\xi_m+\lambda_m\,b\,\xi_m)\,W(s_m,t_m,s_{m+1},t_{m+1},1)+ \\
& (4c+b\,\xi_m)\,\xi_m\,W(s_m,t_m,s_{m+1},t_{m+1},0)+ \\
& \lambda_m\,X(s_m,t_m,s_{m+1},t_{m+1},1)+ \\
& \xi_m\,X(s_m,t_m,s_{m+1},t_{m+1},0)] \qquad \text{(F.22)}
\end{aligned}
$$

$$
\begin{aligned}
I(0,1,0,0,3) \;=\; & \frac{1}{320}\sum_{m=1}^{4}[b\,(1-2\lambda_m)\,W(s_m,t_m,s_{m+1},t_{m+1},2)+ \\
& 2(2\,\lambda_m\,c-b\,\xi_m+\lambda_m\,b\,\xi_m)\,W(s_m,t_m,s_{m+1},t_{m+1},1)+ \\
& (4c+b\,\xi_m)\,\xi_m\,W(s_m,t_m,s_{m+1},t_{m+1},0)+ \\
& \lambda_m\,Y(s_m,t_m,s_{m+1},t_{m+1},1)+ \\
& \xi_m\,Y(s_m,t_m,s_{m+1},t_{m+1},0)] \qquad \text{(F.23)}
\end{aligned}
$$

$$
\begin{aligned}
I(1,0,1,0,3) \;=\; & \frac{1}{960}\sum_{m=1}^{4}[-2\,\lambda_m\,W(s_m,t_m,s_{m+1},t_{m+1},3)+ \\
& 3\,\lambda_m\,\xi_m^2\,W(s_m,t_m,s_{m+1},t_{m+1},1)+ \\
& \xi_m^3\,W(s_m,t_m,s_{m+1},t_{m+1},0)] \qquad \text{(F.24)}
\end{aligned}
$$

$$
\begin{aligned}
I(0,1,1,0,3) \;=\; & \frac{1}{960}\sum_{m=1}^{4}\{b(4\lambda_m-3)\,W(s_m,t_m,s_{m+1},t_{m+1},3)+ \\
& 3\,[2b\,\xi_m\,(1-\lambda_m)+c(1-2\lambda_m)]\,W(s_m,t_m,s_{m+1},t_{m+1},2)+ \\
& 3\xi_m\,(\lambda_m-1)\,(b\,\xi_m+2c)\,W(s_m,t_m,s_{m+1},t_{m+1},1)+ \\
& \xi_m^2(3c+b\,\xi_m)\,W(s_m,t_m,s_{m+1},t_{m+1},0)+ \\
& \frac{3}{4}[(1-2\lambda_m)\,Y(s_m,t_m,s_{m+1},t_{m+1},2)+ \\
& 2\xi_m(\lambda_m-1)\,Y(s_m,t_m,s_{m+1},t_{m+1},1)+ \\
& \xi_m^2\,Y(s_m,t_m,s_{m+1},t_{m+1},0)]\}
\end{aligned}
\tag{F.25}
$$

$$
\begin{aligned}
I(1,0,0,1,3) \;=\; & \frac{1}{960}\sum_{m=1}^{4}\{-2b\,\lambda_m\,W(s_m,t_m,s_{m+1},t_{m+1},3)+ \\
& 3c(2\lambda_m+1)\,W(s_m,t_m,s_{m+1},t_{m+1},2)+ \\
& 3\xi_m[2c\,(\lambda_m+1)+b\,\lambda_m\,\xi_m]\,W(s_m,t_m,s_{m+1},t_{m+1},1)+ \\
& \xi_m^2\,(3c+b\,\xi_m)\,W(s_m,t_m,s_{m+1},t_{m+1},0)+ \\
& \frac{3}{4}[(1+2\lambda_m)\,X(s_m,t_m,s_{m+1},t_{m+1},2)+ \\
& 2\xi_m\,(\lambda_m+1)\,X(s_m,t_m,s_{m+1},t_{m+1},1)+ \\
& \xi_m^2\,X(s_m,t_m,s_{m+1},t_{m+1},0)]\}
\end{aligned}
\tag{F.26}
$$

$$
\begin{aligned}
I(0,1,0,1,3) \;=\; & \frac{1}{960}\sum_{m=1}^{4}\{b^2(4\lambda_m-3)\,W(s_m,t_m,s_{m+1},t_{m+1},3)+ \\
& 6b[c(1-2\lambda_m)+b\xi_m\,(1-\lambda_m)]\cdot \\
& W(s_m,t_m,s_{m+1},t_{m+1},2)+ \\
& 3[b\xi_m\,(\lambda_m-1)\,(b\xi_m+4c)+4c^2\lambda_m]\cdot \\
& W(s_m,t_m,s_{m+1},t_{m+1},1)+
\end{aligned}
$$

$$\xi_m \left(12c^2 + 6cb\,\xi_m + b^2\,\xi_m^2\right) W(s_m, t_m, s_{m+1}, t_{m+1}, 0) +$$
$$\frac{3}{4}[b(1 - 2\lambda_m)\, Z(s_m, t_m, s_{m+1}, t_{m+1}, 2) +$$
$$2(2\lambda_m\, c - b\,\xi_m + \lambda_m\, b\,\xi_m)\, Z(s_m, t_m, s_{m+1}, t_{m+1}, 1) +$$
$$(4c + b\,\xi_m)\,\xi_m\, Z(s_m, t_m, s_{m+1}, t_{m+1}, 0)] +$$
$$\frac{4}{3}[\lambda_m\, A(s_m, t_m, s_{m+1}, t_{m+1}, 1) +$$
$$\xi_m\, A(s_m, t_m, s_{m+1}, t_{m+1}, 0)]\} \qquad \text{(F.27)}$$

APPENDIX G

THE DOUBLE INTEGRALS $\mathbf{I(I,J,I',J',P)}$, $\mathbf{P=-1,1,3}$ WITH LINEAR INDEPENDENT $(\mathbf{X}-\mathbf{X}')$ AND $(\mathbf{Y}-\mathbf{Y}')$

The double integrals $I(i,j,i',j',p)$ with linear independent $(x-x')$ and $(y-y')$ are defined in Section 4.4 and the solution techniques are introduced in Section 4.5.2.

The results of the integrals with all the combinations are expressed in terms of the integrals defined in Appendix E.

$$I(0,0,0,0,-1) = \triangle \sum_{m=1}^{4} GD(s_m, t_m, s_{m+1}, t_{m+1}, 0, 0) \qquad \text{(G.1)}$$

$$\begin{aligned} I(0,0,1,0,-1) &= \triangle \sum_{m=1}^{4} [\alpha_2\, GD(s_m, t_m, s_{m+1}, t_{m+1}, 0, 0) + \beta_2\, GD(s_m, t_m, \\ &\quad s_{m+1}, t_{m+1}, 0, 1) + \gamma_2\, GD(s_m, t_m, s_{m+1}, t_{m+1}, 1, 0)] \end{aligned} \qquad \text{(G.2)}$$

$$\begin{aligned} I(1,0,0,0,-1) &= \triangle \sum_{m=1}^{4} [\alpha_1\, GD(s_m, t_m, s_{m+1}, t_{m+1}, 0, 0) + \beta_1\, GD(s_m, t_m, \\ &\quad s_{m+1}, t_{m+1}, 0, 1) + \gamma_1\, GD(s_m, t_m, s_{m+1}, t_{m+1}, 1, 0)] \end{aligned} \qquad \text{(G.3)}$$

$$I(0,0,0,1,-1) = \triangle \sum_{m=1}^{4} [\alpha_4\, GD(s_m, t_m, s_{m+1}, t_{m+1}, 0, 0) + \beta_4\, GD(s_m, t_m,$$

$$s_{m+1}, t_{m+1}, 0, 1) + \gamma_4\, GD(s_m, t_m, s_{m+1}, t_{m+1}, 1, 0) +$$
$$HD(s_m, t_m, s_{m+1}, t_{m+1}, 0, 0)] \qquad \text{(G.4)}$$

$$I(0,1,0,0,-1) = \Delta \sum_{m=1}^{4} [\alpha_4\, GD(s_m, t_m, s_{m+1}, t_{m+1}, 0, 0) + \beta_4\, GD(s_m, t_m,$$
$$s_{m+1}, t_{m+1}, 0, 1) + \gamma_4\, GD(s_m, t_m, s_{m+1}, t_{m+1}, 1, 0) +$$
$$KD(s_m, t_m, s_{m+1}, t_{m+1}, 0, 0)] \qquad \text{(G.5)}$$

$$I(1,0,1,0,-1) = \Delta \sum_{m=1}^{4} [\alpha_1\alpha_2\, GD(s_m, t_m, s_{m+1}, t_{m+1}, 0, 0) +$$
$$(\alpha_1\beta_2 + \alpha_2\beta_1)\, GD(s_m, t_m, s_{m+1}, t_{m+1}, 0, 1) +$$
$$\beta_1\beta_2\, GD(s_m, t_m, s_{m+1}, t_{m+1}, 0, 2) +$$
$$(\alpha_1\gamma_2 + \alpha_2\gamma_1)\, GD(s_m, t_m, s_{m+1}, t_{m+1}, 1, 0) +$$
$$\gamma_1\gamma_2\, GD(s_m, t_m, s_{m+1}, t_{m+1}, 2, 0) +$$
$$(\beta_1\gamma_2 + \beta_2\gamma_1)\, GD(s_m, t_m, s_{m+1}, t_{m+1}, 1, 1)] \qquad \text{(G.6)}$$

$$I(0,1,1,0,-1) = \Delta \sum_{m=1}^{4} [\alpha_2\alpha_4\, GD(s_m, t_m, s_{m+1}, t_{m+1}, 0, 0) +$$
$$(\alpha_2\beta_4 + \alpha_4\beta_2)\, GD(s_m, t_m, s_{m+1}, t_{m+1}, 0, 1) +$$
$$\beta_2\beta_4\, GD(s_m, t_m, s_{m+1}, t_{m+1}, 0, 2) +$$
$$(\alpha_2\gamma_4 + \alpha_4\gamma_2)\, GD(s_m, t_m, s_{m+1}, t_{m+1}, 1, 0) +$$
$$\gamma_2\gamma_4\, GD(s_m, t_m, s_{m+1}, t_{m+1}, 2, 0) +$$
$$(\beta_2\gamma_4 + \beta_4\gamma_2)\, GD(s_m, t_m, s_{m+1}, t_{m+1}, 1, 1) +$$
$$\alpha_2\, KD(s_m, t_m, s_{m+1}, t_{m+1}, 0, 0) +$$

$$\beta_2\, KD(s_m, t_m, s_{m+1}, t_{m+1}, 0, 1) +$$
$$\gamma_2\, KD(s_m, t_m, s_{m+1}, t_{m+1}, 1, 0)] \qquad \text{(G.7)}$$

$$\begin{aligned} I(1,0,0,1,-1) \;=\; & \triangle \sum_{m=1}^{4} [\alpha_1\alpha_4\, GD(s_m, t_m, s_{m+1}, t_{m+1}, 0, 0) + \\ & (\alpha_1\beta_4 + \alpha_4\beta_1)\, GD(s_m, t_m, s_{m+1}, t_{m+1}, 0, 1) + \\ & \beta_1\beta_4\, GD(s_m, t_m, s_{m+1}, t_{m+1}, 0, 2) + \\ & (\alpha_1\gamma_4 + \alpha_4\gamma_1)\, GD(s_m, t_m, s_{m+1}, t_{m+1}, 1, 0) + \\ & \gamma_1\gamma_4\, GD(s_m, t_m, s_{m+1}, t_{m+1}, 2, 0) + \\ & (\beta_1\gamma_4 + \beta_4\gamma_1)\, GD(s_m, t_m, s_{m+1}, t_{m+1}, 1, 1) + \\ & \alpha_1\, HD(s_m, t_m, s_{m+1}, t_{m+1}, 0, 0) + \\ & \beta_1\, HD(s_m, t_m, s_{m+1}, t_{m+1}, 0, 1) + \\ & \gamma_1\, HD(s_m, t_m, s_{m+1}, t_{m+1}, 1, 0)] \end{aligned} \qquad \text{(G.8)}$$

$$\begin{aligned} I(0,1,0,1,-1) \;=\; & \triangle \sum_{m=1}^{4} [\alpha_4^2\, GD(s_m, t_m, s_{m+1}, t_{m+1}, 0, 0) + \\ & 2\alpha_4\beta_4\, GD(s_m, t_m, s_{m+1}, t_{m+1}, 0, 1) + \\ & \beta_4^2\, GD(s_m, t_m, s_{m+1}, t_{m+1}, 0, 2) + \\ & 2\alpha_4\gamma_4\, GD(s_m, t_m, s_{m+1}, t_{m+1}, 1, 0) + \\ & \gamma_4^2\, GD(s_m, t_m, s_{m+1}, t_{m+1}, 2, 0) + \\ & 2\beta_4\gamma_4\, GD(s_m, t_m, s_{m+1}, t_{m+1}, 1, 1) + \\ & \alpha_4\, LD(s_m, t_m, s_{m+1}, t_{m+1}, 0, 0) + \\ & \beta_4\, LD(s_m, t_m, s_{m+1}, t_{m+1}, 0, 1) + \\ & \gamma_4\, LD(s_m, t_m, s_{m+1}, t_{m+1}, 1, 0) + \end{aligned}$$

$$MD(s_m, t_m, s_{m+1}, t_{m+1}, 0, 0)] \tag{G.9}$$

$$I(0,0,0,0,1) = \Delta \sum_{m=1}^{4} ND(s_m, t_m, s_{m+1}, t_{m+1}, 0, 0) \tag{G.10}$$

$$\begin{aligned} I(0,0,1,0,1) \;=\; & \Delta \sum_{m=1}^{4} [\alpha_2\, ND(s_m, t_m, s_{m+1}, t_{m+1}, 0, 0) + \beta_2\, ND(s_m, t_m, \\ & s_{m+1}, t_{m+1}, 0, 1) + \gamma_2\, ND(s_m, t_m, s_{m+1}, t_{m+1}, 1, 0)] \end{aligned} \tag{G.11}$$

$$\begin{aligned} I(1,0,0,0,1) \;=\; & \Delta \sum_{m=1}^{4} [\alpha_1\, ND(s_m, t_m, s_{m+1}, t_{m+1}, 0, 0) + \beta_1\, ND(s_m, t_m, \\ & s_{m+1}, t_{m+1}, 0, 1) + \gamma_1\, ND(s_m, t_m, s_{m+1}, t_{m+1}, 1, 0)] \end{aligned} \tag{G.12}$$

$$\begin{aligned} I(0,0,0,1,1) \;=\; & \Delta \sum_{m=1}^{4} [\alpha_4\, ND(s_m, t_m, s_{m+1}, t_{m+1}, 0, 0) + \beta_4\, ND(s_m, t_m, \\ & s_{m+1}, t_{m+1}, 0, 1) + \gamma_4\, ND(s_m, t_m, s_{m+1}, t_{m+1}, 1, 0) + \\ & PD(s_m, t_m, s_{m+1}, t_{m+1}, 0, 0)] \end{aligned} \tag{G.13}$$

$$\begin{aligned} I(0,1,0,0,1) \;=\; & \Delta \sum_{m=1}^{4} [\alpha_4\, ND(s_m, t_m, s_{m+1}, t_{m+1}, 0, 0) + \beta_4\, ND(s_m, t_m, \\ & s_{m+1}, t_{m+1}, 0, 1) + \gamma_4\, ND(s_m, t_m, s_{m+1}, t_{m+1}, 1, 0) + \\ & RD(s_m, t_m, s_{m+1}, t_{m+1}, 0, 0)] \end{aligned} \tag{G.14}$$

$$I(1,0,1,0,1) \;=\; \Delta \sum_{m=1}^{4} [\alpha_1\alpha_2\, ND(s_m, t_m, s_{m+1}, t_{m+1}, 0, 0) +$$

$$
\begin{aligned}
&(\alpha_1\beta_2 + \alpha_2\beta_1)\, ND(s_m, t_m, s_{m+1}, t_{m+1}, 0, 1) + \\
&\beta_1\beta_2\, ND(s_m, t_m, s_{m+1}, t_{m+1}, 0, 2) + \\
&(\alpha_1\gamma_2 + \alpha_2\gamma_1)\, ND(s_m, t_m, s_{m+1}, t_{m+1}, 1, 0) + \\
&\gamma_1\gamma_2\, ND(s_m, t_m, s_{m+1}, t_{m+1}, 2, 0) + \\
&(\beta_1\gamma_2 + \beta_2\gamma_1)\, ND(s_m, t_m, s_{m+1}, t_{m+1}, 1, 1)] \qquad \text{(G.15)}
\end{aligned}
$$

$$
\begin{aligned}
I(0,1,1,0,1) \;=\; & \triangle \sum_{m=1}^{4} [\alpha_2\alpha_4\, ND(s_m, t_m, s_{m+1}, t_{m+1}, 0, 0) + \\
&(\alpha_2\beta_4 + \alpha_4\beta_2)\, ND(s_m, t_m, s_{m+1}, t_{m+1}, 0, 1) + \\
&\beta_2\beta_4\, ND(s_m, t_m, s_{m+1}, t_{m+1}, 0, 2) + \\
&(\alpha_2\gamma_4 + \alpha_4\gamma_2)\, ND(s_m, t_m, s_{m+1}, t_{m+1}, 1, 0) + \\
&\gamma_2\gamma_4\, ND(s_m, t_m, s_{m+1}, t_{m+1}, 2, 0) + \\
&(\beta_2\gamma_4 + \beta_4\gamma_2)\, ND(s_m, t_m, s_{m+1}, t_{m+1}, 1, 1) + \\
&\alpha_2\, RD(s_m, t_m, s_{m+1}, t_{m+1}, 0, 0) + \\
&\beta_2\, RD(s_m, t_m, s_{m+1}, t_{m+1}, 0, 1) + \\
&\gamma_2\, RD(s_m, t_m, s_{m+1}, t_{m+1}, 1, 0)] \qquad \text{(G.16)}
\end{aligned}
$$

$$
\begin{aligned}
I(1,0,0,1,1) \;=\; & \triangle \sum_{m=1}^{4} [\alpha_1\alpha_4\, ND(s_m, t_m, s_{m+1}, t_{m+1}, 0, 0) + \\
&(\alpha_1\beta_4 + \alpha_4\beta_1)\, ND(s_m, t_m, s_{m+1}, t_{m+1}, 0, 1) + \\
&\beta_1\beta_4\, ND(s_m, t_m, s_{m+1}, t_{m+1}, 0, 2) + \\
&(\alpha_1\gamma_4 + \alpha_4\gamma_1)\, ND(s_m, t_m, s_{m+1}, t_{m+1}, 1, 0) + \\
&\gamma_1\gamma_4\, ND(s_m, t_m, s_{m+1}, t_{m+1}, 2, 0) + \\
&(\beta_1\gamma_4 + \beta_4\gamma_1)\, ND(s_m, t_m, s_{m+1}, t_{m+1}, 1, 1) +
\end{aligned}
$$

$$\alpha_1 PD(s_m, t_m, s_{m+1}, t_{m+1}, 0, 0) +$$
$$\beta_1 PD(s_m, t_m, s_{m+1}, t_{m+1}, 0, 1) +$$
$$\gamma_1 PD(s_m, t_m, s_{m+1}, t_{m+1}, 1, 0)] \qquad \text{(G.17)}$$

$$\begin{aligned} I(0,1,0,1,1) \;=\; & \Delta \sum_{m=1}^{4} [\alpha_4^2 ND(s_m, t_m, s_{m+1}, t_{m+1}, 0, 0) + \\ & 2\alpha_4\beta_4 ND(s_m, t_m, s_{m+1}, t_{m+1}, 0, 1) + \\ & \beta_4^2 ND(s_m, t_m, s_{m+1}, t_{m+1}, 0, 2) + \\ & 2\alpha_4\gamma_4 ND(s_m, t_m, s_{m+1}, t_{m+1}, 1, 0) + \\ & \gamma_4^2 ND(s_m, t_m, s_{m+1}, t_{m+1}, 2, 0) + \\ & 2\beta_4\gamma_4 ND(s_m, t_m, s_{m+1}, t_{m+1}, 1, 1) + \\ & \alpha_4 TD(s_m, t_m, s_{m+1}, t_{m+1}, 0, 0) + \\ & \beta_4 TD(s_m, t_m, s_{m+1}, t_{m+1}, 0, 1) + \\ & \gamma_4 TD(s_m, t_m, s_{m+1}, t_{m+1}, 1, 0) + \\ & VD(s_m, t_m, s_{m+1}, t_{m+1}, 0, 0)] \end{aligned} \qquad \text{(G.18)}$$

$$I(0,0,0,0,3) = \Delta \sum_{m=1}^{4} WD(s_m, t_m, s_{m+1}, t_{m+1}, 0, 0) \qquad \text{(G.19)}$$

$$\begin{aligned} I(0,0,1,0,3) \;=\; & \Delta \sum_{m=1}^{4} [\alpha_2 WD(s_m, t_m, s_{m+1}, t_{m+1}, 0, 0) + \beta_2 WD(s_m, t_m, \\ & s_{m+1}, t_{m+1}, 0, 1) + \gamma_2 WD(s_m, t_m, s_{m+1}, t_{m+1}, 1, 0)] \end{aligned} \qquad \text{(G.20)}$$

$$I(1,0,0,0,3) \;=\; \Delta \sum_{m=1}^{4} [\alpha_1 WD(s_m, t_m, s_{m+1}, t_{m+1}, 0, 0) + \beta_1 WD(s_m, t_m,$$

$$s_{m+1}, t_{m+1}, 0, 1) + \gamma_1 WD(s_m, t_m, s_{m+1}, t_{m+1}, 1, 0)] \tag{G.21}$$

$$\begin{aligned} I(0,0,0,1,3) &= \triangle \sum_{m=1}^{4} [\alpha_4 WD(s_m, t_m, s_{m+1}, t_{m+1}, 0, 0) + \beta_4 WD(s_m, t_m, \\ &\quad s_{m+1}, t_{m+1}, 0, 1) + \gamma_4 WD(s_m, t_m, s_{m+1}, t_{m+1}, 1, 0) + \\ &\quad XD(s_m, t_m, s_{m+1}, t_{m+1}, 0, 0)] \end{aligned} \tag{G.22}$$

$$\begin{aligned} I(0,1,0,0,3) &= \triangle \sum_{m=1}^{4} [\alpha_4 WD(s_m, t_m, s_{m+1}, t_{m+1}, 0, 0) + \beta_4 WD(s_m, t_m, \\ &\quad s_{m+1}, t_{m+1}, 0, 1) + \gamma_4 WD(s_m, t_m, s_{m+1}, t_{m+1}, 1, 0) + \\ &\quad YD(s_m, t_m, s_{m+1}, t_{m+1}, 0, 0)] \end{aligned} \tag{G.23}$$

$$\begin{aligned} I(1,0,1,0,3) &= \triangle \sum_{m=1}^{4} [\alpha_1\alpha_2 WD(s_m, t_m, s_{m+1}, t_{m+1}, 0, 0) + \\ &\quad (\alpha_1\beta_2 + \alpha_2\beta_1) WD(s_m, t_m, s_{m+1}, t_{m+1}, 0, 1) + \\ &\quad \beta_1\beta_2 WD(s_m, t_m, s_{m+1}, t_{m+1}, 0, 2) + \\ &\quad (\alpha_1\gamma_2 + \alpha_2\gamma_1) WD(s_m, t_m, s_{m+1}, t_{m+1}, 1, 0) + \\ &\quad \gamma_1\gamma_2 WD(s_m, t_m, s_{m+1}, t_{m+1}, 2, 0) + \\ &\quad (\beta_1\gamma_2 + \beta_2\gamma_1) WD(s_m, t_m, s_{m+1}, t_{m+1}, 1, 1)] \end{aligned} \tag{G.24}$$

$$\begin{aligned} I(0,1,1,0,3) &= \triangle \sum_{m=1}^{4} [\alpha_2\alpha_4 WD(s_m, t_m, s_{m+1}, t_{m+1}, 0, 0) + \\ &\quad (\alpha_2\beta_4 + \alpha_4\beta_2) WD(s_m, t_m, s_{m+1}, t_{m+1}, 0, 1) + \\ &\quad \beta_2\beta_4 WD(s_m, t_m, s_{m+1}, t_{m+1}, 0, 2) + \end{aligned}$$

$$
\begin{aligned}
& (\alpha_2\gamma_4 + \alpha_4\gamma_2)\, WD(s_m, t_m, s_{m+1}, t_{m+1}, 1, 0) + \\
& \gamma_2\gamma_4\, WD(s_m, t_m, s_{m+1}, t_{m+1}, 2, 0) + \\
& (\beta_2\gamma_4 + \beta_4\gamma_2)\, WD(s_m, t_m, s_{m+1}, t_{m+1}, 1, 1) + \\
& \alpha_2\, YD(s_m, t_m, s_{m+1}, t_{m+1}, 0, 0) + \\
& \beta_2\, YD(s_m, t_m, s_{m+1}, t_{m+1}, 0, 1) + \\
& \gamma_2\, YD(s_m, t_m, s_{m+1}, t_{m+1}, 1, 0)] \qquad \text{(G.25)}
\end{aligned}
$$

$$
\begin{aligned}
I(1,0,0,1,3) \;=\; & \Delta \sum_{m=1}^{4} [\alpha_1\alpha_4\, WD(s_m, t_m, s_{m+1}, t_{m+1}, 0, 0) + \\
& (\alpha_1\beta_4 + \alpha_4\beta_1)\, WD(s_m, t_m, s_{m+1}, t_{m+1}, 0, 1) + \\
& \beta_1\beta_4\, WD(s_m, t_m, s_{m+1}, t_{m+1}, 0, 2) + \\
& (\alpha_1\gamma_4 + \alpha_4\gamma_1)\, WD(s_m, t_m, s_{m+1}, t_{m+1}, 1, 0) + \\
& \gamma_1\gamma_4\, WD(s_m, t_m, s_{m+1}, t_{m+1}, 2, 0) + \\
& (\beta_1\gamma_4 + \beta_4\gamma_1)\, WD(s_m, t_m, s_{m+1}, t_{m+1}, 1, 1) + \\
& \alpha_1\, XD(s_m, t_m, s_{m+1}, t_{m+1}, 0, 0) + \\
& \beta_1\, XD(s_m, t_m, s_{m+1}, t_{m+1}, 0, 1) + \\
& \gamma_1\, XD(s_m, t_m, s_{m+1}, t_{m+1}, 1, 0)] \qquad \text{(G.26)}
\end{aligned}
$$

$$
\begin{aligned}
I(0,1,0,1,3) \;=\; & \Delta \sum_{m=1}^{4} [\alpha_4^2\, WD(s_m, t_m, s_{m+1}, t_{m+1}, 0, 0) + \\
& 2\alpha_4\beta_4\, WD(s_m, t_m, s_{m+1}, t_{m+1}, 0, 1) + \\
& \beta_4^2\, WD(s_m, t_m, s_{m+1}, t_{m+1}, 0, 2) + \\
& 2\alpha_4\gamma_4\, WD(s_m, t_m, s_{m+1}, t_{m+1}, 1, 0) + \\
& \gamma_4^2\, WD(s_m, t_m, s_{m+1}, t_{m+1}, 2, 0) +
\end{aligned}
$$

$$
\begin{aligned}
&2\beta_4\gamma_4\, WD(s_m, t_m, s_{m+1}, t_{m+1}, 1, 1) + \\
&\alpha_4\, ZD(s_m, t_m, s_{m+1}, t_{m+1}, 0, 0) + \\
&\beta_4\, ZD(s_m, t_m, s_{m+1}, t_{m+1}, 0, 1) + \\
&\gamma_4\, ZD(s_m, t_m, s_{m+1}, t_{m+1}, 1, 0) + \\
&AD(s_m, t_m, s_{m+1}, t_{m+1}, 0, 0)] \qquad \text{(G.27)}
\end{aligned}
$$